CZECH TECHNICAL UNIVERSITY IN PRAGUE

Faculty of Civil Engineering
Department of Materials Engineering and Chemistry

Characterization of hydration processes of cement pastes by means of thermal analysis

DOCTORAL THESIS

Lenka Scheinherrová

Doctoral study programme: Civil Engineering
Branch of study: Physical and Material Engineering

Doctoral thesis supervisor: Assoc. Prof. Anton Trník

Prague, 2018

I hereby confirm on my honor that I personally prepared the present doctoral thesis and carried out the activities directly associated with it by myself.

This doctoral thesis has not been submitted to any other examination authority. I also confirm that I have used no resources other than those declared. All formulations and concepts adopted literally or in their essential content from printed, unprinted or internet sources have been cited according to the rules for academic work.

Lenka Scheinherrová, 10/2018.

Acknowledgements

This thesis was realized at the Department of Material Engineering and Chemistry in collaboration with the University Centre for Energy Efficient Buildings (both CTU in Prague) and with the Institute of Inorganic Chemistry of Academy of Sciences of the Czech Republic. It was mainly founded by the project No. GB105/12/G059 - Cumulative time dependent processes in building materials and structures.

I would like to express my gratitude to all the people who made this work possible:

- Assoc. Prof. Anton Trník, my thesis supervisor, for his guidance, conceptual and technical advice, support and patience.
- Assoc. Prof. Martin Keppert, for helping me to understand the chemical background of hydration mechanisms. I am also grateful for his patience, and motivating and stimulating discussions.
- Dr. Vratislav Tydlitát and Dr. Miloš Jerman for performing the calorimetric experiments.
- M.Eng. Jitka Krejsová for carrying out the SEM analysis. I am very grateful for her kind support.
- Dr. Petr Bezdička, for his contribution in the XRD analysis and fruitful and constructive discussions.
- M.Eng. Magdaléna Doleželová for execution of the MIP analysis and for feeding me when I was too tired to cook for myself.
- M.Eng. Jaroslav Pokorný for performing the Blaine permeability method and Particle size distribution experiments.
- My other colleagues and friends from our department for the good atmosphere and for all interesting discussions linked to this thesis.
- My friends, for their encouragement and patience at the times I could not be available for them as much as I would have wished.

- My great and big family, for always being there when I needed their hugs and kind words, for trusting me in my (many weird and unexpected) choices and for their unlimited support.
- Guilhem, significant other, and a huge distraction in my life, for crossing my path during time when I was lost, looking for the right direction. For calming me down when I needed it or for pushing on me when I got lazy and hopeless. Simply, for always being there for me, no matter what.

Anotace

I přesto, že existuje velké množství odborných studií, které se zabývají mechanismy hydratace cementu, většina z nich omezuje své pozorování pouze na krátký časový interval. Pro správné pochopení hydratačních procesů je nutné co nejvíce rozšířit tento studovaný úsek. Z tohoto důvodu se tato práce zabývá studiem průběhu hydratace cementových past v závislosti na čase až do 360 dní.

Za tímto účelem byly navrženy cementové pasty s různým vodním součinitelem 0.3–0.5. Dále byly připraveny pasty s pucolánově aktivními příměsmi. Cement byl v těchto pastách částečně nahrazen mikrosilikou v rozmezí 0–12 %. Druhým studovaným pucolánem byl zvolen přírodní zeolit, kterým bylo nahrazeno 0–40 % cementu. Dále byl sledován vliv způsobu uložení vzorků (voda/vzduch) na tvorbu a změnu hydratačních produktů.

Hlavní metodou byla zvolena termická analýza. Jedná se o metodu, která je využitelná v jakémkoliv stáří materiálu. Především pomocí termogravimetrie je možné kvantitativně určit zastoupení hlavních hydratačních produktů. Dále byl podrobněji sledován průběh hydratačního tepla, vývoj mikrostruktury, základní fyzikální vlastnosti a mechanické vlastnosti studovaných cementových past.

Klíčová slova: *Hydratace cementu, termická analýza, cementové pasty, pucolán, časová závislost.*

Abstract

Despite the variety of studies dealing with the mechanisms of cement hydration, their observation is usually limited only to short-term intervals. While often neglected, the study of the long-term processes is also essential to fully understand the complex hydration mechanisms. This thesis attempts to extend the limited knowledge in this area through the study of the hydration processes of various cement pastes within a full year.

For this purpose, plain cement pastes with various water-to-cement ratios ratios between 0.3 and 0.5 were prepared, along with pastes containing pozzolana active materials. In these blended pastes, cement was partially replaced by silica fume by 0–12wt.%. The second chosen pozzolan was natural zeolite, which replaced between 0 and 40 wt.% of the cement. The effect of the sample storage (water vs. air) was also examined.

Thermal analysis was selected as the main method, as its performance is not limited by the age of the materials. More precisely, thermogravimetry can quantify the main hydration products and their changes in time. Moreover, the hydration heat development, microstructure evolution, basic physical and mechanical properties of the studied cement pastes were determined.

Keywords: *Hydration of cement, thermal analysis, cement pastes, pozzolan, time dependency.*

List of abbreviations

Abbreviation	Definition
^{1}H NMR	Proton nuclear magnetic resonance spectroscopy
AFm	Monosulfo aluminate
AFt	Ettringite/trisulfoaluminate
C_2S	Dicalcium silicate/larnite
C_3A	Tricalcium aluminate
C_3S	Tricalcium silicate/hartrurite
C_4AF	Calcium alumino-ferrite solid solution/ Ferrite
CBW	Chemically bound water
CH	Portlandite/calcium hydroxide $Ca(OH)_2$
C-S-H	Calcium-silicate hydrates
DSC	Differential scanning calorimetry
DTG	Differential thermogravimetry
MIP	Mercury intrusion porosimetry
NRRA	Nuclear resonance reaction analysis
OPC	Ordinary Portland cement
SEM	Scanning electron microscopy
TA	Thermal analysis
TG	Thermogravimetry
TGA	Thermogravimetric analysis
w/c	Water-to-cement ratio
XRD	X-ray diffraction
XRF	X-ray fluorescence

Contents

Chapter 1

Introduction

1.1. Statement of the problem and objectives

Concrete and cement-based composites are probably the most widely used building materials. The knowledge of their properties, especially understanding of the mechanisms of hydration of cement, along with the ability to predict their behavior for a given time horizon, are the keys to the production of concretes of the best qualities.

The hydration mechanisms can be easily influenced, for example, by the choice of water-to-cement ratio or curing temperature. The water-to-cement ratio, in particular, influences numerous important parameters of fresh and hardened concrete. It modifies the amount and morphology of the hydration products, which leads to changes in mechanical properties.

An important improvement in the technology of concrete can be made thanks to advanced chemical additions and admixtures, which help to enhance some of the parameters of the designed concrete. For this purpose, the utilization of pozzolana active materials, which can be natural or industrially prepared, is very popular nowadays. Moreover, many of these materials are wastes, therefore, their incorporation into concrete helps their further utilization. The addition of pozzolana active materials significantly influences the hydration processes.

It is essential to apply appropriate methods for any type of research study. In this case, hydration processes should be arrested before analyses are performed. Because usually, these experiments cannot be done at the designed day of sample age. Moreover, some methods for hydration stoppage can significantly alter the obtained results.

Several analyses can be successfully used for the study of the cement-based materials at early ages mainly. For example, the hydration heat development can be successfully applied for the first few days.

The microscopy also can help mainly during early age of materials, as the structure of concrete becomes more compact in time, and thus, hydration products are so connected, that it is nearly impossible to analyze them separately.

Thermal analysis is very suitable for this purpose, as it is not limited by the age of the materials. Especially thermogravimetry can be used for the quantification of some selected products, which decompose in a chosen temperature interval. The changes in their production can be therefore recorded and studied.

The main objetives of this study can be summarized as follows:

- To perform detailed analyses on the raw materials chosen for this study, such as ordinary Portland cement and pozzolana active materials, silica fume and natural zeolite.
- To apply classical methods for the study of hydration processes of cement on plain cement pastes with various water-to-cement ratio and on pastes blended with pozzolana active materials.
- To study the hydration products and their changes up to 360 days by means of thermal analysis consisting of thermogravimetry (TG) and differential scanning calorimetry (DSC). While TG gives the most important information about the studied systems, DSC is utilized as a supplementing method.
- From the obtained results, to evaluate the effects of water-to-cement ratio, selected pozzolana active materials and the curing conditions on the hydration processes, especially on the growth of hydration products.
- To propose future possible directions in the study of mechanisms of cement hydration by means of thermal analysis.

1.2. Chapter overview

This work is divided into ten chapters. After the introduction part, the Chapter 2 summarizes the recent literature review about hydration of cement. The mechanisms of early cement hydration are described based on the main phases of cement, such as alite, belite, aluminate phase and ferrite. Properties of the main hydration products are described. Factors influencing properties of hardened cement pastes are discussed thereafter. This chapter is enclosed with an introduction to pozzolana active materials.

Chapter 3 deals with hydration stoppage techniques and summarizes the recent literature about this topic. The impact of direct drying, solvent exchange on the hydration products is discussed.

Chapter 4 describes the classical characterization methods for the determination of properties of cementitious materials, which were studied in this work, such as particle size distribution, Blaine permeability method, X-ray fluorescence, hydration heat, X-ray diffraction, scanning electron microscopy, mercury intrusion porosimetry and basic physical and mechanical properties.

Chapter 5 is focused on thermal analysis method and due to its particular importance for this study, it stands separately. The thermal analysis techniques are introduced. Emphasis is placed on thermogravimetry and differential scanning calorimetry, which were used in this study. The process of the quantification of the main hydration products is described in detail.

Chapter 6 deals with raw materials and composition of the studied cement pates. Generic sample casting is described in this part and the chosen hydration stoppage technique is introduced.

In Chapters 7–9, the main results as obtained in this study, are summarized. Chapter 7 is focused on the characterization of plain cement pastes mixed with different water-to-cement ratio; Chapter 8 shows the results of the cement pastes blended with silica fume, and finally, Chapter 9 summarizes the results of the cement pastes blended with natural zeolite.

Finally, the main conclusions and perspectives of this study are drawn in Chapter 10.

Chapter 2

Hydration of cement

Even though the mechanisms of cement hydration have been widely studied and discussed within the past centuries, they still belong to very interesting topics of nowadays. Understanding what happens immediately after mixing cement with water and at later ages, is essential for both, academic and practical interests. From an academic point of view, the chemical and physical processes that characterize cement hydration, are very complex. Therefore, the determination and deeper description of the individual mechanisms of the parameters defining their rates are difficult. Thus, the basic research about hydration of cement offers significant scientific challenges in various experimental techniques and many theoretical modelling methods. From a more practical aspect, there is an obvious global trend to design and produce more sustainable cementitious materials, especially from secondary mineral additions, which also require more complicated mix designs [1].

In this chapter, the approximate composition of ordinary Portland cements (OPC) is summarized with a brief description how to estimate this parameter. After that, the mechanisms of hydration of the main phases and structure development of fresh and hardened cement pastes are described. The properties of the main hydration products are summarized and the effects of main factors influencing their development, such as various water-to-cement ratios (w/c) or temperature, are discussed. The most frequently used pozzolana active materials are introduced, along with their effects on the properties of blended cement pastes. This chapter is closed with possible ways of stopping hydration processes, which are essential for an appropriate sample preparation for experiments.

2.1. Composition of ordinary Portland cements

As already mentioned, cementitious materials belong to one of the most widely used construction materials in the world. They have been used since pre-Roman times and due to the excellent quality, with which the Roman concrete was produced, allowed the structures to remain durable until today [2, 3]. Romans not only developed the basics of concrete technology, they also gave the name "concretus" to this material, which can be translated as "mixed" or "cast" [4].

Portland cement is made by heating a mixture of limestone and clay, or other materials of similar bulk composition and sufficient reactivity, ultimately to a temperature about 1450 °C. During the final grinding process, the clinker is mixed with a few percent of calcium sulfate (dihydrate) and finely ground, to produce the cement. Calcium sulfate controls the rate of hardening and influences the rate of strength development. Some specifications allow the addition of other materials at the grinding stage [5]. Typical chemical composition of OPC is summarized in Table 2.1.1. These oxides form major phases of cement, and they are called alite, belite, aluminate, and ferrite [6].

Table 2.1.1. Chemical composition of OPC [7].

Oxide	Amount [%]
CaO	58–68
SiO_2	18–25
Al_2O_3	3.1–7.6
Fe_2O_3	0.2–5.8
MgO	0.0–7.1
Alkalies (K_2O, Na_2O)	0.0–1.7
SO_3	0.0–5.4
Free lime	0.0–3.7

The typical composition of these phases is summarized in Table 2.1.2. Several other phases, such as alkali sulfates and calcium oxide, are usually present in minor amounts [5].

Table 2.1.2. The typical phase composition of OPC [5].

Compound	Name of compound	Abbreviated formula	Amount [%]
Alite	Tricalcium silicate	C_3S	50–70
Belite	Dicalcium silicate	C_2S	15–30
Aluminate	Tricalcium aluminate	C_3A	5–10
Ferrite	Tetracalcium aluminoferrite	C_4AF	5–15

Alite is the most important phase of all OPC clinkers, of which it constitutes 50–70%. It is tricalcium silicate (also known as $3CaO{\cdot}SiO_2$; C_3S or hatrurite) modified in composition and crystal structure by ionic substitutions. After mixing cement with water, it reacts relatively quickly. It is the most important constituent phase for strength development; at ages up to 28 days, it is by far the most influential. Pure alite contains 73.7% of CaO and 26.3% of SiO_2. It can be found in 7 different polymorphic forms, depending on the sintering temperature and on the impurities added for the synthesis [5].

Belite represents 15–30% of OPC clinkers. It is dicalcium silicate ($2CaO{\cdot}SiO_2$; C_2S or larnite) modified by ionic substitutions and normally present completely or predominantly as the ß polymorph. Its reaction with water is slow, thus, it contributes only little to the strength during the first 28 days. However, it helps substantially to the further increase in strength at later ages. By one year, the strengths obtainable from pure alite and pure belite are about the same under comparable conditions [5].

Aluminate makes up 5–10% of most OPC clinkers. It is tricalcium aluminate ($3CaO{\cdot}Al_2O_3{\cdot}Fe_2O_3$; C_3A), substantially modified in composition, and sometimes also in structure by ionic substitutions [5]. It exists in several polymorphic forms, all consisting of independent SiO_4 tetrahedra linked by calcium atoms [7]. It reacts rapidly with water, and can cause undesirably rapid setting. To prevent this to happen, a set-controlling agent, such as calcium sulfate (dihydrate), is added to cement [5].

Ferrite represents about 5–15% of OPC clinkers. It is tetracalcium aluminoferrite ($4CaO{\cdot}Al_2O_3{\cdot}Fe_2O_3$; C_4AF, or brownmillerite), significantly modified in composition by a variation in the Al/Fe ratio and ionic substitutions. It appears, that the rate at which it reacts with water is somewhat variable. This can be

caused due to differences in composition or other characteristics. In general, its rate is high initially and low or very low at later ages [5].

Some **minor compounds** can be also present in the composition of OPC, such as MgO, which is generally limited to 4–5%. This restriction is due to the fact that quantities of this component in excess of about 2% can occur as periclase, which through slow reaction with water can be responsible for destructive expansion of hardened concrete. Free lime can behave similarly. Excessive contents of SO_3 can also lead to undesirable expansions. Therefore, it is recommended to use it typically in amounts of 3–5% for OPC. Alkalis (K_2O and Na_2O) can undergo expansive reactions with certain aggregates, and some specifications limit their content, e.g. to 0–6% equivalent Na_2O (Na_2O + 0.66 K_2O) [5].

2.1.1. Determination of the composition

If the raw materials react completely during clinkering to give only the four above mentioned phases, the reactive proportions of these phases can be calculated from the oxide composition of the raw mix [8]. The amounts of clinker phases can be approximately estimated from the well-known Bogue's equations, summarized as follows [6]:

$$C_3S = 4.07(CaO) - 7.60(SiO_2) - 6.72(Al_2O_3) - 1.43(Fe_2O_3) - 2.85(SO_3) \quad (2.1.1)$$

$$C_2S = 2.87(SiO_2) - 0.75(C_3S) \quad (2.1.2)$$

$$C_3A = 2.65(Al_2O_3) - 1.69(Fe_2O_3) \quad (2.1.3)$$

$$C_4AF = 3.04(Fe_2O_3) \quad (2.1.4)$$

Even though these formulas have been widely accepted and used in the past decades; the Bogue calculation takes not into account the solid solution between the phases or of the presence of minor oxides. Therefore, it was found that these calculations give low results for alite and inaccurate values for the other phases. Some authors have proposed new approach for the determination of the OPC composition. For example in 1989, Taylor [9] summarized a list of theoretical requirements for a correct calculation of the cement composition. Based on this list, the original Bogue's equations were modified. It was found that the modified method tended to give high results for aluminate. However, the accuracy of these results was still higher than the original Bogue equations. The

newest revision of the Bogue equations was done in 2014, in a study by Stutzman et al. [10], where a more complex system of multiple sources of uncertainty was considered.

Nowadays, the determination of the proportion of the main cement phases is most often done with the use of modern methods, such as quantitative X-ray diffraction analysis [11, 12], X-ray fluorescence or optical microscopy [13]. Currently, the X-ray fluorescence method is probably the most preferred elemental analysis method in the cement industry.

2.2. Mechanisms of early cement hydration

In this section, the newest findings about hydration mechanisms of the main four phases, which make up OPC, such as alite, belite, aluminate phase and ferrite are reviewed. Emphasis is placed on the description of the alite hydration since almost every review about the Portland cement hydration kinetics [14-17] is focused mainly on the hydration characteristics of alite. Which is in accordance to its dominant presence in the composition of OPC.

2.2.1. Alite hydration

As already mentioned, alite is very reactive during the early hydration period and it is responsible for the early strength evolution and for the formation of the calcium-silicate hydrate (C-S-H), an amorphous or poorly crystalline phase with variable stoichiometry. The C-S-H is one of the main products of hydration [1, 18]. Because it is very challenging to separate all hydration processes, much of the new progress in cement hydration research area has been done either on pure C_3S or alite itself. However, it should be noted that it was proved that triclinic C_3S exhibits a significantly different microstructure and hydration kinetics than impure, monoclinic alite [1, 19].

Historically, the overall progress of hydration of alite has been divided into four (sometimes more) stages, which are defined by somewhat arbitrary points on a plot of hydration vs. time [1]. These stages are displayed in Figure 2.2.1. The rate of alite hydration as a function of time measured by means of isothermal calorimetry therefore consists of (1) initial reaction, (2) period of slow reaction, (3) acceleration period, and finally of (4) deceleration period.

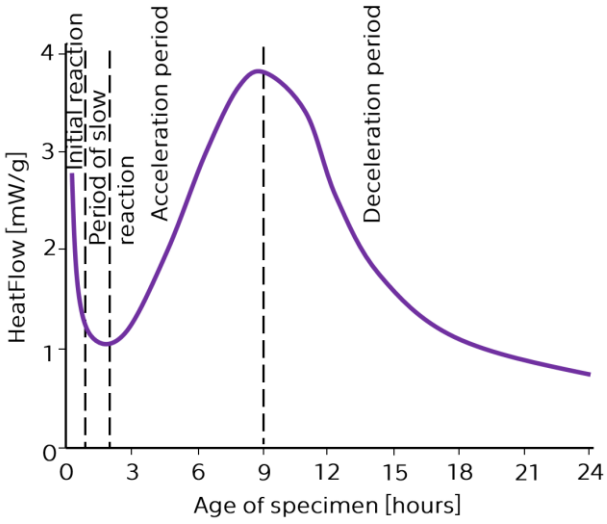

Figure 2.2.1. Typical isothermal calorimetry curve for C_3S paste, from [1].

It still remains difficult to determine precisely the beginning and the end of these stages, but this division helps to provide a more accurate picture of the current state of knowledge [1].

Initial reaction

It is characterized by a strong peak in isothermal calorimetry experiments during the first minutes after mixing cement with water [19]. This initial dissolution of ions upon contact with water takes about 15 minutes and it is followed by a significant reduction in the dissolution rate.

It is well-known that the C_3S dissolution rates decelerate very fast while the solution is still not fully saturated by the end of this period [1, 20]. This behavior is not fully understood and many hypotheses have been proposed to explain the mechanism of this early deceleration of C_3S, as discussed for example in [14-17]. The mostly accepted explanations can be summarized as follows:

- The deceleration could be caused by the rapid formation of a continuous but thin metastable **protective layer/membrane** of hydration products around the grain surface [19]. Gartner and Gaidis [15] have called this layer as C-S-H(m). It effectively passivates the surface by restricting its access to water. This thin layer is proposed to reach equilibrium with the solution at the end of the initial reaction period [1]. Nevertheless, the mechanism for the end of this period is not evident. Even when proved by nuclear

resonance reaction analysis (NRRA) experiments, the evidence for a continuous layer of a metastable barrier was not found using atomic force microscopy [21] nor by high-resolution electron microscopy [22].

- The **slow dissolution step** hypothesis assumes that the C_3S dissolution rates decrease rapidly for some other reason. Barret et al. [23, 24] proposed that a "superficially hydroxylated layer" can be formed on the surface of C_3S in contact with water. When the solution reaches the maximal supersaturation with the respect to C-S-H, it appears that C-S-H nucleates very quickly on surfaces of the C_3S particles and begins to grow slowly because of its initially low surface area. The growth of C-S-H leads to a decrease of the silicate concentration in solution and to an increase of the Ca:Si molar ratio on the other side. Steady state conditions are reached within the first few minutes of hydration in which the solution is supersaturated with respect to C-S-H, but undersaturated with respect to C_3S [1].

Period of slow reaction

During this period, a low heat evolution is determined. It is also known as the "**induction period**". It usually lasts for about 1–2 hours, depending on several parameters (presence of additives, the mineralogy of cement and its particle size). The mechanism that ends the induction period can be explained by two main hypotheses [19]:

- The induction period ends when hydration becomes dominated by the nucleation and growth of the C-S-H [25, 26].
- The product of the initial reaction forms a protective layer on the C_3S particles. The induction period ends when this is destroyed or rendered more permeable by ageing or phase transformation [15, 27-29].

The end of the induction period could be also correlated with the onset of crystallization of Portlandite [30]. Based on the results from scanning electron microscopy (SEM) obtained by Bazzoni [31], where the microstructural development of C_3S pastes was studied (Figure 2.2.2), small precipitates of C-S-H occured on the surface of the cement particles after 1.5 h of hydration. Bazzoni

also spotted etch pits. The induction period of the studied C_3S pastes was finished after 3 hours.

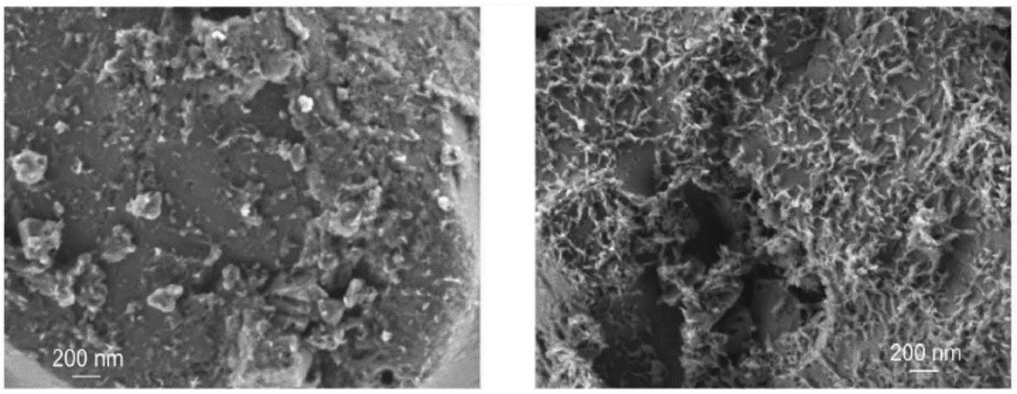

Figure 2.2.2. SEM images of C_3S pastes in secondary electron mode after 1.5 h and 3 h of hydration. Adapted from [31].

Acceleration period

The acceleration period is mainly related to the massive nucleation and growth of the C-S-H and Portlandite [19]. This period begins about 1–3 hours after mixing, depending on when the induction period finishes. As it can be seen in Figure 2.2.1, the reaction rate increases continuously and reaches the maximum after 9–20 hours. The time, at which the peak is reached and the heat is liberated, depends greatly on the particle size of used cement [1, 8]. The rapid formation of hydrates at this period leads to the setting and solidification of the cementitious matrix. A decrease of porosity is also observed during this period [19].

The C-S-H growth mechanism and its proper explanation has been one of the main concerns of many researchers. In a recent study by Zhang et al. [32], morphology evolution and C-S-H growth mechanisms were conducted in a combinatorial approach of experiment and simulation at atomic, nano and micro level. Gartner et al. [16] listed four main proposed mechanisms for the beginning of accelerating period (Table 2.2.1). Each hypothesis has received a certain support in the literature and experimental results have been arguing for or against each other [1]. From these four main mechanisms, the mechanical rupture of a surface barrier has been proved to be most consistent with the NRRA data [33]. Structure of the C-S-H created at the end of this period is poorly

crystalline and consists of sheets of calcium and oxygen surrounded by chains of tetrahedral silica, forming the main layers that are separated by water interlayers [5].

Table 2.2.1. Possible causes of the onset of the nucleation and growth period, reproduced from [1, 16].

Hypothesis/mechanism	Brief description
Nucleation and growth of C-S-H	Nucleation and growth of a stable C-S-H happen at the end of the slow reaction period and are rate-controlling during the acceleration period as a metastable protective layer of hydrate becomes chemically unstable and exposes the high-solubility C_3S.
Growth of stable C-S-H	Nuclei of stable C-S-H, already formed during the initial reaction, grow at a nearly exponential rate. The C-S-H growth is rate controlling. No metastable hydrate barrier layer is invoked.
Rupture of initial barrier	Metastable C-S-H barrier layer is semipermeable. Solution inside is close to saturation with respect to C_3S. Osmotic pressure leads to its rupture.
Nucleation of Portlandite	Nucleation and growth of Portlandite become rate-controlling (and thus indirectly control the rate of growth of C-S-H).

In Figure 2.2.3, the structure of alite paste observed after 9 hours measured by means of scanning electron microscopy (SEM), can be seen. The development and growth processes of the C-S-H highly influence the microstructure of the hydrated cement paste, and therefore, also durability properties of concrete. It has been found that the addition of C-S-H seeds increases C_3S or cement hydration rate by providing more surface. Besides this, it also promotes the hydrate precipitation in the capillary pore space, which is usually not possible in non-seeded systems [34]. The formation of C-S-H can be modified by addition of C-S-H seeds, as demonstrated in Figure 2.2.4. It can be seen that after (a) a few minutes and (b) several hours after mixing ordinary cement paste the hydration products are being slowly created. While with the seeding, hydration products

precipitate on the surface of the particles and on C-S-H seeds after some minutes (c), leading to lower porosity after some hours (d).

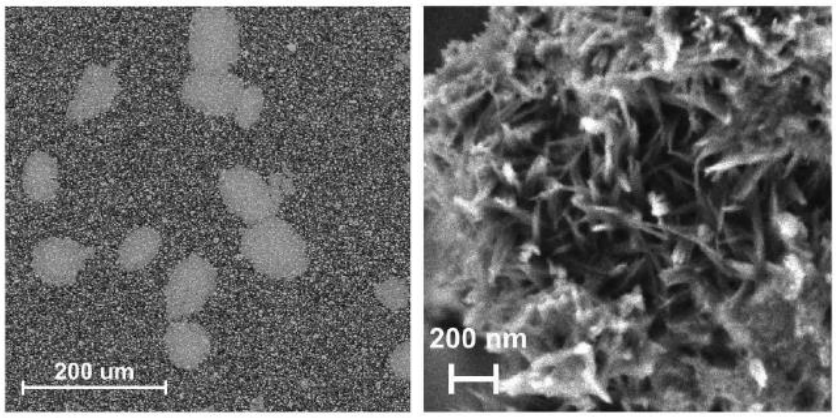

Figure 2.2.3. SEM images of C_3S pastes during the acceleration period, from [31].

SEM performed on the 28-days-old hydrated C_3S clearly showed that the seeding provided a more uniform microstructure with a better distribution of C-S-H and lower porosity [34]. It means that a more homogeneous growth of hydrates impacts positively the microstructure by decreasing the capillary porosity. It can be therefore expected that this will be resulting in better durability properties at equivalent mechanical strengths [18].

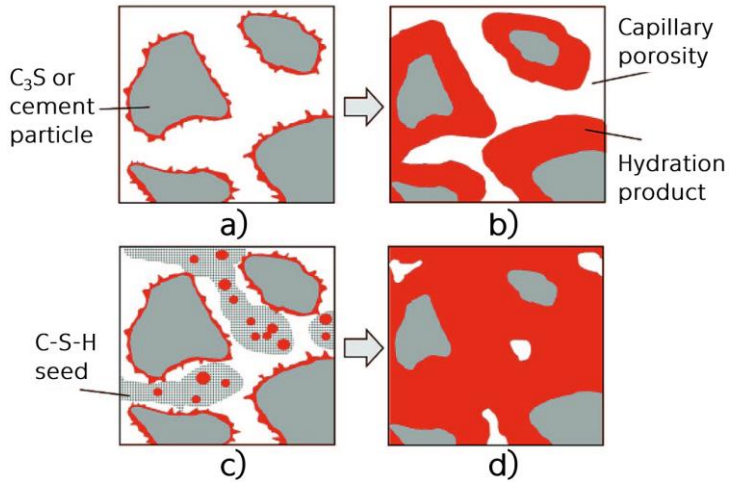

Figure 2.2.4. Schematic illustration of hydration process; from [34].

In [35], the first occurrence of Portlandite in OPC was observed at 4 hours. At 8 hours, more Portlandite was formed and the platelets appeared to bridge between the cement grains. At later hydration ages, a complex network of connected Portlandite platelets was observed. Generally, it appears that the nucleation of Portlandite is favoured in the neighborhood of gypsum grains.

Deceleration period

The acceleration period is followed by a strong decrease of the hydration rate. It is widely considered that at later ages the rate of hydration is controlled by a diffusion process following this pattern [19, 36]. The higher the degree of hydration, the greater is the thickness of the hydrated layer and consequently the slower is the diffusion of water and ionic species though this layer. There are three main factors influencing this period [1]:

- Consumption of small particles, leaving only large particles to react;
- Lack of space, or possibly
- Lack of water.

The last factor is very important in practice, as the total volume of hydrates is slightly lower than the combined volume of the reacting cement mixed with water (by about 5% to 10%). The decrease in total volume is known as chemical or Le Chatelier shrinkage, and it is responsible for the formation of gas-filled porosity after setting. It also leads to a decrease in internal relative humidity causing the decrease of the hydration rate [1].

Higher hydration rates are observed for the cements with the smallest particles, as it can be clearly seen in Figure 2.2.5, where hydration heats of OPC with different surface area are summarized as a function of time [37].

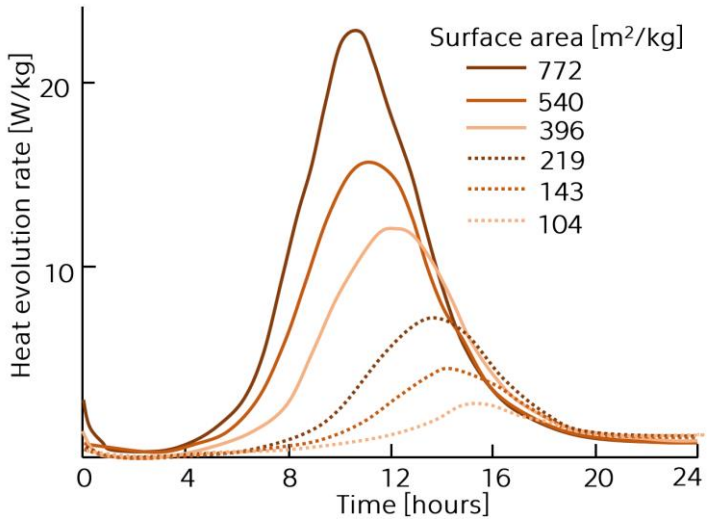

Figure 2.2.5. Effect of surface area on the hydration kinetics, from [37].

Since small particles are being consumed rapidly, the transition time from the acceleration period to the deceleration period occurs earlier for cements with finer particle sizes [19, 38]. Usually, the size of the initial particles of cements ranges from around 50 μm to 60 μm down to smaller than 1 μm. Particles smaller than about 3 μm are found to be completely consumed by about 10 h and particles below 7 μm by 24 h [8].

2.2.2. Belite hydration

It is generally known that C_2S is almost non-reactive compared to alite and it contributes significantly to strengths only after 28 days of hydration [39]. Its low reactivity can be attributed to the regular coordination of its calcium ions with oxygen atoms in the olivine type ($MgSiO_4$) orthorhombic structure, to the absence of holes of atomic dimensions, and to its supposed "through solution" mechanism. Its reactivity also varies with the type and concentrations of impurities [8, 40]. Belite hydration is accompanied with a low release of the hydration heat, which can be used advantageously in special concrete technologies [41, 42].

Along with C_3S, the hydration of β-C_2S produces C-S-H and Portlandite, although much lower amount of Portlandite is formed, which is reflected by the higher porosity of hydrated β-C_2S pastes in comparison to C_3S pastes with the same w/c ratio. The general pattern of reaction of β-C_2S with water follows a very similar trend as that of C_3S, which means that an initial rapid rate of heat evolution is followed by the induction period, accelerating period and a period of deceleration. The induction period lasts usually longer than that for C_3S with the onset of the acceleration period after 5–7 hours [8, 43].

2.2.3. Aluminate phase and ferrite

Generally, in Portland cements, the phase other than alite, that can most affect the hydration kinetics in the first days, is C_3A. The reaction of C_3A in the absence of calcium sulfate is very quick [1]. In comparison with alite, there is no period of slow reaction, and setting is almost instantaneous. It was reported that the firstly formed hydrates are poorly crystallized aluminum hydroxide or AFm phases, generally described as C_2AH_8 and C_4AH_{13} [5]. With time, these metastable phases will transform into a stable product (hydrogarnet) with a formula of C_3AH_6.

This temperature dependent reaction occurs within 25 minutes around room temperature. The rate of the transformation increases with temperature [44].

This fast setting behavior is not desirable in concrete, where a longer period of workability is required. For this reason, calcium sulfate is added to cements, allowing to control the reaction of the aluminate phase. In the presence of calcium sulfate, the pattern of reaction of C_3A is significantly modified. The initial period is characterized by a rapid reaction, after which the rate decreases rapidly within several minutes [45]. The main hydrate phase formed during the initial reaction is ettringite ($C_3A{\cdot}3CaSO_4{\cdot}32H_2O$). When the added calcium sulfate has all been consumed, the rate of reaction rapidly increases again, with a new main product phase – calcium monosulfoaluminate [1]. At sulfate/C_3A ratios normally used in Portland cements, the concentration of sulfate in the solution is exhausted at around 15–18 h and the reaction of C_3A speeds up [17]. In Portland cements, the formation of ettringite continues even after the consumption of sulfate in the solution. Calcium monosulfoaluminate ("monosulfo" or AFm) only forms later in a low broad peak, usually after 24 h. This may often not be well visible in calorimetry curves of OPC [17].

The C_3A phase is generally considered to be more reactive than the ferrite phases. Nevertheless, results presented in [46] indicate that up to 50% of the ferrite phase may react during the first day of hydration. An extensive study of the reactions of the ferrite phase was recently done by Dilnesa et al. [47, 48].

2.2.4. Interaction between silicates and aluminates

For a better understanding of all the mechanisms leading to the development of the main hydration products, it is essential to study besides the pure phases also the interaction between each other. It is important because it could lead to other reactions or kinetics modifications in comparison with those appearing in pure phase systems [18]. Thus, it is crucial to keep silicates, aluminates, and sulfates well balanced [1]. When Portland cement is properly sulfated, it is possible to observe the second aluminate peak in the calorimetry results after the main alite hydration peak occurs (after 10 hours) [1]. The existence of this second sharp peak was discussed already in 1946 by Lerch [49] and later by Tenoutasse [50]. Isothermal calorimetric curves obtained by Tenoutasse are

shown in Figure 2.2.6. In this system, in the absence of sulfates, the aluminate hydration largely suppresses the silicate hydration. It can be seen, that when gypsum is added, the extent of C_3S hydration also increases. The addition of gypsum also causes a delay of the sulfate depletion point. It is interesting that at certain amounts of sulfate (in this case around 4%), there is an inversion of both peaks leading to a movement of the sulfate depletion point right after the main silicate peak [50].

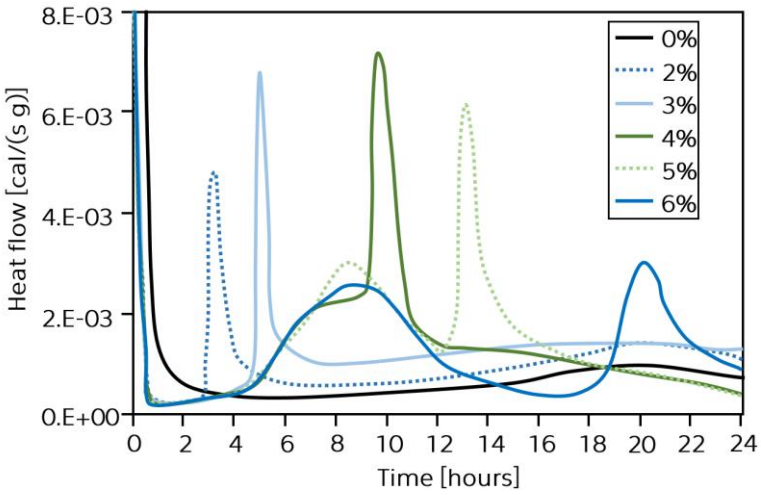

Figure 2.2.6. Isothermal calorimetry of a mixtures of 80% alite and 20% of C_3A in a presence of different amounts of gypsum [50].

The addition of a higher amount of sulfates further leads to certain delays of the sulfate depletion point. However, it does not influence the silicate peak [18]. It was reported that with 2.4% sulfate addition, the sharp peak corresponding to the C_3A reaction leads to the formation of calcium monosulfoaluminate. At higher addition rates (3.5%), the AFm phase was not detected within first 50 hours. From observations done by Bullard et al. [1], it seems that finer cements tend to have higher optimum sulfate requirements.

Figure 2.2.7 illustrates the main hydration products formed during the first hours of hydration of OPC. The large and sharp calorimetry peak corresponding to the AFm phase formation in the cement with 2.4% sulfate addition is often confused with a shoulder peak seen after the main silicate peak. The main aluminate hydration product at this time still seems to be ettringite, possibly formed from sulfate previously absorbed in the C-S-H phase [1, 51]. The

subsequent low broad peak which can be seen between about 20 h and 30 h, is related to the formation of the AFm phase [1].

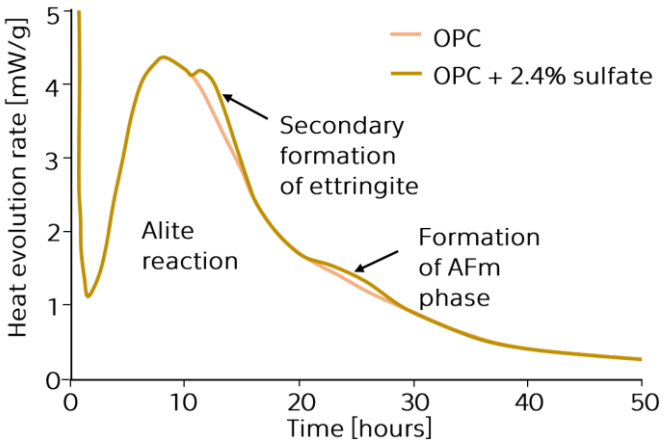

Figure 2.2.7. Calorimetry curves of OPC and OPC with 2.4% of sulfate addition [1].

These reactions between the alite and aluminate phases during hydration are too complex. And thus, there is a need for simulation tools that could deal with the interactions among phases through the ions in the pore solution and the occupation of space by the hydrated phases [1].

2.3. After the first 24 hours of hydration

Most of the reviews dealing with the hydration mechanisms are focused mainly on the early hydration processes (up to first 24 hours). Therefore, deeper knowledge of the mechanisms controlling the hydration kinetics beyond one day has been missing [46]. Especially, the period between 1–28 days is of great practical importance, as about 75% of the designed strength may be developed during this time interval [17]. The later kinetics of hydration was studied for example in [52] by means of proton nuclear magnetic resonance spectroscopy (^{1}H NMR). The state of water was analyzed. The evolution of different states of water in a white cement paste is shown in Figure 2.3.1, where the water in capillary pores, water in gel pores, water in C-S-H interlayer and water in crystalline hydrates (Portlandite and ettringite) can be seen [17, 52]. The amount of water in the crystalline hydrates, in the C-S-H interlayer and in the C-S-H gel pore proportionally increased up to about 2–3 days. Around the same time interval, the amount of water in gel pores was not increasing anymore, despite

the fact that the water in the C-S-H interlayer and crystalline hydrates still kept increasing [52].

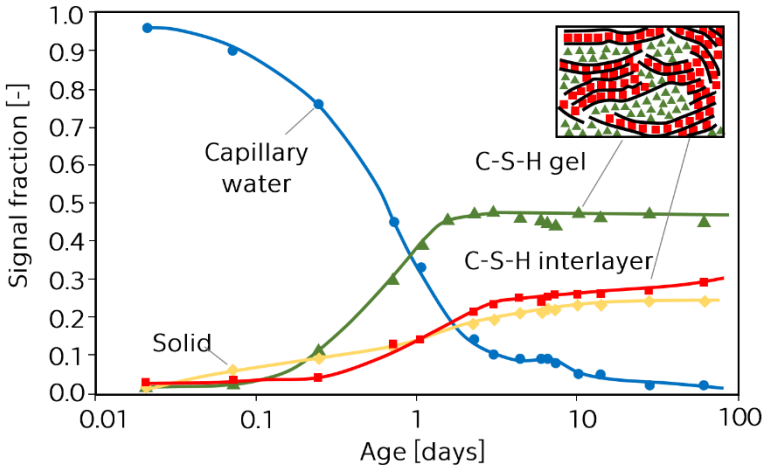

Figure 2.3.1. Evolution of states of water in cement paste with w/c of 0.4 [52].

The size of the capillary pores, still containing water, stabilized at a width of about 8 nm. These results were in a good accordance with mercury intrusion porosimetry, where it was observed, that the pore size did not decrease further in time up to 28 days, even though the total amount of pores intruded continued to decrease [53]. Muller et al. [52] described these pores, which are probably associated with the spaces between the C-S-H "needles", as "interhydrate". Between 6 and 28 days, the hydration processes continued with the formation of the C-S-H, but no more in gel porosity forms. This was documented with increasing the average values of density of the bulk C-S-H from 1.7–1.8 g/cm^3 (24 hours) to about 2.1 g/cm^3 after approaching full hydration [17].

The lack of long-term data about hydration processes that could be generalized is caused partially by the difficulties in carrying out long term measurements as some methods require more time to proceed and they are not precise enough. Another difficulties are related to the particle size of cement grains which reacts with different intensities [17], different compositions of local sources for cement productions, or for example to the age and storage of used cements. In terms of limitations of certain methods; calorimetry curves can be obtained continuously and with high precision up to about 28 days, as the rate of heat evolution is so low that significant errors can arise in the cumulative heat evolution data due to small fluctuations in the base line, etc. Nowadays, only speculations can be done on the mechanisms operating at the long time [17].

2.4. Properties of the main hydration products

This section summarizes selected properties and additional information about four main solid phases, which are formed as a result of hydration processes of OPC. These phases include calcium silicate hydrates, calcium hydroxide, calcium sulfoaluminates and unhydrated clinker grains.

2.4.1. Calcium silicate hydrates

This phase is abbreviated and more known as C-S-H, or C-S-H gels in older literature. It makes up 50–60% of the solid volume in a completely hydrated hardened cement paste. Therefore, it is the most important phase and it is responsible for the main properties of the cement paste. However, it is not well defined, as the Ca/Si ratio varies between 1.5 and 2.0 and its structural water content varies even more significantly. The morphology of the C-S-H is usually poorly crystalline, however, a reticular network can be created. Since the C-S-H tends to cluster, it is therefore possible to determine C-S-H crystals mainly by electron microscopy [54]. The C-S-H has atomic structure close to the ones of tobermorite and/or jennite; two crystalline phases with a lower calcium-to-silicon ratio than the C-S-H [55, 56].

2.4.2. Calcium hydroxide

It is more known as Portlandite. Its crystals constitute about 20–25% of the solid volume in the hydrated cement paste. Contrary to the C-S-H phase, Portlandite has a well-defined stoichiometry, $Ca(OH)_2$. It usually forms large crystals with a distinctive hexagonal-prism morphology. The morphology of Portlandite varies from nondescript to stacks of large plates, and it is greatly affected by the available space, temperature of hydration, and impurities present in the cement paste [54]. In comparison with the C-S-H, the formation of Portlandite has received a relatively little attention. It plays an important role in buffering the pH of the pore solution, and therefore, its presence helps to protect steel reinforcement from corrosion. However, it seems to be more prone to leaching [35]. Glasser [57] identified two types of Portlandite in Portland cements: physically discrete crystallites and labile particles initially present in the C-S-H phase with a high Ca/Si ratio. The second type of Portlandite is responsible

for its capability to donate calcium. The strength-contributing potential of Portlandite is limited due to van der Waals forces. The presence of a higher amount of Portlandite in hydrated cement pastes is not desirable, because it has a negative effect on chemical durability to acidic solutions, which is caused by the higher solubility of Portlandite compared to the C-S-H [54].

2.4.3. Calcium sulfoaluminates

About 15–20% of the solid volume of hydrated cement pastes consists of calcium sulfoaluminates. These compounds have a minor impact on the structure-properties relationships. Ettringite is one of the main products from this group of hydrates. It forms needle-shaped prismatic crystals. SEM pictures of ettringite formed at early hydration processes are shown in Figure 2.4.1. In OPC, ettringite eventually transforms to the monosulfate hydrate, which forms hexagonal-plate crystals. The presence of the monosulfate hydrate in Portland cements makes the concrete vulnerable to sulfate attack [54].

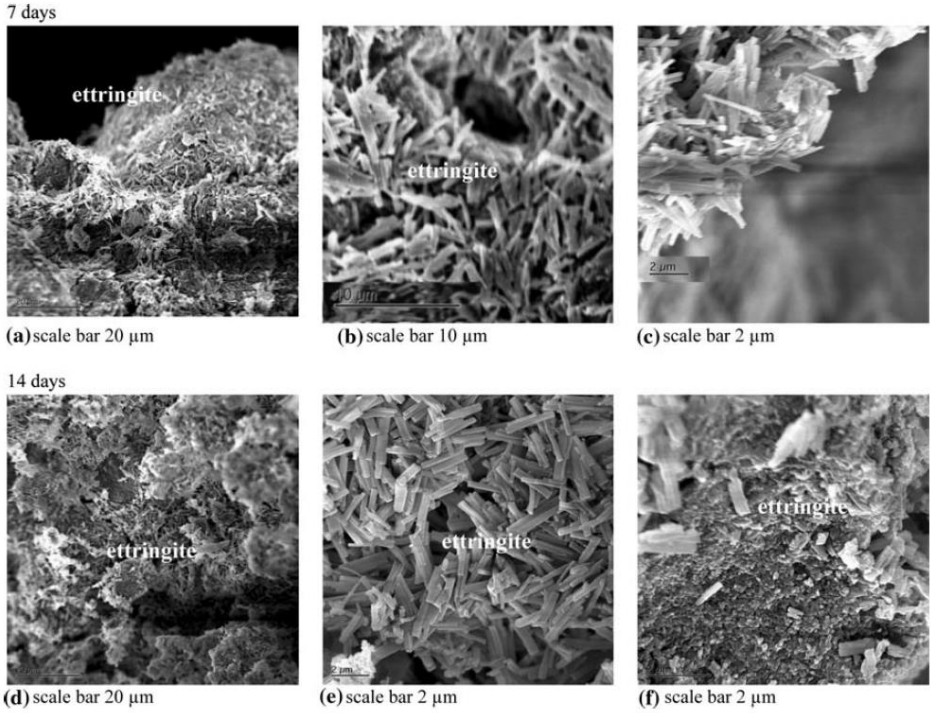

Figure 2.4.1. SEM pictures of ettringite formation from C_3A with gypsum and water at 7 and 14 days, water-to-cement ratio of 0.6 [58].

Ettringite and monosulfate hydrates contain small quantities of iron oxide, which can be substituted with aluminum oxide in the crystal structures [54].

Sometimes, a delayed ettringite formation can appear as a result of high curing temperatures (above 70–80 °C) applied on the fresh concrete, preventing the normal formation of ettringite. Higher curing temperatures can also lead to instability of ettringite [59]. When the cement paste is heated and subsequently stored at room temperature, the sulfate adsorbed on the surface of C-S-H is progressively released and reacts with monosulfate in the exterior product C-S-H to recreate ettringite. This can lead to the expansion and cause cracking of hardened concrete [59, 60].

2.4.4. Unhydrated cement grains

Some unhydrated cement grains (Figure 2.4.2) can be found in the structure of hardened cement paste. The amount of these grains depends on the particle size distribution of the anhydrous cement and the degree of hydration. These grains can appear even long after the hydration processes are finished [54].

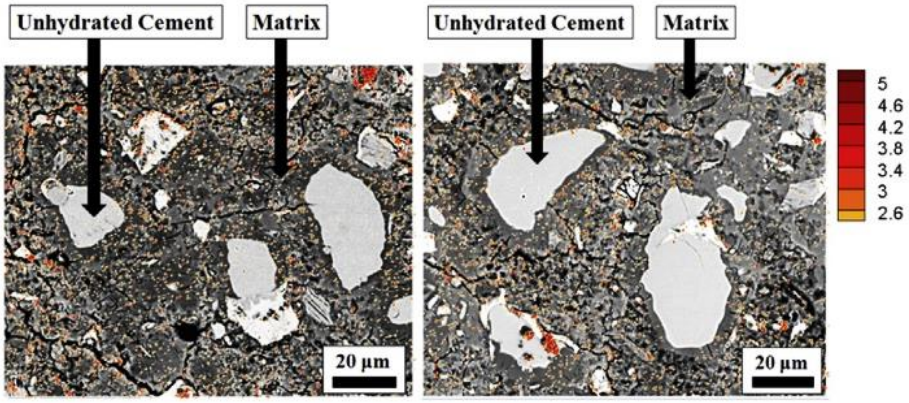

Figure 2.4.2. Unhydrated clinker grains detected by SEM method [61].

The presence of unhydrated clinker grains can lead to undesirable variations in results of mechanical properties, as these particles are not – or barely – taking part in the hardening process and do not contribute to the strength [62].

2.5. Factors influencing properties of hardened cement pastes

This section summarizes the literature review on the most often reported factors influencing properties of fresh and hardened cement pastes, such as water-to-cement ratio and curing temperature. The effect of each parameter on selected properties of mainly hardened cement pastes is discussed.

2.5.1. Water-to-cement ratio

The water content plays an essential role in hydration processes at early age of cement pastes. It can modify the final properties of hardened pastes as well. Therefore, the literature review on the main parameters, which are influenced by the water-to-cement ratio are discussed below.

Hydration heat and microstructure evolution

In early stages of hydration, a higher water content in cement mixtures leads to an extension of the duration of the induction period. Bazzoni [31] reported, that different nucleation rates of C-S-H are being formed in cement pastes with different w/c, as demonstrated in Figure 2.5.1.

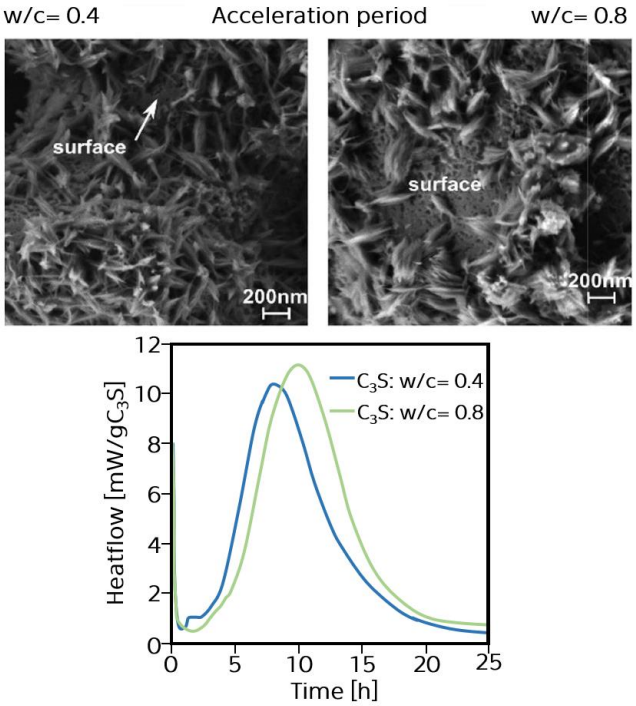

Figure 2.5.1. SEM photographs of surface of C_3S pastes with w/c 0.4 and 0.8 during the acceleration period and calorimetry. Adapted from [31].

Larger C-S-H clumps are created on the surface of C_3S in the more diluted system (w/c=0.8). However, these clumps are more homogeneously distributed on the surface of the less diluted system with the water-to-cement ratio of 0.4. As hydration processes continue, an increase of w/c ratio has an effect to increase the space between particles. According to Bishnoi's and Scrivener's hypothesis [63], the growth of the C-S-H seems not to be limited by a lack of

space. Thus, it is expected that its outward grow would be faster. Later during the acceleration period, the surface of the paste with a higher w/c ratio is less covered by hydrates and there are deeper pits on the surface of the grain (Figure 2.5.1). C-S-H needles seem to be more agglomerated compared to the paste with a lower w/c [31].

Tydlitát et al. [64, 65] also studied the effect of w/c ratio on the early-stage hydration heat development in cement-based composites. It was found that specific hydration heat of the studied cement pastes varied only little with changing w/c, while in the case of mortars, it increased about 3–5% with increasing w/c.

Degree of hydration

The degree of hydration is defined as the fraction of Portland clinker that has fully reacted with water relative to the total amount of cement in the sample. Sometimes it can be associated to the amount of chemically bound water (CBW) [66]. Therefore, the w/c ratio has a significant impact also on this parameter. During the first hours of hydration, the CBW can reach 23% for cement pastes with the w/c of 0.4, and about 29% for the w/c of 0.8 [31]. The degree of hydration in later stages was studied by Cook and Hover [67]. They consistently reported that the degree of hydration increased with an increasing w/c, as it can be clearly seen in Figure 2.5.2.

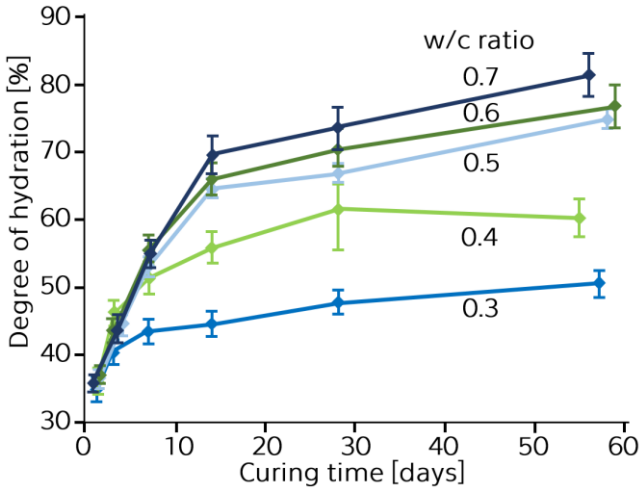

Figure 2.5.2. Dependency of degree of hydration on w/c. Adapted from [67].

As expected, the degree of hydration increases not only with w/c, but also with time. All studied pastes examined by Cook and Hover achieved approximately

35% of hydration after first 24 h of seal curing. After 56 days, hydration ranged from about 51% for the 0.3 w/c paste to about 82% for the 0.7 w/c paste [67].

Porosity

The structure of most building materials is porous. Therefore, the pore structure is a very essential microstructural characteristic because it influences the physical and mechanical properties, and controls the durability of materials [68]. However, it is challenging to estimate a typical pore size distribution of hardened cement pastes, as it encompasses a large range. The larger pores, which are in a range from 10 μm to 10 nm, are called as capillary pores. These pores represent the residual unfilled spaces between cement grains. The finest pores, which can be found in a range from approximately 10 nm to 0.5 nm, are called gel pores since they constitute the internal porosity of the C-S-H phase. The sizes of capillary and gel pores can overlap, and the spectrum of pore sizes in a cement paste is continuous. Structural pores with dimensions of 0.5 nm or smaller are formed by the interlayer spaces of C-S-H gel. These are not true pores because water present in these features is not in the liquid state [69].

As hydration processes proceed, the hydration products grow into the pore space of a hardened cement paste. It means, that with increasing time and decreasing the w/c ratio, the porosity decreases [67, 70], as demonstrated in Figure 2.5.3.

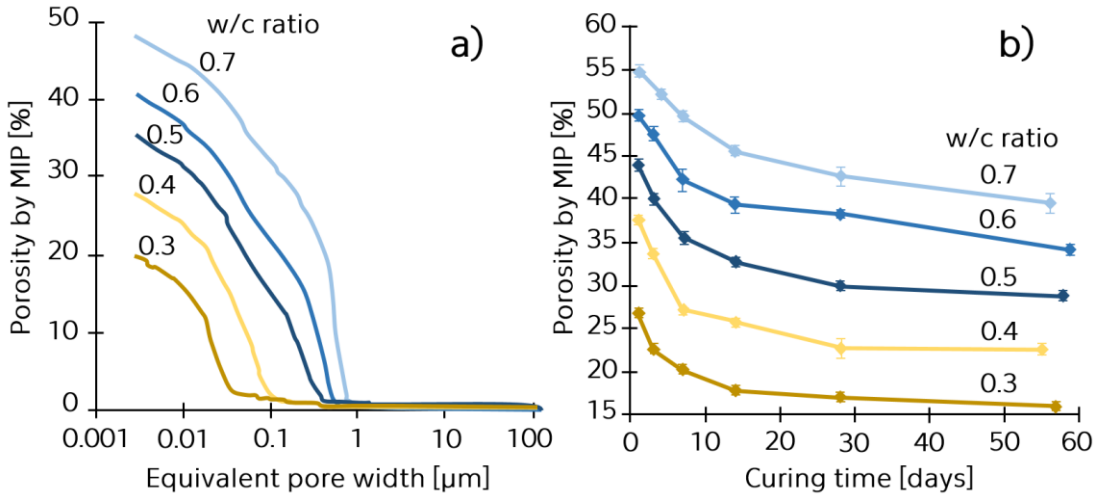

Figure 2.5.3. (a) Effect of w/c ratio on pore size distribution for cement pastes cured for 7 days. (b) Effect of w/c and curing time on total porosity [67].

The initial values of porosity were reported as about 55% after the first day of hydration, for cement pastes with w/c of 0.7. This value decreased to 40% (after 56 days). Porosity at cement pastes with a lower w/c of 0.3 was significantly lower after the first day of hydration (about 27%). This value decreased to almost 15% after 56 days [67].

It was proved by Powers [71, 72] already in early 50s that higher porosity of the system causes a decrease of compressive strength. Therefore, concrete composites with low porosity should be designed to achieve composites of the highest strength.

Mechanical properties

The effect of w/c ratio on mechanical properties was studied for example in [73]. Figure 2.5.4a shows a linear dependence of compressive strength on bulk weight (bulk density in modern literature) and bound water content in hardened cement pastes.

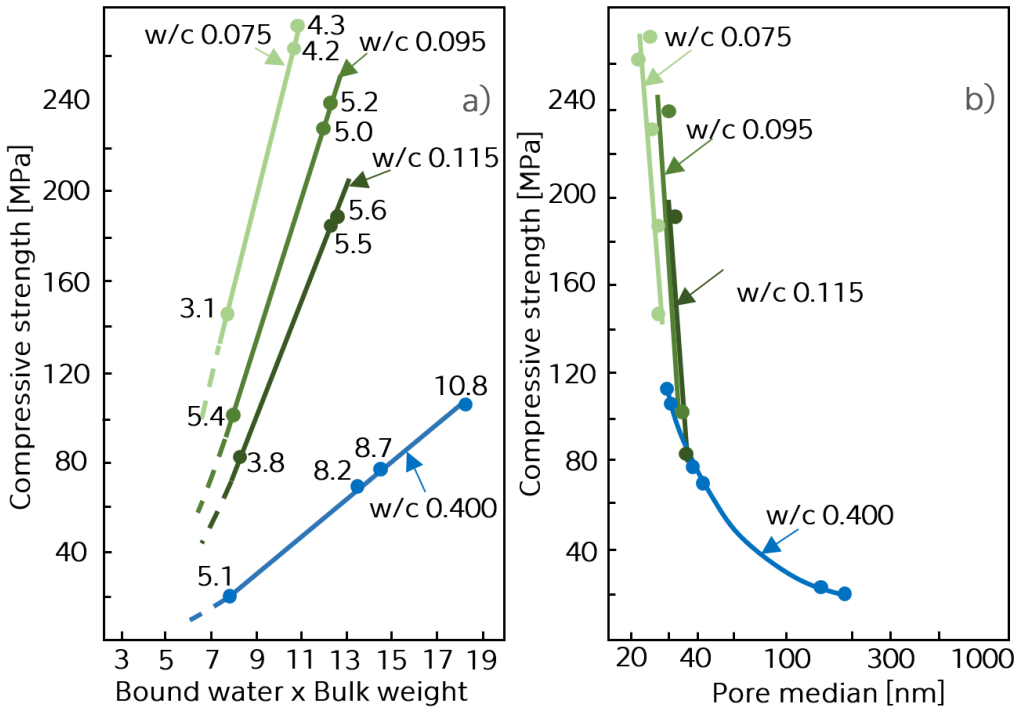

Figure 2.5.4. Relationship between (a) compressive strength and bound water and bulk weight and (b) pore median and compressive strength [73].

It confirms an increase of compressive strength of cement pastes with a decreasing w/c ratio. It was observed that the amount of hydration products was

also lower. This can be explained as a consequence of two factors conducting the effects of w/c ratios decrease:

- Lower amount of hydration products for the filling of the pore space of cement pates is necessary.
- Principal changes of pore structure and matrix occurring with the decrease of w/c ratios.

The relationship between pore median and compressive strength is demonstrated in Figure 2.5.4b, where a significant difference of the character of the pore structure of the studied pastes with various w/c ratios can be seen. Whereas, the pastes with w/c ratio of 0.4 showed a parabolic dependence of the compressive strength on the pore median values, pastes with lower w/c ratios exhibited a linear dependency [73].

2.5.2. Curing temperature

Hydration processes of cement can be easily influenced by temperature, especially during curing at early age of concrete. Generally, higher temperatures lead to initially fast hydration and high early compressive strength [74]. However, the strength of cement pastes hydrated at higher temperature is reduced in later ages compared to those hydrated at room temperature [75]. Higher temperature at the early stage of hydration causes a more rapid precipitation of hydration products during the first hours and days, which is responsible for the observed early strength development. Fast hydration processes lead to a more heterogeneous distribution of the hydration products as the hydrates precipitate around the clinker particles and create a dense inner shell around the clinker grains [74, 76]. Hydration starts slowly at lower temperatures, which allows the dissolved ions more time for diffusion before the hydrates precipitate. This leads to a less dense C-S-H, a more even distribution of hydration products and a lower coarse porosity [74, 76]. Different curing temperatures are not responsible only for changes in the morphology of the solid phases, but they also influence the composition of the liquid phase [74].

Lotenbach et al. [74] analyzed the progress of hydration of sulphate-resisting Portland cement pastes cured at different temperatures by thermal analysis (Figure 2.5.5).

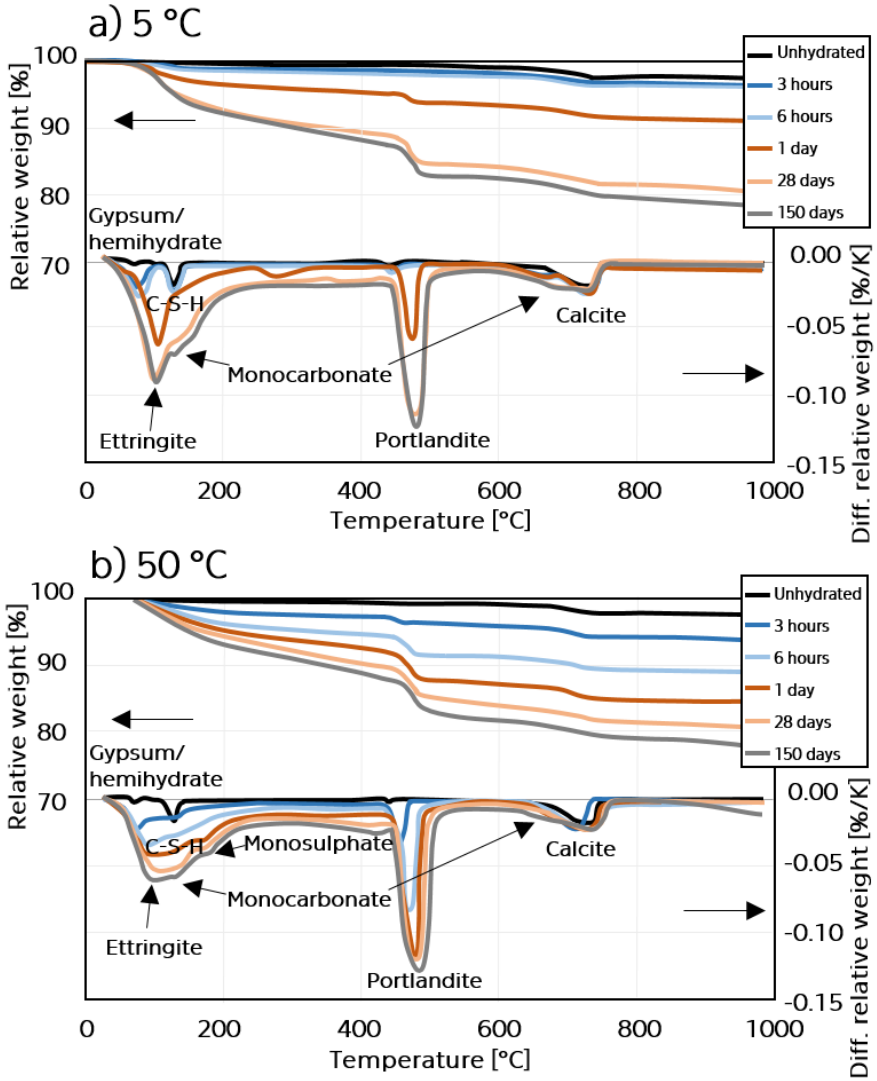

Figure 2.5.5. Thermogravimetric curves and their derivation of sulphate-resisting Portland cement pastes at a) 5 °C and b) 50 °C; from [74].

It can be seen, temperature of 50 °C, kept for three hours, caused the faster precipitation of Portlandite and the C-S-H. At lower temperature of 5 °C, the dissolution of clinkers was relatively slow. The 28 and 91-day compressive strength of the investigated Portland cement mortar and concrete samples with limestone was reduced at curing temperature of 40 °C, while the observed degree of hydration was similar for both temperatures [74].

2.6. Pozzolana active materials

Sometimes it is beneficial to replace cement binder with materials, which can improve the final properties of concrete. The group of these mineral admixtures is called pozzolana active materials. The term pozzolana can be understood in two different ways: The first one has a historical background and refers to the pyroclastic rocks, mainly glassy and sometimes zeolitized, which can be found either in the neighborhood of Pozzuoli or around Rome. The second way how to understand pozzolana active materials, includes all those inorganic materials, either natural or artificial, which harden in water after mixing with calcium hydroxide (lime) or with materials that can release calcium hydroxide (Portland cements) [77]. A more detailed definition describes a pozzolan as a siliceous and aluminous material, which in itself possesses little or no cementitious property but which will, in finely divided form and in the presence of moisture, chemically react with calcium hydroxide at ordinary temperature to form compounds possessing cementing properties. These materials consist mainly of CaO, SiO_2, and Al_2O_3 in different proportional ratios (Figure 2.6.1) [78].

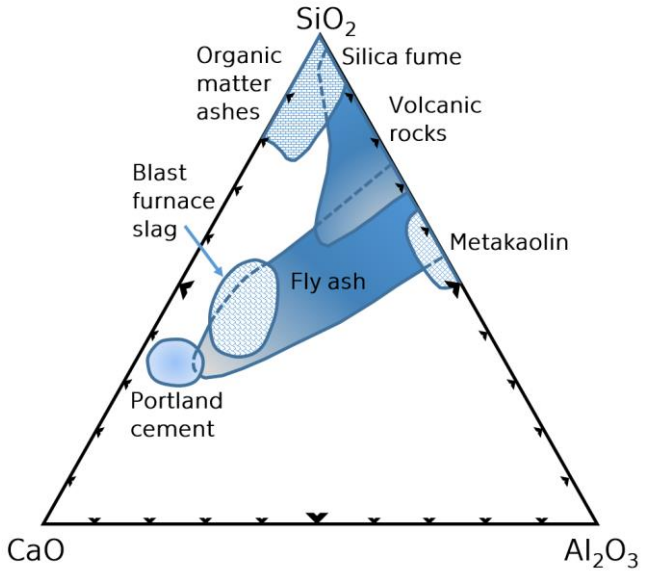

Figure 2.6.1. Ternary CaO-SiO_2-Al_2O_3 diagram (wt.% based) showing the chemical composition of pozzolana active materials. Adapted from [79].

The addition of pozzolanic and cementitious-like materials to the cement and concrete composites has been very popular during the past fifty years. It is due to many benefits derived from the use of mineral admixtures: functional or

engineering benefits, such as improvement in workability, reduction in the heat of hydration, low permeability, high ultimate strength, and control of alkali–silica expansion. Incorporation of pozzolans into structure of concrete also results in economic and ecological advantages [78, 80]. However, as these materials have various properties, it is important to find their appropriate dosage [80].

In this section, the pozzolana active materials, which are the most widely used for concrete production are summarized with their effects on hydration of cement. For a better clarity, they are divided based on their origin into natural and artificially produced pozzolans.

2.6.1. Natural pozzolans

Natural pozzolans have been used for thousands of years, as their utilization can be found in many of the Roman, Greek, Indian or Egyptian cultures. The term "pozzolan" comes from a volcanic ash mixed at Pozzuoli, a village in Italy, following the 79 AD eruption of Mount Vesuvius. Natural pozzolans are sourced from natural mineral and volcanic deposits. They are very reactive since they consist mainly of amorphous silica. The most common natural pozzolans used as a partial substitute for cement in concrete applications today include besides volcanic ash also volcanic glass (pumice and obsidian), zeolites, rice husk ash, calcined clay, calcined shale and metakaolin [78]. Some of these materials, such as volcanic ash, can exhibit pozzolanic behavior in their raw form without calcination or extensive processing. The calcination involves applying significant heat into the material's structure, which causes reactions transforming the material into a pozzolan [81].

Volcanic ash

It is a product of volcanic eruptions. New sources of volcanic materials are being produced steadily. Recently the eruption of volcanoes in Hawaii emitted large quantities of such materials. Of course, these volcanic eruptions are very dangerous catastrophes but they leave very useful materials after the disaster. Volcanic ash is usually finer compared to cement [80]. Similarly to other pozzolana active materials, volcanic ash influences mechanical properties, as with an increase of its content, the strength decreases [82]. This strength increases in time, which was confirmed also at later age at 91 days [80]. From the

reported results, it is recommended to use not more than 20% volcanic ash as a cement replacement to achieve sufficient mechanical properties [83]. It has been also reported that concrete containing volcanic ash exhibits enhanced durability in terms of carbonation rate [84]. The long-term durability of volcanic ash-based geopolymer mortars studied up 180 days recently in [85] also showed promising results under wetting and drying cycles, and a good acid resistance.

Natural zeolites

Zeolites are natural, hydrated aluminosilicates of alkali and alkaline earth cations with a three-dimensional frame structure. They belong to volcanic or volcano-sediment materials. The shape of their crystals exhibits a honeycomb like structure, with very small pores connected with a system of channels. The size of pores varies between 3×10^{-4} and 4×10^{-4} μm. From more than 50 natural and 150 synthetic zeolite minerals, which have been discovered [86], clinoptilolite is one of the most utilized types (Figure 2.6.2).

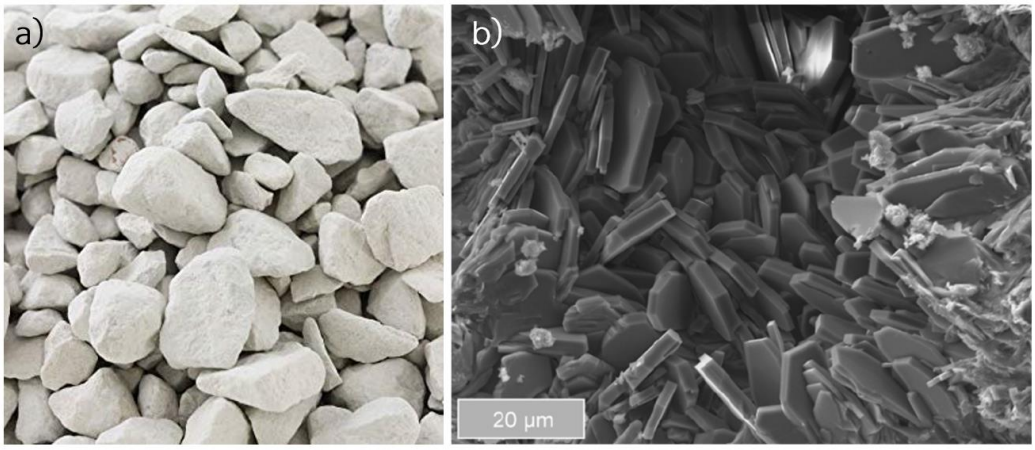

Figure 2.6.2. Photographs of clinoptilolite. Adapted from [79].

The main advantages of zeolites lie in their regular structure, large inner specific surface area (approximately between 600–800 m^2/g), uniform size pores, and good thermal stability. These materials are also very cheap [87, 88]. Zeolites have properties of molecular sieves, they have high absorption capacity at low pressures and low relationship with temperature in the interval of 10–150 °C [89]. Zeolites, as environmentally clean, inert and non-toxic materials, can be successfully utilized in many fields [88]. Especially in China, zeolites are widely used as a partial replacement of cement. Based on [90, 91], it has been reported,

that the total quantity of 30 million tons per year of zeolite is consumed for concrete production. Zeolites can improve final properties of concrete, such as strength, however, it has been reported that zeolite promote the formation of side products (alkali and other complex compounds) [88]. The addition up to 15% of zeolite in concrete can improve the early compressive strength [88, 92, 93]. Ahmadi and Shekarchi [86] reported that based on the thermogravimetric analysis (TGA), although natural zeolite showed lower pozzolanic reactivity than for example silica fume, this pozzolanic active material revealed a high rate of consumption of lime and almost fixed the total produced amount of $Ca(OH)_2$ in cement pastes after 28 days of curing. Generally, the durability properties of concrete can be improved by the addition of natural zeolite. In [93], the most effective application of natural zeolite was observed in the chloride ion penetration, corrosion rate, drying shrinkage and water penetration. Nevertheless, a satisfactory performance was not achieved in acid environment.

Metakaolin

Metakaolin is an anhydrous calcined form of the clay mineral kaolinite (Figure 2.6.3). It is processed from high-purity kaolin clay by the calcination at moderate temperatures between 650 °C and 800 °C. Its utilization as a pozzolanic addition for mortar and concrete production has been widely studied in recent years [94]. The main reasons for the use of such a clay-based pozzolans in mortar and concrete are their availability and the durability enhancement when added into concrete mixtures [95]. Additionally, depending on the calcining temperature and type of clay, strength can be also improved, particularly during the early stages of curing [94]. This enhancement can be observed when the amount of cement replacement is about 5–10% [96, 97]. Synergic effects of metakaolin blended with fly ash were studied recently in [98]. From the results it was clearly seen that the combination of these materials strongly influenced the phase composition, microstructure and long-term behavior of blended pastes. A metakaolin/fly ash ratio of 10:10 led to the highest long-term strength obtained after 91 days of hydration compared to the control concrete. This study showed the potential of combination of fly ash and metakaolin as a low-cost local supplement material for high strength and durable concrete. The synergic effect of metakaolin on a gypsum–lime–metakaolin–water system was also observed

in [99], where a significant improvement of mechanical properties compared to the reference gypsum–lime paste was reported.

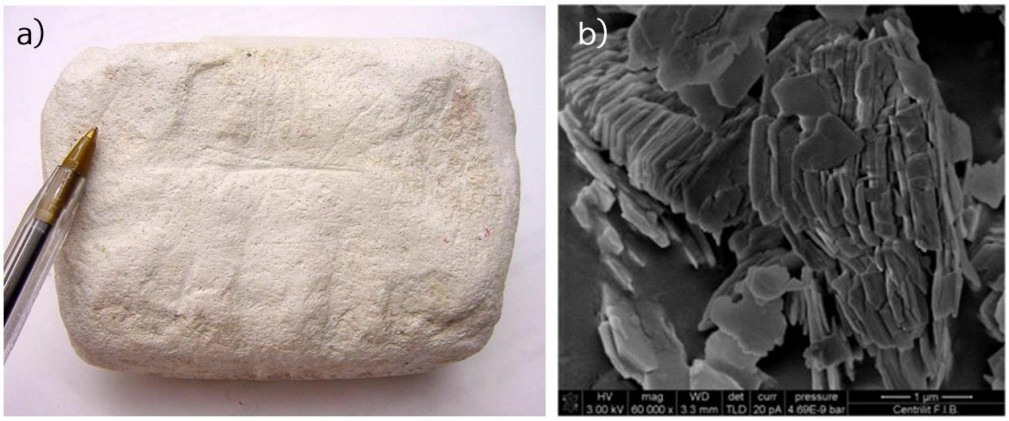

Figure 2.6.3. Photographs of kaolinite (a) before its thermal transformation into metakaolin (b). Adapted from [100, 101].

A similar system was studied in [102], where it was observed that pozzolanic reaction finished already after 8 days of hydration as the Portlandite content was missing in the studied mixtures.

Rice husk ash

This pozzolan is an agricultural waste obtained from the outer covering of rice grains during milling process. It constitutes 20% of the 500 million tons of paddy produced in the world [103, 104]. When this waste is burnt between 550 and 700 °C, the silica content of the created ash transforms into amorphous phase, which activates pozzolanic properties of this material [105]. Reactivity of rice husk ash is then given by its specific surface area [106]. It provides a positive effect on the compressive strength of concretes at early ages [107]. It was reported that the replacement with 30% of rice hush ash leads to a substantial improvement in the permeability properties of blended concrete when compared to OPC [104].

2.6.2. Synthetic pozzolans

By-products, such as fly ash, blast-furnace slag, silica fume or waste from ceramic industry are industrially prepared pozzolans. Also, these materials are mainly siliceous and aluminous and they are produced during various thermal treatments. As these materials are not especially eco-friendly and are generated

in large quantities, there is an increasing interest for their effective utilization. Their incorporation into blended cements has been widely studied in various countries, providing encouraging results regarding the mechanical and durability properties of concrete [108]. The most frequently used synthetic pozzolans in the concrete industry are introduced in this chapter.

Fly ash

It is defined as a by-product of coal-fired electric power stations. It is also known as "pulverized fuel ash". It is composed of the particulates (fine particles of burned fuel), which are driven out of coal-fired boilers together with the flue gases. Fly ash particles are typically spherical, as it can be seen in Figure 2.6.4. It is well-known that its composition is not constant, which is restrictive for its wider utilization. It can be used as a partial cement replacement to improve the durability of concrete [109, 110].

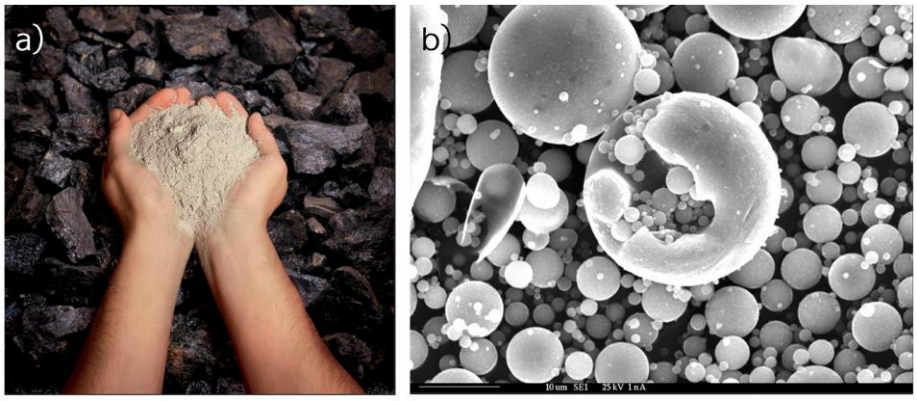

Figure 2.6.4. Photographs of fly ash. Adapted from [111].

It also contributes to concrete strength by pozzolanic and filler effects. Fly ash has been increasingly used in concrete production during last decades. In some cases, a large amount of fly ash (higher than 40%) can be used to achieve desired concrete properties, and thus, to decrease the cost of concrete production [109, 110]. Fly ash exhibits low initial activity, which can be significantly improved by addition of nano-SiO_2. This also leads to an increase of both short-term strength and long-term strength [109]. Similarly, to other pozzolana active materials, the addition of fly ash causes a decrease of strength at early ages. However, after 90 days of hydration, the strength becomes higher compared to the control materials. This significant improvement is given by the higher active silica

content in fly ashes in comparison with cement. In terms of chloride penetration, concrete with fly ash exhibits lower chloride permeability [112]. Recently, it has been reported that fly ash can enhance mechanical properties during accelerated carbonation processes [113].

Blast furnace slag

It is a by-product from the manufacture of pig iron in the blast furnace. It is formed by the combination of earthy constituents of iron ore with limestone flux. When the freshly produced slag is cooled with water, it forms into a fine, granular, almost completely non-crystalline, glassy form, known as granulated slag, having latent hydraulic properties [114]. Similarly, to fly ash, the addition of blast furnace slag can result in a significant decrease in chloride ion diffusion coefficient because it can improve the distribution of pore size and pore shape of concrete. Another reason is, that a higher amount of the C-S-H phase may be formed, which leads to more efficient adsorption of more chloride ions and it blocks diffusing paths [115]. The incorporation of 15% blast furnace slag provides 37.5% reduction in drying shrinkage values compared to concrete without any supplementary cementitious materials [116]. Based on [117], the addition up to 50% slag as a cementitious material is considered suitable in terms of mechanical properties, rates of carbonation and permeability.

Ceramic powder

Another widely utilized by-product is ceramic powder. It is usually obtained during the final cut of bricks, roof tiles, electrical insulators or sanitary ware. Waste ceramic materials are very cheap but almost an equivalent alternative to metakaolin as supplementary material in concrete production. Ceramic powder has been used more frequently as a part of fine aggregates [118, 119]. The bulk density of concrete can be decreased with the addition of fine ground ceramics in its structure. Nevertheless, a higher content of ceramic powder in concrete also leads to an increase of porosity causing a decrease of strength. Therefore, the replacement of 20% of cement by fine ceramic powder was reported to provide satisfactory results in terms of physical, mechanical and water transport properties [118].

Silica fume

During the last few decades, silica fume has become an enormously popular addition for concrete production. It is a by-product obtained from the reduction of high-purity quartz with coal in electric arc furnaces in the manufacture of ferro-silicon alloys and silicon metal. Silica fume is a very fine material, which occurs as near-perfect spheres at the average size of 20–500 nm (Figure 2.6.5). It is an excellent supplementary cementitious material with a good pozzolanic activity due to a high content of amorphous silica. Its advantage is that it has nearly no variation in chemical composition over time [79]. It is well-known that silica fume positively influences mechanical properties of concrete [120, 121]. It has been reported that the optimum 28-day split tensile strength can be obtained in the range of 5–10% silica fume replacement level [122]. The addition of nano-sized SiO_2 leads to a production of a thicker cement paste, and accelerates the cement hydration process [123].

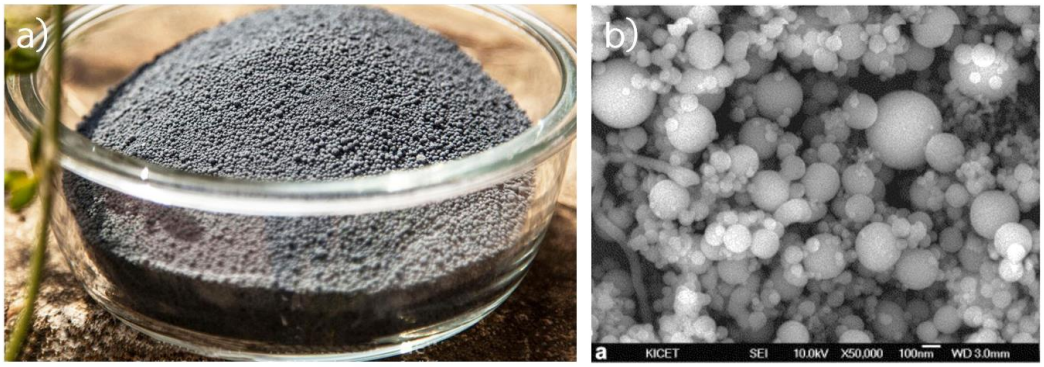

Figure 2.6.5. Photographs of typical silica fume particles, from [124, 125].

Silica fume is considered as a necessary ingredient for production of high performance concrete, as it improves either or both the strength and durability properties of the concrete [126]. Its fine particles are capable to fill empty space between aggregates and cement. Moreover, lower porosity and good permeability results are obtained because it reacts with and consume calcium hydroxides [127, 128]. In terms of durability, the addition of silica fume can improve acid resistance of concrete [129]. The 10% addition of silica fume could result in a chloride ion diffusivity more than 15 times less than that in a comparable concrete made without silica fume [130].

2.7. Summary

The OPC consists mainly of alite, belite, aluminate phases and ferrite. Alite is the most important phase, as it constitutes 50–70 % of OPC. During early hydration, it contributes to the strength development. Following the isothermal calorimetry results, the alite hydration can be divided into several periods. The first, initial period, is characterized by the initial dissolution of ions upon contact with water and it takes about 15 minutes. The period of slow reaction lasts usually for about 1–2 hours. During this period, the C-S-H phase starts growing [25, 26]. The end of the induction period could be correlated with the onset of crystallization of Portlandite. The following acceleration period is mainly related to the massive nucleation and growth of the C-S-H and Portlandite [19]. This period begins about 1–3 hours after mixing, depending on when the induction period finishes. Finally, the acceleration period is followed by a strong decrease of the hydration rate. It is widely considered that at later ages the rate of hydration is controlled by a diffusion process following this pattern [19, 36]. Belite represents about 15–30% of OPC clinkers. It contributes only little to the strength during the first 28 days. Nevertheless, after approximately one year, the strengths obtainable from pure alite and pure belite are about the same under comparable conditions [5]. Aluminate phase makes 5–10% of OPC and it reacts rapidly with water, and can cause undesirably rapid setting. To prevent this to happen, a set-controlling agent is added to cement [5]. Ferrite represents about 5–15% of OPC. Results presented in [46] indicate that up to 50% of the ferrite phase may react during the first day of hydration.

The mechanisms of hydration of cement are very complex, and therefore, they have been widely studied within the past centuries. Nevertheless, most of the reviews dealing with the hydration mechanisms are focused mainly on the early hydration processes (up to first 24 hours). Therefore, deeper knowledge of the mechanisms controlling the hydration kinetics beyond one day has been missing [46]. Especially, the period between 1–28 days is very important because about 75% of the designed strength may be developed during this time interval [17].

The main hydration products which are formed as results of the hydration processes are calcium silicate hydrates (C-S-H), calcium hydroxide (Portlandite) and calcium sulfoaluminates (ettringite, monosulfate hydrate). Some unhydrated cement grains. C-S-H represents 50–60% of the solid volume of cement paste, therefore, it is the most important hydration product, responsible for the main properties of the cement paste. The C-S-H has atomic structure close to the ones of tobermorite and/or jennite [55, 56]. Portlandite constitutes about 20–25% of the solid volume in the hydrated cement paste. It has a well-defined stoichiometry, $Ca(OH)_2$. It usually forms large crystals with a distinctive hexagonal-prism morphology. It plays an important role in buffering the pH of the pore solution, and therefore, its presence helps to protect steel reinforcement from corrosion. However, it seems to be more prone to leaching [35]. About 15–20% of the solid volume of hydrated cement pastes consists of calcium sulfoaluminates. These compounds have a minor impact on the structure-properties relationships.

Hydration processes can be easily modified with the w/c ratio or curing temperature. Higher w/c ratios lead to higher degrees of hydration. However, increasing w/c causes higher porosity of cement pastes, which is reflected by decreasing strength [71, 72]. Higher curing temperature speeds up hydration processes and cause higher initial strength [74]. However, the strength of cement pastes hydrated at higher temperature is reduced in later ages compared to those hydrated at room temperature [75].

Pozzolana active materials for concrete production have been very popular within the past decades. Their properties allow to partially replace cement. Therefore, the utilization of these materials can help to reduce the cement demand, as the cement production leads to a very high production of CO_2 emissions. Moreover, pozzolana active materials can improve the final properties of concrete. Volcanic ash, natural zeolites, metakaolin or for example rice husk ash belong to the most often utilized natural pozzolanic materials. Whereas fly ash, blast furnace slag, ceramic powder or silica fume represent the industrially prepared pozzolans. Especially, silica fume has become an enormously popular addition for concrete production. To obtain concretes of the best qualities, it is essential to find the appropriate dosage of these materials [80].

Chapter 3

Hydration stoppage techniques

This chapter summarizes general information about possible ways of hydration stoppage of cementitious systems, as generally, the hydration of cements is arrested before analysis. Especially, at early hydration times, it is necessary to stop hydration processes to avoid further hydration processes. At samples older than 28 days, the progress of hydration becomes to be slow, and therefore, stoppage procedures are used mainly to remove free pore solution. This is needed before some selected analyses, such as thermogravimetric analysis (TGA), infrared and Raman spectroscopy, or Mercury intrusion porosimetry (MIP). The hydration stoppage also helps to minimize carbonation processes if it is done properly [131]. Generally, the main aim of the stoppage techniques is to remove water present in the pores without removing the water from the hydration products. It is done to avoid alternation of the hydrates and to preserve the microstructure of studied materials. There are two major methods for arresting hydration and removing water: direct drying (removal of water by evaporation or sublimation) and solvent exchange [131].

3.1. Direct drying

In all direct drying techniques, such as oven drying, vacuum drying and freeze drying, water is removed by transforming into vapor. Free water is removed efficiently, which helps to avoid carbonation. On the other hand, generally, the structural water is also removed. This leads to ettringite and AFm phases decomposition [132, 133]. In the case, that the cement paste is kept at room temperature and atmospheric pressure, before the drying technique is applied, then the water inside of the sample is liquid. The interfacial tension from the boundary between the liquid and gas phase creates capillary suction, leading to microcracking and collapse of the subtle microstructure of the cement paste. Consequently, if the transition from the liquid to the gas phase cannot be avoided, the surface tension of the liquid should be minimized [132].

Oven drying

It belongs to one of the most widely used drying methods where temperature is usually maintained between 60 and 105 °C at constant atmospheric pressure (101 kPa). The drying procedure is completed when the sample reaches constant mass, which is typically less than 0.1% of mass change per day [132, 134]. It is necessary to remove CO_2 from the atmosphere to prevent carbonation, which can be done for example by putting solid NaOH with high surface area into the oven [132]. Although oven drying is very effective in term of evaporable water removal, this method has many disadvantages: oven drying at 105 °C for 24 h significantly damages the microstructure of material [135]. It has frequently been reported that the drying process partially destroys or alters the C-S-H structure, causing gas adsorption measurements to measure too low surface area even after adequate drying [135, 136]. Even temperature of 60 °C is unsuitable for preserving the fragile microstructure of hardened cement paste [137]. Moreover, when cementitious samples are dried for longer time period (7 days), the carbonation process is speeded, which was well documented for example by Collier et al. [138] on thermogravimetry (TG) results from 580 to 710 °C, associated with the release of CO_2 from calcite.

Dry ice drying

Dry ice drying or D-drying, was firstly mentioned by Powers [72], but it was proposed as a possible drying technique by Copeland and Hayes [139] a few years later. The apparatus consists of a vacuum desiccator connected to the side arm of a trap by a large bore glass tubing. The trap is cooled by a mixture of solid CO_2 and alcohol at temperature of – 79 °C. The partial pressure of water vapor over dry ice is 0.07 Pa [135]. For sufficient drying, the pressure in the system should be kept below 4 Pa. The removal of pore solution is very slow under these conditions, and it takes approximately 14 days for millimeter-sized samples [135], which also implies that D-drying cannot promptly stop the early hydration at the desired time. This technique is generally accepted as the best standard drying technique because it seems that it can remove all of the physically adsorbed (unbound) water. It is considered as the best microstructure-preserving drying method [133, 135].

Perchlorate drying

A drying method, which is carried out at ambient temperature by placing the sample to be dried over magnesium perchlorate hydrates of analytical grade purity to obtain a partial pressure of water of 1.1 Pa at 25 °C, is called perchlorate drying, or P-drying [139]. This method is based on the stoichiometric calculations where the initial water quantity used for hydration is considered for computations of the approximate degree of hydration reached after 28 days [135].

Vacuum drying

Vacuum drying is usually done in a chamber with lower pressure than 0.1 Pa which results in a vapor pressure of water similar to that obtained in D-drying [133]. It was reported that this type of drying damages ettringite and monosulphate, and it also causes serious damage to the pore structure leading to an increase of the pore volume [133]. Moreover, it was found that this technique removes significantly less water than oven drying at 105 °C [140]. Vacuum-dried samples of hardened cement paste suffer stress and micro-cracks, which are similar to those present in samples dried in an oven at 60 and 105 °C [137]. Additionally, this technique is very slow and does not provide effective early hydration stoppage.

Freeze drying

During freeze drying, the temperature of the sample is reduced immediately to − 196 °C by using liquid nitrogen. Therefore, the water in the liquid state will change to the solid phase. A sample is placed into a freeze dryer under vacuum, resulting in sublimation of ice as the sample is slowly heated to room temperature. No capillary pressure is generated during sublimation, but the freezing process causes potentially damaging stresses from the volume expansion, hydraulic pressure, and crystallization pressure [141, 142]. Upon removal of vacuum, the dry sample returns to its initial conditions of room temperature and atmospheric pressure [132]. After 24 h of vacuum freeze drying, water is effectively removed from millimeter-sized particles of hardened cement pastes [143]. The freezing of pore water inside of the small samples is very quick, therefore, the cement hydration can be arrested immediately. However, the

growth of big ice crystals should be avoided. Gillott [144] recommended, that samples should be immersed in propane or isopentane before subjected to liquid nitrogen, as these compounds have a low freezing point, but a relatively high boiling point. Thus, they are not vaporized as readily by heat from the sample as is nitrogen, which increases the efficiency of cooling [132]. Nevertheless, crystallization of the pore water is unavoidable during these procedures, therefore, the growth of the crystals is expected to harm the microstructure. Moreover, it was reported that high vacuum damages ettringite and monosulphate and it critically influences the pore structure [133].

3.2. Solvent exchange

Hydration of cement pastes can be also arrested by diluting and removing the water present in the pores by a solvent. Selected physical properties of the most often used solvents for water removal are summarized in Table 3.2.1.

Based on the listed characteristics, an ideal solvent would have a small molecular size, which is important for penetration into the smallest pores to replace water. A lower boiling point (higher vapor pressure) facilitates the process of the removal of the solvent without a need of an additional heating to higher temperatures, at which the microstructure and composition of cementitious materials could be affected. The solvent should be miscible with water, and thus, the water in the pores could be replaced. Fast diffusion of the solvent in water can stop the hydration processes effectively. The pore structure damage upon drying can be minimized by lower surface tensions [132, 138].

When the solvent exchange procedure is applied, it is recommended to weight the sample before its immersion in an organic liquid. Upon the immersion, the solvent diffuses into the cement paste and gradually replaces the pore solution. When the mass is stabilized, the solvent is carefully removed by evaporation at ambient or elevated temperatures, under atmospheric pressure or vacuum, depending on the type of sample and the analytical method applied [132]. The time needed for exchange of pore water with the solvents highly depends on the porosity, diffusivity, and the dimensions of the samples [132]. Concerning the sample size, various shapes and dimensions can be found in literature. However, it seems that mainly small samples with 25–30 mm in diameter and 1–2 mm in thickness have been used for solvent exchange [145-

148]. The recommended soaking time varies from 2 days [149] to 10 days [147]. It was reported that for the cylindrical samples of 5.5 × 10 mm, the time needed to reach about 95% exchange of the ethanol was almost 3 weeks. As expected, the bigger sample size is used, the longer time is needed for the successful solvent exchange [150]. The frequency of the solution renewal has been also discussed [132]. To facilitate the diffusion processes, the solvent should be renewed regularly, if the solution-to-water ratio is low.

Table 3.2.1. Selected physical properties of solvents used to exchange water in cement-based materials [132, 151].

Substance	Formula	TB [°C][a]	Solubility in water at 25 °C	D × 10^5 [cm^2/s][b]	γLV [mN/m][c]	pV [kPa][d]
Water	H_2O	100			71.99	3.17
Acetone	$(CH_3)_2CO$	57	Miscible	1.28	23.46	30.80
Ethanol	CH_3CH_2OH	78	Miscible	1.24	21.97	7.87
Isopropanol	$(CH_3)_2CHOH$	82	Miscible	2.02	20.93	6.02
Methanol	CH_3OH	65	Miscible	1.28	22.07	16.90
Benzene	C_6H_6	80	0.8 g/L	1.02	28.22	12.70
Cyclohexane	C_6H_{12}	81	Immiscible		24.65	13.00
Diethyl ether	$(C_2H_5)_2O$	35	69 g/L (20 °C)		72.80	53.30 (18 °C)
Hexane	C_6H_{14}	69	Immiscible		17.89	20.20
Pentane	C_5H_{12}	36	0.1 g/L (20 °C)		15.49	68.30
Toluene	$C_6H_5CH_3$	111	0.47 g/L		27.93	3.79
An ideal solvent		Low	Miscible	Fast	Low	Low

[a] Boiling point at 760 mm Hg. [b] Diffusion coefficient in water. [c] Surface tension at 25 °C. [d] Vapor pressure at 25 °C.

It has been reported that during the first 24 h of the experiment, the solvent should be renewed every hour [152, 153]. A lower frequency is needed if the solution-to-water ratio is higher and the solution is stirred.

The removal of the solvent has been performed using convective heating [154], vacuum drying at ambient temperature [155], evacuation followed by heating [147], or heating under vacuum [149]. There are contradictory opinions about how the solvent should be removed: Feldman and Beaudoin [147] assumed that after the hydration stoppage that was done by isopropanol, subsequent evacuation time and temperature of heating are relatively unimportant to the resulting pore size distribution. Therefore, the water replacement by isopropanol was followed by immediate evacuation and heating at 100 °C for 20 h. Authors claimed that this procedure caused less damage to the cement paste than the replacement by methanol followed by heating for various periods. Afterwards, Beaudoin et al. [148] recommended that samples immersed with isopropanol should be dried under vacuum for 24 h. It is generally agreed that drying after the solvent exchange is less harmful for the original microstructure of hydrated cement-based materials than direct drying of the saturated paste, which is given by the relatively low surface tension of organic solvents [132].

3.3. Comparison of stoppage methods

The main effects of the hydration stoppage by solvent exchange and direct drying are summarized in Table 3.3.1. These findings can be outlined as follows (where ">" means "better") [132]:

a) For avoiding alternations of microstructure: solvent replacement > freeze drying > oven drying.
b) For preservation of composition: freeze drying > oven drying > solvent replacement.
c) For saving time: oven drying > freeze drying > solvent replacement.
d) All techniques more or less cause the dehydration of C-S-H and ettringite.
e) Chemical artifacts are created in the samples by the reaction with hydration products or by the strong adsorption when solvent is applied.
f) D-drying, P-drying, and vacuum drying are similar methods. The hydration stoppage is not effective enough when these techniques are applied. They are more appropriate for microstructural preservation than oven drying, but not as good as solvent replacement.

Table 3.3.1. Advantages and disadvantages of solvent exchange and direct drying methods for hydration stoppage [131].

	Solvent exchange	Direct drying
Advantages	• Easy to perform • Preserves chemically bound water in hydrate phases (depending on solvent) • Preserves microstructure • Removes soluble ions from pore solution	• Oven drying easy to perform, vacuum and freeze-drying need equipment • Supresses carbonation • Short freeze-drying preserves water bound in hydrates
Disadvantages	• Alternation of hydration products and removal of chemically bound water by some organic solvents (esp. methanol) • Organic solvents not completely removed by drying (such as acetone)	• Generally, chemically bound water removed • Microstructure generally altered
Suggested use	• Stoppage of samples for X-ray diffraction (XRD), NMR, MIP and SEM analyses is done with isopropanol. Samples schould be dried at 40 °C for a few minutes to remove the solvent. For TGA the removal of the isopropanol is done with diethyl ether and then drying for a few minutes at 40 °C.	• Freeze-drying or other techniques can be used if only the Portlandite content is of interest. • Gentle freeze-drying can be used for TGA, XRD, NMR and SEM. For MIP, direct drying cannot be recommended.

3.4. Sample storage

The appropriate storage after the hydration stoppage is essential because samples are usually stored before the analyses are performed, which requires a low relative humidity to prevent further hydration [131]. The four main phases of Portland cement clinker do not absorb significant amounts of water vapour if the relative humidity is kept below 55%, as it can be seen in Table 3.4.1.

Table 3.4.1. Relative humidity, at which cement constituents start to take up water vapour. Adapted from [156].

Cement constituent	Relative humidity at which water sorption starts [%]
CaO	< 10
$CaSO_4 \cdot 2H_2O$	24
β-$CaSO_4 \cdot 1/2H_2O$	34
C_3A, orthorhombic	55
$CaSO_4$	58
C_2S, monoclinic	64
C_3S, monoclinic	63
C_4AF, orthorhombic	78
Pure C_3A, cubic	80

The inappropriate sample storage can also lead to carbonation, especially, if the sample is already ground into a very fine powder [131]. The carbonation process is especially of relevance, if Portlandite is present, which can also lead to a partial decomposition of ettringite and the AFm phases. It was reported by Mmusi et al. [157] that the carbonation processes of cement-based composites occur mainly at the relative humidity between 50–80%. Nevertheless, the carbonation products, which are formed due to the consumption of Portlandite has been spotted already at humidity of 30% [158].

3.5. Summary

Generally, the hydration processes are stopped before the analysis is performed. Therefore, this chapter summarized possible ways of doing so. There are two main methods for arresting hydration, such as direct drying and solvent exchange.

In all direct drying techniques, such as oven drying, vacuum drying and freeze drying, water is removed by transforming into vapor. Especially oven drying leads to the removal also of the chemically bound water, which destroys of a part of hydrates and alters the microstructure. Therefore, it is recommended to use solvent exchange with isopropanol or to apply short freeze-drying [131].

The appropriate storage after the hydration stoppage is essential because samples are usually stored before the analyses are performed, which requires a low relative humidity to prevent further hydration. The inappropriate sample storage can lead to carbonation, especially, if the samples are already ground into a very fine powder. Therefore, it is recommended to measure the samples as soon as possible after the hydration stoppage, ideally on the same day [131].

Classical characterization methods for cementitious materials

This chapter summarizes experimental methods and procedures used in this study for the detailed description of the raw powders, such as particle size distribution, Blaine permeability method, X-ray fluorescence, and SEM. Methods for the characterization of the fresh and hardened cement pastes (hydration heat, XRD, MIP, SEM, basic physical and mechanical properties) are also introduced.

Since this study is mainly focused on the utilization of thermal analysis for the characterization of the long-term hydration processes of cement pastes, this method is described more in detail in a separated chapter (Chapter 5).

4.1. Particle size distribution

The particle size distribution is an important parameter affecting cement service properties. It defines the proportion of fine and coarse particles in powdered materials. In the case of cement, the particle size influences water demand, setting and hydration reactions [159, 160]. Moreover, the particle size of cement has a significant impact on the mechanical properties of concrete [160]. Particle size distribution of raw materials, such as natural zeolite, silica fume and cement, was measured on the device Fritsch Analysette 22 – MicroTec plus consisting of a compact measuring unit that can be combined with various dispersion units for dry, respectively, wet measurements. For the analysis, two lasers are utilized: a semiconductor laser with a green light for the measurements of small particles, whereas an infrared-semiconductor laser carries out the large particle size ranges. The measuring range of the applied apparatus covers particle size from 0.08 μm up to 2000 μm. The repeatability of the device according to ISO 13320 [161] is at d50 [μm] ≤ 1%.

4.2. Blaine permeability method

According to the EN 196-6 [162], two methods for determination of the fineness of cement (and powdered materials) are provided: sieving method and air permeability method (Blaine). The second mentioned method is widely used for the analysis of the fineness of powdered materials, and thus, it was utilized in this study. The fineness of powders is measured as their specific surface, which is expressed as the total surface area in square metres of all particles in one kilogram of powder. Thus, the higher value of the specific surface, the finer the studied material is. The principle of the air permeability method is to measure time needed for a specific amount of air flowing through a compacted powder bed of the known mass and porosity. This method is comparative rather then absolute, therefore, a reference material (standardized cement) of known specific surface is required for the calibration of the apparatus.

4.3. X-ray fluorescence

X-ray fluorescence (XRF) was used to determine the composition of the raw powders. Results of the detected elements were reported as their oxide forms. The studied materials were firstly dried and then ignited at 1000 °C for 1 h. Approximately about 1 g of each material was prepared for the analyses. An X-ray fluorescence (XRF) spectrometer, namely, Thermo ARL 9400 XP (Thermo ARL, Switzerland), was used. The obtained data were evaluated by Uniquant 4 software. The XRF analyses were performed in the Central laboratories of Institute of Chemical Technology.

4.4. Hydration heat

Early-stage hydration heat development of the studied cement pastes was measured by means of an isothermal heat flow calorimeter, which was designed by Tydlitát et al. [163]. This type of calorimeter was constructed for the investigation of large-volume samples (up to 1370 cm^3), which suits very well for highly inhomogeneous systems. Before the experiments, it is needed to put the particular components (powders, water) separately into the calorimeter until the equilibration of temperature is reached. Afterwards, the components are carefully mixed by hand for about 3 min. The PE bag, which is used for mixing, is

then sealed, weighted and put in the measuring vessel of the calorimeter. As the output, the time dependence of the heat power [mW] is obtained, which is then recalculated to the specific heat power *N* [mW/g]. When integrated, the total heat [J] or the specific heat *Q* [J/g] can be achieved as a function of time. Each experiment was performed on two samples during first 48 h.

4.5. X-ray diffraction

Changes in the mineralogical composition of the studied materials after 28 days and 360 days of hydration were examined by the XRD method. The diffraction patterns were collected with a PANalytical X´ Pert PRO diffractometer (PANalytical, Almelo, Netherlands) equipped with a conventional X-ray tube (Cu Kα radiation, 40 kV, 30 mA, line focus) and a linear position sensitive detector PIXCel with an anti-scatter shield. Cu X-ray tube was chosen because the amount of Fe (Fe_2O_3) was lower than 2 wt.%. X-ray patterns were measured in the range of 5 to 90° 2 Θ with step of 0.013° and 600 s counting per step, which produces a scan of about 4h 20 min. In this case, a conventional Bragg-Brentano geometry with 0.04 rad Soller slit, 0.25° divergence slit was used, and 15 mm mask in the incident beam, 0.5 anti-scatter slit, 0.04 rad Soller slit and Ni beta-filter in the diffracted beam. The XRD patterns were not pre-treated before the interpretation because no background correction was needed. Around 2 g of a sample was prepared for each studied material. Before the analyses, the powdered samples were mixed with acetone in an achat's bowl. After a thorough mixing (10 minutes) and evaporation of acetone, samples were put into holders and ready for the XRD measurements. Qualitative analysis was performed with the HighScorePlus software package (PANalytical, Netherlands, version 4.7.0) and the JCPDS PDF-4 database [164].

For the quantitative analysis of the XRD patterns, the studied samples were mixed with an inner standard (ZnO, 0.5 g – 20%). The Profex/BGMN software package with structural models based on the ICSD database was used [165, 166]. This program permits to estimate the mass fractions of crystalline phases by means of the Rietveld refinement procedure. The degree of crystallinity was also calculated by means of the Diffrac-Plus Topas program. The XRD analyses were performed with a kind help of Institute of Inorganic Chemistry of the Czech Academy of Sciences.

4.6. Scanning electron microscopy

A Zeiss Merlin high-resolution scanning electron microscope, capable of high-resolution secondary electron imaging with a resolution of 0.8 nm at 15KV and 1.4 nm at 1 kV with an in-lens secondary electron detector, was applied for analysis of the microstructure changes of studied materials after 28 and 360 days of hydration. The microscope is composed of a GEMINI II column, a process chamber with a 5-axes motorized stage (X, Y, Z, Tilt and Rotation) and a semi-automatic airlock providing maintained focus when the sample is tilted at a certain working distance.

The device is equipped with a retractable 4 Quads and in-lens energy selective backscatter detectors for back-scattered electron imaging, a unique charge compensation system for imaging of non-conductive materials, and a scanning transmission electron microscopy (STEM) detector for studying of electron-transparent thin film samples. The samples were placed on the carbon tape. Experiments were carried out in a high vacuum mode (secondary electrons were detected), and accelerating voltage of 7–10 kV. The samples were observed without coating by the conductive metal layer.

4.7. Mercury intrusion porosimetry

As already mentioned, the structure of many types of building materials is porous. The size and shape of pores vary, which significantly influences many properties like thermal conductivity, bulk density, durability, and especially mechanical properties [71]. The pore system is not constant and it changes in time. Therefore, these microstructural changes of the studied materials were determined by means of MIP on 28 days and 360 days old samples. This method is based on the measure of the intrusion of mercury (a non-reactive, non-wetting liquid) into the pores of the studied material at various pressures. The analysis requires a certain equilibrium time for mercury to fill the pore at each pressure level.

The pressure p [Pa] needed for intrusion according to the Washburn-equation is:

$$p = \frac{-2\gamma \cdot \cos\theta}{r} \quad [\text{Pa}], \tag{4.7.1}$$

Where r is the pore radius [m],
γ surface tension of mercury [N/m],
θ contact angle [°].

The pore-size distribution curves were obtained by the instruments Pascal 140 and 440 (Thermo Fisher Scientific), with the ability to determine the volume of pores with a radius greater than 3 nm and lower than 100 μm. The contact surface tension of mercury was assumed to be 480 mN/m with a contact angle 130° and density of 13541 g/cm^3. All measurements were done on homogenous representative samples having the maximum size of 0.7 g per experiment. Each material was examined twice and the values differed within 5%. These values were averaged and presented.

4.8. Basic physical properties

Physical properties, such as bulk density, matrix density and total open porosity were characterized on 28 days and 360 days old samples. The matrix density was measured on fragments of samples by helium pycnometry (Pycnomatic ATC, Thermo Scientific). The bulk density was determined using the measurement of prismatic sample dimensions (40 × 40 × 160 mm) and its dry mass (samples were dried at 105 °C). The total open porosity ψ [%] of studied materials was then calculated by means of the matrix density and bulk density:

$$\psi = 100 \cdot \left(1 - \frac{\rho_b}{\rho_{mat}}\right) \quad [\%], \tag{4.8.1}$$

Where ρ_b is the bulk density [kg/m^3],
ρ_{mat} matrix density [kg/m^3].

The accuracy of the gas volume measurement using this device is ± 0.01% from the measured value, whereas the accuracy of used analytical balances is ±0.0001 g. The expanded combined uncertainty of the bulk density was 2.4%, and 3% for the total open porosity, respectively [167].

4.9. Mechanical properties

The development of mechanical properties, such as flexural and compressive strength, was studied up to 360 days of hydration. These characteristics were obtained according to the procedure described in the technical standard ČSN EN 1015 [168]. At first, measurements of the flexural strength were done on three samples with the dimensions of 40 × 40 × 160 mm using the MTS 100 loading device in a three-point bending test with 100 mm span length. The flexural strength f_f [MPa] was calculated as:

$$f_f = \frac{3F_{max}L}{2bd^2} = \frac{M_{max}}{W} \quad [\text{MPa}], \tag{4.9.1}$$

Where F_{max} is the maximal load (force) at the fracture point [N],
L length of the support span (100 mm),
b/d width/thickness of studied sample [mm],
M_{max} maximal bending moment [N.mm],
W bending section modulus [mm^3].

The bending moment is dependent on the force and the distance between the support span, while the modulus depends on the cross-section type (round, square, rectangular, complex). Then, the measurements of the compressive strength f_c [MPa] were done on the halves of broken prisms with a loading area A about 1600 mm^2:

$$f_c = \frac{F_{max}}{A} \quad [\text{MPa}]. \tag{4.9.2}$$

The expanded combined uncertainty of the flexural strength method was 1.6%, and 1.4% for the compressive strength, respectively [167].

Chapter 5

Thermal analysis

This chapter deals with thermal analysis, which was selected as the main method for the study of hydration processes of analyzed cement (blended) pastes from 2 to 360 days of age under various curing conditions. After a brief introduction of thermal analysis techniques, TGA and DSC are described more in detail, as these two techniques were coupled, and mass change and heatflow changes of studied materials were determined simultaneously in this study.

5.1. Thermal analysis techniques

The terms thermal analysis and calorimetry cover various measuring methods, which are related to the changes in temperature of the analyzed sample. These methods are capable of time dependency measurements of a sample temperature when the sample is exposed to a heating program. Using thermal analysis, it is possible to analyze changes in compositions and certain properties of studied materials [169].

A more exact definition, proposed in 1991, describes thermal analysis as a group of techniques in which a property of the sample is monitored against time or temperature while the temperature of the sample, in a specific atmosphere, is programmed. The program can involve heating or cooling at a fixed rate of temperature change, or holding the temperature constant, or any sequence of these [170].

Measurements are usually performed with increasing temperature but isothermal measurements are also possible. Table 5.1.1 summarizes a selection of thermal analysis techniques showing the breadth of the field. Possibly, any measuring technique can be a part of thermal analysis techniques by adding a thermal control [171].

Table 5.1.1. Primary classification of thermoanalytical and calorimetric methods, adapted from [169].

Studied changes	Method	Abbreviation
Temperature	(Classical) thermal analysis	TA
Temperature difference	Differential thermal analysis	DTA
Enthalpy, heatflow	Differential scanning calorimetry	DSC
Mass	Thermogravimetric analysis/thermogravimetry	TGA TG
Dimension/mechanical properties	Thermomechanical analysis	TMA
Electrical properties	Thermoelectrical properties	TEA
Optical properties	Thermooptical analysis	TOA

Techniques of thermal analysis can be utilized in many fields. In the field of cement science, TGA and DSC methods are reported to be used most frequently. Especially when coupled, these techniques can provide a more powerful tool for the study of hydration processes [131].

5.2. Thermogravimetry

TGA is used to observe the mass loss of materials as a function of temperature or time at a controlled temperature [172]. This method provides information related to certain physical and chemical reactions, such as continuous phase transition, vaporisation, sublimation, absorption, adsorption, desorption, chemisorption, desolvation (dehydration), decomposition, oxidative degradation, solid-state reactions and solid- gas reactions (oxidation or reduction). Nevertheless, TGA cannot provide any information about crystalline transitions, fusions and those solid-state reactions that occur without change of mass [173]. The application of TGA spreads among minerals, inorganic substances, metals, ceramics, electronics materials, polymers, and even various organic substances [174]. The main advantage of this method is that it can be used as a means of determining devolatilization characteristics and to determine

kinetic parameters, such as activation energy [175-179]. When TGA is used in a precise approach, it is possible to obtain a "fingerprint" of material, which can be used as a quality control check [180]. In the field of cement science, it is often used for measurements of the CBW and Portlandite content to follow the reaction of Portland cement or to evaluate the reactivity of supplementary cementitious materials. TGA can identify amorphous hydrates, such as C-S-H or AH_3, which can be used complementarily to other techniques, which cannot provide more details about amorphous phases, such as XRD [131].

5.2.1. Thermogravimetric apparatus

There are two main types of thermogravimetric devices: vertical TGA instruments and horizontal TGA instruments [172]. The main difference between these types lies in the manner how the sample/reference holders are supported. In the case of the horizontal type, there is a need to make a correction for the influence of the thermal expansion on the length of the balance-arm during heating [172, 181]. Generally, the atmosphere of the system is controlled by inert gases (i.e., nitrogen, argon) [182].

5.2.2. Obtained results

The information about a studied material are extracted from a TG curve, which is generated by TGA measurements. Figure 5.2.1 shows an example of this curve and its derivation, which is used for the determination of the beginning and end of the detected reactions.

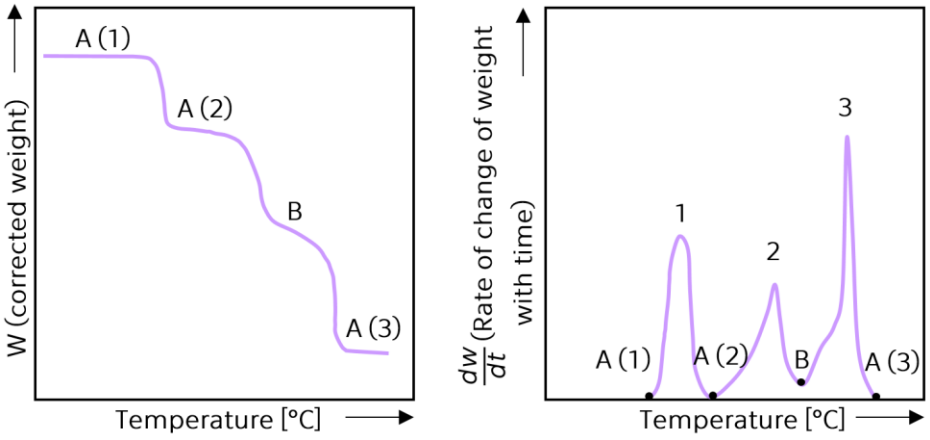

Figure 5.2.1. Examples of a mass-temperature curve and a differential thermogravimetric curve. Adapted from [173].

The second graph may be explained in parallel with the first one. The three points A (1 to 3) represent plateau, which means that exactly at this moment, the mass of the compound does not change during the increase of the temperature. The three peaks (1 to 3) observed in the differential thermogravimetric curve describe the decomposition of the studied material. The faster the decomposition, the higher the peak is. At the B point, it seems that the mass loss curve becomes a plateau. However, this shape of curve shows, that immediately after the decomposition of the material A(2), there is another decomposition. There are also some points of reflexion/inflexion, which mean that the mass change remains constant at this moment. This involves the presence of an intermediate compound (successive reactions) [173].

5.2.3. Accuracy limitations of TGA

In this section, the parameters, which significantly influence the accuracy of the TGA results, are presented.

Small size and mass of materials

Most of materials are composed of two or more components with different size distributions. However, since quite small amounts of samples are used for TGA measurements, it would be difficult to prepare a homogenous representative sample of the material of interest. The samples are usually used in the form of small pieces (1–2 mg/piece, but normally up to 100 mg is used depending on the type of material). This limited mass is employed with the aim to improve heat transfer distribution in the whole material [183, 184].

Heat/mass–transfer limitation

In conventional TGA, the sample plays two roles. Firstly, it is the heat source in which heat of reaction, fusion, transition, etc. are evolved or absorbed (i.e., exothermic or endothermic reactions). Secondly, it has a function of the thermal barrier in which temperature gradient occurs in proportion to the heat flow to the sample (i.e., heat transfer limitation) because the thermocouple junction was inserted into the sample [174]. The heat/mass-transfer limitation is caused by the differences between the heat capacities of sample–crucible–furnace interfaces. The crucible and the sample are heated up with some lag to each other. To obtain

the most accurate results, the crucible must transfer heat uniformly to the sample. The most important characteristic of the crucible, which directly influences these limitations, is its thermal conductivity. There are also differences in heat transfer between a normal crucible and the one with a disc fitted at the bottom [185]. The type and efficiency of heat transfer is also influenced whether the crucible is covered with a lid or not [186]. There is also such comparable lag to the set program of heating. To minimalize this heat/mass – transfer intrusions, the measurement must be done at a low heating rate [184].

Low heating

As it was already mentioned above, to overcome the temperature gradient of the sample and the crucible in the conventional TGA, a low heating rate should be used [187]. However, in order to study a process such as pyrolysis, it is necessary to heat the sample up much faster [188].

Poor gas-solid and solid-solid mixing throughout the sample

Ebrahimpour et al. [188] studied the diffusional effects on the oxidation of SiC powders under air in cylindrical crucible using TGA. It was found that the particle size had a marked influence on the oxidation rate. The results obtained from dynamic TGA indicated that for nano-sized particles, oxidation reaction started at temperatures much lower than micro-sized particles.

Balance inclination

There are many sources and magnitudes of forces, which worsen the accuracy of microbalance in mass measurements, such as convective, thermomolecular, electromagnetic and electrostatic forces; thermal dilatation, buoyancy, mechanical vibration and Brownian motion [189, 190]. In addition, instability of the system, either mechanically or electrically, render the measurement quite time-consuming, which is not user friendly [191, 192], such that even very small changes in microbalance inclination can introduce significant mass errors [190].

Non-quantified method

Last but not least, TGA is not capable of resulting evidence about the composition of materials. This technique typically needs to be combined with other methods to address this issue. Besides, it also cannot be considered as a method in which the changes of molecular weight of materials are obtained [193, 194].

5.2.4. TGA for study of cement hydration processes

Thermogravimetry and its derivation (DTG) have been used to identify the amount of chosen substances included in concrete pastes and their changing ratio during aging. These results have been discussed in several research studies [195-200]. As already mentioned in the Section 2.2, where mechanisms of hydration were described in detail, the hydration of cement starts immediately after its contact with water and it is quite completed in about 28 days. Understanding the reactions, which take place during hydration, is the key how to design and produce concretes of the highest qualities. The information about the formation of hydration products, especially of the Portlandite, is very important because this component influences significantly the properties of concrete. There have been several studies analyzing the amounts of products of hydration using TGA [201, 202]. In [201], a combined XRD/TG method were used to quantify the phase composition of hydrated Portland cements during aging up to first 56 days. In [202], TGA was used to analyse the hydration steps of cements at different times during the first 4 weeks of setting.

TGA has been successfully used to study the cement hydration processes with the effect of different pozzolanic active materials, such as fly ash [203-206], metakaolin [70, 207, 208], blast-furnace slag [209], bentonites [210] or clays [211, 212], different wastes from silica [213], bricks [214], porcelain [215], or an organic materials, such as sugarcane biomass waste [216], even of natural and heated wood [217] or polysaccharide [218], or fluid catalytic cracking catalyst residue [166, 196, 219].

From these numerous examples, it can be therefore seen, that TGA represents a very important tool for studying the hydration processes of OPC.

5.3. Differential scanning calorimetry

The DSC method is one of the most essential techniques of thermal analysis. It has been utilized in many different industries. DSC measures the enthalpy changes, which are related to glass transitions. It can characterize pure phases or the glass fraction in blast furnace slags or fly ash. However, in hydrated cements, this technique is generally not used quantitatively but it is rather used to assess the presence of glassy phases or certain hydrates with a characteristic heat development [131].

All DSC instruments heat the studied sample and a reference with a furnace. The experimental arrangement can have one furnace (heat flux DSC) or two furnaces (power compensation DSC). The principles of these arrangements are slightly different [170]:

Heat flux DSC

A single furnace is used for heating both, the sample and reference crucibles (Figure 5.3.1). There are two temperature sensors inside of the furnace recording the temperature changes of both samples. The reference sample is an empty crucible made of an inert material. The studied material is placed in a crucible with the same dimensions and from the same material like the reference one. Both crucibles are placed on the sensors. During the heating, both samples will be initially heated at the same rate and there will be no temperature difference between them. If a transition occurs within the sample, for example if an endothermic reaction occurs, which requires more energy, then the temperature difference between the studied material and the reference will be negative [170].

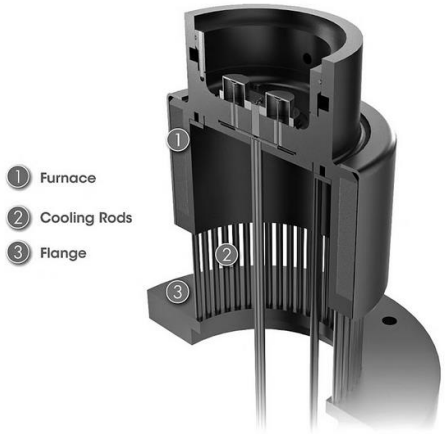

Figure 5.3.1. Schematic representation of a heat flux DSC; from [170].

It can be written that the heat flow (q) is proportional to the temperature difference (ΔT) as follows [170]:

$$\frac{dq}{dt} \sim \Delta T. \tag{5.3.1}$$

In the case, that the temperature difference is only recorded and not converted to a heat flow signal, then this is referred to as a differential scanning calorimetry (DTA) signal. Analysers, which do not have heat flux capability (usually older systems) are referred to as DTA analysers [170]. The conversion of the ΔT signal to power is done by multiplication by an experimentally determined cell constant (k) [170]:

$$\frac{dq}{dt} = k\Delta T. \tag{5.3.2}$$

The value of the constant k can be determined using a certified reference material, such as highly pure metals with defined melting temperatures and enthalpies of fusion [170].

Power compensation DSC

In power compensation DSC, the measuring system consists of two identical furnaces of the same type made of a platinum-iridium alloy. Each furnace contains a temperature sensor and a heating resistor. During heating, the same heating power is supplied to both furnaces, and therefore, the temperature of both furnaces is always the same. When a transition occurs, a temperature difference results between the furnace with the studied material and the reference. The temperature difference is the measurement signal and it also works as an input signal for the compensation of the reaction heat flow rate, which is balanced with electric energy, by increasing or decreasing power [220].

5.3.1. DSC/DTA for study of cement hydration processes

When DSC is compared with differential thermal analysis (DTA), which is suited for the determination of characteristic temperatures; DSC additionally allows the determination of caloric values, such as the heat of fusion or heat of crystallization. For the heat flux DSC and DTA, the primary measuring signal during a measurement is the temperature difference between a sample and

reference in μV (thermal voltage). However, for the power compensation DSC, this temperature difference is usually converted into a heat flow difference in mW by means of an appropriate calibration, as shown in Eq.(5.3.2). This possibility does not exist for a purely DTA instrument [221].

Similarly to TGA, DSC analysis have been successfully used for study of development of hydration products of cement as a function of time [222]. The heatflow and enthalpy results of blended cement pastes with zeolites were studied for example in [223]. The influence of metakaolin on the formation of the hydration products of the hardened pastes analyzed by DSC, DTA and TGA was presented lately in [224]. It was recently reported that in hydrated blast furnace slags or blends of Portland cements with slag, a quantification of the heat generated by the crystallization reaction was nearly impossible, as a strong change in the background was observed [131, 225]. The large contribution of the background was already noted in previous DSC analyses of plain OPC [222, 225]. However, it seems to be promising to couple DSC with selected methods to obtain a more powerful tool. Recently, the DSC together with the MIP were successfully used to determine the changes of the pore structures of concrete [226].

5.4. Factors influencing results

This section summarizes the main factors, which may influence the results determined by thermal analysis (especially TG and DSC methods), such as the architecture of the measuring device, heating rate, sample mass, particle size, used crucible/pan, atmosphere, radiation effects, and pre-treatment of the sample. These parameters make it nearly impossible to transfer measurements done at one laboratory to the another one. Therefore, one of the main rules to perform reliable TA measurements is to keep, as much as possible, the same procedure for all measurements within a laboratory [131].

Heating rate, open and closed crucibles and gas flow

The heating rate together with the type of crucible affect the position of dehydration reactions. Higher heating rates cause that the peaks are better-defined and wider but they also cause higher observed dehydration and dehydroxylation temperatures [131].

For example, gypsum dehydration proceeds via hemihydrate to anhydrite and at higher vapour pressures, the dehydrations can be differentiated because the dehydration process of hemihydrate to anhydrite takes place at slightly higher temperatures. Normally, under TGA conditions, the dehydration of gypsum is observed at about 140 °C. This exact temperature can vary significantly, depending on the vapour pressure present. The dehydration temperature of gypsum was observed at 50 °C, in equilibrium with only 1 Pa vapour pressure, while some researchers reported that at higher pressure, the temperature of dehydration rises up to 150 °C or even higher [227, 228]. Similar behavior can be seen in Figure 5.4.1. When the crucible is closed, the vapour pressure over the sample is increased. It is because water can escape only slowly through the small opening [131].

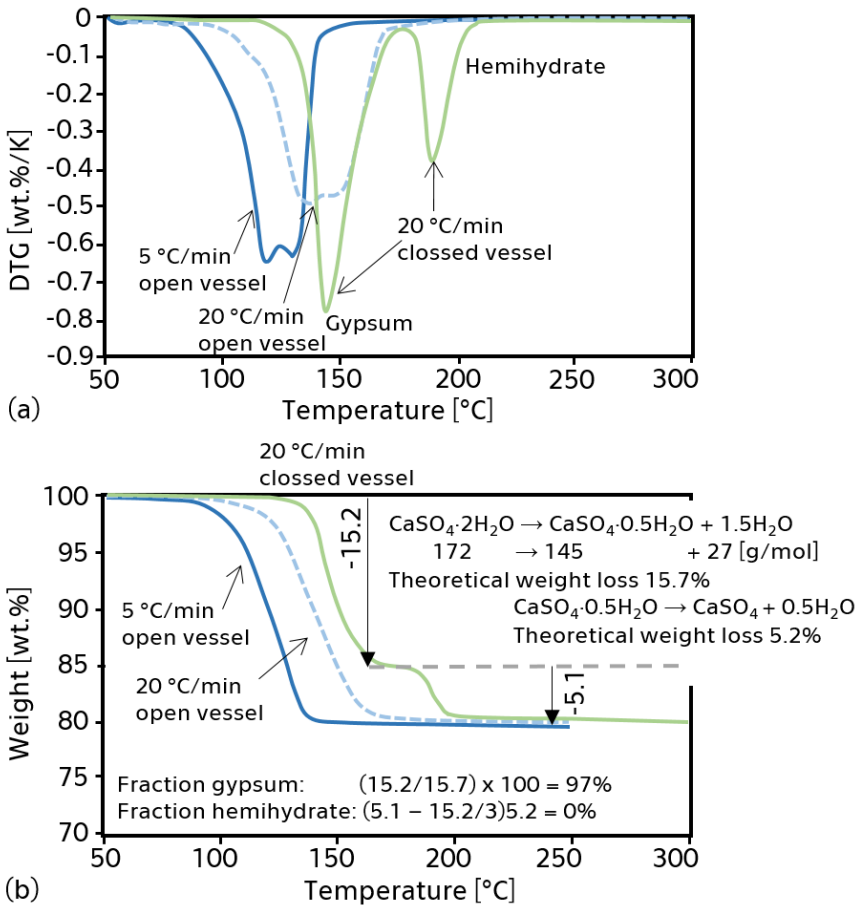

Figure 5.4.1. (a) DTG and (b) mass loss recorded by TGA for gypsum under different conditions. Adapted from [131].

Also, the gas flow affects the main mass loss area. Higher gas flow decreases temperatures where the mass loss is observed but also causes the worse differentiation between different peaks. Similarly, the geometry of the pan/crucible affects the vapour pressure, and thus, the temperature of the main mass loss [131].

Sample mass (size)

The sample mass is an important factor (see Figure 5.4.2), which affects the temperature of the main mass loss. Especially, if the differential data are normalised to 100 wt.% (Figure 5.4.2b). In the normalised plots, higher quantities of a phase lead to a seemingly higher dehydration temperature and broader peaks. In the illustrating picture, the dehydration of a larger quantity of gypsum releases more water, which results in higher vapour pressure in the environment of the solid. Therefore, higher temperatures are needed to dehydrate gypsum to anhydrite [131].

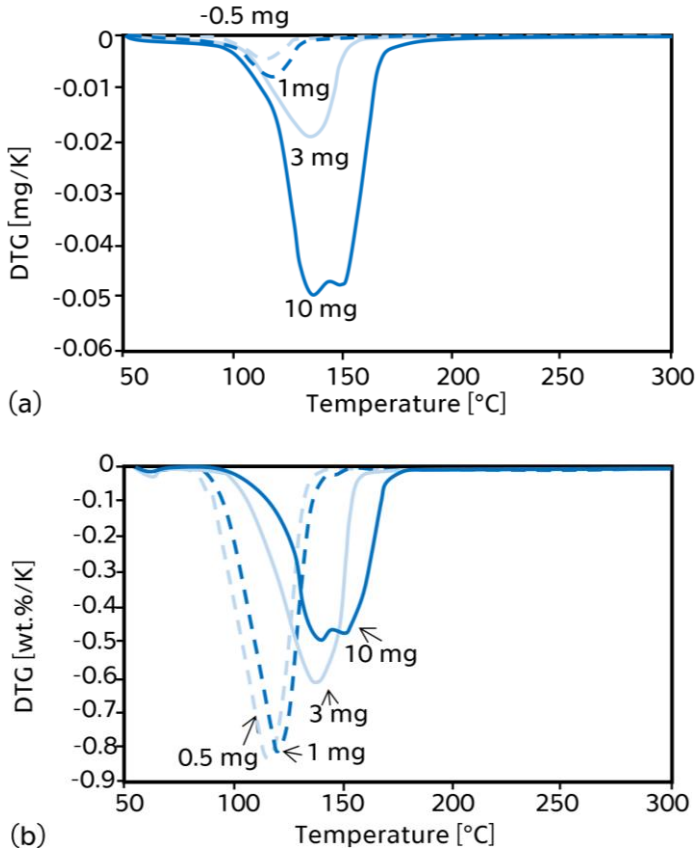

Figure 5.4.2. Influence of the sample mass on the peak position and shape of the dehydration peak of gypsum. Adapted from [131].

The sample mass can influence the TGA curve in these ways [173]:

a) The higher mass of a sample, the higher is the deviation between the temperature of sample and the heating program.
b) The void space around the solid particles influences the degree of diffusion of the product gas. The atmosphere immediately surrounding the reacting particles will be governed by the bulk of the material in the crucible.
c) If the studied material has a low thermal conductivity, it can bring the possible unevenness of the temperature throughout the sample.
d) The smaller mass of a sample may also influence the temperature determination in the cases when the thermocouple is not in the direct contact with the sample. It may cause a thermal lag between thermocouple temperature and the sample temperature [229].

Sample pre-treatment

There is a range of sample preparation methods for TG analysis of hydrated cement paste as summarized recently for example in [132], where cement pastes hydrated for 113 days were studied. Samples were dried by freeze drying, or by solvents replacement with isopropanol, tetrahydrofuran, ethanol or acetone. These techniques were compared to a measurement of a control sample without drying. It was found that all TGA curves were similar below 600 °C. Above this temperature, the curves without drying and after freeze-drying showed a plateau, which means that the sample was not carbonated. In the case of solvent-exchanged samples, the utilization of acetone caused the largest mass loss above 600 °C, whereas isopropanol replacement caused the least mass loss.

Similar results were reported in [131]. Figure 5.4.3 illustrates the main effects of different drying techniques on TGA results using: (a) isopropanol compared with freeze drying, (b) drying at 105 °C, (c) freeze drying compared with re-equilibration over saturated $CaCl_2$, and finally (d) ethanol.

From these results, it seems that the longer soaking time in the case of isopropanol can lead to higher levels of carbonation of cementitious materials.

Therefore, Zhang and Scherer [132] recommended to remove the sample from the solvent as soon as possible.

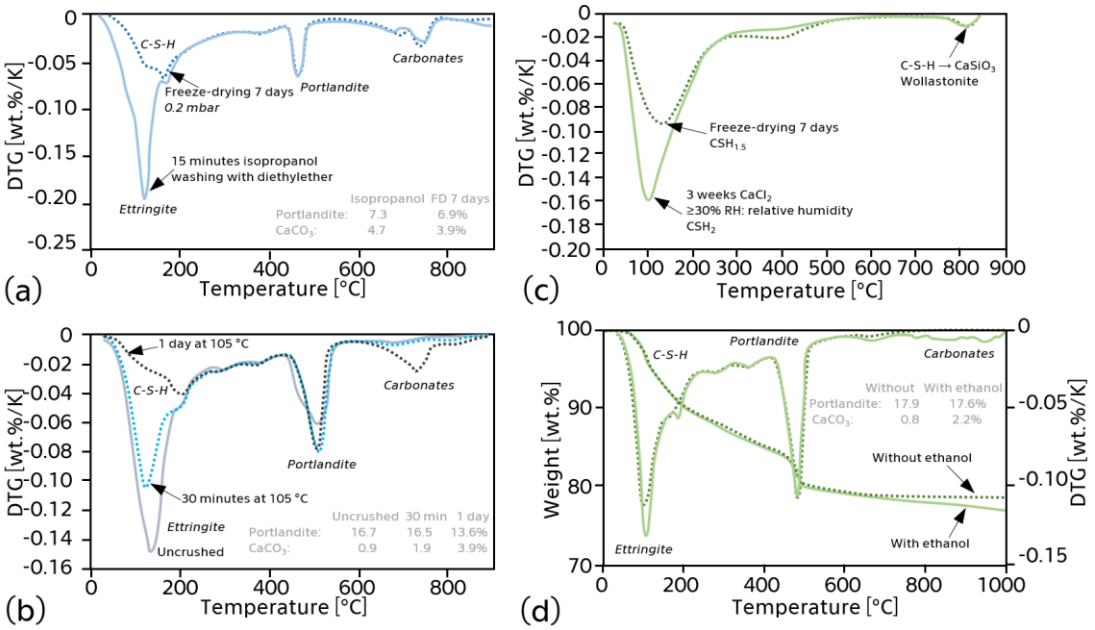

Figure 5.4.3. Effects of various drying techniques on TGA results; from [131].

However, if the time for soaking is limited, the pore water, especially in the smaller pores, will not be completely replaced by the solvent [131], and the hydration stoppage will not be efficient enough. It should be noted that Zhang and Scherer [132] analyzed early-aged cement up to 3 days of hydration. However, based on the most recent review on hydration stoppage techniques [131], in the case of TGA, the use of isopropanol seems to be the most efficient drying method.

5.5. Simultaneous thermal analysis

In this study, a simultaneous thermal analysis (STA) consisting of DSC and TGA methods was used to find and quantify hydration products of all studied samples (Figure 5.5.1). The setup consists of two identical crucibles made of an inert material, alumina (Al_2O_3), of size of 100 mm^3. One is filled with the studied sample and the other one remains empty (reference sample). Both are covered by a lid and they are placed on a system of very sensitive balance. The heat flow (power) and mass changes of the studied sample during heating are recorded simultaneously. Since the experiments are running at a constant pressure, heat

flow is considered to be equivalent to enthalpy changes. The STA was carried out using a Labsys Evo device (Setaram, France).

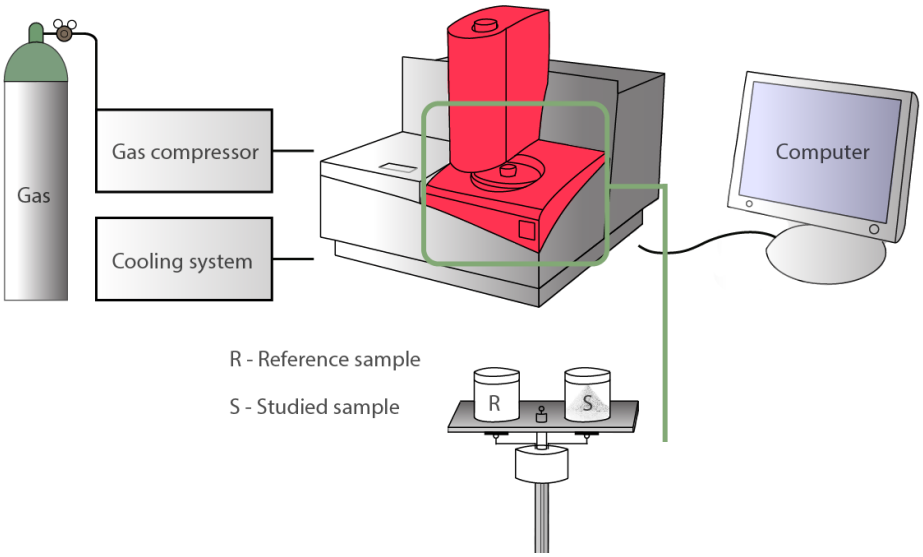

Figure 5.5.1. Schematic representation of the STA arrangement.

The experiments were done in the temperature range from 25 to 1000 °C in an argon atmosphere with a flow rate of 40 mL/min. The heating rate was 5 °C/min. About 50 mg of powdered sample was used.

5.6. Quantification of the main hydration products

This section describes the methods used in this study for the quantification of the main hydration products of the studied cementitious systems. These methods are mainly related to the TGA because this analysis provides very accurate results of mass changes of studied samples during heating. It can be used for a precise quantification of certain hydration products, such as Portlandite and carbonates in cementitious systems. Using TGA results, it is also possible to determine the amount of bound water, which refers to the degree of hydration. Therefore, TGA represents an important technique for a long term study of hydration processes [131].

In spite of the fact that DSC method is a powerful tool for analysis of pure phases, DSC instruments are generally not used for quantification of complex

systems, but rather for assessing the presence of glassy phases or specific hydrates with a characteristic heat development, such as M-S-H [230].

5.6.1. Bound water, degree of hydration

Chemically bound water (CBW) is the non-evaporable water that combines chemically with the cement i.e. the water, which is bound in the hydrate phases [231]. The determination of the CBW content is important to assess the degree of reaction of Portland cements. However, as it is difficult to separate the CBW from the physically bound water and free water, there have been many various studies looking for the most appropriate procedure.

Plain cement pastes

Based on one of these studies [232], the CBW can be obtained from the difference between the mass losses of samples dried to 105 and at 1000 °C. This method assumes that only pore water is removed from the structure until 105 °C, as C-S-H, ettringite and monosulfate lose part of their chemically combined water below this temperature. Additionally, the mass loss caused by the decomposition of carbonates is included when the temperature interval

I from 105 to 1000 °C is selected, which decreases the accuracy of the results, as discussed more in detail in [131].

Another possibility how to obtain the amount of the CBW lies in the use of the difference between the mass after solvent exchange, and the mass after drying at 500 or 550 °C [203] to differentiate the CBW from the mass loss from decarbonation. It can be done based either on the direct weighing or on TGA measurements [131]. The amount of the CBW can be therefore expressed as % of the initial sample mass at 40 °C (w_{40}) and the dry sample mass at approximately 550 °C (w_{550}), in accordance with the end of the Portlandite decomposition (taken from the derivative curve (DTG)) [203]:

$$\mathrm{CBW} = \frac{W_{40} - W_{550}}{W_{550}} \times 100 \quad [\%]. \tag{5.6.1}$$

This approach, proposed by **De Weerdt et al.** [203], seems to be more accurate. However, it depends on the procedure of the solvent exchange, as in

larger but not crushed samples, there is a possibility that they will contain water, which will participate in hydration processes until the experiments are done.

To determine the degree of hydration of Portland cement (α_c), which is directly related to the CBW content, it is assumed that the hydration of 1 g of anhydrous cement produces 0.23 g of the CBW, and thus, it can be written as follows [233]:

$$\alpha_C = \frac{CBW}{0.23} \quad [\%]. \tag{5.6.2}$$

However, the value of 0.23, which represents the maximum CBW required to hydrate a cement particle entirety, can vary between 0.23 and 0.25 depending on literature [234, 235].

Blended cement pastes

In blended cement pastes, the pozzolanic reactions lead to the consumption of Portlandite, which is gradually transformed into C-S-H. Due to an uncertain incorporation of additional water, there is a possibility for the formation of C-S-H (from various reactions) with different water contents. It means that C-S-H can be formed from OPC calcium silicates and also from the pozzolanic reaction, which makes it difficult to directly compare the amount of the CBW present in plain and blended cements. Therefore, as one of the solutions, it was proposed in [232] to compare the amount of the CBW that excludes Portlandite water losses during heating, as it allows to compare the amount of the CBW only from the hydrates in the both types of cements.

The methodologies proposed by Pane et al. [236] and Bhatty [235] for the degree of hydration assessment of blended cement pastes by thermal analysis were reviewed in detail and modified in a recent study [234].

The method by **Bhatty** [235] can be summarized as:

$$CBW = Ldh + Ldx + 0.41\,(Ldc) \quad [\%], \tag{5.6.3}$$

$$\alpha_C = \frac{CBW}{0.24} \times 100 \quad [\%]. \tag{5.6.4}$$

Where Ldh, Ldx and Ldc are mass losses for the different decomposition reactions occuring in the approximate temperature ranges given in Table 5.6.1.

The value of 0.41 is a conversion factor based on which the CBW derived from the carbonated Portlandite can be determined. The origin of this value was explained by Rivera Lozano [237].

Table 5.6.1. Temperature ranges based on the Bhatty's method.

Region	Temperature range [°C]
Ldx	440–580
Ldc	580–1000
Ldh	105–440

The temperature range for the Portlandite decomposition should be determined individually for each studied material; for example with the utilization of the DTG curve.

In the method proposed by **Pane et al.** [236], the mass loss is considered within a temperature range of 140–1100 °C. The starting temperature of 140 °C instead of 105 °C reflects the authors experimental results in which stilled water alone turned completely into gas at 140 °C [234]. The method by Pane et al. [236] can be summarized as:

$$CBW = Ldh + Ldx + (Ldc - Ldc_a) \quad [\%], \tag{5.6.5}$$

$$\alpha_c = \frac{CBW}{CBW_\infty} \times 100 \quad [\%]. \tag{5.6.6}$$

Where Ldh, Ldx and Ldc are mass losses for the different decomposition reactions occuring in the approximate temperature ranges given in Table 5.6.2.

Table 5.6.2. Temperature ranges based on the Pane's method.

Region	Temperature range [°C]
Ldx	440–520
Ldc	520–1100
Ldh	140–440

The Eq.(5.6.5) involves consideration of the decarbonation mass loss entirely without the conversion factor of 0.41. However, not all the mass loss found during the decarbonation is caused by Portlandite that has been carbonated during the hydration processes, as the carbonation of the anhydrous material is included as

well [234]. The only related correction is the substraction of the anhydrous material of carbonation (Ldc_a), as deduced from the totall loss of carbonation in the temperature range from 530–1100 °C. In [234], these values were determined to be 1.117% for OPC and 0.918% for silica fume. In the Eq.(5.6.6), the CBW_∞ is not a fixed value, but it depends on the mineral admixture, which was used. More details are provided in [236].

When these methods are compared, the method by Pane et al. [236] gives significantly higher values than the Bhatty's method [234]. It should be noted, that there are contradictory opinions, if the mass loss from the carbonation processes should be included into these computations [131].

5.6.2. Portlandite

Portlandite ($Ca(OH)_2$) usually decomposes between 400 and 500 °C to CaO and H_2O, following Eq.(5.6.7). The quantification of Portlandite can be very challenging, especially in the temperature interval from 40 °C to 600 °C, where mass loss from C-S-H is also observed [131].

$$Ca(OH)_2 \rightarrow CaO + H_2O. \tag{5.6.7}$$

The mass loss caused by the evaporation of water in this temperature interval ($WL_{Ca(OH)_2}$ in %) can be used for the calculation of the amount of Portlandite present in a studied system. This can be done with the utilization of molecular masses of Portlandite ($m_{Ca(OH)_2}$ = 74 g/mol) and water (m_{H_2O} = 18 g/mol) [131]:

$$Ca(OH)_{2,measured} = WL_{Ca(OH)_2} \times m_{(Ca(OH)_2} / m_{(H_2O)} = WL_{Ca(OH)_2} \times \frac{74}{18} \text{ [\%]}. \tag{5.6.8}$$

Because the sample mass of the solid fraction of the sample changes during hydration, sometimes there is a need to rescale the obtained results, to either paste or anhydrous, as explained further in [131]. In practise, there are two techniques to quantify Portlandite: stepwise (horizontal) or tangential, as demonstrated in Figure 5.6.1. The stepwise method (Figure 5.6.1a) is the simplest one and is often used to determine Portlandite content in hydrated cements. However, it seems that even when this method tends to agree reasonably well with XRD results, it overestimates the real Portlandite content as it includes besides the mass loss of Portlandite also the mass loss associated to the C-S-H

(and other phases decomposing in this temperature interval). In terms of the tangential method, the mass change originated due to the presence of C-S-H (or other phase) observed before and after the peak will continue (linearly) in the region with the Portlandite decomposition. This technique therefore allows to determine the mass loss of Portlandite only and it is equivalent to the integration of the peak area (Figure 5.6.1c) [131].

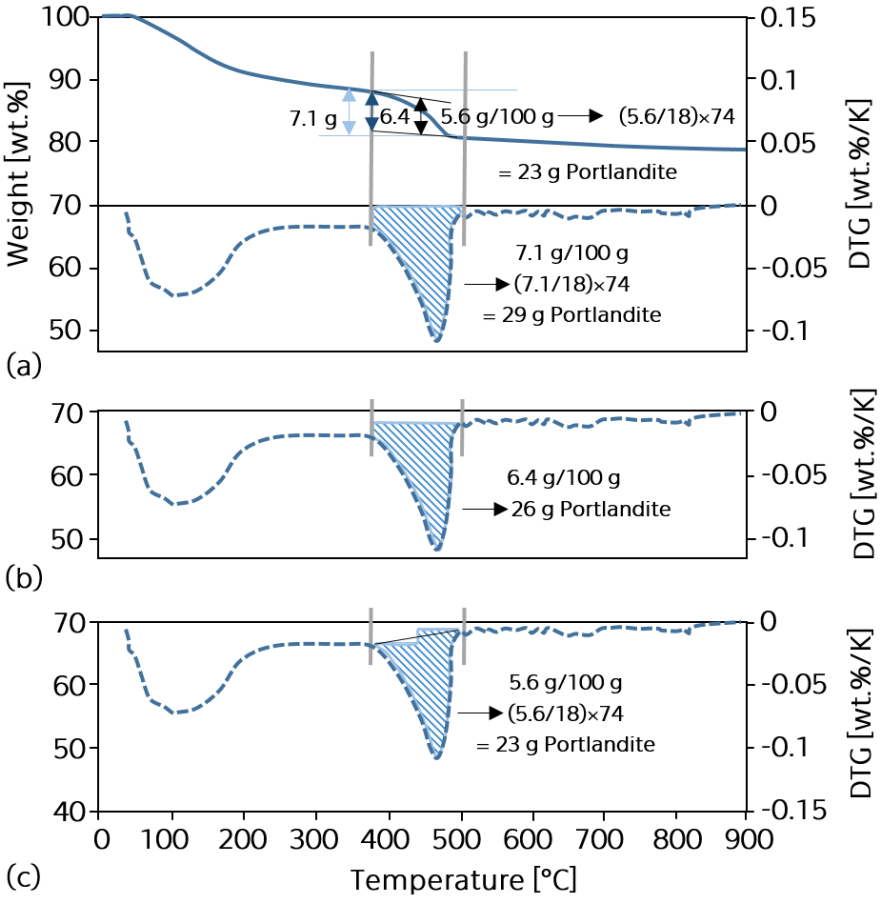

Figure 5.6.1. Effects of tangential and stepwise methods on the quantification of Portlandite. Adapted from [131].

Software related to the TGA instrument usually allow the direct quantification of the mass loss either by the stepwise, the tangential method or by the integration of the derivative curve. However, in the cause of the tangential method, some instruments use the start temperature instead of the median temperature (Figure 5.6.1b); resulting in a higher mass loss [131]. Other software would compute the difference at the temperature where the mass loss reaches the maximum. Therefore, it is recommended to integrate the peak area, which corresponds to the real results the most (Figure 5.6.1c) [131].

5.6.3. Calcite

Calcium carbonate ($CaCO_3$) usually decomposes above 600 °C into CaO and CO_2, following the Eq.(5.6.9). Aragonite and vaterite, which are two other crystalline calcium carbonate polymorphs, recrystallize without mass change at about 450 °C to calcite, while amorphous calcium carbonate decarbonates partially between lower temperatures 400–600 °C, forming CaO and calcite [131].

$$CaCO_3 \rightarrow CaO + CO_2. \tag{5.6.9}$$

The exact position of the calcite decomposition strongly depends on many factors, such as the presence of hemi- and monocarbonates, the amount of calcium carbonate and its fineness. Under certain conditions, calcium carbonate can decompose within two peaks. The CO_2 mass loss peak observable at around 720 °C is caused by the presence of relatively coarse calcite whereas the second mass loss peak, present at lower temperatures from 600 to 650 °C, is associated to the presence of mono- or hemicarbonates originated from the carbonation of Portlandite, and possibly C-S-H [131].

In the case of calcite, the quantification is simpler compared to Portlandite, except in cases where amorphous calcium carbonate has formed. Similarly, to Porlandite, the mass loss obtained in this temperature interval (WL_{CaCO_3}) can be used for calculation of the amount of calcium carbonate present in the studied system, with the utilization of the molecular masses of $CaCO_3$ (m_{CaCO_3} =100 g/mol) and CO_2 (m_{CO_2} =44 g/mol) [131]:

$$CaCO_{3,measured} = WL_{CaCO_3} \times m_{(CaCO_3)} / m_{(CO_2)} = WL_{CaCO_3} \times \frac{100}{44}. \tag{5.6.10}$$

Since the decomposition of calcite is not influenced by any potentially overlapping reaction, the stepwise method is appropriate enough for the determination of the mass loss in this temperature interval.

5.6.4. Enthalpy results

The exothermic reactions occurring during heating can theoretically be used for quantification of the amount of unreacted pozzolans. In [238], authors used DTA method for finding the amount of unreacted slag in supersulfated cement

pastes (HR-SSC). Unfortunately, in this case, a precise quantification of the heat generated by the crystallization reaction was nearly impossible because the background was not constant (see Figure 5.6.2).

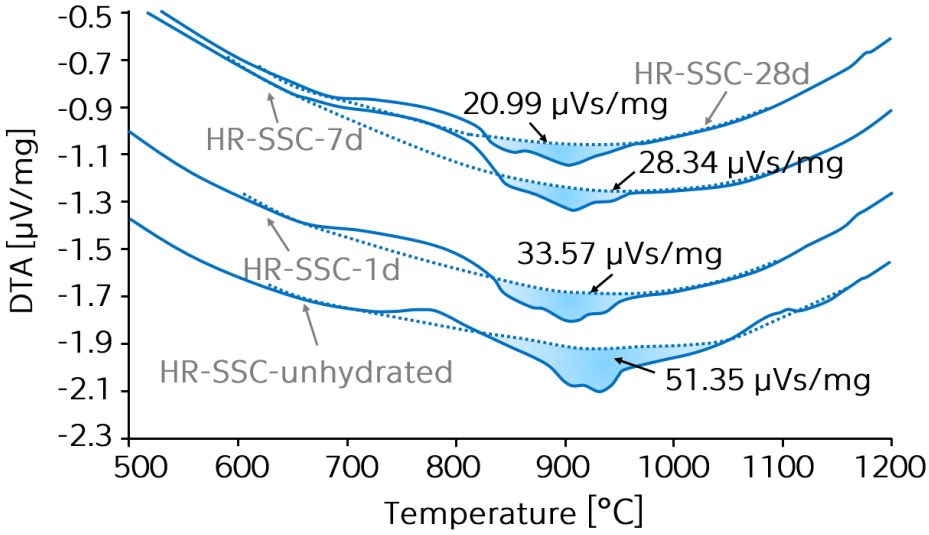

Figure 5.6.2. DTA curves for unhydrated and hydrated (1, 7 and 28 days) HR-SSC with manually fitted baselines and the calculated area under each curve [238].

However, there are many studies [119, 230, 239, 240], where the enthalpy results were successfully used for the description of the development of hydration products. For example, in the study about the effect of burnt clay shale on the evolution of hydration products of high-performance concrete [239], the enthalpy results helped to analyze the Portlandite and calcite decomposition. Moreover, spinel formation, as a side product during heating, was described and its enthalpy referred to the amount of unhydrated burnt clay shale at higher levels of its addition.

For a quantification of the degree of reaction of used pozzolan, it is important to choose an anhydrous material, in which the recrystallization peaks occur in the studied temperature interval, such as slag [225, 238]. Nevertheless, as stated at the beggining of this section, the successfull utiliziation of the enthalpy results is limited by a difficulty to obtain a constant background, which is necessary for the comparison of the results.

5.7. Summary

This section describes This chapter summarized the main methods of thermal analysis, such as TGA and DSC, because these techniques were coupled and used for this study. After a brief description of TGA method, obtained results and its accuracy limitations, such as small size and mass of materials, heat/mass-transfer limitation, low heating or for example balance inclination issues were described. In addition, TGA does not provide the information about the composition of the studied materials. However, it is a very powerful technique, which can be used for the study of hydration processes of cement because it can quantify changes in the production of the main hydration products. In addition, its important advantage lies in its sensitivity towards XRD amorphous materials, such as C-S-H, M-S-H or AH_3, as it is often used as a technique complementary to XRD [131]. On the other side, DSC has been widely used in many various industries, as it provides information about pure phases or the glass fraction (for example in blast furnace slags or fly ash). In hydrated cements, this technique is generally not used quantitatively. Two main experimental arrangements, such as heat flux DSC and power compensation DSC were described. In order to demonstrate the use of DSC in the study of hydration processes, a brief literature review was provided. The information about studied materials can be significantly extended when DSC is coupled with some other methods.

The factors influencing the quality of the obtained results were discussed. One of the main factors, is the heating rate, open or closed crucibles, gas flow, selected sample mass, and especially the chosen sample pre-treatment. As already discussed in the previous Chapter 3, where the hydration stoppage techniques were introduced, hydration processes must be arrested before analyses are done. Therefore, the effect of various hydration stoppage techniques on the TGA results was discussed.

Finally, a simultaneous thermal analysis consisting of TGA and DSC was introduced. The main used parameters were described and the process of quantification of the main hydration products was explained along with a brief literature review. The main parameters determined in this study therefore are the CBW content, Portlandite and calcite. The enthalpy results were used for the study of crystallization processes occurring at higher temperatures.

Studied materials

This chapter describes raw materials, which were selected for this study, such as ordinary Portland cement, silica fume and natural zeolite. After the introduction of these unhydrated powders, the composition and production of studied cement pastes are described. The plain cement pastes were prepared with three different w/c and they were cured under water. The blended pastes with pozzolana active materials (silica fume or natural zeolite) were prepared with one fixed water-to-cement ratio and they were also stored in water. The influence of water environment on the hydration processes, especially on the development of hydration products within the time interval from 2 days to 360 days of age of studied cement pastes was analyzed using several techniques, with emphasis on thermal analysis method. Additionaly, an extra set of all designed cement pastes was prepared and cured in air for a better understanding of the mechanisms of hydration processes. These analyses were performed by means of thermal analysis.

6.1. Raw materials

Ordinary Portland cement CEM I 42.5 R was used as the only one type of the cementitious binder. It was produced by Českomoravský cement, as. (Mokrá, Czech Republic). The main reactive components were with approximately 67% C_3S, 11% C_2S, 7% C_3A, 11% of C_4AF, and about 1.4% MgO, according to the technical lists provided by the company [241].

For this study, two types of finely ground pozzolana active materials, such as natural zeolite ZeoBau 50 provided by the ZEOCEM Corp. (Bystré, Slovak Republic), and industrially prepared silica fume Stachesil S (Stachema CZ, Kolín, Czech Republic) were chosen (Figure 6.1.1). In the case of natural zeolite, clinoptilolite was selected for its unique structure and properties. It contains between 50–60% of amorphous SiO_2. This kind of zeolite is used mainly because of its adsorption, ion-exchange, molecular sieve and catalytic properties [242].

Silica fume is used in a form of very fine powder. As already discussed in the chapter with pozzolana active materials, its utilization has a positive impact on rheological properties of concrete, as it improves mechanical properties and durability. Based on the product sheet, it is recommended to use it in amounts of 5–10 wt.% [243].

Figure 6.1.1. Raw materials used for the study. From the left: natural zeolite, silica fume, ordinary Portland cement.

The chemical composition of the raw powders, as determined by means of the XRF method, is summarized in Table 6.1.1. The chemical composition of cement is usually measured more frequently because it can vary within different batches. The cement 1 was used for the study of plain cement pastes with different cement to water ratio and stored in different environments (in air for thermal analysis study and under water for basic physical and mechanical properties).

Table 6.1.1. Chemical composition of the raw materials in wt.%.

Component	SiO_2	Fe_2O_3	Al_2O_3	CaO	MgO	SO_3	Na_2O	K_2O	d_{50} (μm)
Cement 1	19.9	3.8	5.7	63.3	1.0	3.3	0.1	1.1	11.3
Cement 2	21.9	3.8	5.6	62.3	1.0	2.9	0.1	0.9	-
Cement 3	19.0	2.4	4.3	62.9	1.8	3.2	0.1	0.8	-
Silica fume	94.6	0.5	0.4	0.5	0.5	0.8	0.3	1.6	0.5
Zeolite	74.5	1.6	15.4	3.3	0.7	-	0.6	3.5	24.3

The cement 2 with a very similar composition was used for the study of the blended cement pastes. The last batch was used for a preparation of small samples for thermal analysis study of all studied pastes stored under water.

From the results summarized in Table 6.1.1, it can be therefore seen that the cement used in this study consisted mainly of CaO and SiO_2. Minor components, such as Al_2O_3, SO_3 and Fe_2O_3 were also detected in its composition. It was confirmed that silica fume contained almost 95% of SiO_2. And finally, the natural zeolite consisted mainly of SiO_2 and Al_2O_3. The specific surface area (based on the Blaine method) was the lowest for cement, about 385 m^2/kg; it was 1560 m^2/kg for natural zeolite, and the highest specific surface area was determined for silica fume, where it reached the value of 4830 m^2/kg. The mineralogical composition of natural zeolite was determined using the Rietveld method. It consisted mainly of clinoptilolite (54.8%), cristobalite (10.7%), quartz (2.6%), albite (6.7%), muscovite (2.9%), and amorphous (glassy) phase (22.3%). SEM photographs of all studied powders are shown in Figure 6.1.2.

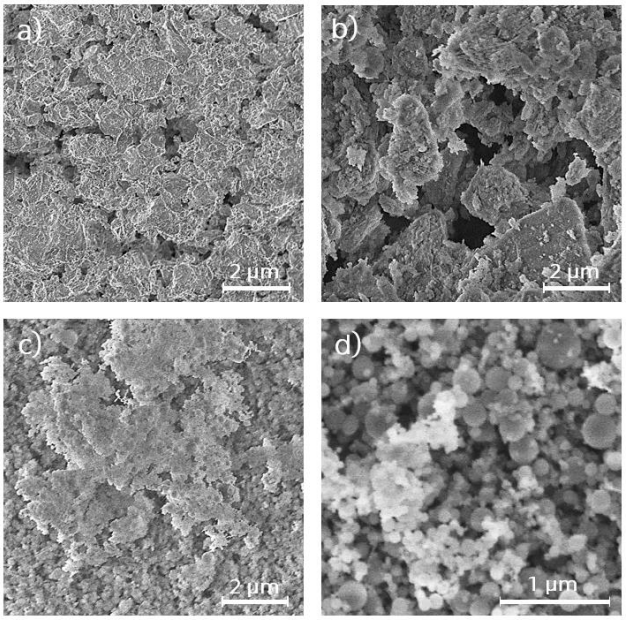

Figure 6.1.2. SEM photographs of the raw powders: a) cement, b) natural zeolite, c) and d) silica fume.

Cement and natural zeolite were measured with the same magnification (10000x), whereas silica fume, as the finest powder, was determined also more in detail (10000x and 30000x, Figures 6.1.2c and d, respectively). While silica fume tended to agglomerate and create clusters, natural zeolite particles seemed to form rather flat layers surrounded by large voids. Particle size distribution curves of the powders analyzed by a laser diffraction method are given in Figure 6.1.3.

They show distinct differences between the powdered materials. The median particle size d50 of each powdered material is summarized in Table 6.1.1.

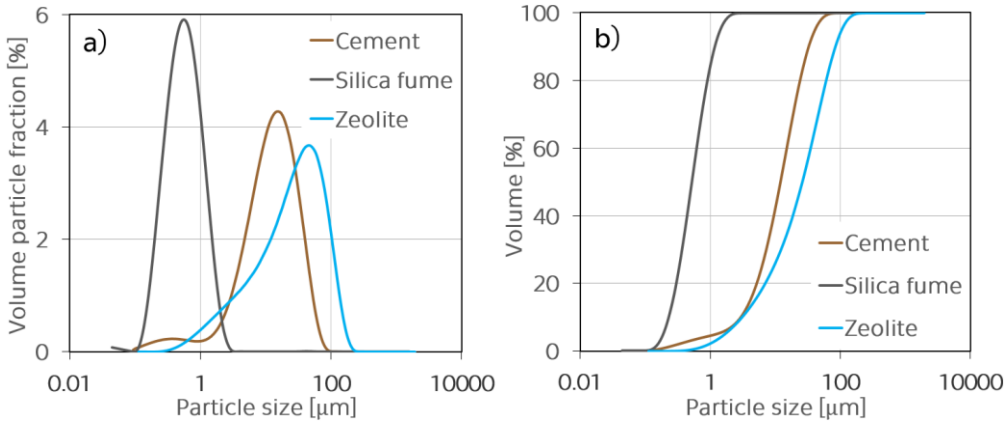

Figure 6.1.3. (a) Particle size distribution curves and (b) cumulative particle size distribution curves of the raw powders.

The quality check of the used cement was done by simultaneous thermal analysis in cases where the same cement was used during the first three months from the opening of the selected batch (cement 1). The quality check was done every month. From the results demonstrated in Figure 6.1.4, it can be therefore seen that the storage of cement in well-closed plastic bags was sufficient enough to keep the initial state of the used cement for the sample preparation during this period. The quality check was not done when the cement was used only once, immediately after the batch was opened (cement 2 and 3).

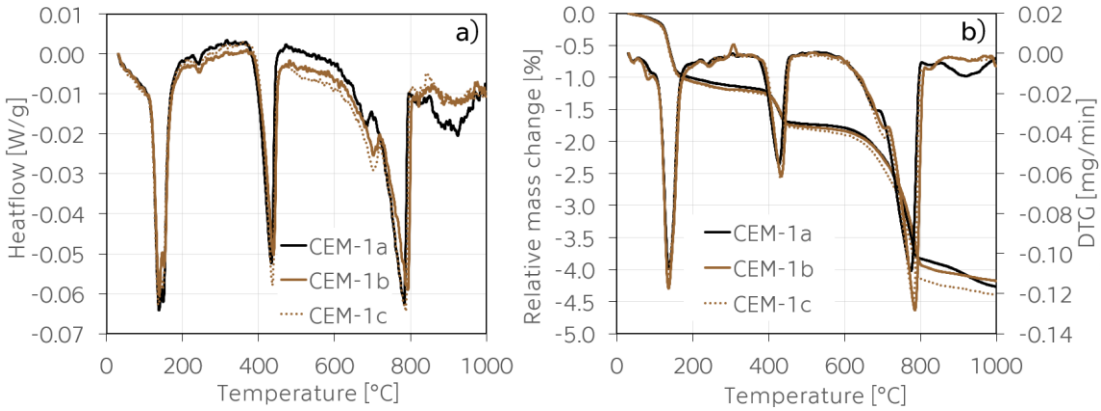

Figure 6.1.4. (a) Heatflow and (b) TGA/DTG curves of studied cement 1.

However, it should be noted that the initial state of used cement exhibited pre-hydration behavior, as in fresh cements, only minor mass losses, mainly

between 110 and 150 °C can be found. They are associated to gypsum and hemihydrate. Ettringite can be formed in the aged samples [131]. In this study, also small peaks related to Portlandite decomposition (360–480 °C) and $CaCO_3$ decomposition at higher temperatures (490–810 °C) were found. It is given by the ageing history of the cement due to its production and storage until its delivery. Nevertheless, the mass loss in the Portlandite decomposition stage was only about 0.5%, and in the case of $CaCO_3$ it was between 2.1–2.3%.

In terms of silica fume and natural zeolite, the thermal analysis results were used to describe their thermal stability (Figure 6.1.5). Silica fume has a complex phase diagram as it undergoes several structural changes when heated. The exothermal peak starting around 170 °C and finishing around 240 °C could be associated to recrystallization of a metastable cristobalite, which is commonly present in silica fume, or less possibly to a metastable tridymite, as discussed deeper in [244, 245].

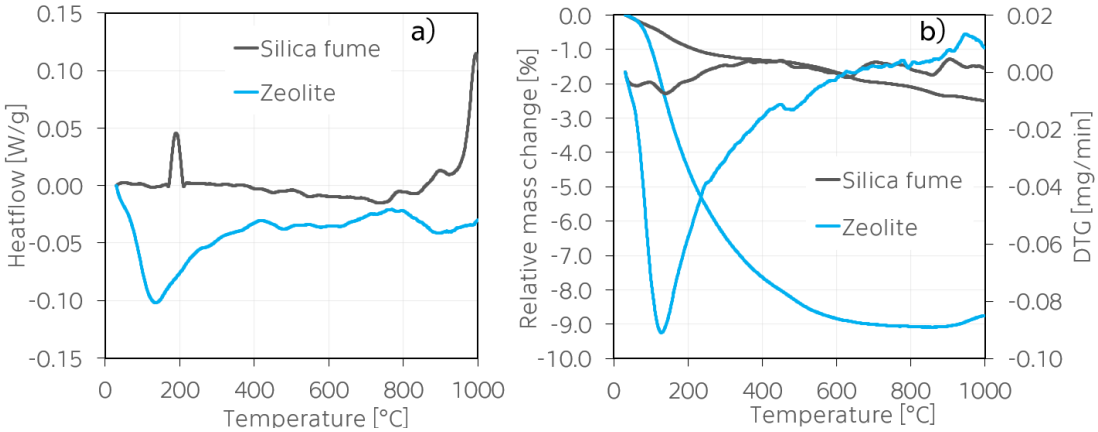

Figure 6.1.5. Heatflow curves of silica fume and natural zeolite.

Above 900 °C, an unfinished exothermal peak could be related to formation of a stable modification of cristobalite [244, 245], resulting in a compact structure of silica fume due to the reconstruction of the broken bonds caused by the dehydration reaction [246]. The related mass changes, as a result of these processes, are not significant, as the total mass loss was lower than 3% after the analysis (Figure 6.1.5b). In the case of natural zeolite, one main endothermal peak was detected in the temperature interval from 25 °C to about 400 °C (Figure 6.1.6a). The associated mass loss was continuous during heating. The main mass loss is related to loss of hygroscopic water and of the water residing in the

channels and the cavities of the zeolite framework, respectively [247]. It was reported that there are two forms of water in the structure of clinoptilolite – intact molecules and OH groups present in the structure of silicate minerals. Intact water can be eliminated at temperatures below 100 °C, whereas for the removal of hydroxyl groups it is needed to apply temperatures above 400 °C [248]. More precisely, the structural water (OH groups) is eliminated from clinoptilolite after 360 °C [249]. The total mass loss observed in this study was about 9%, which is slightly lower than in [250]. The increasing trend of mass change (mass gain) at the end of the measurement was probably caused by some impurities in the studied material.

6.2. Composition of studied cement pastes

Several cement pastes were designed for this study. Their composition with used system of labelling is summarized in Table 6.2.1. The plain cement pastes contained only cement and water with the w/c ratio of 0.3, 0.4, and 0.5. The blended cement pastes with pozzolana active materials were prepared with the fixed water-to-cement ratio of 0.5.

Table 6.2.1. The detailed composition of studied cement pastes.

Material	Water [kg]	CEM* [kg]	NZ* [kg]	SF* [kg]	Label
Reference paste (w/c of 0.5)	1	2	-	-	REF
Paste with w/c of 0.4	0.8	2	-	-	R04
Paste with w/c of 0.3	0.6	2	-	-	R03
Paste with 8 wt.% of ZeoBau 50	1	1.84	0.16	-	CZ8
Paste with 16 wt.% of ZeoBau 50	1	1.68	0.32	-	CZ16
Paste with 24 wt.% of ZeoBau 50	1	1.52	0.48	-	CZ24
Paste with 40 wt.% of ZeoBau 50	1	1.20	0.80	-	CZ40
Paste with 4 wt.% of Stachesil S	1	1.92	-	0.08	MS4
Paste with 8 wt.% of Stachesil S	1	1.84	-	0.16	MS8
Paste with 12 wt.% of Stachesil S	1	1.76	-	0.24	MS12

*CEM–cement, NZ–natural zeolite, SF–silica fume.

Natural zeolite (with no additional preparation) was used as a partial replacement for the cement in the amounts 8, 16, 24, and 40 wt.%. As silica fume is recommended to be used in lower amounts, it partially replaced only 4, 8 and 12 wt.% of cement.

6.3. Generic sample casting

The procedure of the sample preparation was as follows: In the case of cement pastes with various water-to-cement ratios, fresh cement was firstly homogenized by hand and then it was added to a desired amount of water. The mixture was mixed in a laboratory mixer for 60 s at low speed and another 30 s at higher speed, whipped off, and mixed again for another 60 s at high speed. Thereafter, the mixture was removed from the mixer and put into the molds. The samples for physical and mechanical properties were prepared with the dimensions of 160 × 40 × 40 mm, the samples for SEM, XRD, MIP and thermal analysis were put in small plastic vessels and were covered by a plastic foil.

In the case of blended cement pastes, which contained natural zeolites or silica fume, respectively, cement and pozzolana were mixed together first until homogenized. Except this first step, the procedure of mixing was the same like in the case of the plain cement pastes. After putting into the molds, samples were covered by a plastic foil. All samples were stored in laboratory conditions for first 24 hours. After this time, samples were put in water, where they were cured up 360 days. Most of the analyses were performed after 28 days and 360 days of hydration, only mechanical properties and thermal analysis were studied more frequently. Additionally, one extra set of all studied pastes was prepared and let to hydrate in the laboratory conditions (atmospheric air, constant temperature of 25 °C). These pastes were studied by thermal analysis only.

It should be noted that in the case of plain cement pastes with w/c ratio of 0.5, the "actively" used amount of water, which would be participating during the hydration processes, was slightly lower than expected – a separated layer of water was created at the top of fresh samples during first hours of hydration. This water was collected. After measuring the mass of this redundant water, it was computed that the real w/c ratio used in this study was approximately 0.45. This effect was not observed in the case of blended cement pastes.

6.4. Hydration stoppage

As already discussed in the Chapter 3, due to the limited time for analyses, the hydration of cements is usually stopped to avoid alternation of the hydrates and to preserve the microstructure of studied materials. It is done by removing water present in the pores, without removing the water from the hydration products [131]. The hydration stoppage techniques used in this study are summarized in Table 6.4.1.

Table 6.4.1. Stoppage techniques used to arrest hydration.

Method	Days of hydration					
	2	7	28	90	180	360
SEM-W	-	-	Iso/S	-	-	Iso/S
XRD-W	-	-	Iso/S	-	-	Iso/S
MIP-W	-	-	Iso/S	-	-	Iso/S
Basic physical properties-W	-	-	Ov	-	-	Ov
Mechanical properties-W	SD	SD	SD	SD	SD	SD
DSC/TGA-W	Iso/S	Iso/S	Iso/S	Iso/S	Iso/S	Iso/S
DSC/TGA-A	SD	SD	SD	SD	SD	SD

Iso–isopropanol; S–samples were sealed during curing; Ov–oven drying at 105 °C; SD–performed at a selected day; W–cured in water; A–cured in air.

Plain and blended cement pastes, which were stored in air in laboratory conditions at 25 °C, were analyzed only in terms of thermal analysis (DSC/TGA-A). These experiments were performed at the selected days of hydration, thus, there was no need to arrest the hydration processes. Samples were ground into powders at the same day of the analysis. The measurements of mechanical properties were also done at the selected days of hydration on the wet samples as taken from the curing boxes. Samples for basic physical properties were dried at selected days of hydration in oven at 105 °C until constant mass. Finally, samples for SEM, XRD, MIP and DSC/TGA analyses were immersed in isopropanol at selected days of hydration, where they were kept for three months. At the time, where these analyses were done (2016), there was no information about removing the isopropanol with diethyl ether, mentioned later in [131]. Therefore, the samples were let in air for couple of hours before the analyses were done.

Characterization of plain cement pastes

This chapter summarizes experimental results of the effect of w/c ratio on the hydration processes of plain studied cement pastes labelled as R03, R04 and REF. At first, the early-stage hydration heat development is described. This study is mainly oriented on the description of the long term hydration processes, therefore the most of the presented characteristics, such as SEM, XRD, MIP and basic physical properties, are determined on cement pastes at 28 and 360 days of hydration. Only mechanical properties, similarly to thermal analysis, are determined more frequently at 2, 7, 28 and 360 days. All results presented in sections 7.1–7.4 were obtained from experiments performed on samples cured in water.

7.1. Hydration heat

The results of the early-stage hydration heat development of studied plain cement pastes with various w/c ratio are shown in Figure 7.1.1. The description of the results follows the division of the Figure 2.2.1, based on which the hydration mechanisms of alite were explained. The positions of the extremes of the time-dependent specific hydration power $N(t)$ (Figure 7.1.1a) were influenced by the w/c ratio as follows: The initial reaction reached the highest values in the R04 paste and it was found to be the lowest in the REF paste. The differences between the R03 and REF pastes were very low, while in the case of the R04 paste, the specific hydration power was significantly higher. The following period of slow reaction, representing the first local minimum, was observed within the time range of 3.5–5 h. Its time position increased with increasing w/c. The N value at this minimum was almost the same, independent of w/c. The following acceleration period, appearing within the time period of 12–15 h, was influenced by w/c ratio the most visibly. Its position increased with increasing w/c.

N reached the highest value for the lowest w/c, and gradually decreased with increasing w/c. Finally, the deceleration period (within 20–30 h) was characteristic by the decrease of *N*. The most visible shift into lower values was observed for the R03 pastes, the highest values were found for the REF pastes.

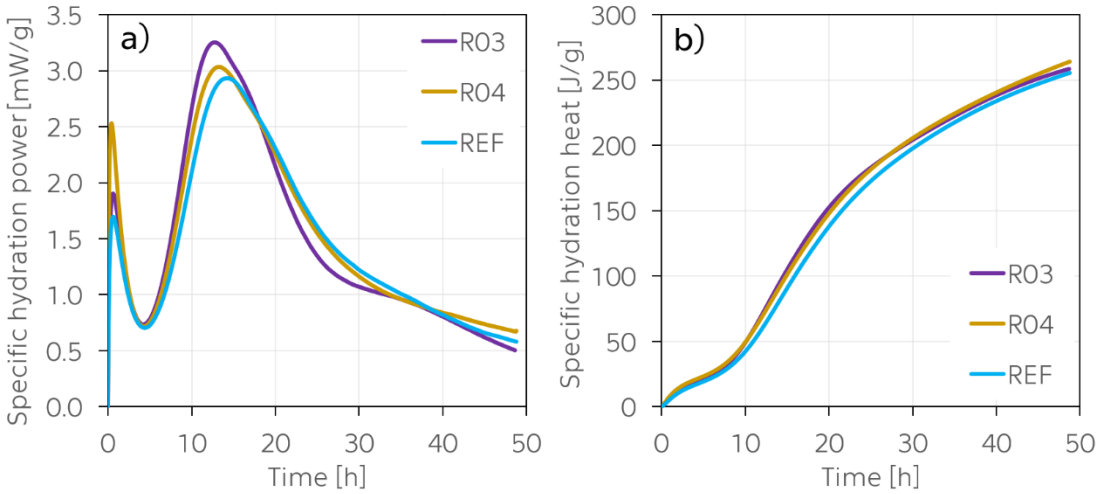

Figure 7.1.1. Specific hydration power (a) and specific hydration heat (b) of cement pastes as a function of time and w/c ratios.

This phenomenon was also observed for example in [251], where it was clearly seen that as w/c ratio decreased, the peak of the heat evolution of studied cementitious materials was shifted slightly to the left. One of the possible explanations is that the initial ion concentration for mixes with different w/c was not the same. For the materials with a lower w/c, more particles were dispersed in a given volume of water compared to those materials with a higher w/c. It could mean that due to the relatively higher chemical ion concentration in the low w/c system, a more rapid hydration occurred. Therefore, a slightly higher rate of heat evolution was determined. After a certain time of hydration, the materials with a lower w/c started to set earlier, which was caused by the hydration products coated on the surface of the unhydrated cement particles, and filled the limited spaces among the unreacted cement particles. This led to a decceleration of the cement hydration (the shift to the left) [251]. Some similar studies on the impact of w/c ratio on the hydration heat development of cement pastes were done by other investigators [64, 252-255]. In [252], a similar decrease of the second local maximum at cement pastes with the w/c ratio of 0.35–0.425 was observed. The initial reation was faster in [252] when compared to this study, which could be given by the different compositions of the used cement.

7.2. Microstructural development

The evolution of microstructure of the studied pastes was determined by means of various methods, such as SEM, XRD, and MIP. The representative SEM micrographs taken using 20000x magnification are displayed in Figure 7.2.1.

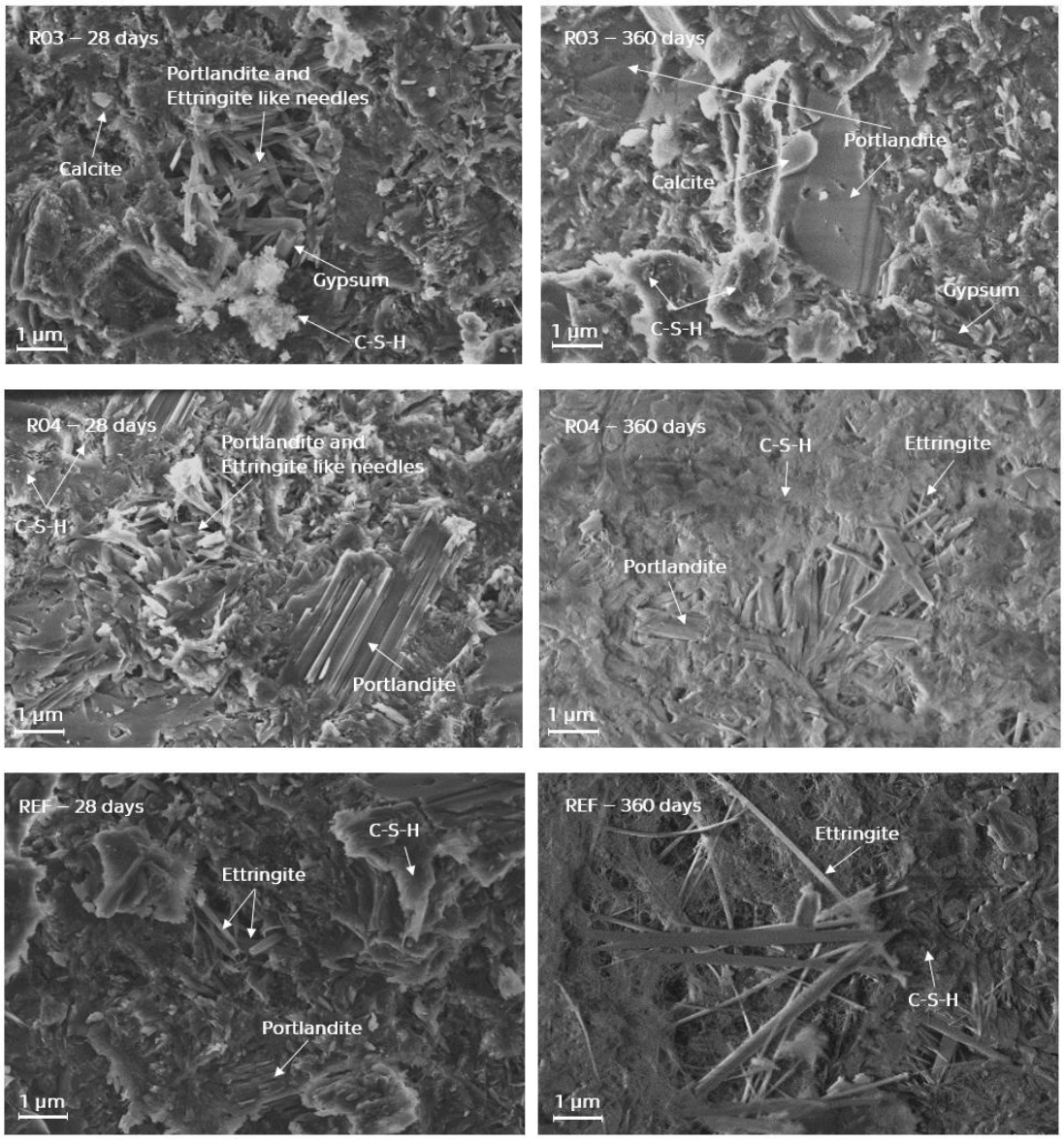

Figure 7.2.1. SEM micrographs of cement pastes after 28 and 360 days.

Observations were made across several points on the surface of each sample. It was clearly seen that the w/c ratio influenced the morphology and homogeneity of the hydration products of studied pastes, which was in a good agreement with results published in [256], where it was reported that a lower w/c ratio led to an increase in the homogeneneity of hydration products and it caused

a reduction of the content of crystalline hydrates, primarily Portlandite. The structure of R03 pastes with the lowest w/c ratio contained besides hydration products also a higher amount of unhydrated cement grains, even after 360 days. Portlandite and ettringite were observed in a form of needles on the surface of all studied pastes after 28 and 360 days of hydration. However, in pastes with a higher w/c ratio (R04 and REF), it was observed that Portlandite formed larger, rather lamellar (shape of columms) crystals, similar to those reported in [256]. After 360 days of hydration, the surface of the studied pastes was fully covered by dense hydration products. The presence of these hydration products was confirmed also by the XRD method.

The XRD patterns of the studied cement pastes are summarized in Figure 7.2.2. Based on these results, it can be seen that the w/c ratio affected the evolution of hydration products only slightly – mainly the intensity of the Portlandite peaks. The amounts of the crystalline and amorphous phases were calculated based on the internal standard phase, 20 wt.% of ZnO. Unfortunately, the XRD method cannot provide a more detailed information about the composititon of the amorphous phase. It might be consisting besides C-S-H also from amorphous $CaCO_3$ or some other phases not detectable by XRD. The computed results are summarized in Table 7.2.1.

Table 7.2.1. Mineral composition of the studied pastes in wt.%.

Material	After 28 days			After 360 days		
	R03	R04	REF	R03	R04	REF
Alite	10.1	10.6	7.5	10.7	8.4	7.3
Amorphous	61.6	60.9	63.1	62.0	67.5	66.7
Belite	3.7	4.5	4.4	4.5	2.7	2.6
Calcite	4.4	3.4	3.2	2.8	2.9	3.2
Ettringite	1.7	2.5	4.7	4.0	3.8	4.5
Ferrite	5.4	3.3	3.5	3.8	1.5	1.4
Gypsum	1.6	1.4	1.2	1.1	1.0	1.2
Portlandite	11.4	13.0	12.3	10.9	11.8	12.8
Quartz	0.2	0.4	0.2	0.3	0.4	0.3

The amount of amorphous phase was very similar for all studied pastes after 28 days of hydration, and it was around 61–63 wt.%. It had an increasing trend in time, except for R03, which could mean that the main part of hydration processes

was finished already after 28 days of hydration in this paste. Alite and belite were found in higher amounts in R03 and R04 pastes compared to the REF paste.

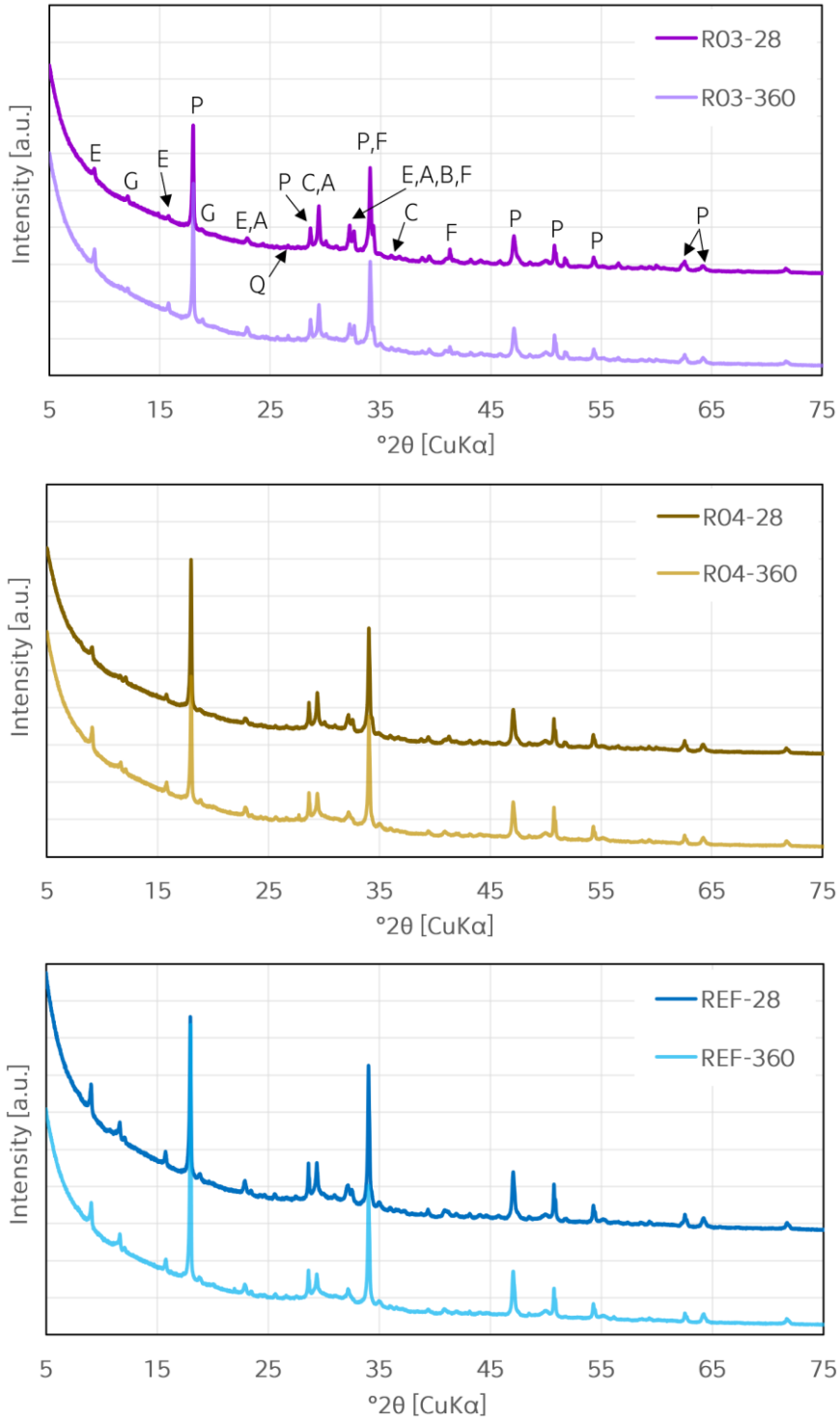

Figure 7.2.2. XRD patterns of studied cement pastes after 28 and 360 days: A–alite, B–belite, C–calcite, E–ettringite, F–ferrite, G–gypsum, P–Portlandite, Q–quartz.

Their amounts decreased in time in R04 and REF pastes, while it remained almost at the same level in R03. It is in a good agreement with the SEM analysis, where alite and belite were spotted in forms of unhydrated cement grains in the R03 paste. The amount of ettringite increased in pastes with increasing w/c ratio after 28 days, while it was found to be a very similar in all pastes after 360 days. It could mean that at the early age, water content helped with its creation, while at later ages, these initial differences disappeared. The highest amount of ferrite was found in pastes with the lowest w/c ratio after 28 days and its content gradually decreased with increasing w/c ratio and time. The amount of Portlandite was found to be very similar in all studied pastes. In time, it slightly decreased in R03 and R04, while in REF paste its increase was probably caused more likely by the uncertainty of the analysis. Therefore, the water environment with a low CO_2 content prevented carbonation processes. Moreover, the amount of calcite even tended to decrease in R03 and R04 with time. This phenomenon will be discussed deeper in the chapter with the thermal analysis results.

The effect of w/c on the development of the porous system was also studied by the MIP method. Cumulative intruded pore volume curves and pore size distribution obtained for the studied cement pastes are summarized in Figure 7.2.3.

As expected, the curves of the REF paste with the highest w/c exhibited the highest porosity values after both, 28 and 360 days. The lowest porosity was observed in the R03 paste. The cumulative pore volume curves (Figure 7.2.3a, c) showed a continuous trend for all pastes, with the highest amounts of pores with diameters between 0.01 μm and 0.1 μm. As hydration processes continued, the structure of the pastes had become more compact, and therefore less porous, which can be seen especially in the R03 samples with the lowest w/c ratio, where the amounts of pores decreased most visibly (Figure 7.2.3b, d). The significant shift, which occurred on the cumulative pore volume curve of the R04 paste after 28 days, was probably caused be a group of larger pores. These larger pores are also visible on the related graph of the pore size distribution between 10 μm and 100 μm (Figure 7.2.3b).

From the results from SEM, XRD and MIP method, it can be clearly seen that different w/c influenced the evolution of microstructure of the studied cement pastes. These results can be summarized as follows: A lower w/c ratio led to an

increase in the homogeneity of hydration products and it caused a reduction of the content of crystalline hydrates, primarily Portlandite.

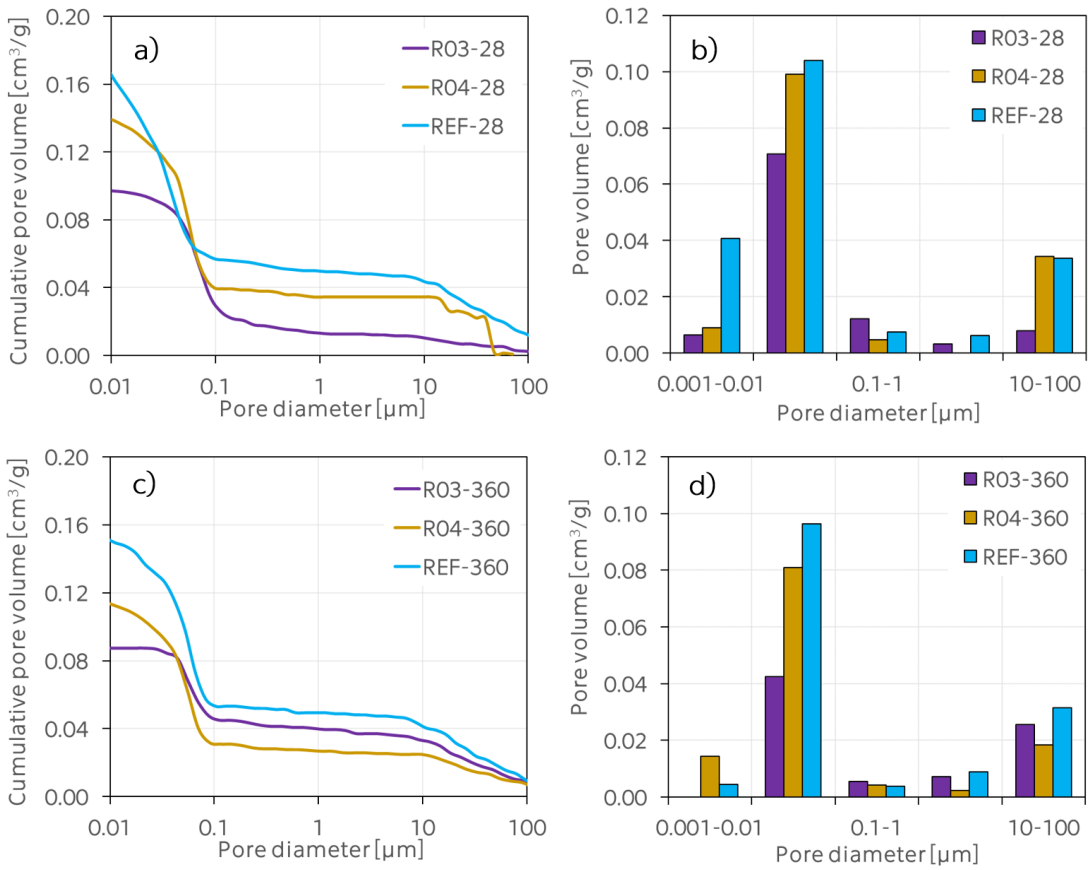

Figure 7.2.3. Dependence of the cumulative pore volume curves and pore size distribution of studied pastes on the w/c ratio.

The amount of Portlandite was found to be very similar at all studied pastes. In time, it slightly decreased at R03 and R04, while for the REF paste its increase was probably caused more likely by the uncertainty of the analysis. Because Portlandite was not consumed by the carbonation processes (the amount of calcite even slightly decreased in time), it can be seen that the water environment with a low CO_2 content prevented carbonation of the plain cement pastes. In terms of the cumulative pore volume curves, they showed a continuous trend at all pastes, with the highest amounst of pores with diameters between 0.01 µm and 0.1 µm. In time, as hydration processes continued, the structure of the pastes had become more compact, and therefore less porous. This effect was most visible for pastes with the lowest w/c ratio.

7.3. Basic physical properties

Basic physical properties, such as matrix density, bulk density and total open porosity were analyzed for pastes after 28 and 360 days. Before the analysis, the studied pastes were dried at 105 °C until constant mass was achieved. The results are summarized into Table 7.3.1. In terms of the matrix density, the highest value was determined in the R03 paste after 28 days, where it reached 2359 kg/m^3 in average. It significantly decreased with increasing w/c ratio, by about 6% in the REF paste. The matrix density slightly decreased in time in all studied pastes.

Table 7.3.1. Basic physical properties of studied pastes

Paste	Age [days]	Matrix density [kg/m^3]	Bulk density [kg/m^3]	Total open porosity [%]
R03	28	2359	1808	23.4
R04	28	2248	1638	27.1
REF	28	2229	1550	30.5
R03	360	2212	1891	14.5
R04	360	2132	1793	15.9
REF	360	2062	1702	17.5

The bulk density showed a similar tendency to the matrix density, as it reached the highest values also in pastes with the lowest w/c ratio, 1808 kg/m^3 in average and it exhibited a decreasing trend with increasing w/c ratio. The bulk density in the REF pastes reached about 15% lower values than the R03 pastes. An increasing trend of the bulk density with time is a result of hydration processes. The open porosity of the studied pastes was about 30.5% in the REF pastes after 28 days and it was slightly lower in pastes with lower w/c ratios. It is in a good agreement with the MIP results presented in Figure 7.2.3. After 360 days of hydration, the open porosity decreased by up to 13% in the case of the reference paste and about 8.9% for the R03 paste. In summary, the lower w/c ratio is chosen, the more compact and less porous the final structure of cement pastes is. These results are in a good accordance with the data found in literature [67, 70, 257].

7.4. Mechanical properties

The results of the mechanical properties are shown in Figure 7.4.1. The R03 pastes reached the highest compressive and flexural strength results at all selected days of study, which is in a good agreement with the porosity results and the results of basic physical properties, and with data reported in [233].

After 28 days of hydration, the pastes with the lowest w/c ratio exhibited the highest compressive strength, 70.88 MPa, which was about 28% higher than the REF pastes. Very similar values of compressive strength after 7 and 28 days were observed for these pastes (R03), which could be caused by an uncertainty of the measurements or by the lack of water available to support the hydration processes. At the end of the studied period, 360 days, the compressive strength for R03 paste was 93.79 MPa, which was about 15% and 36% higher than for the R04 and REF pastes, respectively.

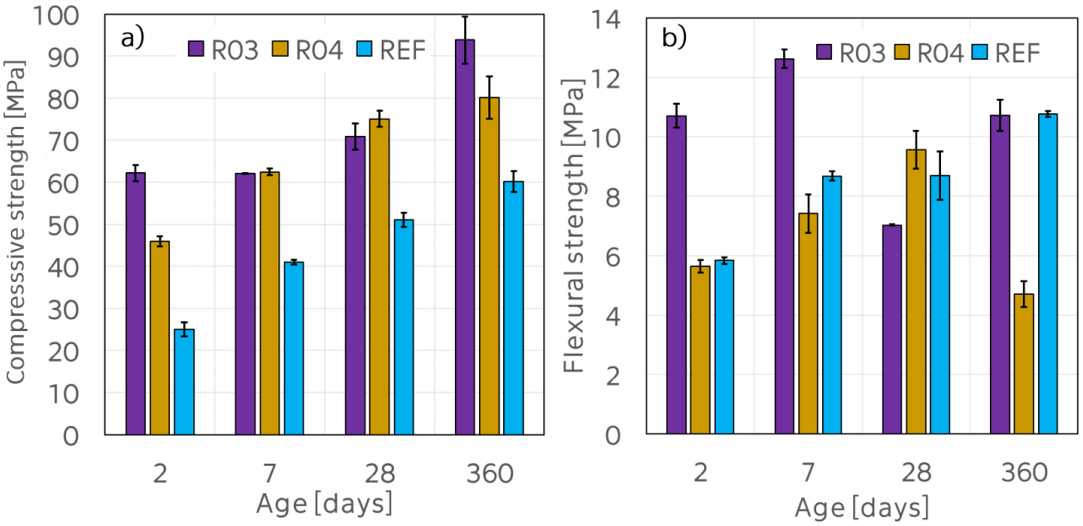

Figure 7.4.1. Mechanical properties of the studied pastes: a) compressive and b) flexural strength as a function of w/c and time.

In terms of flexural strength, the R03 paste reached relatively high values after 2 and 7 days of hydration (10.7 and 12.6 MPa) compared to the other pastes. Nevertheless, this initial increase in strength was higher than the values for 28, 90 and 180 day-strength. It could be caused by inhomogeneity of the studied samples, as there were unhydrated cement grains present in their structure. The final flexural strength for R03 was 13.6 MPa. The initial flexural strength was

6.9 MPa and 5.8 MPa for R04 and REF pastes, respectively. After 360 days of hydration, these values increased slightly above 12 MPa for both pastes.

From the trends of both, compressive and flexural strength results, it can be clearly seen that the higher w/c is used in cement pastes, the lower values of mechanical properties are, which is in a good agreement with results published in [73].

7.5. Thermal analysis results

In this section, the thermal analysis was used to determine the effect of w/c ratio on the hydration products when samples were stored in two different environments. For this purpose, the results of thermal analysis of plain cement pastes stored in water (W) are compared to those cured in air (A). These results are summarized in Figures 7.5.1–7.5.3.

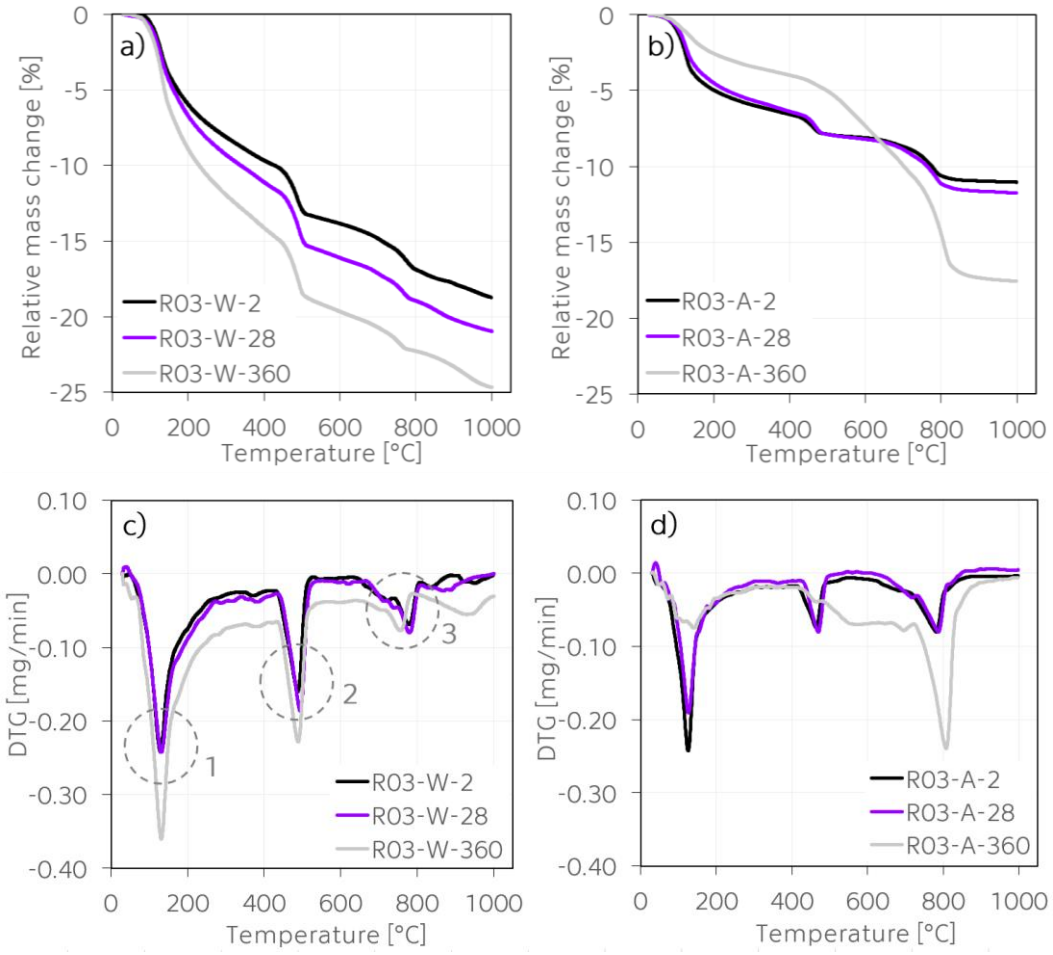

Figure 7.5.1. Thermal analysis results for R03 paste stored in:
(a, c) water and (b, d) air.

Each designed paste was analyzed 3-times when cured in air, and 2-times when cured under water after 2, 7, 28, 90, 180 and 360 days of hydration (30 experiments in total per a paste). Thus, for an easier orientation in the obtained results, only selected experiments after 2, 28 and 360 days of hydration of relative mass change [in %] and its derivation [in mg/min] are shown for both studied environments. However, the related computations are done with the utilization of all experiments. The results of heatflow curves are not provided in this section, as they are used for a description of crystallization processes at cement pastes blended with pozzolana active materials.

A further analysis of the TGA results is divided based on the most significant mass changes spotted by DTG, as illustrated in Figure 7.5.1c.

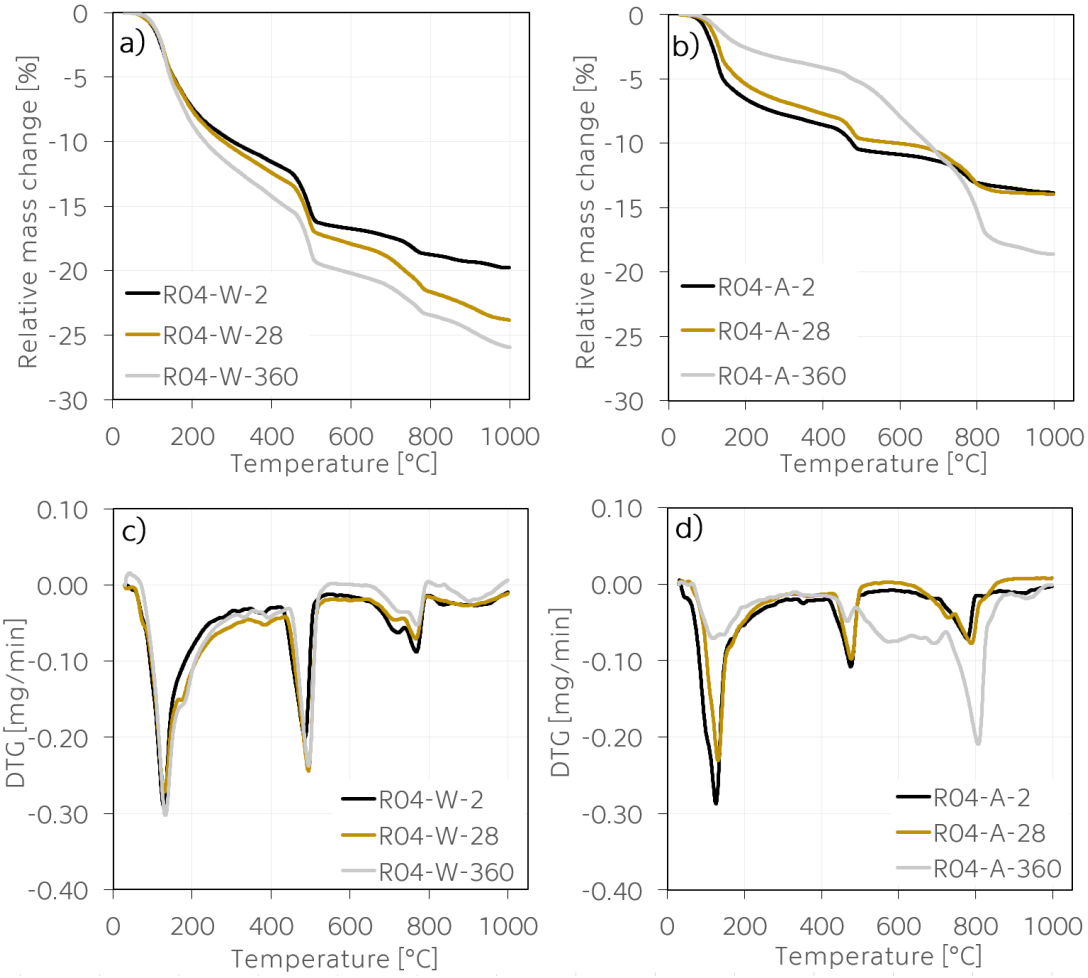

Figure 7.5.2. Thermal analysis results for R04 paste stored in:
(a, c) water and (b, d) air.

These three peaks can be found in all studied pastes. The first peak, labelled as 1, usually occurring in the temperature interval from 25 °C to about 330 °C, is related to the decomposition of C-S-H, ettringite and gypsum [131]. It is characterized by a release of the physically bound and a part of the CBW. Because all these mentioned components decompose in a very similar temperature interval, it is nearly impossible to quantify their specific amounts in the structure of the studied pastes by thermal analysis.

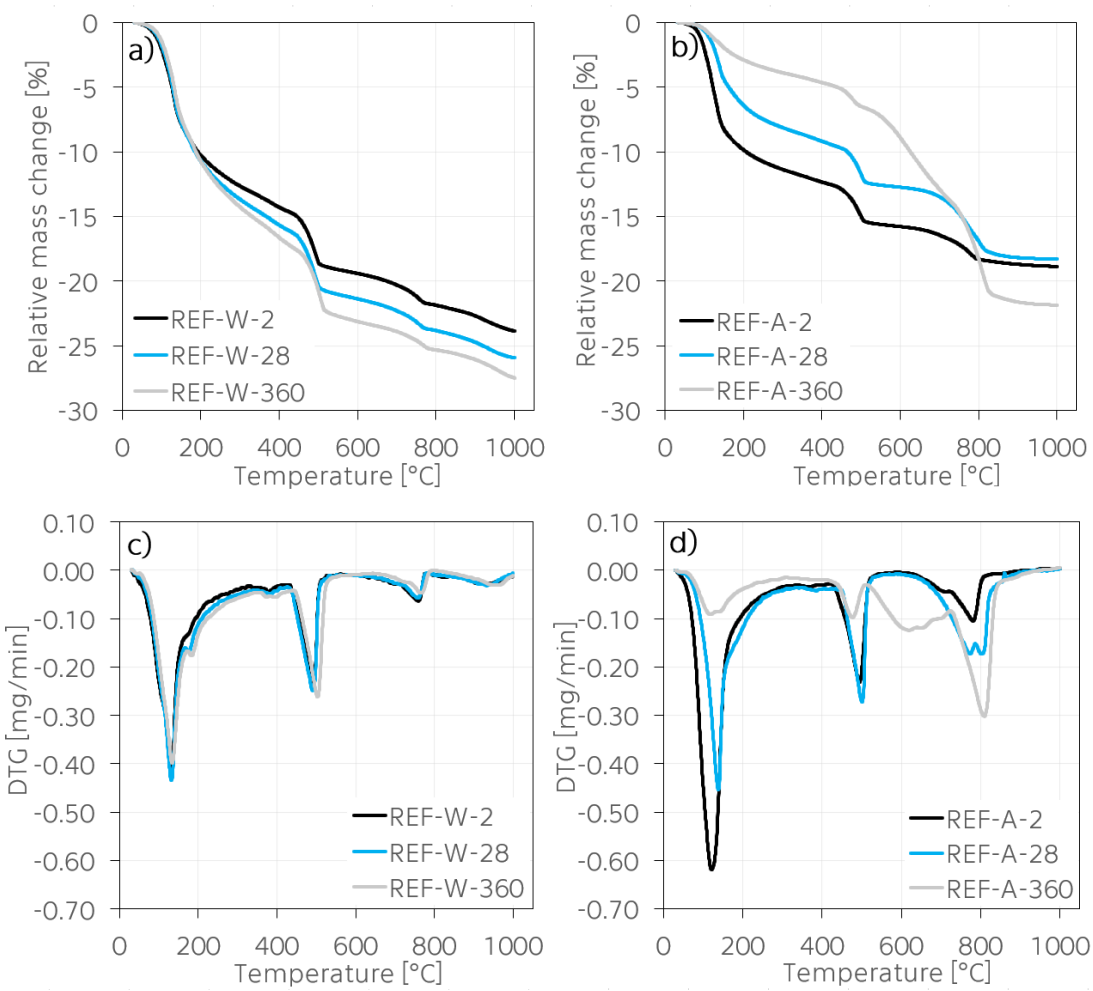

Figure 7.5.3. Thermal analysis results for REF paste stored in:
(a, c) water and (b, d) air.

Thus, the analysis of this peak area is rather focused on the determination of the amount of the CBW, which is released not only in the first temperature area, but also during the decomposition of Portlandite, which occurs between 400 and 550 °C (labelled as 2). The changes in the Portlandite and calcite (3) contents as a function of time and w/c are analyzed in the following separated sections.

7.5.1. Chemically bound water

In order to determine the CBW of studied pastes, two methods suggested by De Weerdt et al. [203] and Bhatty [235] were utilized. These methods were described in detail in Section 5.6.1. To ensure that the computations are done only with the CBW content, the initial mass of measured samples was taken at 135 °C. This temperature was determined experimentally and it is also in a good accordance with [5, 236, 258]. Therefore, the CBW was estimated by the difference in mass between 135 °C and the end of the decomposition of Portlandite for the method proposed by De Weerdt et al. [203], while this interval was extended up to 1000 °C in the case of the Bhatty's method [235]. The ranges used for these calculations are given in Table 7.5.1. Since the CBW content is mainly used for the determination of the degree of hydration, this section deals only with pastes stored in water, because the hydration processes were fully supported only in this environment.

Table 7.5.1. Temperature ranges of different solid phases.

Region	Temperature range [°C]
Ldh – dehydration	135–400
Ldx – dehydroxylation	400–600
Ldc - decarbonation	600–1000

Selected mass change values, as obtained from the TGA experiments, are presented in Table 7.5.2.

Table 7.5.2. Selected mass loss values [in mg] determined by TGA.

Paste	Age [days]	M_{sample}	$M_{135°C}$	$M_{400°C}$	$M_{600°C}$	$M_{1000°C}$
R03-W	2	50.4	48.53	44.93	43.27	40.42
	28	50.4	48.64	44.46	42.56	39.51
	360	51.1	48.74	43.53	41.35	38.49
R04-W	2	50.6	48.58	45.18	43.23	40.29
	28	50.1	48.22	43.49	41.23	38.39
	360	49.5	47.30	41.62	39.31	36.19
REF-W	2	51.2	48.19	43.97	41.70	39.15
	28	51.2	48.57	43.28	40.85	38.25
	360	50.4	47.61	41.57	39.01	36.54

The mass changes from the decomposition of Portlandite were determined individually for each sample. For the method proposed by De Weerdt et al. [203], the highest values of the CBW (Figure 7.5.4a) were obtained in the cement pastes with the highest w/c ratio (REF-W) during the whole studied time interval. The CBW content was determined as 15.6% after 2 days of hydration and it reached 21.8% after 360 days. This trend was in a good agreement with [203, 232, 233].

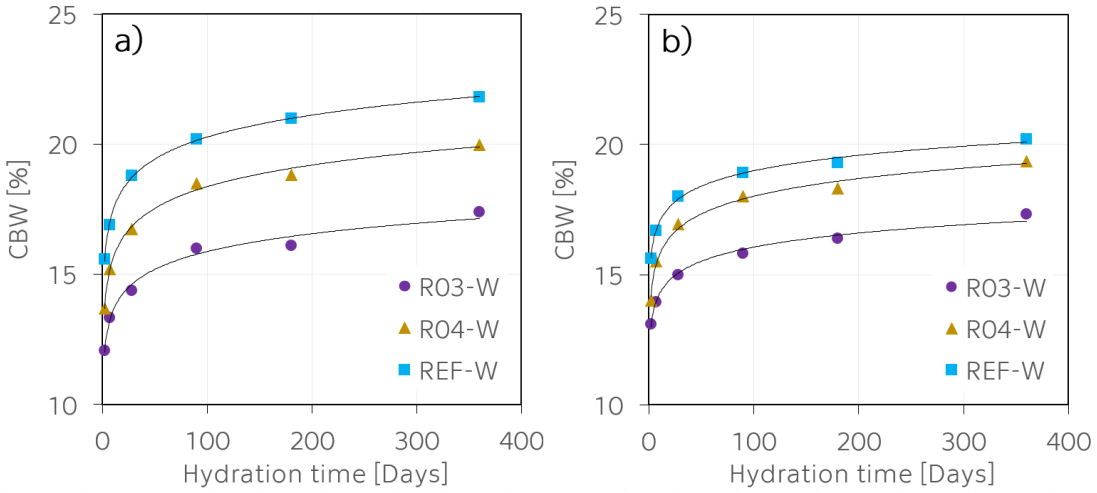

Figure 7.5.4. The amount of CBW determined using methods proposed by (a) De Weerdt and (b) Bhatty.

In [232], it was reported that cement paste with w/c of 0.5 reached 16.5% of the CBW after 3 days, and about 23.5% after 360 days. However, because authors heated samples at 120 °C for an hour and then ignited them at 950 °C for another hour, they determined the CBW content also with the mass loss from the calcite decomposition, which takes place at temperatures above 600 °C [131]. Therefore, their values were slightly higher than those computed in this study. Lam et al. [233] reported that cement pastes with the w/c of 0.5 reached 15 and 18.6% after 7 and 90 days of hydration, respectively, which were slightly lower values than those observed in this study. To determine the CBW content, authors dried samples at 110 °C for 3 h, and then ignited them at 950 °C for another hour.

With a decreasing w/c ratio, the CBW content decreased. After 2 days of hydration, the CBW was 13.7 and 12.1% for R04-W and R03-W pastes, respectively, and it reached 20 and 17.4% after 360 days, following the decreasing trend with a decreasing w/c ratio. In [233], the CBW of cement pastes with w/c of 0.3 was studied in the interval from 7 to 90 days. It increased from

14.2 to 15.7% after 7 and 90 days, respectively. The CBW computed in this study for the R03-W pastes was 13.3 and 16% after the same days of hydration.

The associated logarithmic trendlines describing the development of the CBW content of the studied plain cement pastes, determined with the method by De Weerdt et al. [203], can be expressed as follows:

$$CBW_{R03\text{-}W} = 0.987 \ln(d)+11.332, \quad (7.5.1)$$

$$CBW_{R04\text{-}W} = 1.197 \ln(d)+12.859, \quad (7.5.2)$$

$$CBW_{REF\text{-}W} = 1.219 \ln(d)+14.666. \quad (7.5.3)$$

Where d represents the hydration time in days, and it is ≥ 2. These equations can theoretically be used until the results reach the maximal theoretical value of 23%. However, because it is uncertain if the plain cement pastes with various w/c ratio will actually reach this maximal value, it is recommended to use these equations within the scope of this study.

In the case of the results obtained using the Bhatty's method [235] (Figure 7.5.4.b), the obtained trend is very similar, and it can be written as:

$$CBW_{R03\text{-}W} = 0.784 \ln(d)+12.446, \quad (7.5.4)$$

$$CBW_{R04\text{-}W} = 0.983 \ln(d)+13.486, \quad (7.5.5)$$

$$CBW_{REF\text{-}W} = 0.857 \ln(d)+15.047. \quad (7.5.6)$$

Where d refers to the hydration time in days, and it is ≥ 2. Similarly, to the previous equations, it is recommended to use them up to d = 360 days. It can be seen, that it provides very similar results, which are generally slightly lower about 0–9% compared to the firstly discussed method.

7.5.2. Degree of hydration

The CBW was used to estimate the degree of hydration for the studied plain cement pastes. This was done again based on methods suggested by De Weerdt et al. [203] and Bhatty [235]. The degree of hydration as a function of w/c and time is shown in Figure 7.5.5.

The degree of hydration, as computed with the utilization of the first mentioned method, is shown in Figure 7.5.5a. It reached 67.7% for the REF-W paste and increased up to 94.8% after 360 days. These results are in a good quantitative agreement with [232, 233, 258], where similar values were reported.

It can be seen that with a decreasing w/c ratio, the degree of hydration also decreased. It was 59.6 and 52.5% for the R04-W and R03-W pastes after 2 days and it reached 86.9% and only 75.7% after 360 days, respectively.

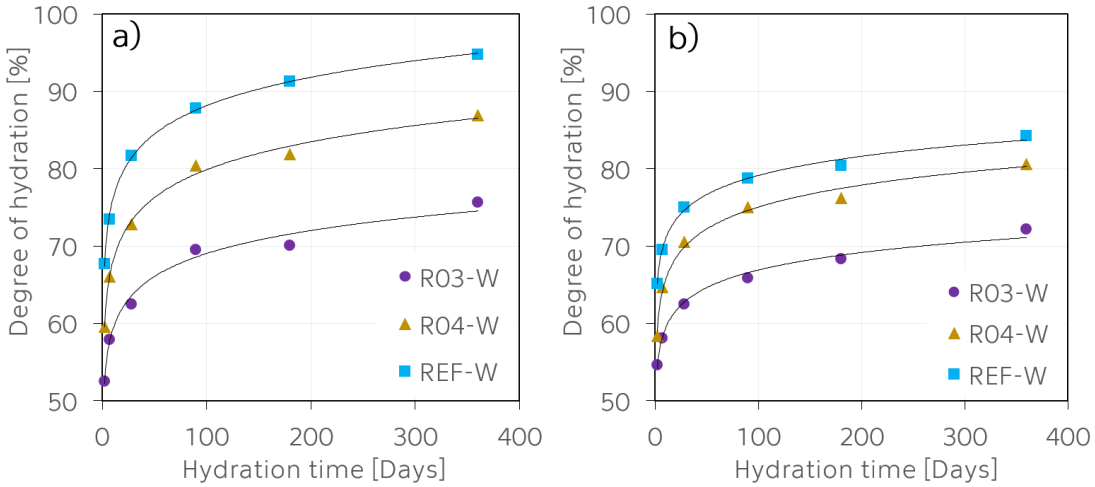

Figure 7.5.5. Degree of hydration of studied plain cement pastes determined using methods proposed by (a) De Weerdt et al. and (b) Bhatty.

The lower degree of hydration for the plain cement pastes with lower w/c ratios can be attributed to the insufficient space available to contain more hydration products [6, 233].

The associated logarithmic trendlines describing the development of the degree of hydration (DOH) of the studied plain cement pastes can be written as follows:

$$DOH_{R03\text{-}W} = 4.293 \ln(d)+49.268, \quad (7.5.7)$$

$$DOH_{R04\text{-}W} = 5.205 \ln(d)+55.909, \quad (7.5.8)$$

$$DOH_{REF\text{-}W} = 5.298 \ln(d)+63.764. \quad (7.5.9)$$

Where d represents the hydration time in days, and it is ≥ 2. These equations can theoretically be used until the results reach the maximal possible value of 100%. However, because it is uncertain if the plain cement pastes with various w/c ratio will actually reach this maximal value, it is recommended to use these equations within the scope of this study.

When the Bhatty's method [235] was applied, the degree of hydration was significantly lower, which was expected from the generally lower results of the CBW reported in the previous section. And also because a lower coefficient

of 0.24 was used in this method. These results were about 0–11% lower compared to the previous method.

The associated trendlines describing the obtained trends can be expressed:

$$DOH_{R03\text{-}W} = 3.021 \ln(d)+50.291, \quad (7.5.10)$$

$$DOH_{R04\text{-}W} = 3.899 \ln(d)+54.141, \quad (7.5.11)$$

$$DOH_{REF\text{-}W} = 3.520 \ln(d)+58.820. \quad (7.5.12)$$

Where d represents the hydration time in days, and it is ≥ 2. These equations can theoretically be used until the results reach the maximal possible value of 100%.

7.5.3. Portlandite evolution

The development of Portlandite, one of the main hydration products, was analyzed by the utilization of TGA method. Portlandite decomposes in the temperature interval from 450 to 550 °C, and this endothermal reaction is characterised by a sharp peak on DSC/TG thermographs [222]. The mass losses related to this decomposition reaction were obtained from TG by two methods (stepwise vs. tangential) for pastes stored in water, and these results were compared with pastes exposed to atmospheric air. The amount of Portlandite was computed based on the Eq.(5.6.8). The results of studied plain cement pastes are presented in Figure 7.5.6.

Generally, it is considered that a fully hydrated Portland cement with a typical composition will consume about 20 to 25 wt.% of water to produce about 20 to 25 wt.% of Portlandite [7, 233, 259].

When the studied cement pastes were stored in water (Figure 7.5.6a, b), the amount Portlandite gradually increased within the studied time interval, and its values were higher with increasing w/c ratio. This trend was in a great accordance with [198]. It was 18% in the REF-W paste after 2 days of hydration and it increased up to almost 21% after 360 days when the stepwise method was applied (Figure 7.5.6a), which was in a very good accordance with [234].

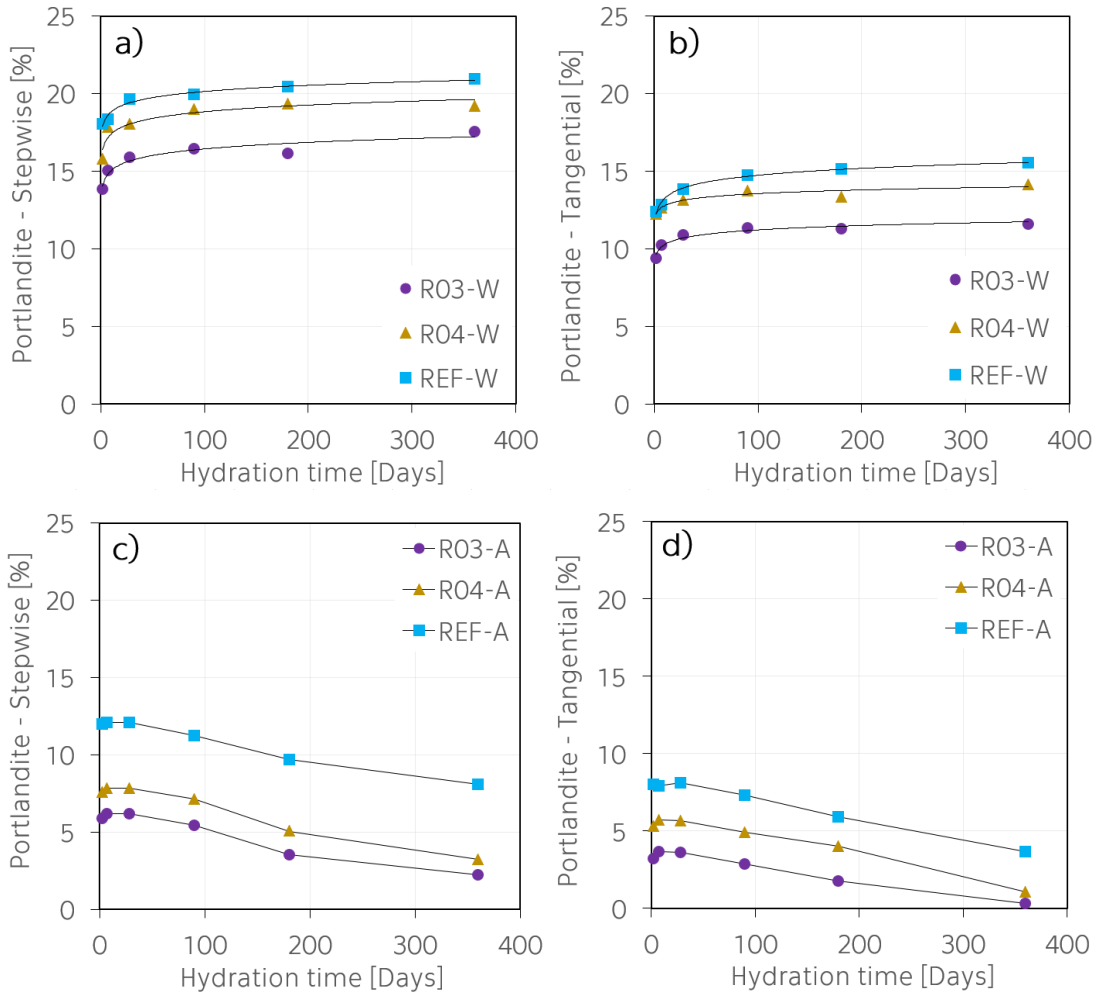

Figure 7.5.6. Portlandite evolution as a function of w/c and time at studied plain pastes determined by (a, c) stepwise and (b, d) tangential methods.

In the case of the R03 and R04 pastes, its values were lower, as it reached 13.8% and 15.8% after 2 days with the increasing w/c ratio. After 360 days of hydration, the amount of Portlandite increased up to 17.5 and 19.2% for the R03 and R04 pastes, respectively. In [232], the evolution of Portlandite was studied on the cement pastes with w/c of 0.5, cured in water at 20 °C. The maximum concentration of Portlandite for the studied cement pastes was relatively low (~16%) after 360 days compared to this study (~21%). Lothenbach et al. [260] predicted quantitatively the amount of hydrates by coupling of thermodynamic modelling with a set of kinetic equations. For their study, an ordinary Portland cement with w/c of 0.4 was used. The reported Portlandite evolution as a function of time exhibited a very similar increasing trend, and it reached about 24% after 90 days (it was about 19% in this study). However, it was

not mentioned, which method (stepwise or tangential) was applied for their computations, and what was the curing temperature of the studied pastes.

Based on the results of the stepwise method (Figure 7.5.6a), the Portlandite evolution (CH) of cement pastes stored in water can be expressed as:

$$CH_{R03\text{-}W} = 0.608 \ln(d)+13.632, \quad (7.5.10)$$

$$CH_{R04\text{-}W} = 0.620 \ln(d)+15.971, \quad (7.5.11)$$

$$CH_{REF\text{-}W} = 0.570 \ln(d)+17.506. \quad (7.5.12)$$

Where d refers to the hydration time in days, and it is ≥ 2. Similarly, to the previous equations, it is recommended to use these equations up to d = 360 days.

In terms of the tangential method, which is considered to be more accurate in comparison to the stepwise method [131], these results are displayed in Figure 7.5.6b. The obtained trend was very similar compared to the stepwise method. However, the computed values reached between 66–75% of the values of the stepwise method. These lower values obtained by the tangential method are in a very good agreement with the XRD results presented earlier in this study. The Portlandite evolution, as determined by the tangential method, can be described as follows:

$$CH_{R03\text{-}W} = 0.408 \ln(d)+9.335, \quad (7.5.13)$$

$$CH_{R04\text{-}W} = 0.338 \ln(d)+11.998, \quad (7.5.14)$$

$$CH_{REF\text{-}W} = 0.641 \ln(d)+11.783. \quad (7.5.15)$$

Where d refers to the hydration time in days, and it is ≥ 2. It is recommended to use these equations up to d = 360 days.

For the pastes stored in air, the Portlandite development exhibited the opposite trend: it decreased with curing time. More precisely, its content increased during the first 28 days of hydration in all studied pastes where it reached its maximum. It was about 12.1% for the REF-A paste, 7.9% for the R04-A paste and finally only about 6.2% for the R03-A paste. After this time, it gradually decreased. In the case of the stepwise method (Figure 7.5.6c), the difference between the REF-A paste and the other studied pastes was more obvious, whereas in the case of the tangential method (Figure 7.5.6d), the results for all studied pastes exhibited almost a constant shift.

7.5.4. Carbonation progress

The evolution of the calcium carbonate content (in this study present only in a form of calcite) was determined from the TG curves using the Eq.(5.6.10). These computed results are shown in Figure 7.5.7.

Generally, the amount of $CaCO_3$ increases in time, as its formation is related to carbonation processes in concrete structure. It begins when CO_2 penetrates into the cement matrix, which leads into a dissolution of the pore solution producing HCO_3^- and CO_3^{2-} ions, which react with Ca^{2+} from Portlandite, C-S-H and the hydrated calcium aluminates and ferro-aluminates. As a result, calcium carbonate ($CaCO_3$), silica gel and hydrated aluminium and iron oxides are formed [261, 262], following these formulas [263]:

$$Ca(OH)_2 + CO_2 \rightarrow CaCO_3 + H_2O \; [Ca^{2+} + CO_2^{2-} \rightarrow CaCO_3] \quad (7.5.16)$$

$$3CaO \cdot 2SiO_2 \cdot 3H_2O + 3CO_2 \rightarrow 3CaCO_3 + 2SiO_2 + 3H_2O \quad (7.5.17)$$

$$4CaO \cdot 2Al_2O_3 \cdot 13H_2O + 4CO_2 \rightarrow 4CaCO_3 + 2Al(OH)_3 + 10H_2O \quad (7.5.18)$$

The impact of the atmospheric CO_2 on the studied cement pastes, which were stored in water and sealed in plastic bottles, was almost negligible, as it can be seen on the Figure 7.5.7a. It can be also seen on the increasing trend of Portlandite content in these pastes, as it was discussed earlier. At the beginning of the hydration processes, the amount of calcite was the lowest in the REF-W paste, 6% after 2 days. Slightly higher values 8.6 and 9.6% were observed in the R04 and R03 pastes, respectively. These differences might be caused by the drying procedure done with isopropanol. It seems that this procedure of free water removal was more effective in the case of the pastes with a lower water content (lower w/c). Because samples were stored in several plastic bags before the analyses were performed, even the limited contact with the atmospheric CO_2 activated the carbonation processes in these samples. It is interesting that the evolution of the amount of calcite exhibited a decreasing trend in all studied plain pastes stored in water until 90 days of hydration.

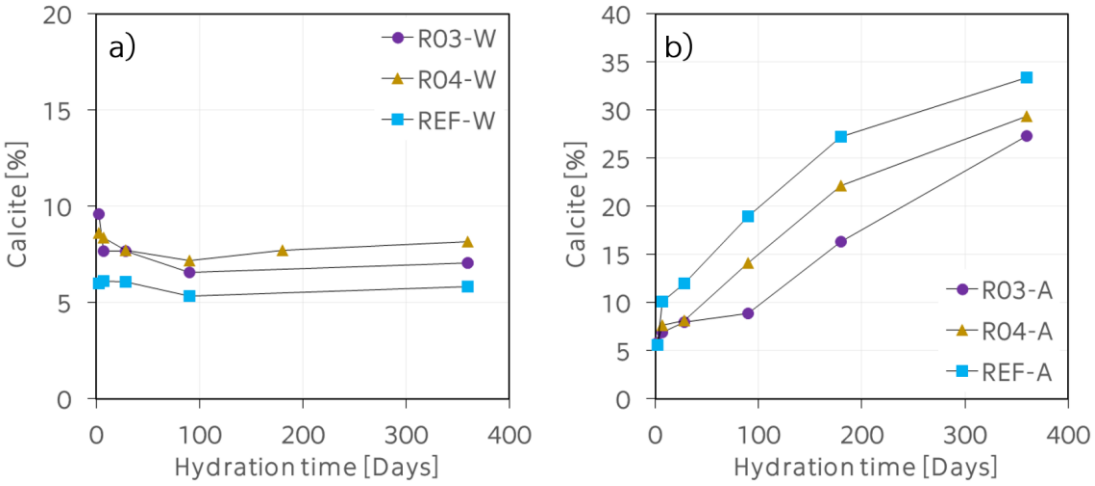

Figure 7.5.7. Evolution of the calcite content as a function of w/c ratio for cement pastes stored in (a) water and (b) air.

This phenomenon could be related to the ability of calcium carbonate to dissolve in water under specific conditions [264, 265]. Generally, calcium carbonate is only slightly soluble in pure water, but its solubility is improved when CO_2 is present in water, and with decreasing temperature [266-268]:

$$CaCO_3 + 2CO_2 + H_2O \leftrightarrow Ca^{2+} + 2HCO_3^- \quad (7.5.19)$$

Nevertheless, the description of calcium carbonate dissolution is a very challenging topic, as it is dependent besides on CO_2 content and temperature also on pH, quality of water (amount of Ca^{2+}), NaCl content etc [268]. Unfortunately, none of these parameters were analyzed in this study. However, it can be seen that when the studied pastes were kept in water and sealed at constant temperature of 25 °C, the calcite content slightly decreased up 90 days of hydration. It reached about 5.3% in the REF-W, 7.2% in the R04-W, and 6.6% in the R03-W paste. Since these values are very low, the following increase after 360 days can be a result of uncertainty of experiments.

Another interesting observation was done on the surface of the studied samples after 360 days of hydration, as it can be seen in Figure 7.5.8. This additional white layer formed on the surface of samples is probably caused by water leaking through the samples and dissolving Portlandite from the matrix. Portlandite thereafter reacts with the atmospheric CO_2 which leads to the formation of calcium carbonate layer (or calcium sulphate). If the level of leaching

is high enough, it can form stalactites, as explained more in detail in a recent study [269].

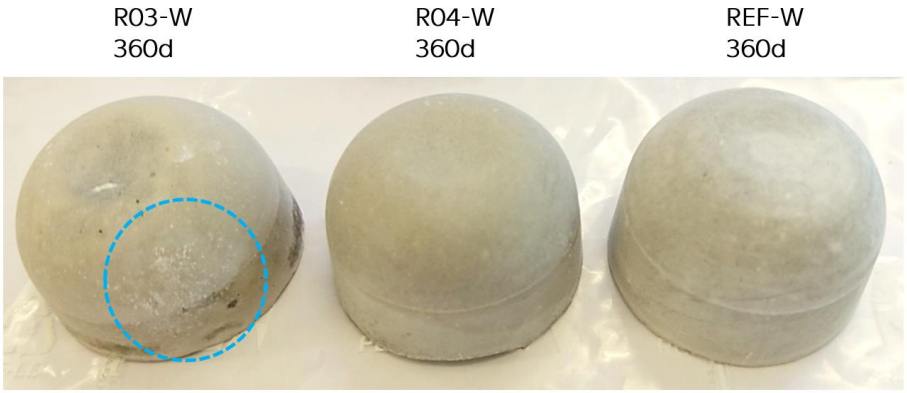

Figure 7.5.8. Additional calcium carbonate layer observed on the surface of studied samples as a result of lime leaching.

When cement pastes were stored in air (Figure 7.5.7b), the calcite content significantly increased with increasing w/c and time. This is in a good agreement with the trend of the decrease of Portlandite and CBW content observed for these pastes. The samples were exposed constantly to the atmospheric air and it seems that the shape of their surface supported the carbonation processes. From the results, it can be seen that the carbonation proceeded faster at samples with a higher w/c ratio. In this case, the calcite content was almost the same in all studied samples, and it was about 5.6–5.9% after 2 days. Its amount gradually increased within the studied time interval. It reached 33.4% in the REF-A, 29.4% in the R04-A and finally, the lowest values were observed for the R03-A, where the calcite content was 29.4% after 360 days.

These observed trends are in a good agreement with data published in [270], where the curing effects on carbonation of concrete with various w/c ratios were analyzed. The carbonation depth was determined by infrared spectroscopy and compared with results from the phenolphthalein method. It was found that samples cured in water for 28 days became more carbonated to only 53% of the level for air-cured samples. In this study, it was 50.6% for the REF pastes, whereas in the case of the pastes with the lower w/c ratio, they reached about 95% of the air-cured values after 28 days.

7.6. Summary

This chapter summarized experimental results of the effect of w/c ratio on the hydration processes of plain studied cement pastes labelled as R03, R04 and REF. With the utilization of the classical methods along with thermal analysis, it was found that a lower w/c ratio led to:

- A faster beginning of the hydration processes, which was probably caused by the relatively high chemical ion concentration in pastes with the lower w/c ratio.
- An increase in the homogeneity of hydration products, observed after 28 and 360 days.
- Formation of denser hydration products, which affected basic physical properties and the pore size distribution of the pastes.
- Significant improvement of the compressive and flexural strength.
- Lower amount of the CBW, and therefore, the lower degree of hydration.
- Lower formation of Portlandite. Its content increased with time in all pastes stored in water, whereas it had an opposite trend for pastes stored in air.
- Lower amount of calcite. Carbonation processes were arrested in the water environment. However, some variations in the results were observed when isopropanol was used to stop hydration processes. When samples were cured in air, the amount of calcite significantly increased about 27 % for the reference sample (it was slightly lower in the other pastes).

Chapter 8

Characterization of cement pastes blended with silica fume

In this chapter, experimental results of the cement pastes blended with silica fume are presented. This pozzolana active material was chosen as a partial replacement of cement by up to 12 wt.%. Studied pastes were labelled as MS4 and MS12, in accordance with the percentage of the cement replacement. Thermal analysis was performed also on pastes with 8 wt.% replacement of silica fume to obtain a more comprehensive analysis of hydration processes. All studied materials were cured in water until they were analyzed.

At the beginning, there was an intention to directly compare results of both pozzolana active materials (silica fume and natural zeolite) chosen for this study, but because silica fume is recommended to be used in lower amounts than natural zeolite, the highest amount of silica fume used in this study was only 12 wt.%. Samples with 16 wt.% of silica fume were prepared at first, but these samples were significantly damaged due to their significant expansion during hydration in water environment, which led to a massive cracking, especially at later ages after 28 days of curing. Therefore, these samples were replaced with samples with 12 wt.%, where this effect was not observed.

8.1. Hydration heat

The early-stage hydration heat development of the studied cement pastes blended with silica fume is shown in Figure 8.1.1. It can be seen that silica fume modifies the heat evolution within the studied time interval up to 50 hours. The first peak (initial reaction), which is not clearly seen in Figure 8.1.1a, decreased with increasing amount of silica fume in studied pastes. The pastes with silica fume released much lower heat during the first minutes compared to the plain cement paste.

The same trend wa s found also in [271], where cement pastes containing up 30% of silica fume were studied. It has been reported that the pozzolanic reactivity of silica fume causes an immediate consumption of calcium due to its rapid dissolution [234, 272]. It results in the lack of Portlandite leading to a reduced speed of early hydration processes since these reactions depend on the concentration of Portlandite [271]. Based on other studies, the SO_3 content could be another factor responsible for the delay of the aluminate reaction [273]. In calorimetric measurements, this can be seen during the induction period where the heat exchange with the medium decreases. The reactions occuring during this period are responsible for the reduction of the porosity and a consequent increase of strength [234]. This decrease of heat during the induction period was very low in this study, since the induction period of all studied pastes exhibited a very similar trend. In the acceleration period, the effect of silica fume was more obvious. The main hydration peak decreased with increasing silica fume, which is in a good accordance with data presented in [271].

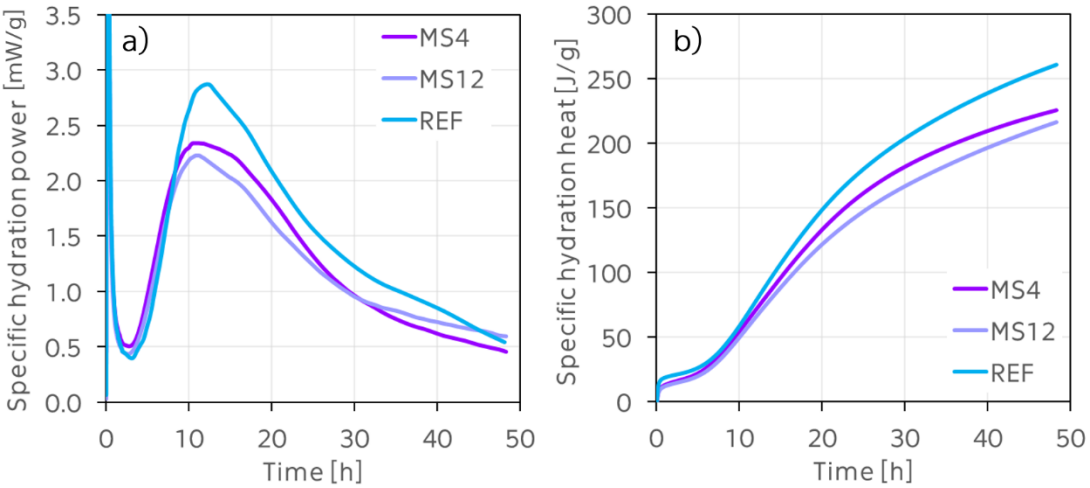

Figure 8.1.1. Specific hydration power (a) and specific hydration heat (b) of cement pastes blended with silica fume.

The decerelation period showed very broad shoulders for pastes with silica fume, which were probably related to the pozzolanic reaction. It appears that the pozzolanic reaction was activated at later age, more precisely after 45 h for the paste with a higher amount of silica fume, and after 57 h for the MS4 paste. The activation of the pozzolanic reaction of studied pastes was slower in comparison to the literature [271].

8.2. Microstructural development

The SEM photographs, demonstrating the evolution of hydration products of cement pastes blended with silica fume, are shown in Figure 8.2.1. It can be seen that silica fume particles, along with a relatively high w/c ratio of 0.5, modified the formation of the main hydration products. In the case of the MS4 paste after 28 days, the C-S-H phase exhibited a "honeycomb" structure, while Portlandite was found in a form of column aggregates [274]. The porous morphology of the C-S-H phase indicated the space that was originally water-filled. It was also reported in literature [275] that when C_3S and C_2S was blended with condensed silica fume, it led to an increase of the C-S-H mean chain length compared to mixes without silica fume, which was also observed in this study. Ettringite needles were found situated mainly close to Portlandite. After 360 days of hydration, plates of Portlandite were spotted in the MS4 paste. Separated particles of silica fume, which did not participate during the hydration processes, were found mainly on the surface of Portlandite.

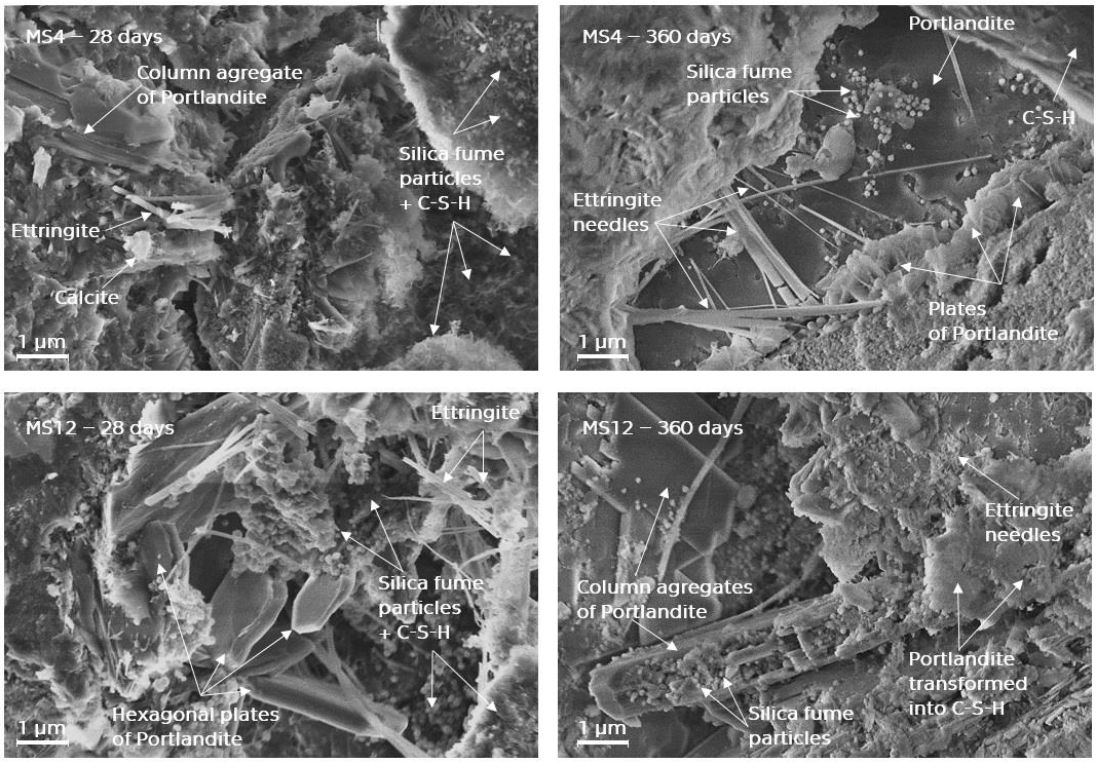

Figure 8.2.1. SEM micrographs of cement pastes blended with silica fume after 28 and 360 days.

The long ettringite needles were randomly distributed across the other hydration products. As the microstructure became more compact with time, the morphology of the C-S-H phase was also more massive without any characteristic shape. The higher content of silica fume in the MS12 paste caused changes in the morphology of Portlandite and C-S-H phase. After 28 days, Portlandite was found mainly in a form of massive, hexagonal crystals, surrounded with clustered particles of silica fume. These crystals were transformed into larger column aggregates of Portlandite and denser C-S-H after 360 days of hydration. In [276], the porous structure of C-S-H formed in white cement blended with similar amount of silica fume, 10 wt.%, was described as "foil-like". The morphology of the C-S-H was found mainly in a form of dense, connected layers. In [276], it was also reported that the addition of a similar amount of silica fume caused a significant decrease of the Ca/Si ratio of the C-S-H. It seems that the higher volume of silica fume in the MS12 pastes led to the formation of shorter ettringite needles.

The influence of silica fume on the amount of formed hydration products was analyzed by XRD method. The corresponding XRD patterns are shown in Figure 8.2.2. The amounts of crystalline and amorphous phases were calculated based on the internal standard phase, 20 wt.% of ZnO. These computed results are summarized in Table 8.2.1.

Table 8.2.1. Mineral composition of MS pastes in wt.%.

Material	After 28 days			After 360 days		
	REF	MS4	MS12	REF	MS4	MS12
Alite	7.5	8.9	8.4	7.3	7.0	8.8
Amorphous	63.1	65.9	71.1	66.7	69.6	71.1
Belite	4.4	3.0	3.1	2.6	2.5	2.4
Calcite	3.2	3.3	3.2	3.2	2.6	2.9
Ettringite	4.7	4.1	3.7	4.5	4.5	4.0
Ferrite	3.5	1.7	0.9	1.4	1.0	1.6
Gypsum	1.2	1.7	1.9	1.2	1.3	2.1
Portlandite	12.3	11.1	7.5	12.8	11.3	7.0
Quartz	0.2	0.2	0.3	0.3	0.3	0.2

The addition of silica fume led to the formation of higher amount of amorphous phase (mainly to C-S-H) in blended pastes compared to the reference paste. Amorphous phase constituted 71.1% in the MS12 paste after

28 days, which was about 5% and 8% more than in the case of the MS4 and REF pastes, respectively.

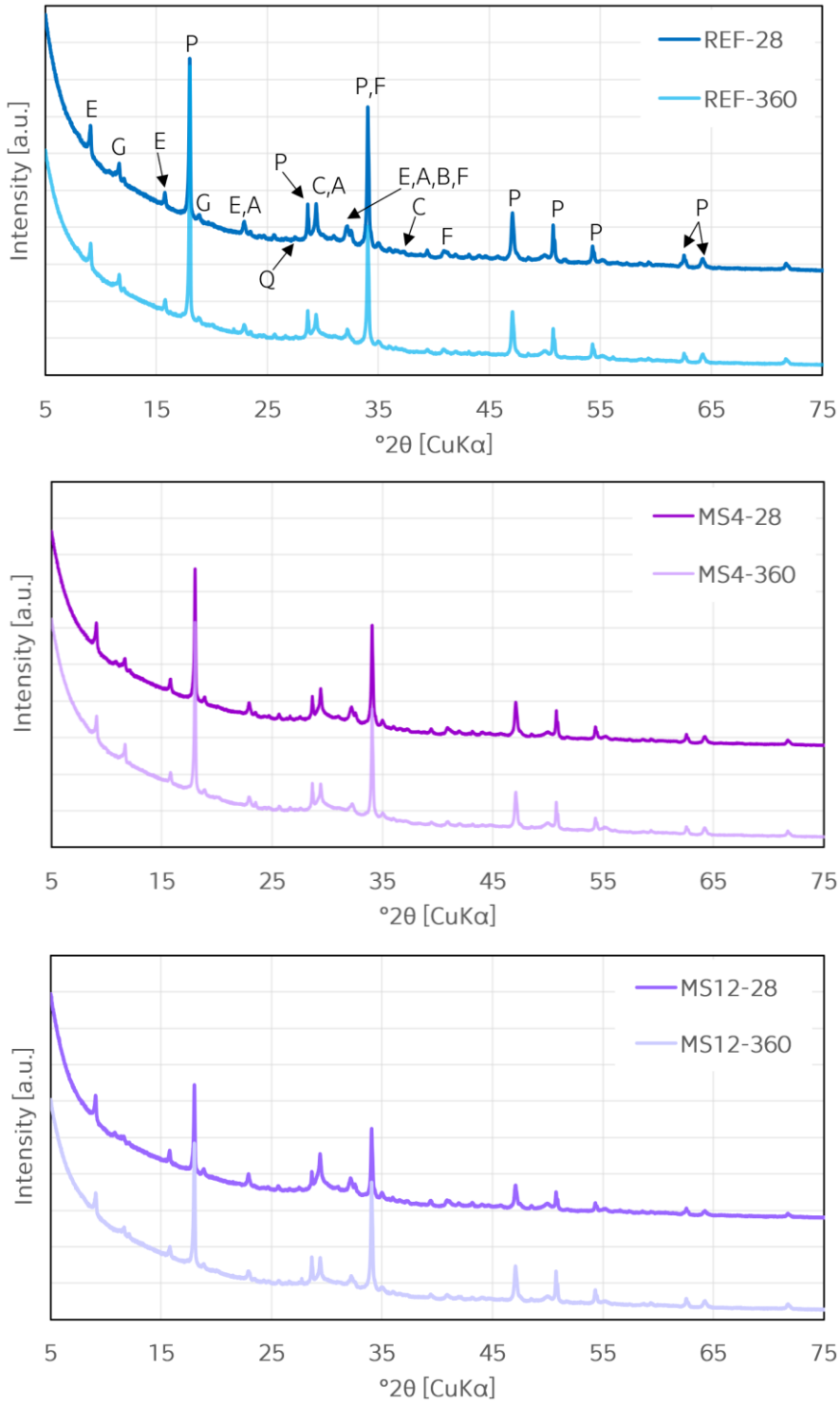

Figure 8.2.2. XRD patterns of cement pastes blended with 4 and 12 wt.% of silica fume after 28 and 360 days: A–alite, B–belite, C–calcite, E–ettringite, F–ferrite, G–gypsum, P–Portlandite, Q–quartz.

Amorphous phase remained at the same level in the MS12 paste after 360 days, while it slighly increased in the reference paste and the paste with 4 wt.% of silica fume. It can mean, besides the uncertainty of the measurements, that pastes with 12 wt.% were saturated with the active part of silica fume mainly after 28 days of hydration, and the rest of the unhydrated silica fume particles acted partially as a chemical inert filler [277]. The content of alite exhibited an increasing trend with increasing amount of silica fume in pastes after 28 days. Its amount decreased in time as it was gradually consumed by the continuing hydration and pozzolanic processes. The addition of silica fume led to a higher consumption of belite in the blended pastes after 28 days in comparison to the reference paste. Nevertheless, it was found in very similar amounts after 360 days. The ettringite content remained almost at the same levels in all studied blended pastes. Its formation into tricalcium–monosulfo–aluminate hydrate (AFm) was not detected by the XRD method. The impact of silica fume on the hydration processes can be also seen on the decreasing amount of Portlandite, which was formed and gradually consumed with an increasing amount of silica fume in blended cement pastes. However, after 360 days of hydration in water, the amount of Portlandite was at the same levels like after 28 days, which was reported also in [276], where samples were sealed throughout the hydration without sample drying. Muller et al. [276] also noted that because all measurements were performed on sealed systems, it could have led to a chemical isolation of the calcium hydroxide. It was also seen that the calcium content of the C-S-H was lower in the silica fume system, indicating that this calcium was also available for the pozzolanic reaction [276]. It is an interesting phenomenon, as it would be expected that the water environment will support the hydration processes, and thus, the Portlandite content should be significantly decreasing in time. Similarly like in the case of the plain cement pastes, the amount of calcite exhibited a decreasing trend with an increasing time with no reference to the silica fume content. This effect will be discussed in the section with thermal analysis results.

The development of the porous system of the cement pastes blended with silica fume was analyzed by means of the MIP method. The cumulative intruded pore volume curves and pore size distribution are shown in Figure 8.2.3. From the results of pore size distribution measured after 28 days of hydration

(Figure 8.2.3b), it can be seen that from the studied pastes, the paste with 4 wt.% of silica fume exhibited the lowest porosity in the range from 0.01 μm to 0.1 μm (gel pores), while it contained a higher amount of the larger pores from 0.1 to 100 μm (capillary pores) in comparison to the MS12.

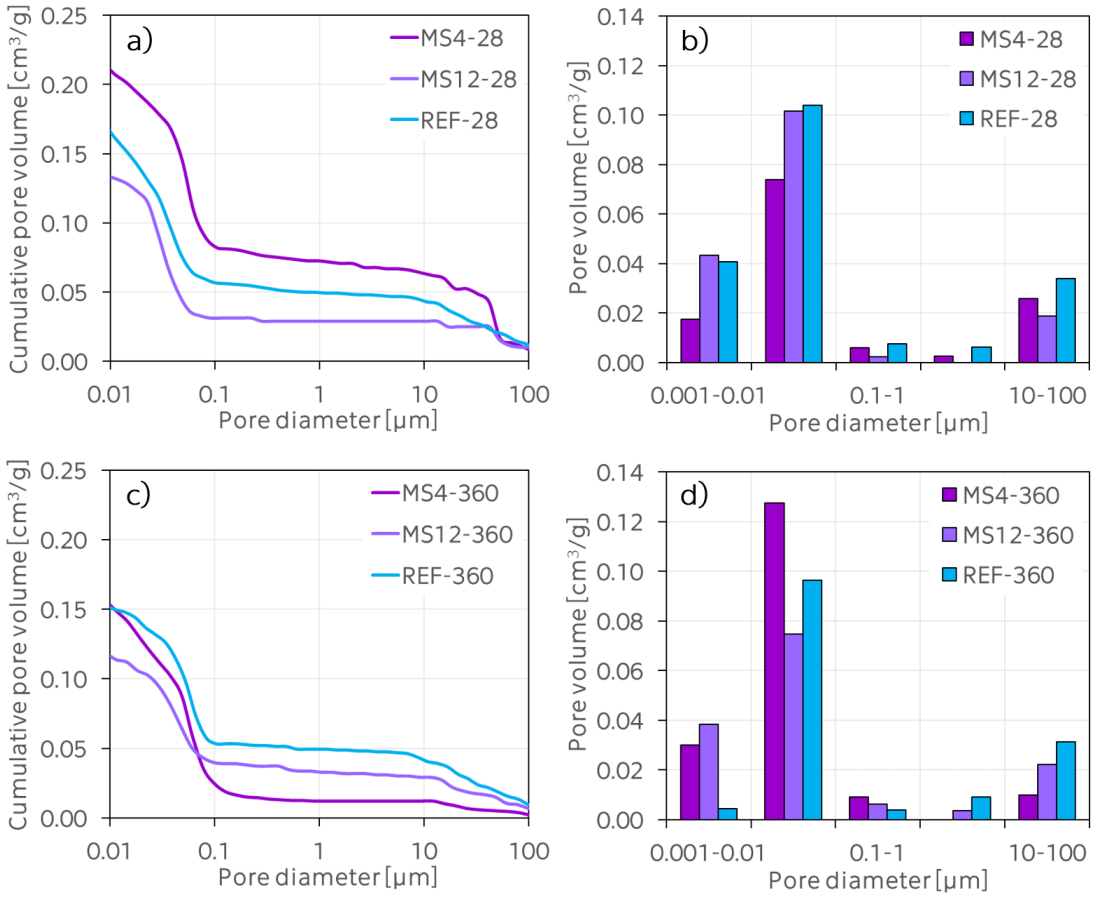

Figure 8.2.3. Dependence of the cumulative pore volume curves and pore size distribution of studied blended pastes on the level of silica fume addition.

After 360 days of hydration, the volume of the capillary pores gradually decreased (Figure 8.2.3c, d) in REF and MS4 paste, while it remained at the same level in the case of MS12. As the hydration processes continued and the resulting microstructure of the studied pastes became more compact, the capillary pores were gradually transformed into gel pores appearing mainly in the range from 0.01 μm to 0.1 μm. These pores are related to the formation of the C-S-H. This transformation was the most visible in the MS4 paste. However, these changes were in a range of the uncertainty of the measurements.

In summary, a higher content of silica fume in studied pastes caused changes in the morphology of hydration products, especially in the case of Portlandite and C-S-H phase. The amount of Portlandite decreased only moderately with time, which implies that the sealed systems might have caused a chemical isolation of Portlandite. This hypothesis was supported by a slight decrease of the calcite content. In terms of the porosity, as the hydration processes continued, the resulting structure of the studied pastes was more compact. It was associated with a gradually transformation of capillary pores into gel pores appearing mainly in the range from 0.01 μm to 0.1 μm. However, no clear trend related to the silica fume content was found.

8.3. Basic physical properties

Results of the matrix density, bulk density and the total open porosity are summarized in Table 8.3.1. The highest matrix density values were obtained in the case of the reference paste, 2229 kg/m^3 after 28 days, having a decreasing trend with an increasing amount of silica fume. The lowest value of the matrix density was achieved for the MS12 paste, 1794 kg/m^3, as expected. These values gradually decreased in time as the hydration products were formed. The bulk density exhibited a similar trend in comparison to the matrix density, as it was found to be the highest in the REF paste after 28 days of hydration and the lowest for the MS12 paste, 1550 kg/m^3 and 1343 kg/m^3, respectively, showing an increasing trend in time.

Table 8.3.1. Basic physical properties of studied pastes blended with silica fume.

Paste	Age [days]	Matrix density [kg/m^3]	Bulk density [kg/m^3]	Total open porosity [%]
REF	28	2229	1550	30.5
MS4	28	2163	1481	31.5
MS12	28	1794	1343	25.1
REF	360	2062	1702	17.5
MS4	360	2017	1632	19.1
MS12	360	1690	1436	15.0

In terms of total open porosity, pastes containing 4 wt.% of silica fume exhibited similar porosity like the reference paste after 28 days of hydration.

These results are quantitatively in a good accordance with the cement pastes with w/c ratio of 0.4 blended with 5, 10 and 15 wt.% of silica fume presented in [278]. Therefore, it appears that the pozzolanic reaction in pastes blended with silica fume proceeded relatively slowly, as the porosity of the studied pastes was at the same levels after 28 days of hydration when compared to the reference paste, which was also discussed in [128, 277].

8.4. Mechanical properties

The results of compressive and flexural strength are shown in Figure 8.4.1. The compressive strength (Figure 8.4.1a) of all studied pastes gradually increased with time. The effect of silica fume was not significant until 28 days of hydration. After this time, the highest compressive strength was obtained in the MS12 pastes.

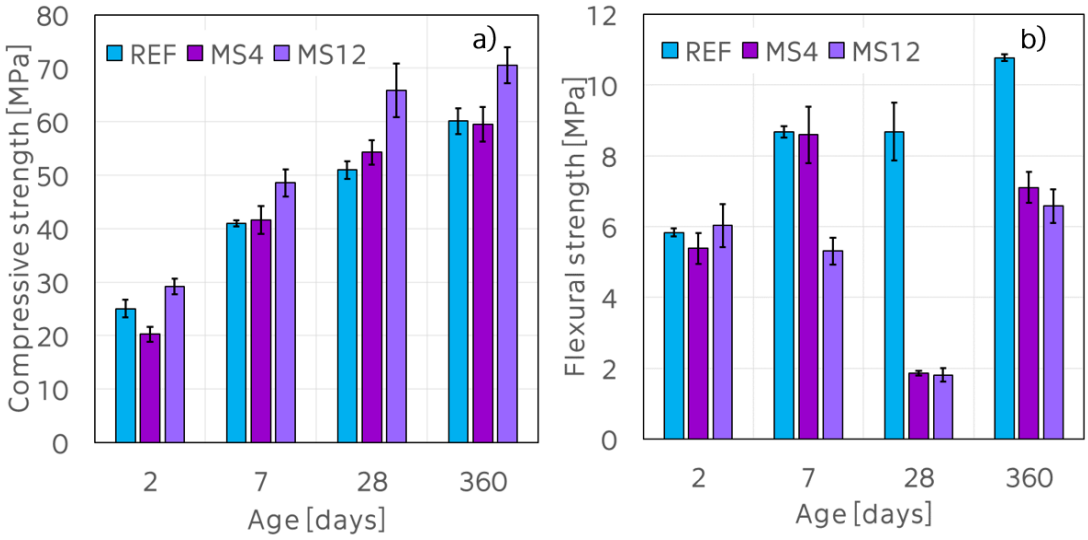

Figure 8.4.1. Mechanical properties of the blended pastes: a) compressive and b) flexural strength as a function of a silica fume replacement and time.

It became more obvious after 360 days, where the compressive strength reached 70.54 MPa in the MS12 paste, which was about 10 MPa higher than for the reference paste. Similar results were observed in [279], where it was discussed that coarse silica fume agglomeration could lead to an improvement on compressive strength. It should be noted that the compressive strength in the MS4 pastes after 2 days of hydration was in a good agreement with the hydration

heat development, where it was observed that the pozzolanic reaction was activated after 57 hours of hydration.

The results of the flexural strength (Figure 8.4.1b) did not show any specific trend, which could be caused by inhomogeneity of the studied samples, as there were unhydrated cement grains present in their structure (spotted by SEM). Especially the reason of the significant drop of the flexural strength for pastes with silica fume, as obtained after 28 days, remains unclear.

8.5. Thermal analysis results

Changes of the production of hydration products in cement pastes blended with 4 and 12wt.% of silica fume stored in diferent environments were determined by means of thermal analysis. The results obtained from TGA analysis for the storage in water (W) and in air (A) are summarized in Figures 8.5.1–8.5.3.

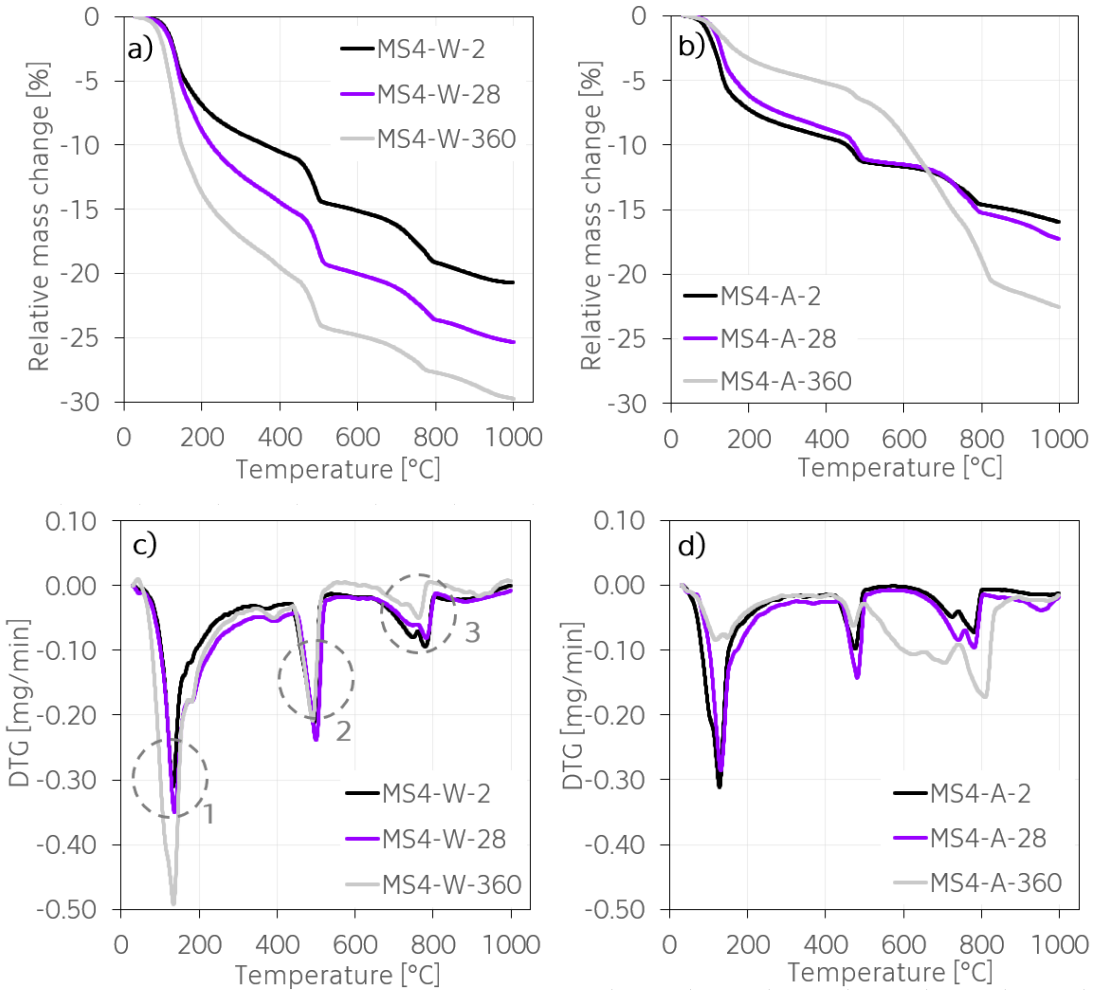

Figure 8.5.1. Thermal analysis results for MS4 pastes stored in:
(a, c) water and (b, d) air.

In addition, pastes with 8wt.% of silica fume were analyzed as well, for a better understanding of hydration processes of studied pastes. Similarly to the plain cement pastes: each designed paste was analyzed 3-times when cured in air, and 2-times when cured under water after 2, 7, 28, 90, 180 and 360 days of hydration (30 experiments in total per a paste). Only selected experiments after 2, 28 and 360 days of hydration of relative mass change [in %] and its derivation [in mg/min] are shown for both studied environments. However, the related computations are done with the utilization of results of all experiments. A further analysis of the TGA results is divided based on the most significant mass changes spotted by DTG, as illustrated in Figure 8.5.1c.

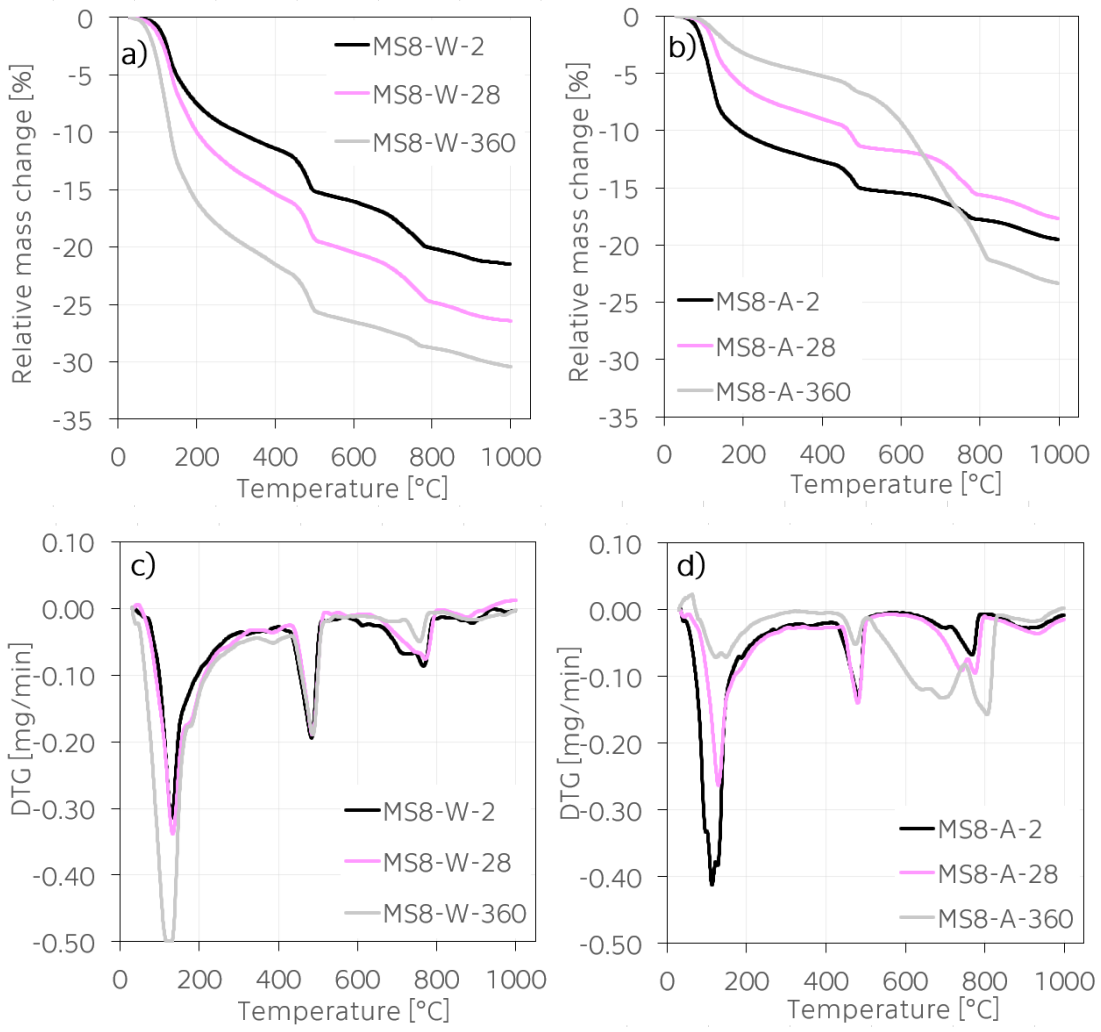

Figure 8.5.2. Thermal analysis results for MS8 pastes stored in:
(a, c) water and (b, d) air.

In accordance with the previously discussed results of the plain cement pastes, the first peak is related to the decomposition of C-S-H, ettringite and gypsum. The analysis of this peak area is focused on the determination of the CBW, which is released also during the decomposition of Portlandite occuring between 400 and 550 °C (labelled as 2). The degree of hydration of these blended pastes is computed based on the methods proposed by De Weerdt et al. [203] and Bhatty [235] and presented in a separated section, showing the impact of different levels of the silica fume addition as a function of time.

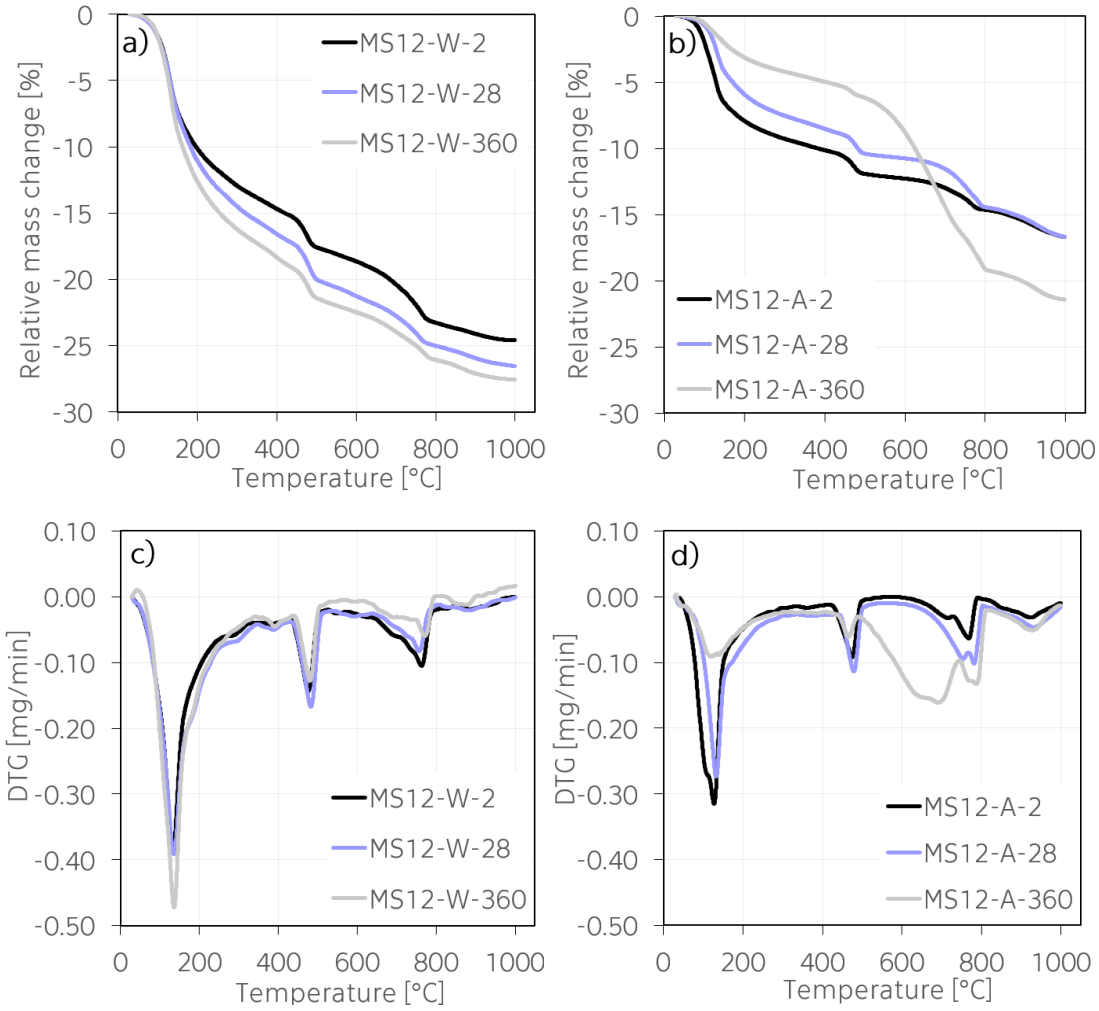

Figure 8.5.3. Thermal analysis results for MS12 pastes stored in: (a, c) water and (b, d) air.

The changes of the Portlandite content (2), which refers to the pozzolanic reactivity of silica fume, are described by stepwise and tangential methods, similarly like in the case of the plain pastes. These results are analyzed and

compared to the literature. The impact of different amounts of silica fume on the consumption of this hydration product is disccused.

The changes of the amount of calcite (3) are analyzed thereafter. It can be clearly seen that when samples are stored in diffrerent environments, the levels of this product, which is related to the carbonation procesess, are affected.

Finally, in the last section, the results of heatflow are also presented. Because when studied pastes were stored in air and heated, an exothermic reaction occurred at higher temperatures around 900 °C, without significant mass changes. This time-dependent reaction was spotted in literature in similar cement systems [280]. Its origin and effect on the hydration procesess are discussed in a separated section.

8.5.1. Chemically bound water

Similarly, like in the case of the plain cement pastes, the content of the CBW of pastes with silica fume, stored in water, was determined based on the methods proposed by De Weerdt et al. [203] and Bhatty [235]. Also the same approximate temperature ranges, as provided earlier in Table 7.5.1, were used for these calculations. Selected mass change values, as obtained from the TGA experiments, are presented in Table 8.5.1. The mass changes from the decomposition of Portlandite were determined individually for each sample.

Table 8.5.1. Selected mass loss values [in mg] determined by TGA.

Paste	Age [days]	M_{sample}	$M_{135°C}$	$M_{400°C}$	$M_{600°C}$	$M_{1000°C}$
MS4-W	2	49.3	47.54	43.80	41.95	38.92
	28	51.4	49.31	43.39	41.18	38.46
	360	51.0	46.56	40.36	38.14	35.71
MS8-W	2	50.4	48.58	45.18	43.23	40.29
	28	51.4	49.06	43.34	41.43	38.09
	360	49.5	44.26	38.37	36.60	34.27
MS12-W	2	49.9	47.14	42.36	41.05	37.62
	28	51.2	48.39	42.46	40.83	37.62
	360	51.1	47.82	41.31	40.07	37.00

Based on these values, the CBW content was computed. The obtained results are summarized into Figure 8.5.4. The results of the reference paste are also provided for a better comparison. The results obtained using the method proposed by De Weerdt et al. [203] show that different levels of silica fume modified the amount of CBW produced by OPC at pastes stored in water (Figure 8.4.4.a). While the results of the MS4-W exhibited a very similar trend like the REF-W pastes, it can be seen that the greater the silica fume addition is, the lower amount of the CBW relative to the plain cement pastes can be expected.

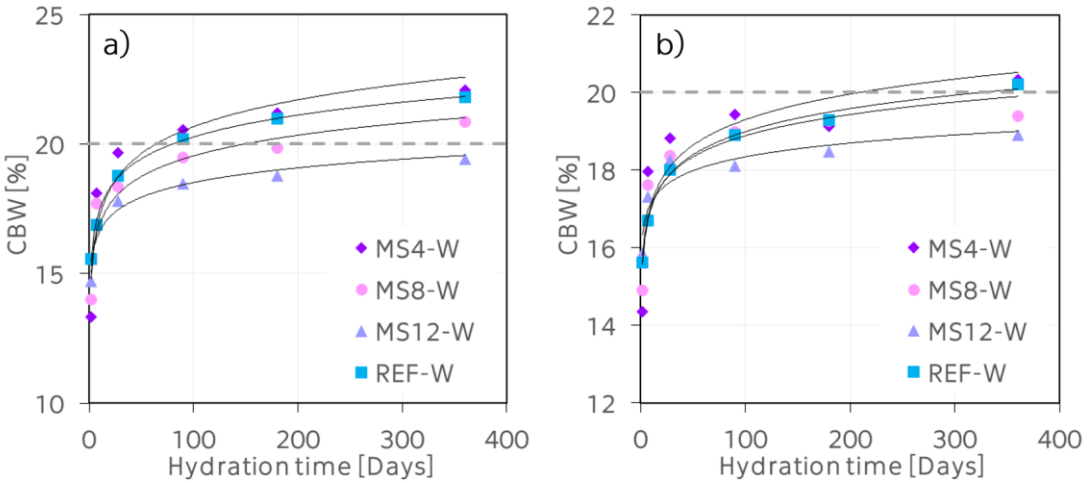

Figure 8.5.4. The amount of CBW determined using methods proposed by (a) De Weerdt and (b) Bhatty.

The CBW content was determined as 13.3% in the MS4-W, 14.0% in the MS8-W, and finally 14.7% in the MS12-W after 2 days. The highest value of 15.6% was observed for the REF-W paste. With increasing time, these values gradually increased. It is interesting that this enhancement was about 40%, 33% and 24% of the original values for MS4-A, MS8-W and MS12-W, respectively. Which also implies that the capacity for production of CBW was higher for pastes with a lower silica fume addition.

The associated logarithmic trendlines describing the development of the CBW content of the studied cement pastes stored in water can be expressed as follows:

$$CBW_{MS4\text{-}W} = 1.499\ln(d)+13.766, \quad (8.5.1)$$

$$CBW_{MS8\text{-}W} = 1.150\ln(d)+14.250, \quad (8.5.2)$$

$$CBW_{MS12\text{-}W} = 0.818\ln(d)+14.750. \quad (8.5.3)$$

Where *d* represents the hydration time in days, and it is ≥ 2. These equations can theoretically be used until the results reach the maximal theoretical value of 23%. However, because it is uncertain if the blended cement pastes will actually reach this maximal value, it is recommended to use these equations within the scope of this study.

The trend of the decreasing CBW with increasing amount of silica fume in cement pastes was explained in literature in several ways: Some authors [128] attributed the lower amount of the CBW to the increased average chain length of polysilicates in the C-S-H phase, with both silica fume content and time, which probably resulted in the release of water, hence lower amount of CBW. Atlassi [281] proposed that the water from Portlandite participating in the pozzolanic reaction is released as evaporable water, which leads to lowering the total amount of chemically bounded water per hydrated cement content in blends with silica fume. Another explanation could be that, at high contents of silica fume, the availability of water for silicate hydration is restricted by the impermeability of the paste that resulted after the refinement of the microstructure [232, 282]. In [283], it was proposed that silica fume reacts directly with Portlandite to produce C-S-H binding no additional water.

When the Bhatty's method [235] was applied, the CBW content moved into lower values, as already observed in the case of the plain cement pastes. However, the obtained trend was a very similar compared to the previous method: the addition of silica fume led to a decrease of the CBW content. This decrease was more obvious with increasing addition of the used silica fume. Because the variation between the results was too high, the associated trendlines could not be expressed mathematically.

8.5.2. Degree of hydration

In terms of the determination of the degree of hydration, it is very challenging to find the most appropriate approach applicable for TGA results of blended cement pastes. Because Portlandite, which is gradually formed during hydration processes, is consumed not only by the formation of C-S-H, but also by the pozzolanic reactions. Thus, the CBW content is modified. The methodologies proposed by Pane et al. [236] and Bhatty [235] for the degree of hydration assessment of blended cement pastes by thermal analysis were reviewed in

detail and modified in a recent study [234]. These methods were already described in detail in the chapter dealing with thermal analysis (Section 5.6.1).

However, for an easier comparison of the results, the same methods, which were utilized in the case of the plain cement paste, were applied. It should be noted that the method proposed by De Weerdt et al. [203] is more reliable for the plain cement pastes, as it is mainly based on the amount of Portlandite content, which can be used for the determination of hydration processes rather than for the description of the CBW content, and related degree of hydration in the case of blended cement pastes. Therefore, the results summarized in Figure 8.5.5a are more illustrative.

The results of the degree of hydration computed by the Bhatty's method [235], are shown in Figure 8.5.5b. It reached about 59.8% for the MS4 paste after 2 days of hydration, and about 65.1% for the reference paste. The highest value was achieved for the MS12 paste, where the degree of hydration was 66.1%. These results were in a good agreement with those from the hydration heat and mechanical properties presented eairler. With time, these values gradually increased up to about 85% after 360 days for the reference paste and the paste with the lowest silica fume content. The higher silica fume addition, the lower the degree of hydration was observed.

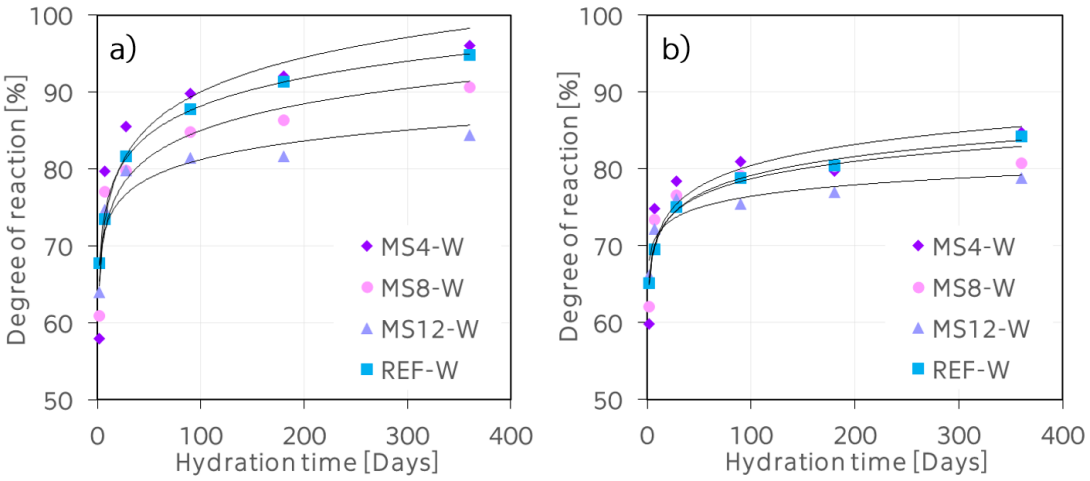

Figure 8.5.5. Degree of hydration of studied plain cement pastes determined using methods proposed by (a) De Weerdt et al. and (b) Bhatty.

It was reported that the reaction degree of 10 wt.% of silica fume in white cement pastes at w/c of 0.5 was 65% of silica fume reaction by 100 days [284],

which is about 10% lower values than computed in this study for the pastes with 12wt.% silica fume. In another study [276], ^{29}Si nuclear magnetic resonance spectroscopy experiments were carried out on white cement pastes with the same dosage of silica fume after 3, 7, 14 and 28 days of hydration. The degree of reaction of silica was computed and it was found that about 34% of the silica fume reacted by 3 days and up to 67% after 28 days of hydration. These data are in a good agreement with the results published in [277], where the pozzolanic reaction between silica fume and lime formed during cement hydration occured after 3 days of hydration. Therefore, its was concluded also by this study [277] that the pozzolanic reaction had no affect on reaction mechanisms during the early stage of hydration in Portland cement–silica fume systems.

Thus, the data of the hydration degree presented in this study were slightly higher compared to the literature review. However, for a more precise comparision of results, the hydration degree highly depends on the type and composition of Portland cement, w/c ratio and the type and fineness of silica fume used, which was probably different in this study. Nevertheless, the obtained results clearly showed that blended pastes with silica fume needed more time to activate the pozzolanic reaction, as confirmed by other measurements disscused in this study.

8.5.3. Portlandite evolution

The Portlandite development, as a function of silica fume addition and time, was determined from the TGA experiments with the utilization of the Eq.(5.6.8). These results are displayed in Figure 8.5.6.

When stored in water (Figure 8.5.6a), the silica fume addition at all levels led to a decrease of Portlandite compared to the reference paste. After 2 days of sealed curing, the amount of Portlandite was 15.4% for the MS4-W, 14.7% for the MS8-W, and finally 11.0% for the MS12-W paste, as obtained by the stepwise method. These results were quantitatively in a good agreement with data published in [280]. The amount of Portlandite slightly increased at all studied pastes until 90 days of hydration. After this time, Portlandite was gradually consumed. The most significant drop in its amount can be seen in the MS12-W pastes, where it decreased to about 10%.

The results of the tangential method (Figure 8.5.6b) were in a very good accordance with results from the XRD method, as the amount of Portlandite in the MS4-W and MS12-W pastes was 11.0% and 6.5% after 2 days of hydration, and after 360 days, these values were determined as 11.2% and 5.4%, respectively.

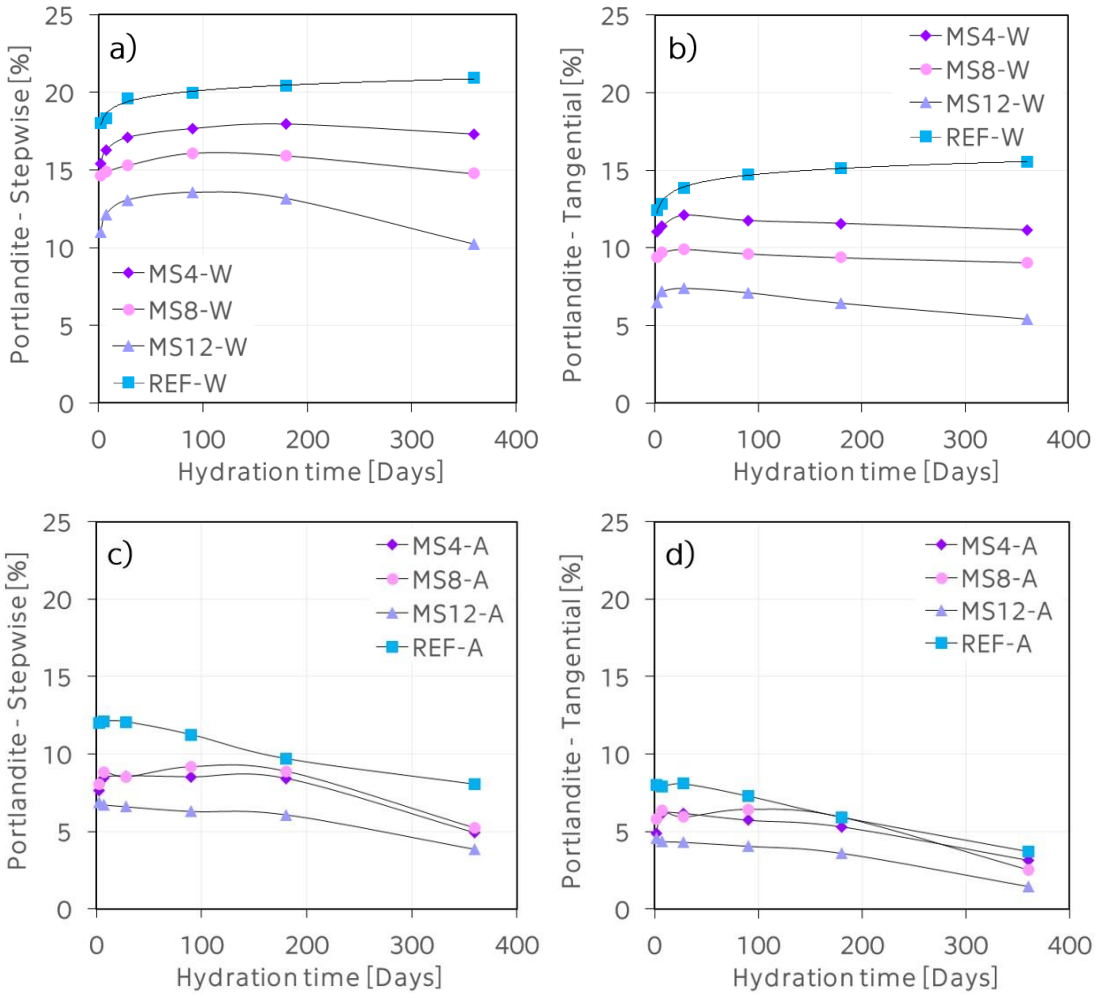

Figure 8.5.6. Portlandite evolution at studied pastes blended with silica fume determined by (a, c) stepwise and (b, d) tangential methods.

When pastes were stored in the air environment (Figure 8.5.6c, d), there was an interesting shift in the amount of Portlandite between the MS4-A and MS8-A pastes after reaching 90 days of hydration. However, this difference was numerically almost negligible. Generally, the Portlandite content in pastes stored in air reached only about 50–60% of the water-cured values. This significant difference was caused by the fact that Portlandite was consumed not only by the pozzolanic reactions, but also by the carbonation processes when exposed to the atmospheric air.

8.5.4. Carbonation progress

The changes in the calcium carbonate content were determined from the TG curves using the Eq.(5.6.10). These results are summarized in Figure 8.5.7. At first sight, it can be seen that the water environment, similarly like in the case of the plain cement pastes, preserved samples and protected them from carbonation (Figure 8.5.7a). Whereas pastes stored in air were exposed to CO_2, and thus, the carbonation processes started already after several days of hydration, as indicated by the increase of amount of calcite (Figure 8.5.7b).

At the beginning of the hydration processes, the amount of calcite was the lowest in the REF-W paste, 6.0% after 2 days. Higher values were observed with increasing amount of silica fume in pastes, which is not clear. These differences might be caused by the drying procedure done with isopropanol or/and some non-specified processes.

Similarly like in the case of plain cement pastes, the evolution of calcite content exhibited a decreasing trend until 90 days of hydration. As already discussed, this can be caused by the ability of calcium carbonate to dissolve in water under specific conditions [264, 265]. The amount of calcite was determined as 5.3% for the REF-W. It reached about 7.3% in the MS4-W paste, and it slightly increased with increasing amount of silica fume.

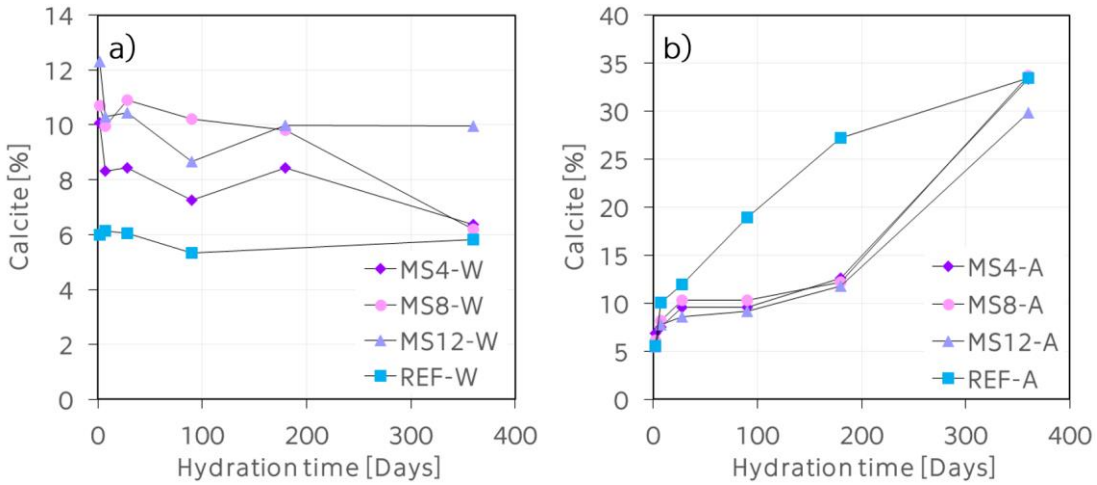

Figure 8.5.7. Evolution of the calcite content for blended cement pastes stored in (a) water and (b) air.

However, the maximal value was found in the MS8-W, 10.2%. With time, the amount of calcite decreased in all studied pastes to the similar level (5–6%),

except for the MS12-W paste, where it remained about 10% after 360 days. The trend of an increasing amount of calcite in pastes with increasing silica fume content was not expected, because Portlandite was consumed by pozzolanic reactions, and thus, a lower amount of this component could be consumed also by carbonation processes. Therefore, it seems that there was another factor leading to a higher production of calcite in pastes with higher silica fume addition.

The same observation like for the plain cement pastes was done on the surface of the studied samples stored in water after 360 days of hydration, documented by Figure 8.5.8. As already discussed, this additional white layer formed on the surface of samples was probably caused by water leaking through the samples and dissolving Portlandite from the matrix, leading to the formation of calcium carbonate layer (or calcium sulphate) [269].

When blended pastes were stored in air (Figure 8.5.7b), the trend of the calcite content was significantly affected by the addition of silica fume. The higher amount of silica fume was added, the lower was the level of carbonation, which was in a good agreement with literature [285-287]. Besides the lower amount of Portlandite available for carbonation, also changes in pore size distribution due to pozzolanic reactions have been reported [288], resulting in diminishing diffusion of CO_2 in structure of sample and the level of carbonation. As a result of these two (opposing) phenomena, it is challenging to a-priori assess the resistance of blended cement paste to carbonation [285].

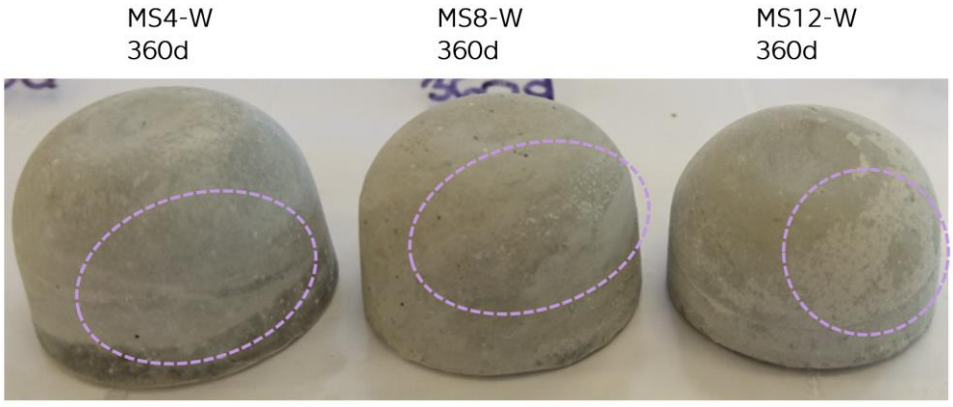

Figure 8.5.8. Additional calcium carbonate layer observed on the surface of studied samples as a result of lime leaching.

However, after 360 days, all samples were carbonated almost equally in this study. The amount of calcite was determined as 33.4% for the reference paste, which was almost equal compared with the pastes with the 4 and 8wt.% silica fume. A slightly lower value was reached for the MS12-W paste, where it was 29.8%.

8.5.5. Crystallization

When the studied samples were heated above 790 °C, an exothermic reaction occured in DSC thermographs. This reaction was not accompanied with mass change. Its origin is discussed below. The selected results of heatflow of blended pastes are displayed in Figure 8.5.9. Experiments were performed in the same time interval like TGA (2, 7, 28, 90, 180 and 360 days). This exothermic reaction was not observed in the case of samples stored in water environment.

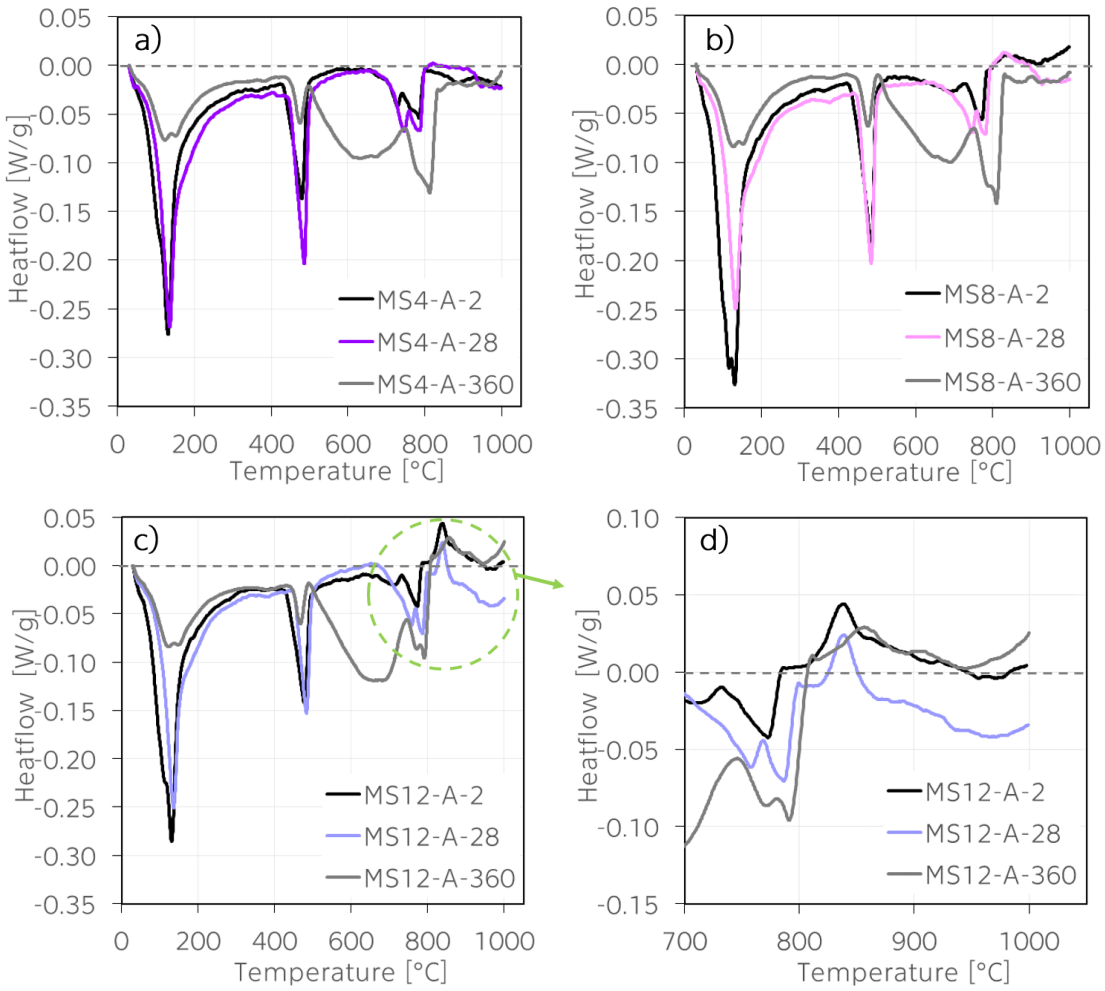

Figure 8.5.9. Heatflow results of studied pastes blended with silica fume.

In Figure 8.5.9d, results of heatflow curves for the MS12-A pastes are displayed in detail. It can be seen that the background was not constant at all experiments, which made the computation of enthalpy more difficult, as discussed in [238]. However, it is clearly visible, that in the case of pastes blended with the lowest amount of silica fume, this exothermic reaction was missing. In the MS8-A paste, it disappeared after 90 days of hydration. It can be therefore assumed that the size and intensity of this reaction was somehow dependent on the amount of available silica fume. With increasing time, silica fume was gradually consumed by the pozzolanic reaction, and therefore, a lower amount could be transformed at higher temperatures to participate in the exothermic reaction. For the pastes blended with the highest amount of silica fume, this exothermic peak remained present even after 360 days. Its size was time-dependent. The related temperature intervals, onset, maximal temperatures and computed enthalpies for the paste containing a higher amount of silica fume are summarized in Tables 8.5.2 and 8.5.3, respectively.

Table 8.5.2. Enthalpy results for the MS8-A pastes.

Age [Days]	Interval [°C]	Onset [°C]	Max.Temp. [°C]	Enthalpy [°C]
2	792-912	796.3	829.9	-10.8
7	800-906	809.2	834.9	-8.0
28	797-887	802.4	828.6	-7.6
90	811-882	838.3	838.3	-2.7

Table 8.5.3. Enthalpy results for the MS12-A pastes.

Age [Days]	Interval [°C]	Onset [°C]	Max.Temp. [°C]	Enthalpy [°C]
2	805-900	816.5	837.6	-14.7
7	806-900	820.7	838.0	-11.4
28	806-900	821.5	838.4	-11.4
90	813-876	823.6	838.8	-10.8
180	814-865	825.6	839.6	-9.5
360	816-892	831.1	856.7	-7.6

In the MS8-A pastes, the exothermal reaction was not observed in the same temperature interval at all studied days. After 2 days, this reaction was found between 792–912 °C and it moved into lower values after 360 days (811–882 °C).

The determined enthalpies showed a decreasing trend, probably indicating the speed with which the silica fume was consumed during pozzolanic reactions. When silica fume was fully consumed (after 90 days of hydration), the exothermal reaction vanished in the MS8-A pastes.

For the MS12-A pastes, the temperature interval of the exothermal reaction was almost constant during the first 28 days (806–900 °C). Then, its beginning moved into slightly higher values (813–816 °C), which also moved the onset of the reaction. The maximal temperature was very consistent (838–840 °C) within 2–180 days of hydration. It moved into a higher value of 857 °C at the end of the studied interval. In terms of the enthalpy, it can be seen that it gradually decreased with time. After 360 days, it reached 52% of its original value, as determined after 2 days of hydration.

The results of computed enthalpies are demonstrated in Figure 8.5.10. The most significant shift was achieved between 2–7 days of hydration for both pastes with a higher silica fume content, which was related to the activation of the pozzolanic reaction. This led to a significant consumption of silica fume, which decreased the enthalpy results about 26% in the MS8-A, and about 22% in the MS12-A after 7 days. The subsequent decrease in enthalpy was more distinct in the case of the MS8-A, while its trend was almost linear for the MS12-A until 360 days, indicating a slower consumption of silica fume in time in these pastes.

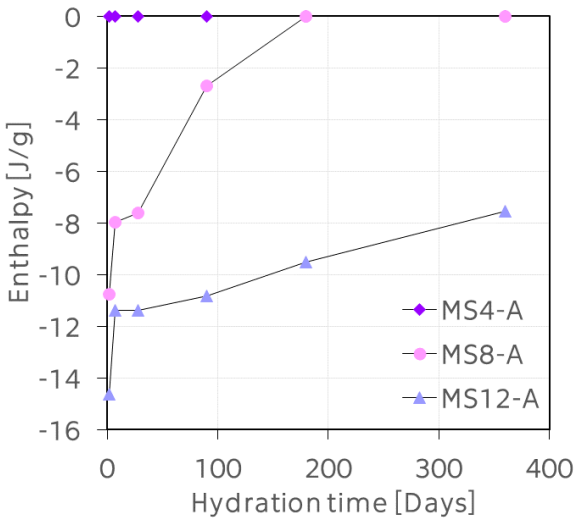

Figure 8.5.10. Enthalpy results for the crystallization peak at blended pastes.

As already mentioned, Esteves [280] spotted a similar peak in a cementitious system with 15% silica fume. He concluded that the peak was growing with the curing time and it was related to the degree of crystallization between Ca and Si. However, the trend in this study was the opposite (decreasing). The origin of this reaction is therefore unclear. In some other studies [289, 290], it was reported, that wollastonite ($CaSiO_3$) was formed under specific conditions in the same temperature interval in systems with silica fume and CaO. It should be noted, that in the case of unhydrated silica fume, an exothermic peak was observed in Figure 6.1.5. This peak could be potentially used for the quantification of unreacted silica fume. However, it occured at higher temperatures above 1000 °C, which were not included in this study.

8.6. Summary

The obtained findings of the study of the the early and long-term hydration processes of cement pastes blended with 0–12 wt.% of silica fume can be summarized as follows:

- A lower beginning of the hydration processes was observed, which was probably caused by slower activation of the pozzolanic reactions.
- The resulting structure of studied pastes was more compact in time, as expected. However, in terms of pore size distribution, there was no clear trend, related to the silica fume content.
- After 360 days, the total porosity was the lowest in the pastes with the highest silica fume addition, which led to higher compressive strength results at later ages.
- A lower the CBW was determined with increasing dosage of silica fume in pastes, and therefore, the degree of hydration was also lower.
- Portlandite slightly increased in pastes stored in water until 90 days. Thereafter, a part of Portlandite, which was produced during the hydration processes, was consumed by the pozzolanic reactions. This consumption was more significant in pastes with the higher silica fume addition.
- In terms of calcite, when samples were stored in water, a decrease of its content was observed similarly to the plain pastes. However, when stored in air, the trend of the calcite content was significantly affected by the addition of silica fume. The higher amount of silica fume was added, the

lower was the level of carbonation, which is related to the lower amount of Portlandite available for carbonation processes.

- An exothermic reaction occurred in DSC thermographs when samples were heated above 790 °C. Its origin was not clear but it was time-dependent and somehow related to the silica fume content.

Characterization of cement pastes blended with natural zeolite

This chapter describes the experimental results of the cement pastes blended with natural zeolite (clinoptilolite). This pozzolana active material was chosen as a partial replacement of cement by up to 40 wt.%. Similarly like in the case of cement pastes blended with silica fume, the studied pastes were labelled as CZ8 and CZ40, referring to the percentage of the cement replacement.

For a more detailed description of the long-term hydration processes, the results of basic physical properties and mechanical properties are extended with the CZ16 and CZ24 pastes, and these are also included in the thermal analysis results. All studied pastes were cured in water until the analyses were performed. Additionally, the effect of two environments on the growth of the main hydration products was determined by means of thermal analysis.

9.1. Hydration heat

The early-stage hydration heat development of studied cement pastes blended with natural zeolite is shown in Figure 9.1.1. It can be seen that natural zeolite modified the heat evolution within the studied time interval up to 50 hours. Similar trends were observed in [291]. In the initial period up to about 4 hours and the following period of slow reaction, the specific hydration heat power (Figure 9.1.1a) significantly increased with increasing amount of natural zeolite in blended pastes. It means that the onset of C_3S hydration was accelerated due to the presence of natural zeolite in the pastes. This observation was in a good accordance with results presented in [292], where it was reported that the onset of C_3S hydration, Portlandite precipitation and AFt formation was substantially advanced by the addition of a natural clinoptilolite-rich tuff of low crystallinity. During the accelerating period, the maximal values were obtained between 10–12 hours for pastes with no or a lower addition of natural zeolites.

The highest value of specific hydration power was found in the reference paste, and it significantly decreased with increasing amount of natural zeolite in studied pastes. However, the second local maximum in the CZ40 pastes was found after 7.5 hours, implying the acceleration of the hydration processes in these pastes, compared to the other mixes under the study. At 12 hours, the specific hydration heats (Figure 9.1.1b) of all analyzed pastes were at the same level, regardless the zeolite content. For cements blended with 40 wt.% of natural zeolite, an extra peak was observed at 12 hours, emphasized even more the accelerating effect of zeolite on the hydration process. This peak could be related to the transformation of the AFt to the AFm phase [293]. It was not observed in the other studied pastes. During the later time periods after 20 hours, the specific hydration heat significantly decreased with increasing addition of natural zeolite.

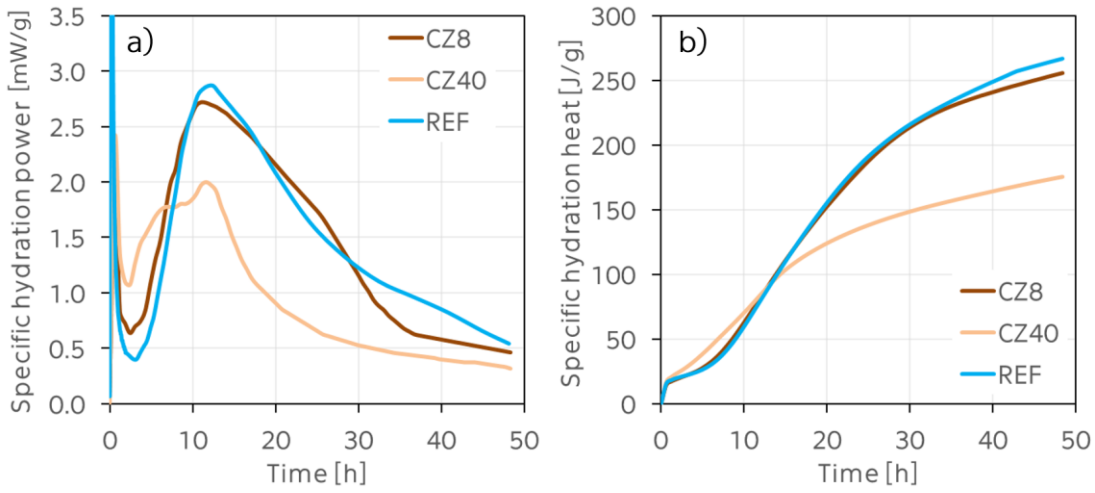

Figure 9.1.1. Specific hydration power (a) and specific hydration heat (b) of cement pastes blended with natural zeolite.

In terms of the pozzolanic reaction, it was reported that silica fume is more reactive than natural zeolite [91], and therefore, the lower values, of mechanical strength can be expected when natural zeolite is used to partially replace cement binder, especially at early ages [293]. In [293], the replacement of Portland cement in an amount of 10% by mass by natural zeolite was recommended as a limit for its effective use. Above this amount, a substantial part of zeolite did not participate in the hydration process and played a role of a fine filler instead.

9.2. Microstructural development

The evolution of microstructure of cement pastes blended with natural zeolite determined by means of SEM is shown in Figure 9.2.1. After 28 days, the CZ8 paste exhibited relatively dense microstructure in comparison to the CZ40 paste, where the C-S-H was found mainly in the form a network of tiles forming a three-dimensional structure referred to as "honeycomb" [294]. Portlandite formed flat layers, which were built into the structure of the C-S-H phases.

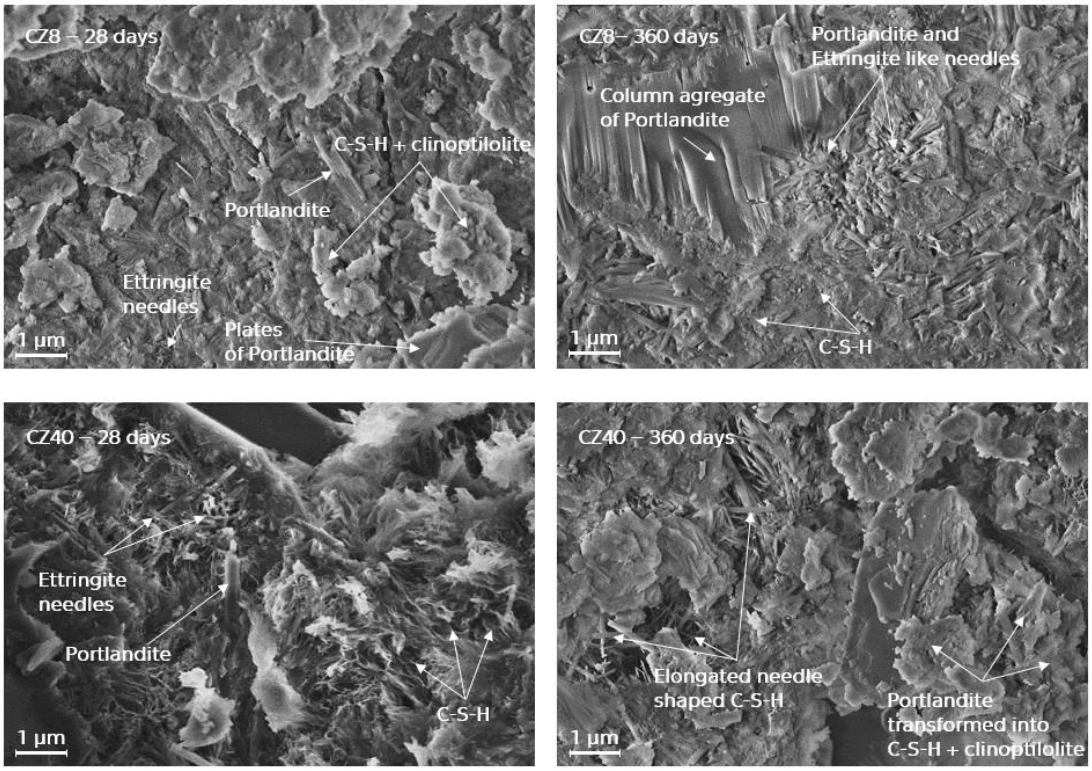

Figure 9.2.1. SEM micrographs of cement pastes blended with natural zeolite after 28 and 360 days.

Especially in the case of the CZ8 paste, these thin layers of Portlandite were transformed into massive column agregates in time. Portlandite was barely not spotted in the microstructure of the CZ40 paste already after 28 days. Usually, ettringite crystals are found in the form of elongated needles with a circular cross-section, creating distinctive clusters filling the empty spaces between the aggregated clusters of C-S-H phases [294], and these needles can be seen in the CZ8 pastes after 360 days. The "honeycomb" structure of C-S-H observed in the CZ40 paste after 28 days was transformed into elongated needle-shaped C-S-H

crystals located in voids and fissure [295]. In both studied pastes blended with natural zeolite, the clusters of clinoptilolite crystals were covered by the surrounding hydrated matrix.

The influence of natural zeolite on the amount of formed hydration products was analyzed by means of the XRD method. The corresponding XRD patterns are shown in Figure 9.2.2. The amounts of crystalline and amorphous phases were calculated based on the internal standard phase, 20 wt.% of ZnO. These computed results are summarized in Table 9.2.1. The addition of natural zeolite led to the formation of a very similar amount of amorphous phase (C-S-H) in blended pastes in comparison to the reference paste. The amorphous phase constituted 65.1% in the CZ8 paste after 28 days, which was about 2% more than in the REF paste. The lowest amount of the amorphous phase was found in the CZ40 paste, which indicates that a lower amount of the C-S-H phase was formed. With time, the amount of amorphous phase slightly increased in all studied pastes, and it remained the lowest in the CZ40 paste. Alite and belite exhibited a decreasing trend with increasing amount of natural zeolite in pastes after 28 and 360 days. They were gradually consumed due to the pozzolanic reactions.

Table 9.2.1. Mineral composition of the CZ pastes in wt.%.

Material	After 28 days			After 360 days		
	REF	CZ8	CZ40	REF	CZ8	CZ40
Albite	-	-	5.7	-	-	6.1
Alite	7.5	8.1	7.9	7.3	6.7	6.0
Amorphous	63.1	65.1	61.2	66.7	68.3	65.7
Belite	4.4	4.6	1.8	2.6	3.4	1.9
Calcite	3.2	3.0	2.1	3.2	3.3	4.8
Clinoptilolite	-	3.1	10.9	-	2.4	7.7
Ettringite	4.7	2.3	2.3	4.5	3.7	3.2
Ferrite	3.5	-	1.6	1.4	0.9	1.0
Gypsum	1.2	1.7	2.1	1.2	1.6	1.0
Portlandite	12.3	11.6	3.1	12.8	9.1	1.3
Quartz	0.2	0.5	1.4	0.3	0.6	1.4

The amount of ettringite was significantly lower in pastes blended with natural zeolite compared to the reference paste. Its amount slighly increased with time in the blended pastes, while it remained at the same level in the REF paste. Its formation into tricalcium–monosulfo–aluminate hydrate (AFm) was

not observed. However, it might have been present in the structure of pates, but its amount could be under the detection limit.

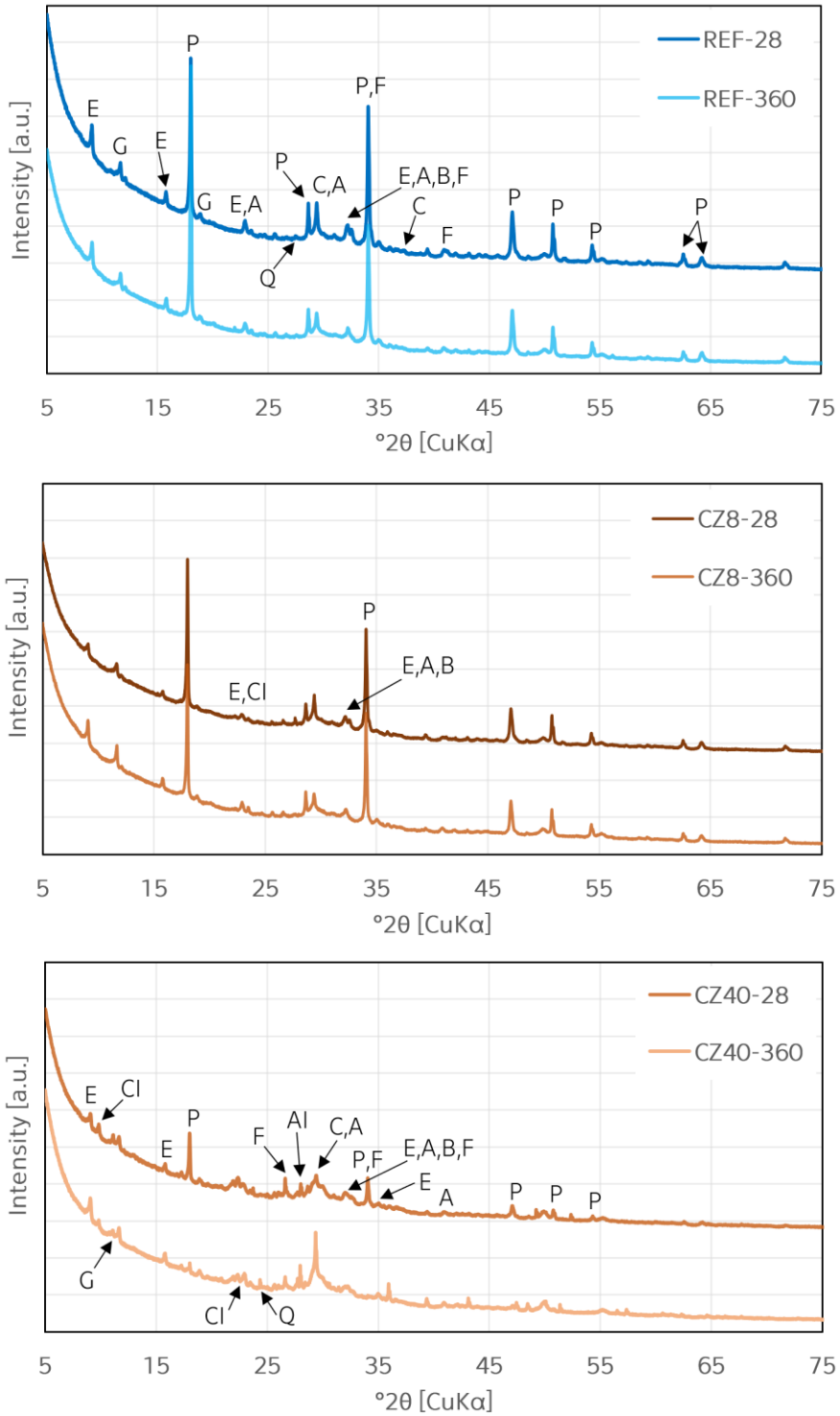

Figure 9.2.2. XRD patterns of cement pastes blended with 8 and 40 wt.% of natural zeolite after 28 and 360 days: A–alite, Al–albite, B–belite, C–calcite, Cl–clinoptilolite, E–ettringite, F–ferrite, G–gypsum, P–Portlandite, Q–quartz.

The impact of natural zeolite on the hydration processes of cement pastes can be also seen on the changing amount of Portlandite. After 28 days of hydration, the Portlandite content was at very similar levels in the CZ8 and the REF pastes, whereas its content was about four times lower in the CZ40 pastes. It refered to the pozzolanic reaction, which was speeded up with the higher addition of natural zeolite in the pastes [296]. While the amount of Portlandite decreased about 3% in the CZ8 paste after 360 days, only 1% was determined in the CZ40 pastes.

The amount of calcite slightly increased from 3% to 3.3% for the CZ8 pastes and from 2.1% to 4.8% for the CZ40 after 28 and 360 days, respectively. It was with a good accordance with the decreasing Portlandite content. About 3% of clinoptilolite was detected in the CZ8 pastes after 28 days and it decreased to 2.4% at the end of hydration. It was found in higher quantities in the CZ40 pastes, about 11% and 8% after 28 and 360 days, respectively. In addition, about 6% of a mineral albite was found in the composition of the CZ40 pastes after both selected days of hydration. This remaining amount of clinoptilolite and albite (both were present in the structre of natural zeolite) played a role of an inert filler.

The cumulative intruded pore volume curves and pore size distribution of the cement pastes blended with natural zeolite were determined at 28 and 360 days of age by means of MIP, and these results are shown in Figure 9.2.3. After 28 days of hydration, the volume of the gel pores, appearing in the range from 0.01 μm to 0.1 μm, increased significantly in the CZ40 pastes compared to the reference paste (Figure 9.2.3a, b). The increase of pore volume was mainly due to fine pores of diameter below 0.1 μm, which is characteristic for zeolites in general, as reported in [297, 298]. Therefore, it can be expected that an increasing addition of natural zeolite in cementitious materials will primarily lead to an increase of pore volume in the range below 0.1 μm [297], as can be seen in this study as well. However, the addition of 8 wt.% of natural zeolite exhibited a lower amount of gel pores compared to the reference paste (Figure 9.2.3a). It can be caused by the pozzolanic reactions, which effectively consumed natural zeolite up to 10 wt.% of its cement replacement [293]. In the case of the larger (capillary) pores, which are ranging from 0.1 μm to 100 μm, the CZ40 paste also contained a higher amount of these pores compared to the REF paste. This effect can also

be seen as a significant shift in the cumulative pore volume curve in Figure 9.1.3a in this area.

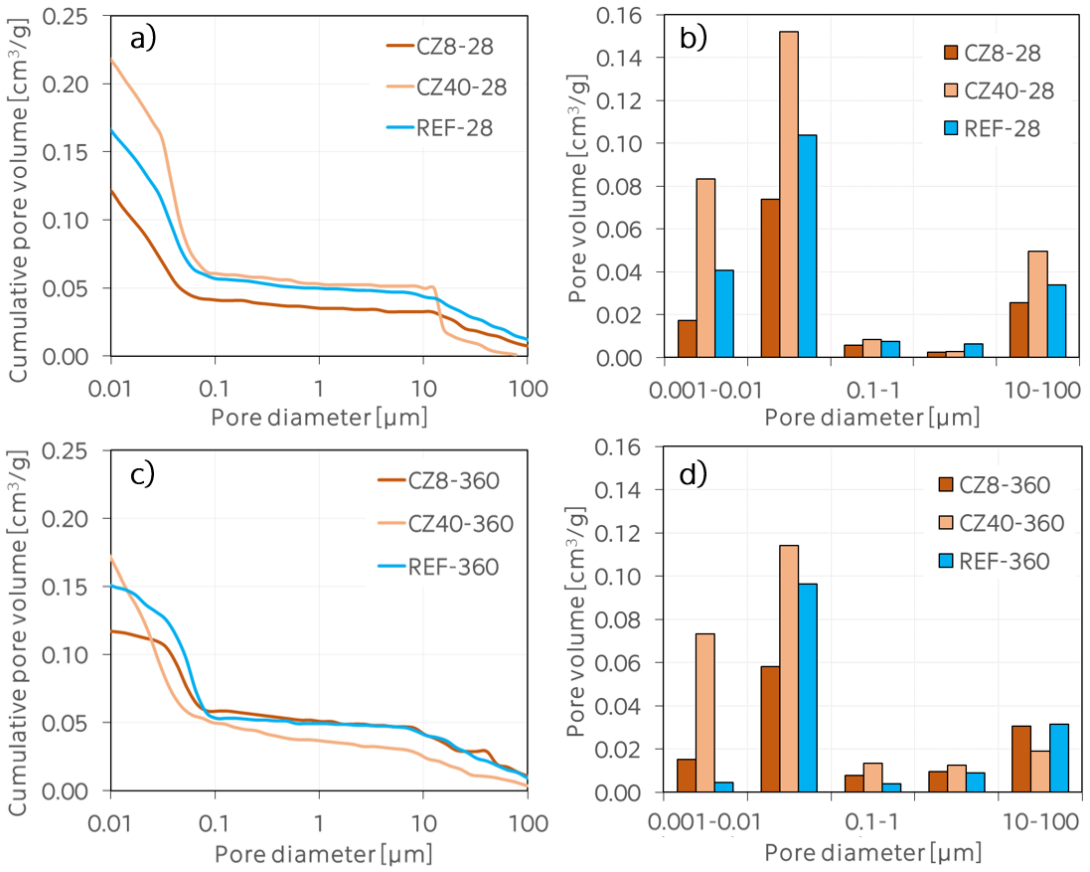

Figure 9.2.3. Dependence of the cumulative pore volume curves and pore size distribution of studied pastes on the level of the addition of natural zeolite.

After 360 days of hydration, the volume of the capillary pores gradually decreased (Figure 9.1.3c, d) in all studied pastes, the most visibly in the CZ40 paste. The capillary pores were gradually transformed into gel pores, appearing mainly in the range from 0.01 µm to 0.1 µm. However, this transformation cannot be properly seen in the Figure 9.2.3d, because natural zeolite was gradually consumed by the pozzolanic reactions, which led to a decrease of the pores in the range with gel pores.

In summary, the addition of natural zeolite (clinoptilolite) into cement pastes modified the morphology of the hydration products. In the CZ8 paste, Portlandite formed flat layers, which were transformed into massive column aggregates in time. Portlandite was barely not found in the CZ40 paste, which means that it was gradually consumed by the pozzolanic reactions already within 28 days. A higher

content of clinoptilolite detected in the CZ40 pastes after 360 days implies that a higher addition of natural zeolite played a role of inert filler rather than a pozzolana active material. In terms of the pore structure, it was found that the replacement of 40 wt.% of cement by natural zeolite led to an increase of pore volume in the range below 0.1 μm, which is characteristic for the natural zeolite itself, after 28 days of hydration. After 360 days, both, capillary and gel pores decreased in the structure of the blended cement pastes, which indicated that natural zeolite was gradually consumed by the pozzolanic reactions.

9.3. Basic physical properties

Table 9.3.1 shows results of the matrix density, bulk density and the total open porosity of the studied pastes. In addition, the results of CZ16 and CZ24 pastes are also presented in this section. The highest matrix density values were obtained for the reference paste, 2229 kg/m^3, after 28 days, showing a decreasing trend with an increasing amount of natural zeolite. The lowest value of the matrix density was achieved for the CZ40 paste, 1898 kg/m^3, as expected. These values gradually decreased in time as the hydration products were formed.

Table 9.3.1. Basic physical properties of studied pastes.

Paste	Age [days]	Matrix density [kg/m^3]	Bulk density [kg/m^3]	Total open porosity [%]
REF	28	2229	1550	30.5
CZ8	28	2145	1455	32.2
CZ16	28	2056	1373	33.2
CZ24	28	1982	1308	34.0
CZ40	28	1898	1235	34.9
REF	360	2062	1702	17.5
CZ8	360	1986	1523	23.3
CZ16	360	1895	1421	25.0
CZ24	360	1789	1335	25.4
CZ40	360	1735	1268	26.9

The 28-days bulk density exhibited a similar trend in comparison to the matrix density, as it was the highest in the REF paste whereas it was the lowest in the CZ40 paste, 1550 kg/m^{3}and 1235 kg/m^3, respectively, showing an

increasing trend in time. In terms of total open porosity, pastes containing up to 8 wt.% of natural zeolite exhibited similar porosity (32.2%) like in the reference paste, 30.5%. It increased with an increasing amount of natural zeolite in blended pastes by up to 35% in the CZ40 paste. The total open porosity showed a decreasing trend with time, however, pastes blended with natural zeolite exhibited about 6–9% higher values compared to the reference paste after 360 days.

9.4. Mechanical properties

The effect of natural zeolite on the mechanical properties is shown in Figure 9.4.1. The development of the compressive strength (Figure 9.4.1a) was not improved after 2 days of hydration, as the maximal compressive strength was observed for the reference paste. This trend was expected based on the results of the hydration heat, presented in the Section 9.1. The pozzolanic reaction was probably activated after 7 days, when the CZ8 paste reached 43.96 MPa, which was about 3 MPa higher than for the REF paste. The pastes containing higher levels of natural zeolite exhibited lower compressive strength values. These results were in a good agreement with [299], where the slower increase of compressive strength was explained by a lack of sufficient Portlandite, caused by slow development of hydration despite the sufficient amount of reactive SiO_2 in the studied mortars.

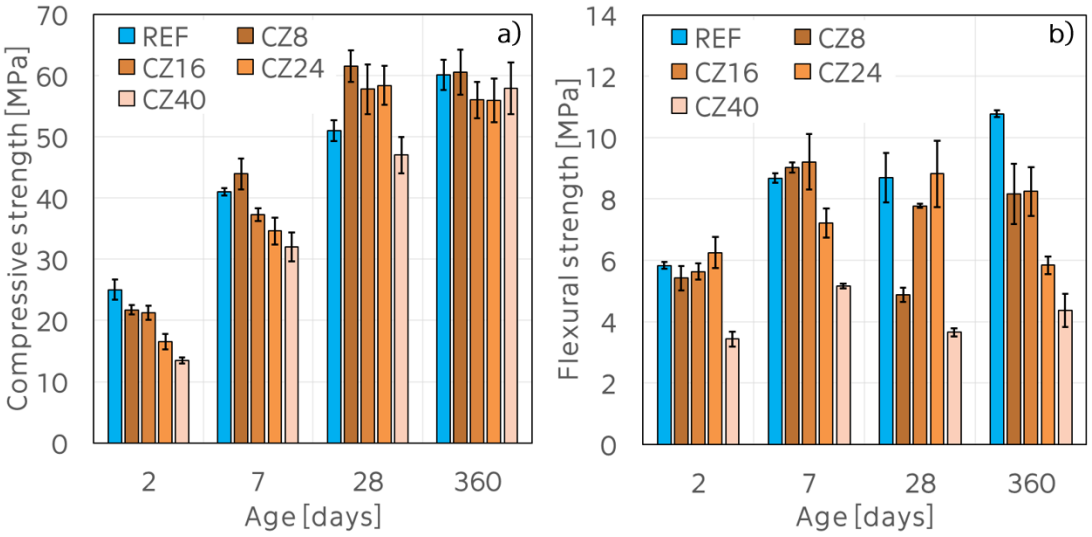

Figure 9.4.1. Mechanical properties of the blended pastes: a) compressive and b) flexural strength as a function of a natural zeolite replacement and time.

After 28 days, the effect of natural zeolite on the studied pastes became more significant, as the compressive strength determined for the CZ8, CZ16 and CZ24 was higher in comparison to the reference paste. The highest value was observed again for the CZ8 paste, 61.57 MPa, which was about 17% higher than for the REF paste. After 360 days, the differences between the studied pastes were very low. Nevertheless, the reference paste and the paste blended with the lowest amount of natural zeolite gave the best performance. Similar results were observed in [300].

In terms of the flexural strength, the reference paste exhibited an increasing trend in time, while the pastes containing natural zeolite did not show any specific trend. It is interesting that after 360 days of hydration, the flexural strength for all blended pastes decreased compared to the 7-days values.

9.5. Thermal analysis results

The development of hydration products of cement pastes blended with up to 40 wt.% of natural zeolite when stored in diferent environments were determined by means of thermal analysis. The results obtained from TGA analysis for storage in water (W) and in air (A) are summarized in Figures 9.5.1–9.5.4.

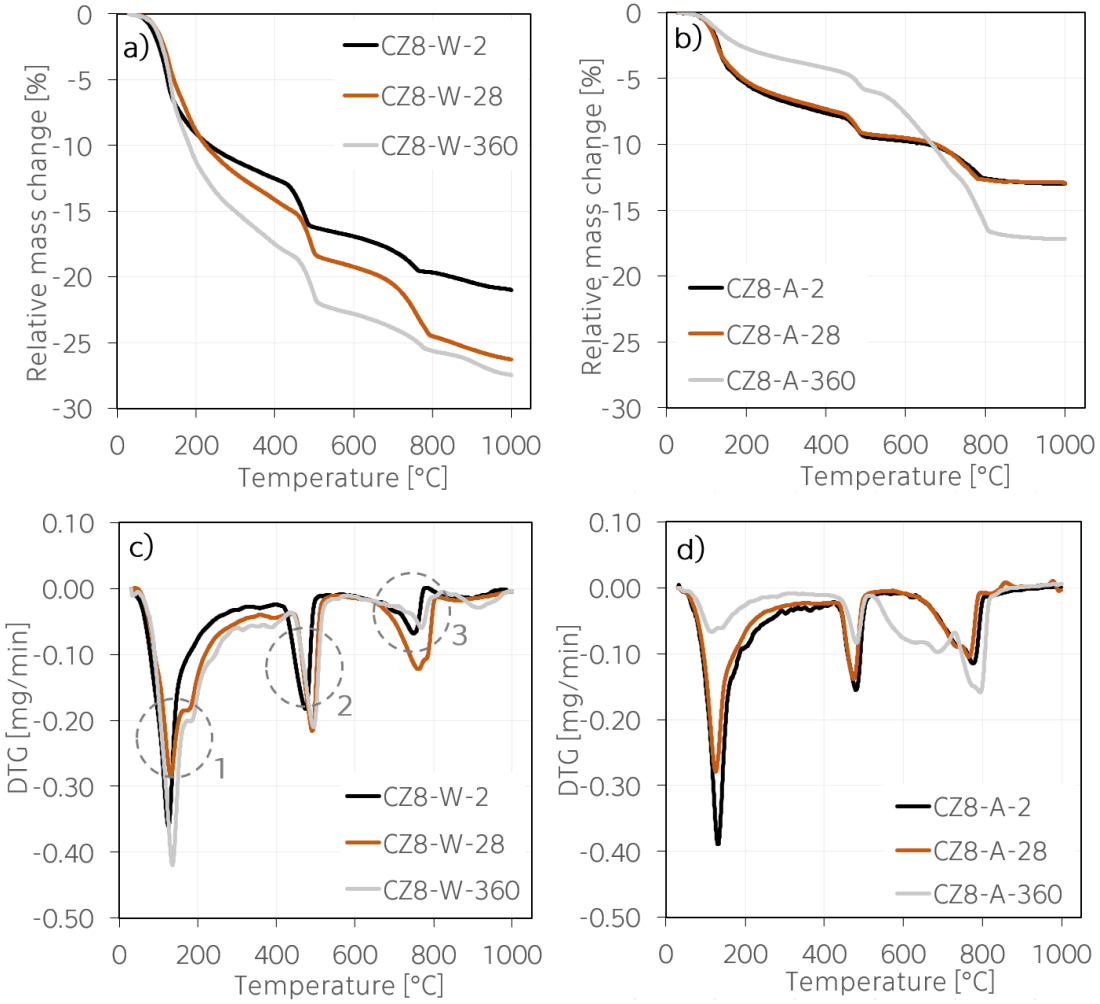

Figure 9.5.1. Thermal analysis results for pastes blended with 8 wt.% of natural zeolite stored in: (a, c) water and (b, d) air.

Similarly to the previously presented pastes, each designed paste was analyzed 3-times when cured in air, and 2-times when cured under water after 2, 7, 28, 90, 180 and 360 days of hydration (30 experiments in total per a paste). Only selected experiments after 2, 28 and 360 days of hydration of relative mass change [in %] and its derivation [in mg/min] are shown for both studied

environments. Nevertheless, the related computations are done with the utilization of results from all experiments.

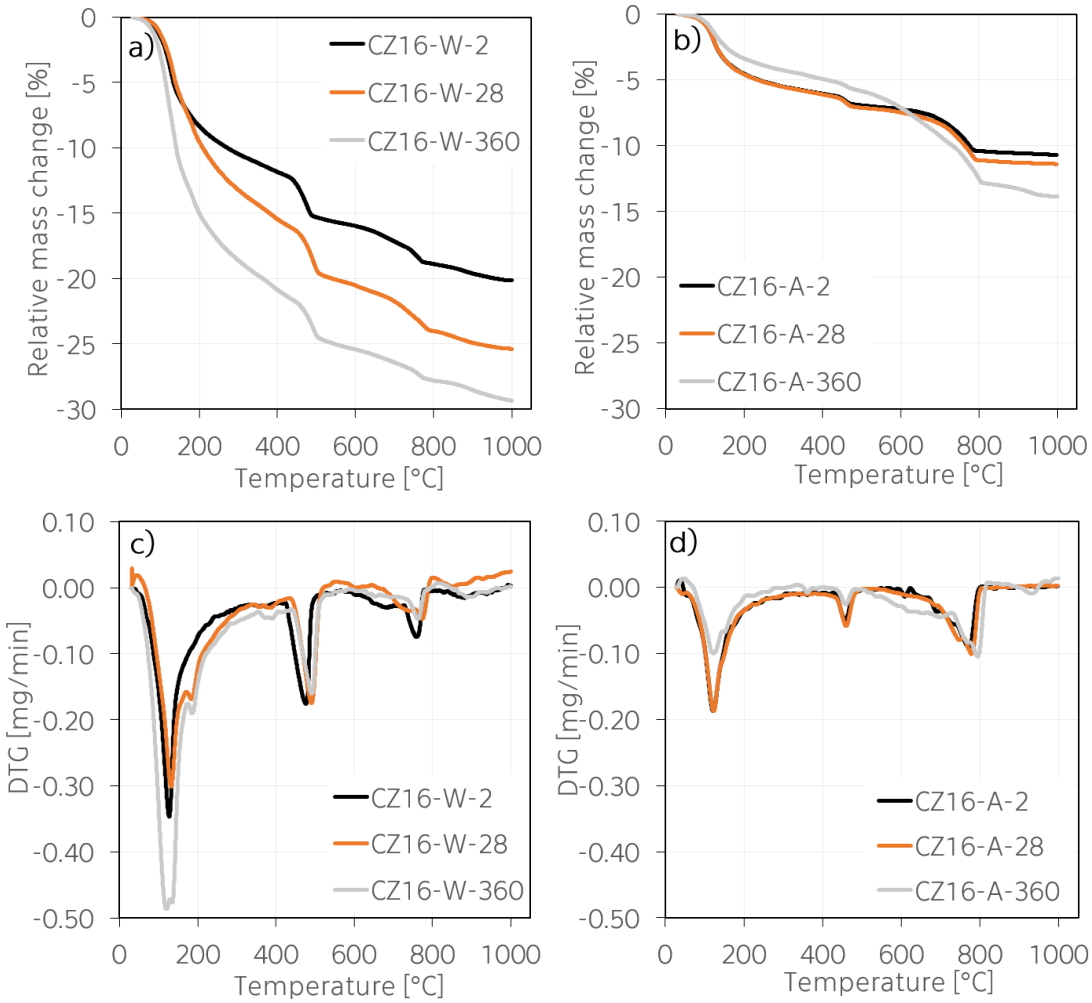

Figure 9.5.2. Thermal analysis results for pastes blended with 16 wt.% of natural zeolite stored in: (a, c) water and (b, d) air.

Also in the case of pastes blended with natural zeolite, a further analysis of the TGA results is divided based on the area with the most significant mass changes spotted by DTG, as illustrated in Figure 9.5.1c. In accordance with the previously discussed results of the plain cement pastes and those blended with silica fume, the first peak is related to the decomposition of C-S-H, ettringite and gypsum. The analysis of this peak area is focused on the determination of the CBW, which is released also during the decomposition of Portlandite occuring between 400 and 550 °C (labelled as 2). The degree of hydration of these blended pastes is computed based on the methods proposed by De Weerdt et al. [203]

and Bhatty [235], and it is presented in a separated section, showing the impact of different levels of the natural zeolite addition as a function of time.

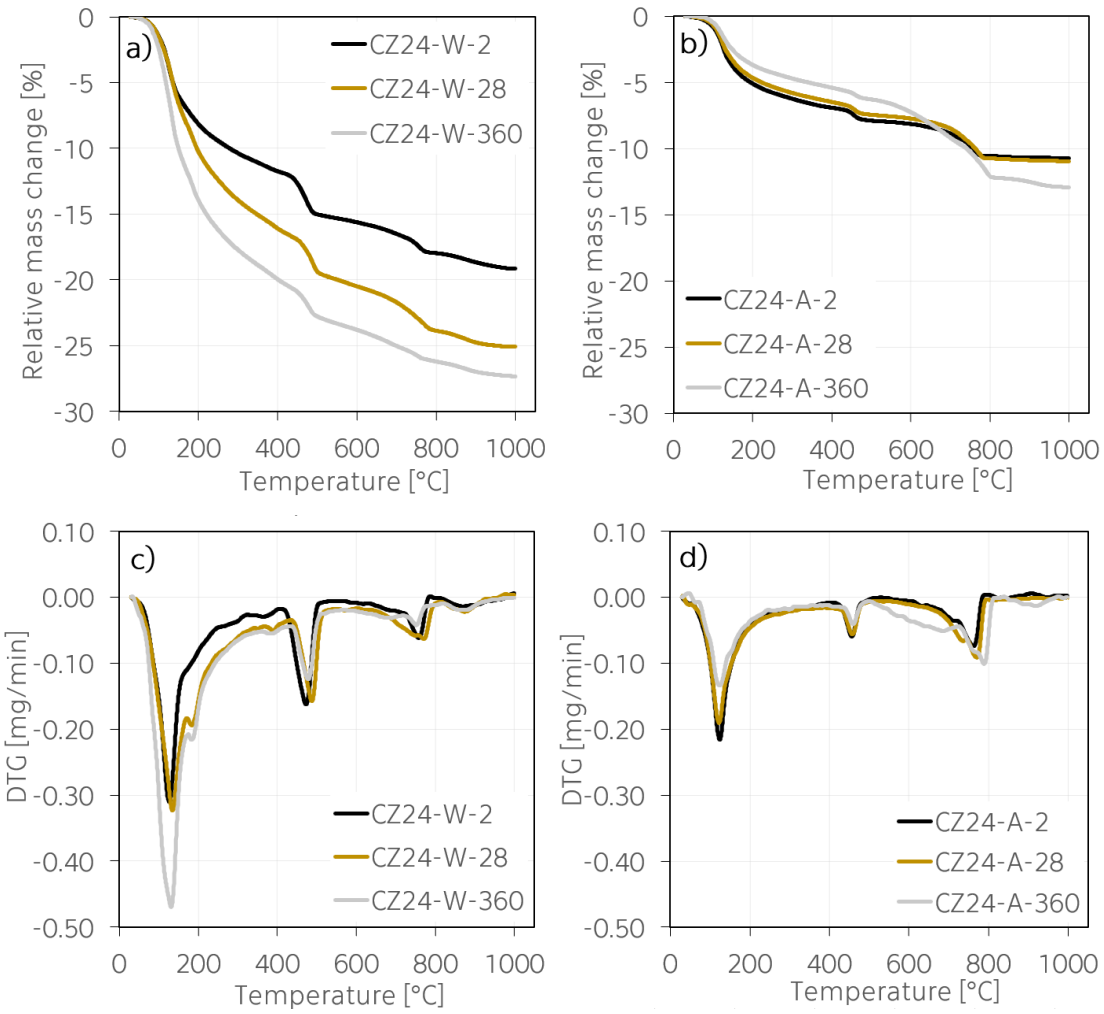

Figure 9.5.3. Thermal analysis results for pastes blended with 24 wt.% of natural zeolite stored in: (a, c) water and (b, d) air.

The changes of the Portlandite amount (2), which refers to the pozzolanic reactivity of natural zeolite, are described by the stepwise and tangential methods. Results obtained using these methods are analyzed and compared to the literature. The impact of different amounts of natural zeolite on the consumption of this hydration product is disccused.

The changes in the amount of calcite (3) are analyzed thereafter. It can be clearly seen that the different storage of the samples significantly affects the formation of this product, that is related to the carbonation procesess.

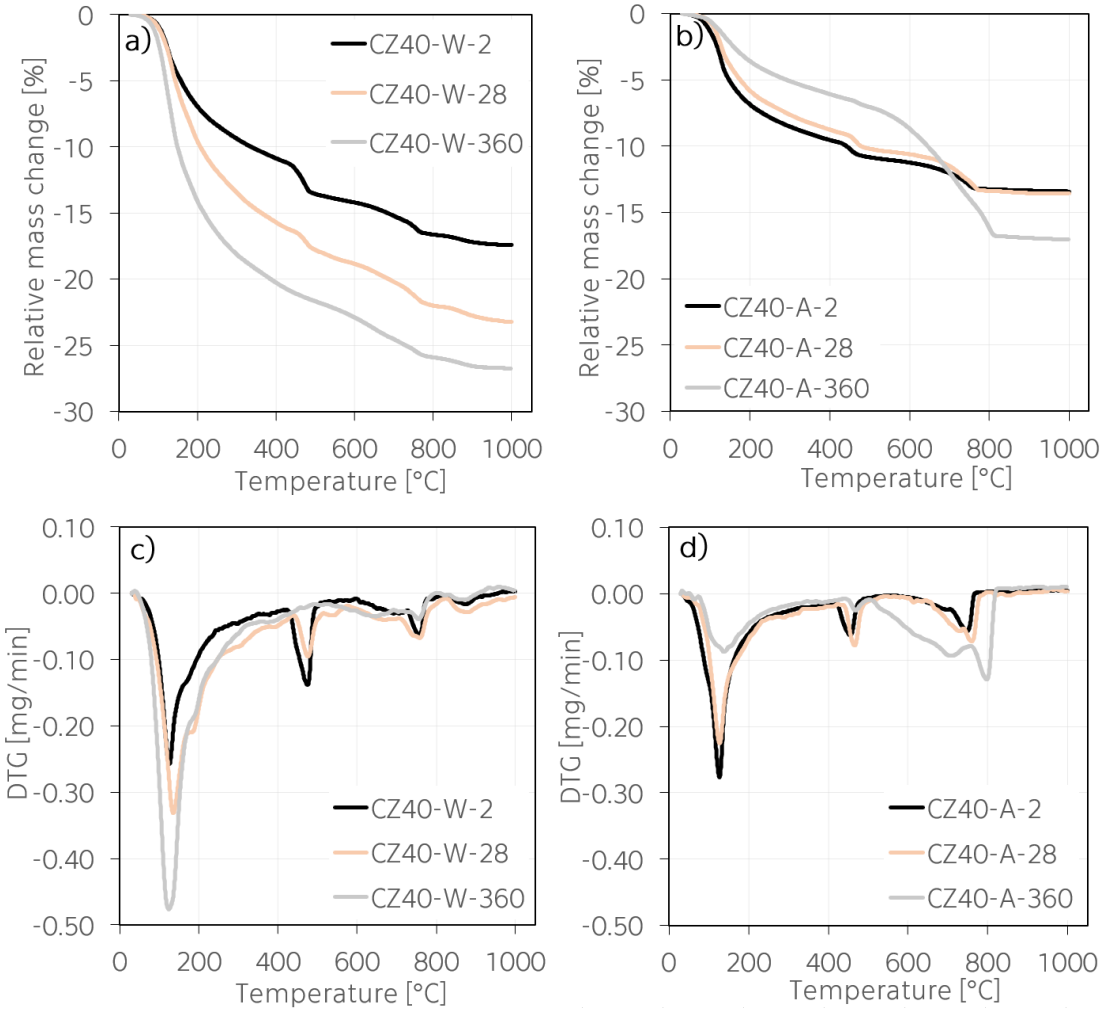

Figure 9.5.4. Thermal analysis results for pastes blended with 40 wt.% of natural zeolite stored in: (a, c) water and (b, d) air.

Finally, in the last section, the results of heatflow are also presented. Similarly, to pastes blended with silica fume and stored in air, an exothermic reaction occurred in the similar temperature interval (above 790 °C). This reaction was not accompanied with a mass change. Nevertheless, this exothermic reaction was time-dependent and it was found in similar cement systems [223]. Its origin and effect on the hydration procesess are discussed in a separated section.

9.5.1. Chemically bound water

The content of the CBW of pastes blended with different levels of natural zeolite, stored in water, was determined based on the methods proposed by De Weerdt et al. [203] and Bhatty [235]. The same approximate temperature ranges, as provided earlier in Table 7.5.1, were used for these calculations. Selected mass changes obtained from the TGA experiments are presented in Table 9.5.1. The mass changes from the decomposition of Portlandite were determined individually for each sample.

Table 9.5.1. Selected mass loss values [in mg] determined by TGA.

Paste	Age [days]	M_{sample}	$M_{135°C}$	$M_{400°C}$	$M_{600°C}$	$M_{1000°C}$
CZ8-W	2	50.5	47.45	44.12	42.24	39.90
	28	50.5	48.36	42.95	41.03	37.22
	360	50.3	47.64	41.11	39.10	36.50
CZ16-W	2	49.7	47.12	43.67	42.04	39.67
	28	49.7	47.43	41.67	39.75	37.06
	360	50.4	45.87	39.47	37.88	35.60
CZ24-W	2	51.0	48.49	44.95	43.28	41.22
	28	50.0	47.55	41.67	40.13	37.45
	360	51.1	47.05	40.52	39.34	37.12
CZ40-W	2	50.2	48.38	44.63	43.34	41.45
	28	51.0	48.96	42.71	41.85	39.15
	360	50.7	46.71	39.99	39.74	37.12

Based on these values, the CBW content was computed. The obtained results are summarized into Figure 9.5.5. The results of the reference paste are also provided for a better comparison. Compared to the previously discussed plain and pastes blended with silica fume, the resulting curves are less smooth. The addition of natural zeolite at all levels significantly decreased the amount of the CBW after 2 days of hydration. The CBW determined using the method proposed by De Weerdt et al. [203] was about 12.1% for the CZ8 paste, and the lowest amount was observed for the CZ40, where it was 11.3%. These results were very similar for both applied methods.

After the pozzolanic reaction was activated (7 days approximately), the CBW content increased up to about 17.7% for pastes with 16 wt.% of natural zeolite, reaching approximately higher values compared to the reference paste (16.9%). Pastes with a higher pozzolan content exhibited lower values in the CBW content during the whole studied interval. Moreover, it seems that pastes with 24 and 40 wt.% of natural zeolite reached the maximal "saturation" after 180 days, as the CBW content remained almost the same after 360 days. However, because it was expected to obtain an increasing trend of the CBW content in pastes blended with certain amounts of natural zeolite, the method proposed by De Weerdt et al. [203] seemed to be more suitable for the plain cement pastes or for pastes with a lower expected CBW.

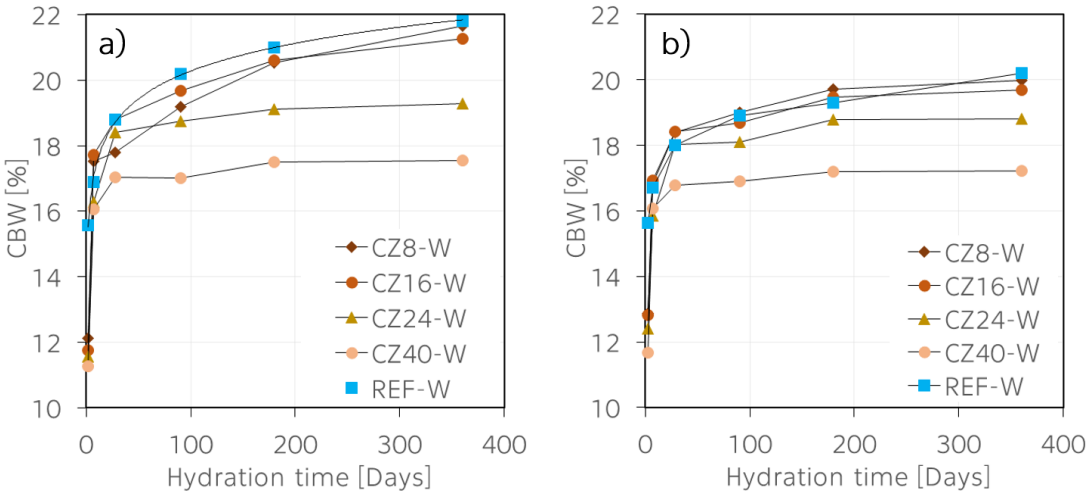

Figure 9.5.5. The amount of CBW determined using methods proposed by (a) De Weerdt and (b) Bhatty.

When the Bhatty's method [235] was applied (Figure 9.5.5b), the amount of the CBW moved into lower values, as already observed in the case of both previously discussed cement pastes. However, the obtained trend showed shifts in the CBW for pastes up to 16 wt.% of natural zeolite above the reference sample after 7 days of hydration until 360 days. The higher CBW content in hydration products in zeolite pastes indicated that the presence of zeolite modified the amount and/or the kind of hydration products [301].

Because the variation between the results was too high, the associated trendlines cannot be expressed mathematically.

9.5.2. Degree of hydration

The computed degree of hydration of studied pastes is summarized in Figure 9.5.6. The results computed using the method proposed by De Weerdt et al. [203] are summarized in Figure 9.5.6a, and similarly like in the case of the pastes blended with silica fume, they are displayed mainly for illustrative purposes.

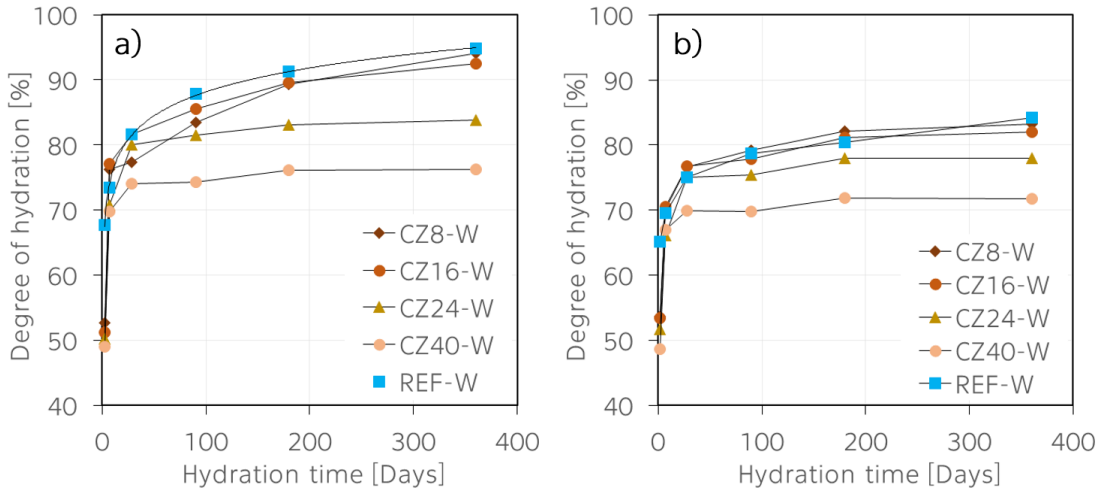

Figure 9.5.6. Degree of hydration of studied plain cement pastes determined using methods proposed by (a) De Weerdt et al. and (b) Bhatty.

The results of the degree of hydration computed by the Bhatty's method [235], are shown in Figure 9.5.6b. It reached about 53.7% for the CZ8 paste after 2 days of hydration, and about 65.1% for the reference paste. The lowest value was achieved for the CZ40 paste, where the degree of hydration was 48.6%. These results were in a good agreement with the hydration heat and mechanical properties presented earlier. A significant shift into higher values was observed after 7 days of hydration for all studied blended pastes. These values gradually increased up to about 85% after 360 days for the reference paste and the paste with the lowest natural zeolite content. The higher addition of natural zeolite, the lower the degree of hydration was observed. It reached about 71.8% in the CZ40 pastes after 360 days. From the Figure 9.5.6b, it also seems that the highest amount of zeolite was consumed until 180 days, as the degree of hydration increased only moderately in pastes with 16–40 wt.% of zeolite. It was reported that after 14 days of reaction 89% of the K-clinoptilolite, 88% of Na-clinoptilolite, 79% of the Ca-clinoptilolite and 45% of the chabazite were

consumed in cement pastes [292]. These high values of the clinoptilolite consumption could explain the significant shifts in the degree of hydration between 2 and 7 days, observed in this study. It was reported in [91], that lower w/c ratio of 0.25 and 0.3 significantly prolonged the hydration processes, when OPC was mixed with up to 25% of zeolite, as the degree of its pozzolanic reaction was approximately only 5% for both pastes after 3 days (computed from the insoluble residues and ignited samples).

9.5.3. Portlandite evolution

The Portlandite development as a function of the addition of natural zeolite and time was determined from the TGA experiments using the stepwise and tangential methods. These results are displayed in Figure 9.5.7.

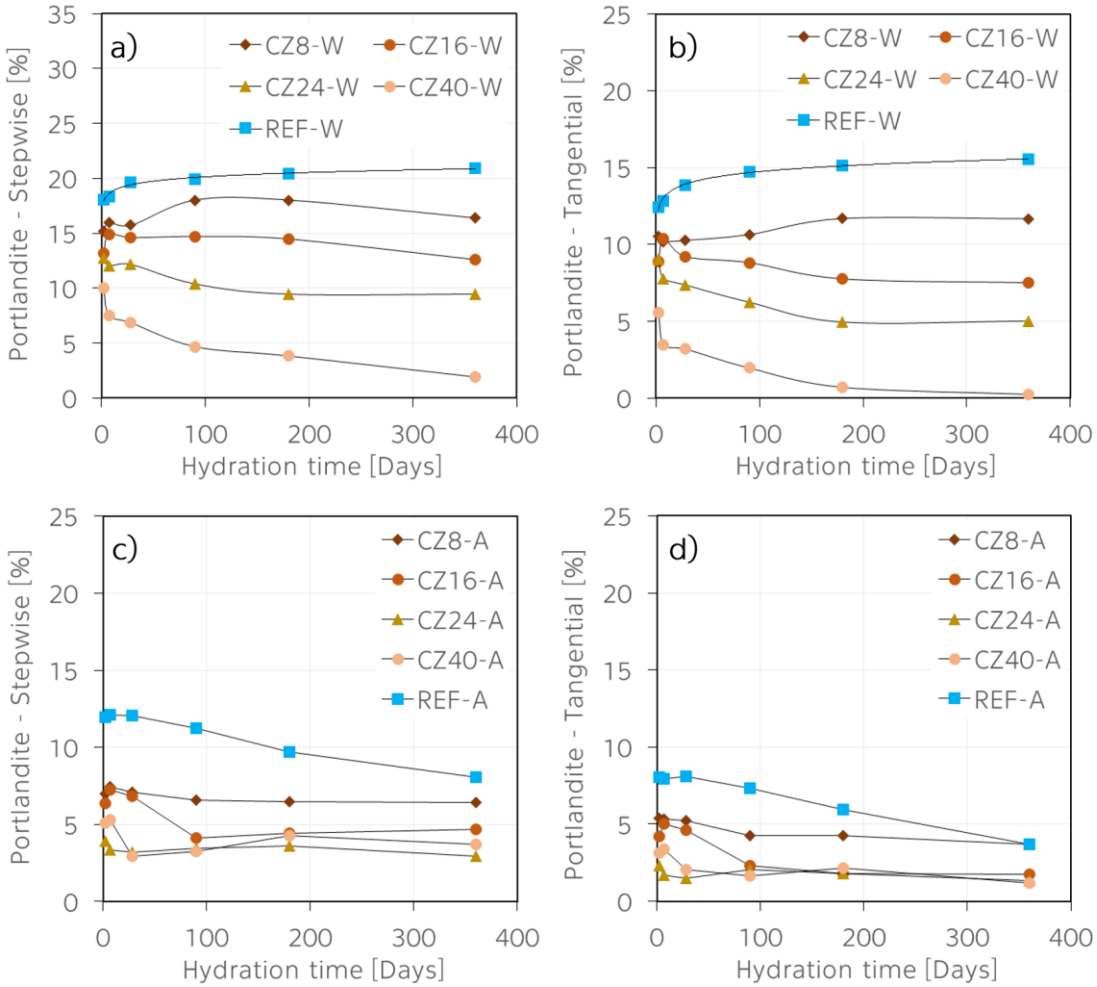

Figure 9.5.7. Portlandite evolution at studied pastes blended with natural zeolite determined by (a, c) stepwise and (b, d) tangential methods.

When pastes were stored in water (Figure 9.5.7a, b), the addition of natural zeolite at all levels led to a significant decrease of Portlandite compared to the reference paste. After 2 days of sealed curing, the amount of Portlandite was 15.2% for the CZ8-W, and only 10.0% for the CZ40-W as obtained by the stepwise method (Figure 9.5.7a). After 7 days, the amount of Portlandite slightly increased in the pastes with up to 16 wt.% of zeolite while an opposite trend was observed for pastes with a higher zeolite content. In the pastes with 8 wt.% of zeolite, the increase of Portlandite was observed until 90 days of hydration, indicating that a higher amount of Portlandite was produced during the hydration processes, than it was consumed by the pozzolanic reaction. In the pastes with more than 24 wt.% of zeolite, the highest amount of Portlandite was observed after 2 days of hydration, and thereafter, it was gradually consumed up to 360 days (a higher amount of Portlandite was consumed than produced). Its amount decreased to 10.4% in the CZ24-W paste, and it was only 4.7% in the CZ40-W paste. Similar results were reported in [301-303].

The results of the tangential method (Figure 9.5.7b) were in a good agreement with those from the XRD method, as the amount of Portlandite in the CZ8-W and CZ40-W pastes was 10.5% and 5.6% after 2 days of hydration, and after 360 days, these values were determined as 11.7% and 0.3%, respectively.

When pastes were stored in the air environment (Figure 9.5.7c, d), very similar results were determined using both, stepwise and tangential methods because the Portlandite content was generally lower in pastes stored in air. In the case of the stepwise method, the CZ8-A reached about 7.0% of Portlandite. Its amount slightly increased after 7 days (7.5%), when it reached its maximum. After 360 days of hydration, its value remained around 6.4%. Portlandite had a decreasing trend with increasing amount of zeolite in pastes. However, it seems that its amount remained almost the same at all studied blended pastes between 180 and 360 days. The tangential method provided similarly low results. Except for the CZ8-A paste, the Portlandite content was found lower than 5% for all studied pastes. Its amount gradually decreased within the studied interval up to 360 days. These results also demonstrated that there was a lack of water supporting, besides hydration processes, also the pozzolanic reactions.

9.5.4. Carbonation progress

The changes in the calcium carbonate content were determined from the TG curves using the Eq.(5.6.10). These results are summarized in Figure 9.5.8. At first sight, it can be seen that the water environment, similarly like in the case of the plain and cement pastes blended with silica fume, preserved samples and protected them from carbonation (Figure 9.5.8a). Whereas pastes stored in air were exposed to CO_2, and thus, the carbonation processes started already after several days of hydration, as indicated by the increase of amount of calcite (Figure 9.5.8b).

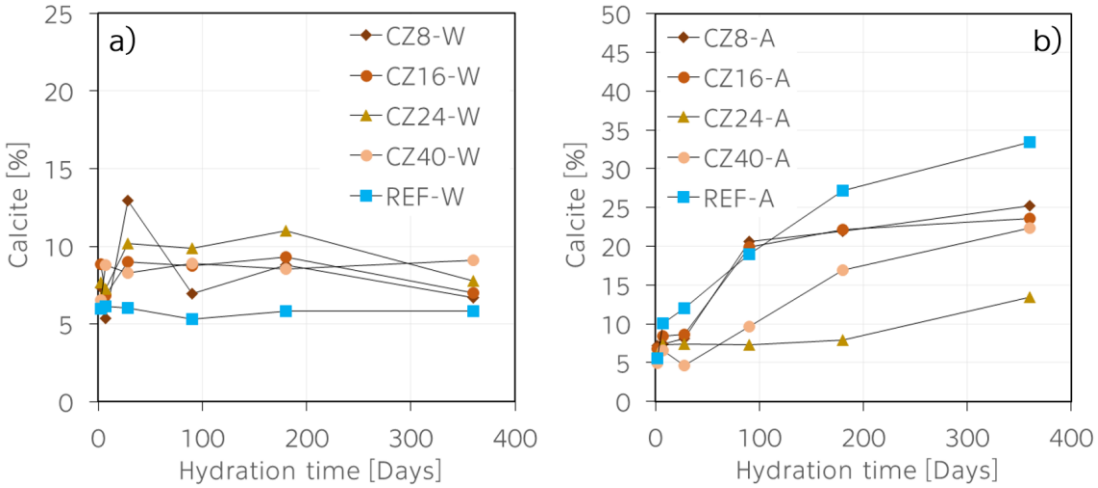

Figure 9.5.8. Evolution of the calcite content for blended cement pastes stored in (a) water and (b) air.

At the beginning of the hydration processes, the lowest amount of calcite was found in the REF-W paste, 6.0% after 2 days. Higher values were obtained with increasing amount of natural zeolite in pastes, which was observed in the pastes blended with silica fume as well. However, there was no specific pattern indicating if an increasing amount of zeolite in pastes could lead to higher amounts of calcite in pastes. Nevertheless, theoretically, the higher amount of Portlandite available for carbonation processes was produced in the pastes with up to 24 wt.% of natural zeolite. This expected trend can somehow be seen in Figure 9.5.8a in the CZ24-W paste, while its effect was not that significant for the CZ8-W paste. The evolution of calcite content exhibited a decreasing trend until 90 days of hydration. As already discussed, this can be caused by the ability of calcium carbonate to dissolve in water under specific conditions [264, 265]. The

amount of calcite was determined as 5.3% for the REF-W. It reached about 6.9% for the CZ8-W paste and it slightly increased with increasing addition of natural zeolite. After 360 days of hydration, the highest calcite content was observed in the CZ40-W paste, 9.1%, and it decreased with increasing zeolite content. It was the lowest for the blended pastes with the lowest amount of zeolite, 6.7%. The reference paste was not affected by the carbonation processes during the studied interval.

A similar observation like in the case of the plain cement pastes and pastes blended with silica fume was done on the surface of the studied samples after 360 days of hydration, and it was documented in Figure 9.5.9. As already discussed, this additional white layer created on the surface of samples was probably caused by water leaking through the samples and dissolving Portlandite from the matrix. This later led to the formation of calcium carbonate layer (or calcium sulphate) [269] on the surface of the samples.

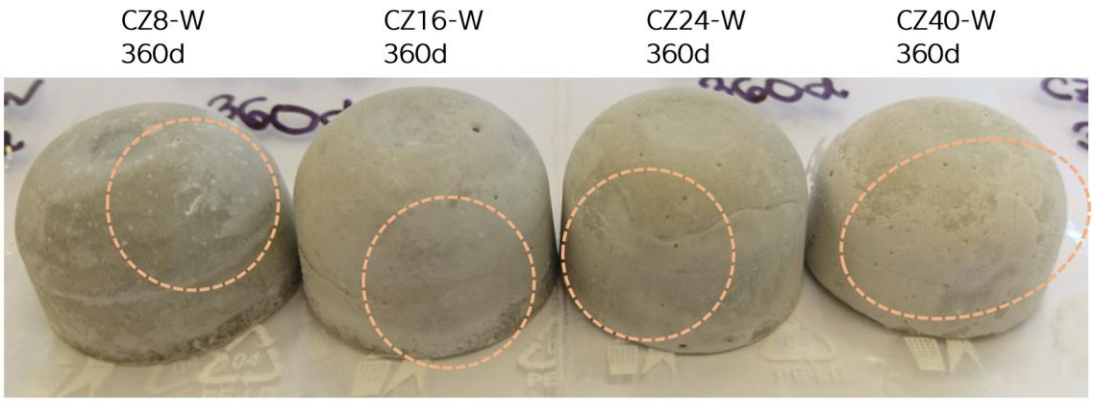

Figure 9.5.9. Additional calcium carbonate layer observed on the surface of studied samples as a result of lime leaching.

When blended pastes were stored in air (Figure 9.5.8b), the trend of the calcite content was significantly affected by the addition of natural zeolite. The higher amount of natural zeolite was added, the lower was the level of carbonation, which was in a good agreement with literature [304], where positive effects of clinoptilolite on the carbonation depth of mortars containing clinoptilolite after 90 days of hydration were reported. In the carbonation tests, samples were cured in the humidity chamber (21 ± 1 °C, 50% RH). In this study,

the amount of calcite was about 25% and 33% lower in the CZ8-A and CZ40, respectively, compared to the reference paste after 360 days.

There is a lack of studies dealing with the effects of natural zeolites on the carbonation processes. However, the positive impacts of this natural pozzolan on the durability parameters has been reported frequently [300, 305, 306]. From these studies, the main conclusion was that natural zeolite is less effective than silica fume in terms of improving durability. However, its is significantly cheaper [306].

9.5.5. Crystallization

Similarly, to the pastes blended with silica fume, an exothermic reaction occured during heating at higher temperatures above 790 °C. This crystallization was spotted for example in [223], where its origin was discussed. In a study by Sha and Pereira [222] an exothermic peak was observed in a similar temperature range, but it was probably caused by the transformation of metakaolin into spinel ($MgAl_2O_4$). In [223], it was concluded, that the newly formed phase was wollastonite ($CaSiO_3$). It was caused by the products of the pozzolanic reaction between OPC and natural zeolite. Its size corresponded to the degree of crystallization between Ca and Si, as proposed in [280]. Because in this study, the used clinoptilolite was rich in SiO_2, it is assumed, that the newly formed phase in this study could be wollastonite or gehlenite ($Ca_2Al_2SiO_7$) [307].

The selected results of heatflow of blended pastes containing various levels of natural zeolite are displayed in Figure 9.5.10. The experiments were performed in the same time interval like TGA (2, 7, 28, 90, 180 and 360 days). Even though the exothermic reaction was observed in samples stored in both environments, the consequent analyses of heatflow were done only in the case of pastes stored in air because the background was less stable (not constant) for the pastes stored in water. Additional lines displayed in Figure 9.5.10 demonstrate that the background was not perfectly constant neither for the pastes stored in air, which made the computations of enthalpy more difficult, as discussed in [238].

As it can be seen in Figure 6.1.5, where the heatflow of unhydrated natural zeolite is shown, there is no exothermic reaction above 800 °C. Therefore, the crystallization occurring in blended pastes could not be used for monitoring of the amount of unreacted natural zeolite. However, the crystallization reaction

occurring above 800 °C seems to be time-dependent and the size and intensity of its peak varied with the amount of natural zeolite addition.

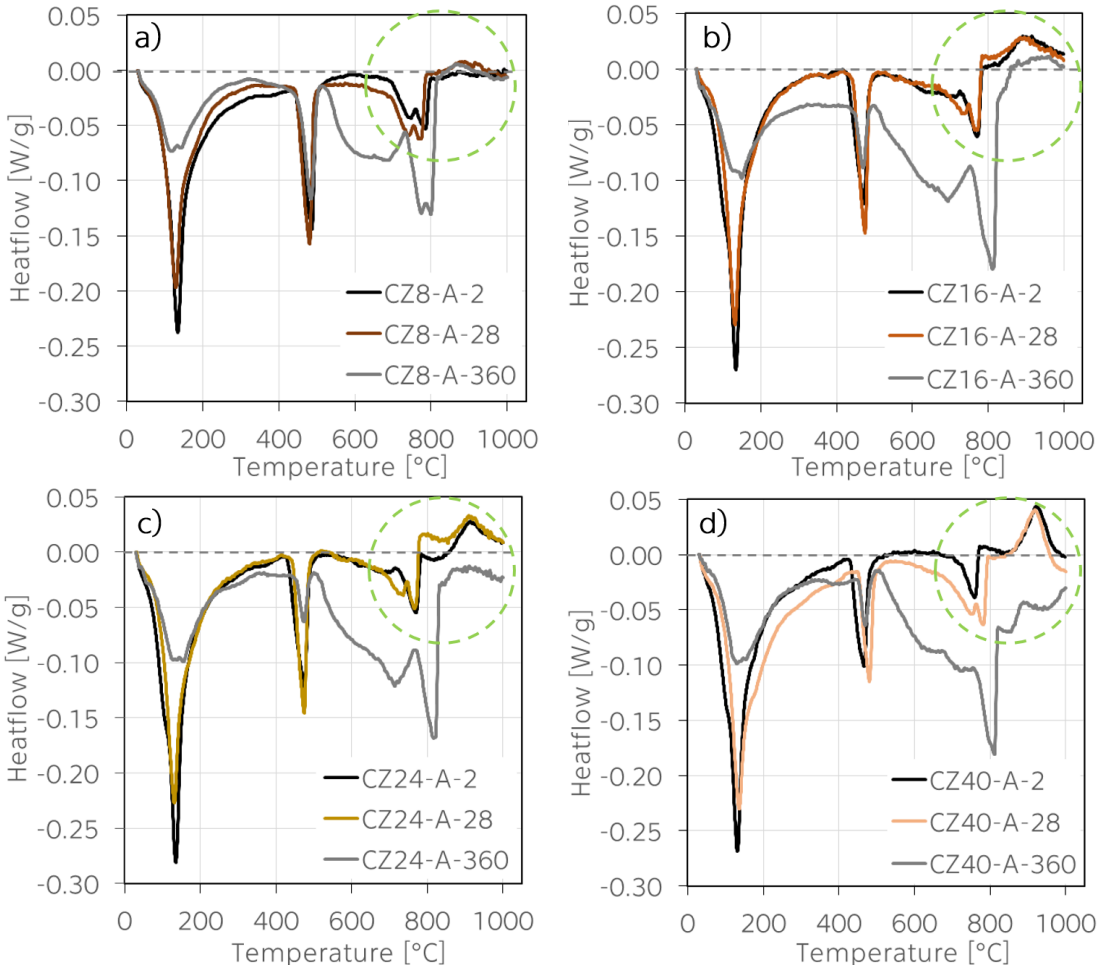

Figure 9.5.10. Heatflow results of studied pastes blended with natural zeolite.

The related temperature intervals, onsets, maximal temperatures and enthalpies of the crystallization peak were determined by manual method and these results are summarized into Tables 9.5.2–9.5.5.

Table 9.5.2. Enthalpy results for the CZ8-A pastes.

Age [Days]	Interval [°C]	Onset [°C]	Max.Temp. [°C]	Enthalpy [°C]
2	-	-	-	-
7	789-973	816.4	886.4	-11.8
28	801-977	888.3	888.3	-11.9
90	802-900	840.0	840.0	-4.7
180	837-938	844.9	874.7	-7.7
360	822-946	864.1	864.1	-8.4

Table 9.5.3. Enthalpy results for the CZ16-A pastes.

Age [Days]	Interval [°C]	Onset [°C]	Max.Temp. [°C]	Enthalpy [°C]
2	828-985	877.3	981.4	-19.7
7	846-961	862.4	884.9	-9.9
28	822-970	897.3	897.3	-15.1
90	834-986	905.2	905.2	-8.8
180	893-967	893.6	923.2	-6.7
360	820-833	859.2	870.5	-7.4

Table 9.5.4. Enthalpy results for the CZ24-A pastes.

Age [Days]	Interval [°C]	Onset [°C]	Max.Temp. [°C]	Enthalpy [°C]
2	850-980	881.2	924.4	-15.5
7	859-988	894.6	912.3	-15.3
28	854-1013	881.3	918.2	-12.1
90	856-969	871.1	911.6	-7.2
180	856-993	905.9	930.0	-7.1
360	835-905	848.0	870.0	-5.8

Table 9.5.5. Enthalpy results for the CZ40-A pastes.

Age [Days]	Interval [°C]	Onset [°C]	Max.Temp. [°C]	Enthalpy [°C]
2	8601-994	895.6	929.2	-20.0
7	858-977	887.4	922.1	-18.9
28	857-976	883.5	921.3	-20.0
90	845-974	845.8	899.3	-16.4
180	865-986	866.9	926.4	-21.1
360	839-962	862.8	887.4	-14.0

In the case of the CZ8-A, the exothermic reaction was not observed after 2 days of hydration. At 7 and 28 days, its size and intensity were almost equal and also determined values of enthalpy were very similar. With increasing time, the obtained trend was not clear, as the enthalpies varied. Which was a consequence of the changes in the background of heatflow curves during experiments. Similar difficulty was observed in the case of the other studied pastes blended with natural zeolite. The results summarized into Tables 9.5.2–9.5.5 are also displayed

in Figure 9.5.11. It seems that enthalpies obtained for all pastes had a similarly decreasing trend with time. This decrease was the slowest in the pastes containing the highest amount of natural zeolite. These results indicate that the size and intensity of the crystallization reaction depended on the amount of natural zeolite available to create this reaction. As the pozzolanic reaction gradually consumed natural zeolite in blended pastes, the effect of the crystallization reaction was less strong.

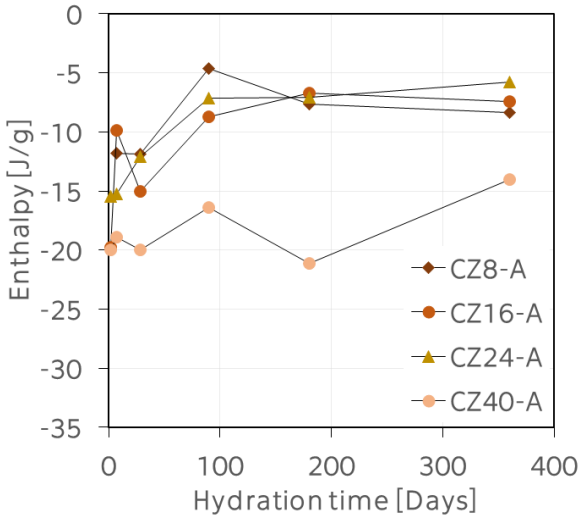

Figure 9.5.11. Enthalpy results for the MS12-A paste.

However, it should be noted that the manual method for the determination of enthalpy from the DSC results is very subjective, and it does not provide accurate results. Therefore, these results support the conclusions drawn in [225], where the DSC method was used to describe the recrystallization peaks of unhydrated slag and blended cement pastes with this pozzolan. It was concluded that the DSC method is unreliable due to the large error produced by the background.

9.6. Summary

In terms of the cement pastes blended with 0–40 wt.% of natural zeolite, the obtained findings can be summarized as follows:

- Low dosages up 8 wt.% of natural zeolite did not influence the hydration heat development. The pozzolanic reaction was probably activated at later ages compared to the silica fume (7 days).

- The pore structure was significantly affected by the higher additions of natural zeolite, as an increase of pores in the range below 0.1 μm was observed. This size is characteristic for natural zeolite itself. The total open porosity increased with increasing amount of natural zeolite, which affected mechanical properties.
- The long-term mechanical properties were not improved by the addition of natural zeolite at any level compared to the reference paste. However, 8 wt.% addition of natural zeolite provided similar performance compared to the reference paste after 360 days.
- A lower amount of the CBW was determined with increasing dosage of natural zeolite in pastes, and therefore, the degree of hydration was also lower. Moreover, it seemed that samples with 24 wt.% and higher addition were fully saturated after 180 days, as the CBW content remained almost the same after 360 days.
- The addition of natural zeolite at all levels led to a significant decrease of Portlandite compared to the reference paste, when pastes were stored in water. For the pastes blended with 8 wt.%, it had an increasing trend until 90 days, then it reached its maximum in these pastes, and it was gradually consumed by the pozzolanic reaction. When a higher amount of natural zeolite was added, the amount of produced Portlandite was significantly lower. It seems that additions higher than 8 wt.% of natural zeolite played a role of an inert filler. When samples were stored in air, this trend was more obvious.
- Similar results of calcite amount compared to other pastes were observed, when samples were stored in water, with no clear effect of natural zeolite on carbonation processes. When stored in air, pastes with the highest addition of natural zeolite exhibited the lowest carbonation levels. Compared to the silica fume, the addition of natural zeolite at all levels slowed the carbonation processes. Nevertheless, it could be caused by higher additions of natural zeolite, and therefore by the lack of Portlandite, which could be consumed by the carbonation processes.
- Also in these pastes, an exothermic reaction occurred in DSC thermographs when samples were heated above 790 °C. Its origin was discussed with literature.

Chapter 10

Conclusions and perspectives

The aim of this work was to study mechanisms of hydration processes of cement pastes by means of thermal analysis along with classical characterization methods for cementitious materials. In that respect, the main contribution was the extension of frequently studied early cement hydration also with long-term data up to 360 days. For this purpose, plain cement pastes with various water-to-cement ratios and pastes blended with pozzolana active materials, such as silica fume and natural zeolite, were prepared.

The important point was to apply an appropriate hydration stoppage technique, which would not alter hydration products. Based on the literature review, solvent exchange method was chosen for arresting hydration. However, the removal of the isopropanol, which was recommended in [131], with diethyl ether and then drying samples for a few minutes at 40 °C was not applied, as this recommendation was published in 2016.

After the detailed analysis of the raw materials, plain cement pastes were first studied. It was found that the designed w/c ratio of 0.5 used for the reference paste was not effective, as an additional layer of water was released at the top of the samples. This water was collected, and it was computed that the real w/c ratio was 0.45 in these pastes. This problem was not observed for the other pastes. Samples were cured at 25 °C in water or air. At the desired age of the samples, selected analyses were performed.

It was found that the best performance of the studied cement pastes was obtained for the plain pastes with the w/c of 0.3, which was mainly a result of the compact structure with a low porosity. In terms of the hydration products, in these pastes, stored in water, the amount of Portlandite gradually increased in time, whereas it decreased when samples were exposed to the atmospheric CO_2. Generally, the amount of Portlandite was higher in pastes with a higher w/c for both environments. Therefore, the pastes with higher amount of Portlandite were more prone to the carbonation, especially, when stored in air.

In the case of the blended pastes, the addition of 12 wt.% of silica fume led to a significant improvement of the compressive strength. The lower addition of 4 wt.% provided similar results compared to the reference sample between 7 and 360 days of hydration. Portlandite was gradually consumed by the pozzolanic reaction, which resulted in its lower amounts in all blended pastes. Therefore, its amount decreased in time and it was lower in pastes with a higher addition of silica fume. This effect was observed for both curing environments. Generally, the lower generated/consumed amount of Portlandite led to lower carbonation levels in pastes with silica fume, when stored in air.

When pastes were blended with natural zeolite, the 8 wt.% addition of natural zeolite provided the best performance of studied blended pastes. However, after 360 days of hydration, the compressive strength of this paste reached similar values compared to the reference paste. Generally, higher additions of natural zeolite led to saturation of the pastes, and therefore, the natural zeolite played a role of inert filler. This was clearly seen on the results of the CBW, degree of hydration, and Portlandite development. In terms of the carbonation, the addition of 24 and 40 wt.% of natural zeolite significantly improved the resistance of the blended pastes.

Methodology

In order to compare the utilized methods, these observations can be drawn:

- Isothermal heat flow calorimeter used for the determination of hydration heat development could be effectively used only within the first few days of hydration.
- SEM was a very important method up to 28 days of hydration. After this time, hydration products were too connected for a further analysis.
- Performance of TGA was not influenced by the age of studied samples. However, an appropriate hydration stoppage technique is required.
- XRD results were in a good agreement with those from TGA, when the tangential method for the Portlandite determination was applied. XRD was not measured as frequently as TGA, which led to the small differences in results, which were sometimes contradictory to TGA. In addition, XRD cannot provide details about amorphous phase, which are detectable by TGA.

Perspectives

The process of evaluation and identification of thermal analysis results may be time-consuming and requires users' expertise, since there is no universally accepted search-based software library. Therefore, for the correct interpretation, researchers have to compare their own results with literature or textbook data [308-310]. On the other hand, as the number of parameters increases with the complexity of the studied system, the evaluation based only on existing publications is limited, since these publications certainly do not describe every material or every measurement condition applied. The most important disadvantage of existing collections of data is the fact, that they do not allow a direct software-based comparison [311].

Recently, the first database system in the thermal analysis field has been introduced [312, 313]. It proposes an automatic evaluation, identification and classification of measurements based on advanced algorithms such as image recognition. Nevertheless, this promising solution to a non-existing thermal analysis database has a few important limitations, such as multiple possible interpretations, as TGA and DSC curves are not a unique identifier for a material. The other limitations are the dependence on the measurement conditions (heating rate, mass weight, atmosphere), and also the limited amount of data available so far [313].

Since the calculations for this study were obtained by treating about 300 curves, the main possible utilization of these data could lie in a design of a well-structured database model, which could be utilized as follows:

- Design and implementation of graph templates in graphic libraries (i.e. ggplot for R or pyplot in python) for a fast and personalized visual exploration of the results.
- Automated computation of custom characteristic (i.e. product of hydration contents etc.) allowing to accelerate the analysis process.
- Comparison of a wider range of materials sharing similar characteristics (comparison of historical data with current ones).

References

1. Bullard, J.W., et al., *Mechanisms of cement hydration.* Cement and Concrete Research, 2011. 41(12): p. 1208-1223.
2. Kocaba, V., *Development and evaluation of methods to follow microstructural development of cementitious systems including slags*. 2009, École Polytechnique Fédérale de Lausanne.
3. Öner, M., K. Erdoğdu, and A. Günlü, *Effect of components fineness on strength of blast furnace slag cement.* Cement and Concrete Research, 2003. 33(4): p. 463-469.
4. Camões, A. and R. Ferreira. *Technological evolution of concrete: from ancient times to ultra high-performance concrete*. in *Structures & Architecture: ICSA 2010-1st International Conference on Structures & Architecture, July 21-23 July, 2010 in Guimaraes, Portugal*. 2010. CRC Press.
5. Taylor, H.F., *Cement chemistry*. 1997: Thomas Telford.
6. Neville, A.M., *Properties of concrete*. Vol. 4. 1995: Longman London.
7. Lea, F., *The chemistry of Cement and concrete, 1970.* Publisher Frederick Edward Arnold Ltd, 1970: p. 406.
8. Scrivener, K.L., *The development of microstructure during the hydration of Portland cement*. 1984, University of London.
9. Taylor, H.F., *Modification of the Bogue calculation.* Advances in Cement Research, 1989. 2(6): p. 73-77.
10. Stutzman, P., et al., *Uncertainty in Bogue-calculated phase composition of hydraulic cements.* Cement and Concrete Research, 2014. 61: p. 40-48.
11. Odler, I., S. Abdul-Maula, and P. Nuedling, *Mineralogical and oxidic composition of industrial Portland cement clinkers.* ZKG, Zement-Kalk-Gips, Edition A, 1981. 34: p. 445-9.
12. Gutteridge, W. *Quantitative X-ray powder diffraction in the study of some cementive materials*. in *Proc. Br. Ceram. Soc.* 1984.
13. Kristmann, M., *Portland cement clinker: Mineralogical and chemical investigations: Part I Microscopy, X-ray fluorescence and X-ray diffraction.* Cement and Concrete Research, 1977. 7(6): p. 649-658.
14. Taylor, H.F.W., et al., *The hydration of tricalcium silicate.* Matériaux et Construction, 1984. 17(6): p. 457-468.
15. Gartner, E.M. and J.M. Gaidis, *Hydration mechanisms: I.* Materials Science of Concrete III, I, 1 pp., 1989. 95.
16. Gartner, E., et al., *Hydration of Portland cement.* Structure and performance of cements, 2002. 13: p. 57-108.
17. Scrivener, K.L., P. Juilland, and P.J.M. Monteiro, *Advances in understanding hydration of Portland cement.* Cement and Concrete Research, 2015. 78: p. 38-56.
18. Marchon, D. and R.J. Flatt, *8 - Mechanisms of cement hydration*, in *Science and Technology of Concrete Admixtures*. 2016, Woodhead Publishing. p. 129-145.
19. Costoya Fernández, M.M., *Effect of particle size on the hydration kinetics and microstructural development of tricalcium silicate.* 2008.
20. Garrault, S. and A. Nonat, *Hydrated layer formation on tricalcium and dicalcium silicate surfaces: experimental study and numerical simulations.* Langmuir, 2001. 17(26): p. 8131-8138.
21. Garrault, S., et al., *Study of C-S-H growth on C_3S surface during its early hydration.* Materials and structures, 2005. 38(4): p. 435-442.

22. Juilland, P., et al., *Dissolution theory applied to the induction period in alite hydration.* Cement and Concrete Research, 2010. 40(6): p. 831-844.
23. Barret, P. and D. Ménétrier, *Filter dissolution of C_3S as a function of the lime concentration in a limited amount of lime water.* Cement and Concrete Research, 1980. 10(4): p. 521-534.
24. Barret, P., D. Ménétrier, and D. Bertrandie, *Mechanism of C_3S dissolution and problem of the congruency in the very initial period and later on.* Cement and Concrete Research, 1983. 13(5): p. 728-738.
25. Fierens, P. and J. Verhaegen, *Hydration of tricalcium silicate in paste—kinetics of calcium ions dissolution in the aqueous phase.* Cement and Concrete Research, 1976. 6(3): p. 337-342.
26. Odler, I. and H. Dörr, *Early hydration of tricalcium silicate II. The induction period.* Cement and Concrete Research, 1979. 9(3): p. 277-284.
27. Stein, H. and J. Stevels, *Influence of silica on the hydration of 3CaO, SiO_2.* Journal of Applied Chemistry, 1964. 14(8): p. 338-346.
28. Jennings, H.M., *Aqueous solubility relationships for two types of calcium silicate hydrate.* Journal of the American Ceramic Society, 1986. 69(8): p. 614-618.
29. Brown, P.W., J. Pommersheim, and G. Frohnsdorff, *A kinetic model for the hydration of tricalcium silicate.* Cement and Concrete Research, 1985. 15(1): p. 35-41.
30. Young, J., H. Tong, and R. Berger, *Compositions of solutions in contact with hydrating tricalcium silicate pastes.* Journal of the American Ceramic Society, 1977. 60(5-6): p. 193-198.
31. Bazzoni, A., *Study of early hydration mechanisms of cement by means of electron microscopy.* 2014.
32. Zhang, L., et al., *Hydration for the Alite mineral: Morphology evolution, reaction mechanism and the compositional influences.* Construction and Building Materials, 2017. 155: p. 413-426.
33. Livingston, R., et al., *Characterization of the induction period in tricalcium silicate hydration by nuclear resonance reaction analysis.* Journal of Materials Research, 2001. 16(3): p. 687-693.
34. Thomas, J.J., H.M. Jennings, and J.J. Chen, *Influence of nucleation seeding on the hydration mechanisms of tricalcium silicate and cement.* The Journal of Physical Chemistry C, 2009. 113(11): p. 4327-4334.
35. Gallucci, E. and K. Scrivener, *Crystallisation of calcium hydroxide in early age model and ordinary cementitious systems.* Cement and Concrete Research, 2007. 37(4): p. 492-501.
36. Gauffinet, S., et al., *Direct observation of the growth of calcium silicate hydrate on alite and silica surfaces by atomic force microscopy.* Comptes Rendus de l'Academie des Sciences Series IIA Earth and Planetary Science, 1998. 4(327): p. 231-236.
37. Bye, G.C., *Portland cement: composition, production and properties*. 1999: Thomas Telford.
38. Tenoutasse, N. and A. De Donder, *The kinetics and mechanism of hydration of tricalcium silicate.* Silicates Ind, 1970. 35: p. 301-307.
39. Sharara, A., et al., *Hydration characteristics of β-C_2S in the presence of some pozzolanic materials.* Cement and concrete research, 1994. 24(5): p. 966-974.
40. Skalny, J. and J. Young. *Mechanisms of Portland cement hydration*. in *Proceedings, 7th International Symposium Chemical of Cement, Paris*. 1980.
41. Jinyu, L., et al., *Development and research of high belite cement dam concrete with low heat and high crack resistance.* Sustainable Development and Concrete Technology, 2004: p. 251.
42. Chatterjee, A.K., *High belite cements—Present status and future technological options: Part I.* Cement and Concrete Research, 1996. 26(8): p. 1213-1225.

43. Fierens, P. and J. Tirlocq, *Nature and concentration effect of stabilizing elements of beta-dicalcium silicate on its hydration rate.* Cement and Concrete Research, 1983. 13(2): p. 267-276.
44. Corstanje, W., H. Stein, and J. Stevels, *Hydration reactions in pastes $C_3S+C_3A+CaSO_4.2aq+H_2O$ at 25 Cl.* Cement and Concrete Research, 1973. 3(6): p. 791-806.
45. Minard, H., et al., *Mechanisms and parameters controlling the tricalcium aluminate reactivity in the presence of gypsum.* Cement and Concrete Research, 2007. 37(10): p. 1418-1426.
46. Scrivener, K.L. and A. Nonat, *Hydration of cementitious materials, present and future.* Cement and Concrete Research, 2011. 41(7): p. 651-665.
47. Dilnesa, B.Z., *Fe-containing hydrates and their fate during cement hydration: thermodynamic data and experimental study.* Ecole Polytechnique Federale de Lausanne, 2011.
48. Dilnesa, B.Z., et al., *Fe-containing phases in hydrated cements.* Cement and Concrete Research, 2014. 58: p. 45-55.
49. Lerch, W., *The influence of gypsum on the hydration and properties of Portland cement pastes*. 2008.
50. Tenoutasse, N., *The Hydratation Mechanism of C_3A and C_3S in the Presence of Calcium Chloride and Calcium Sulphate*. 1969: CRIC.
51. Gallucci, E., P. Mathur, and K. Scrivener, *Microstructural development of early age hydration shells around cement grains.* Cement and Concrete Research, 2010. 40(1): p. 4-13.
52. Muller, A.C.A., et al., *Densification of C–S–H measured by 1H NMR relaxometry.* The Journal of Physical Chemistry C, 2012. 117(1): p. 403-412.
53. Berodier, E.M.J., *Impact of the supplementary cementitious materials on the kinetics and microstructural development of cement hydration.* 2015.
54. Mehta, P.K. and P.J. Monteiro, *Concrete microstructure, properties and materials*. 2001.
55. Bonaccorsi, E., S. Merlino, and H. Taylor, *The crystal structure of jennite, Ca9Si6O18 (OH) 6· 8H2O.* Cement and Concrete Research, 2004. 34(9): p. 1481-1488.
56. Bonaccorsi, E., S. Merlino, and A.R. Kampf, *The crystal structure of tobermorite 14 Å (plombierite), a C–S–H phase.* Journal of the American Ceramic Society, 2005. 88(3): p. 505-512.
57. Glasser, F.P., *The role of $Ca(OH)_2$ in Portland cement concretes*, in *Materials of Science and Concrete, Calcium Hydroxide in Concrete*. 2001.
58. Kirchheim, A., et al., *Analysis of cubic and orthorhombic C_3A hydration in presence of gypsum and lime.* Journal of materials science, 2009. 44(8): p. 2038-2045.
59. Taylor, H.F.W., C. Famy, and K.L. Scrivener, *Delayed ettringite formation.* Cement and Concrete Research, 2001. 31(5): p. 683-693.
60. Asamoto, S., et al., *Effect of carbonate ions on delayed ettringite formation.* Construction and Building Materials, 2017. 147: p. 221-226.
61. Cao, Y., et al., *The influence of cellulose nanocrystals on the microstructure of cement paste.* Cement and Concrete Composites, 2016. 74: p. 164-173.
62. Talaber, J., *Factors influencing the quality of cement.* Periodica Polytechnica Civil Engineering, 1982. 26(1-2): p. 27-39.
63. Bishnoi, S. and K.L. Scrivener, *Studying nucleation and growth kinetics of alite hydration using μic.* Cement and Concrete Research, 2009. 39(10): p. 849-860.
64. Tydlitát, V., et al., *Application of large-volume calorimetry for monitoring the early-stage hydration heat development in cement-based composites as a function of w/c.* Thermochimica Acta, 2012. 546: p. 44-48.
65. Tydlitát, V., T. Matas, and R. Černý, *Effect of w/c and temperature on the early-stage hydration heat development in Portland-limestone cement.* Construction and Building Materials, 2014. 50: p. 140-147.

66. Fagerlund, G., *Chemically bound water as measure of degree of hydration: method and potential errors*. 2009: Division of Building Materials, Lund Institute of Technology.
67. Cook, R.A. and K.C. Hover, *Mercury porosimetry of hardened cement pastes.* Cement and Concrete Research, 1999. 29(6): p. 933-943.
68. Aligizaki, K.K., *Pore structure of cement-based materials: testing, interpretation and requirements*. 2014: CRC Press.
69. Thomas J.J. and H.M. Jennings. *The pore system and classification of pores*. 2014.
70. Frías, M. and J. Cabrera, *Pore size distribution and degree of hydration of metakaolin–cement pastes.* Cement and Concrete Research, 2000. 30(4): p. 561-569.
71. Powers, T.C., *Structure and physical properties of hardened Portland cement paste.* Journal of the American Ceramic Society, 1958. 41(1): p. 1-6.
72. Powers, T.C. and T.L. Brownyard. *Studies of the physical properties of hardened Portland cement paste*. in *Journal Proceedings*. 1946.
73. Živica, V., *Effects of the very low water/cement ratio.* Construction and Building Materials, 2009. 23(12): p. 3579-3582.
74. Lothenbach, B., et al., *Effect of temperature on the pore solution, microstructure and hydration products of Portland cement pastes.* Cement and Concrete Research, 2007. 37(4): p. 483-491.
75. Escalante-Garcıa, J. and J. Sharp, *The microstructure and mechanical properties of blended cements hydrated at various temperatures.* Cement and Concrete Research, 2001. 31(5): p. 695-702.
76. Kjellsen, K.O. and R.J. Detwiler, *Reaction kinetics of Portland cement mortars hydrated at different temperatures.* Cement and Concrete Research, 1992. 22(1): p. 112-120.
77. Massazza, F., *Pozzolana and pozzolanic cements.* Lea's chemistry of cement and concrete, 1998. 4: p. 471-631.
78. Malhotra, V.M. and P.K. Mehta, *Pozzolanic and cementitious materials*. 2014: CRC Press.
79. Snellings, R., G. Mertens, and J. Elsen, *Supplementary cementitious materials.* Reviews in Mineralogy and Geochemistry, 2012. 74(1): p. 211-278.
80. Uzal, B. and L. Turanli, *Studies on blended cements containing a high volume of natural pozzolans.* Cement and Concrete Research, 2003. 33(11): p. 1777-1781.
81. Tironi, A., et al., *Assessment of pozzolanic activity of different calcined clays.* Cement and Concrete Composites, 2013. 37: p. 319-327.
82. Hossain, K.M.A. and M. Lachemi, *Strength, durability and micro-structural aspects of high performance volcanic ash concrete.* Cement and Concrete Research, 2007. 37(5): p. 759-766.
83. Hossain, K.M.A., *Volcanic ash and pumice as cement additives: pozzolanic, alkali-silica reaction and autoclave expansion characteristics.* Cement and Concrete Research, 2005. 35(6): p. 1141-1144.
84. Taniguchi, M., T. Takahashi, and T. Sagawa, *Effect of Pozzolanic Reactivity of Volcanic Ash in Hokkaido on the Durability of Volcanic Ash Concrete*, in *High Tech Concrete: Where Technology and Engineering Meet*. 2018, Springer. p. 2177-2184.
85. Yankwa Djobo, J.N., et al., *Mechanical properties and durability of volcanic ash based geopolymer mortars.* Construction and Building Materials, 2016. 124: p. 606-614.
86. Ahmadi, B. and M. Shekarchi, *Use of natural zeolite as a supplementary cementitious material.* Cement and Concrete Composites, 2010. 32(2): p. 134-141.
87. Babel, S. and T.A. Kurniawan, *Low-cost adsorbents for heavy metals uptake from contaminated water: a review.* Journal of hazardous materials, 2003. 97(1-3): p. 219-243.

88. Nagrockiene, D. and G. Girskas, *Research into the properties of concrete modified with natural zeolite addition.* Construction and Building Materials, 2016. 113: p. 964-969.
89. Wojsz, R. and M. Rozwadowski, *An attempt to determine the function defining capillary structure of microporous adsorbents.* Chemical engineering science, 1987. 42(12): p. 2877-2881.
90. Feng, N.-Q. and G.-F. Peng, *Applications of natural zeolite to construction and building materials in China.* Construction and Building Materials, 2005. 19(8): p. 579-584.
91. Poon, C., et al., *A study on the hydration rate of natural zeolite blended cement pastes.* Construction and Building Materials, 1999. 13(8): p. 427-432.
92. Tseng, Y.-S., C.-L. Huang, and K.-C. Hsu, *The pozzolanic activity of a calcined waste FCC catalyst and its effect on the compressive strength of cementitious materials.* Cement and concrete research, 2005. 35(4): p. 782-787.
93. Najimi, M., et al., *An experimental study on durability properties of concrete containing zeolite as a highly reactive natural pozzolan.* Construction and Building Materials, 2012. 35: p. 1023-1033.
94. Sabir, B.B., S. Wild, and J. Bai, *Metakaolin and calcined clays as pozzolans for concrete: a review.* Cement and Concrete Composites, 2001. 23(6): p. 441-454.
95. Badogiannis, E., et al., *Evaluation of chloride-penetration resistance of metakaolin concrete by means of a diffusion – Binding model and of the k-value concept.* Cement and Concrete Composites, 2015. 63: p. 1-7.
96. Singh, M. and M. Garg, *Reactive pozzolana from Indian clays—their use in cement mortars.* Cement and Concrete Research, 2006. 36(10): p. 1903-1907.
97. Wild, S. and J. Khatib, *Portlandite consumption in metakaolin cement pastes and mortars.* Cement and concrete research, 1997. 27(1): p. 137-146.
98. Sujjavanich, S., et al., *Synergistic effect of metakaolin and fly ash on properties of concrete.* Construction and Building Materials, 2017. 155: p. 830-837.
99. Vimmrová, A., et al., *Calcined gypsum–lime–metakaolin binders: Design of optimal composition.* Cement and Concrete Composites, 2014. 52: p. 91-96.
100. Unknown. *Kaolinite*. Available from: https://wgnhs.uwex.edu/minerals/kaolinite/
101. Kleen E. *Calcined clays in modern building materials: Potential applications in concrete and composite cements*. 2013.
102. Tydlitát, V., et al., *Application of isothermal calorimetry and thermal analysis for the investigation of calcined gypsum–lime–metakaolin–water system.* Journal of Thermal Analysis and Calorimetry, 2015. 122(1): p. 115-122.
103. Bhanumathidas, N. and P.K. Mehta, *Concrete mixtures made with ternary blended cements containing fly ash and rice-husk ash.* Special Publication, 2001. 199: p. 379-392.
104. Ganesan, K., K. Rajagopal, and K. Thangavel, *Rice husk ash blended cement: Assessment of optimal level of replacement for strength and permeability properties of concrete.* Construction and Building Materials, 2008. 22(8): p. 1675-1683.
105. Boateng, A. and D. Skeete, *Incineration of rice hull for use as a cementitious material: the Guyana experience.* Cement and Concrete Research, 1990. 20(5): p. 795-802.
106. Mehta, P.K., *Rice Hush Ash-A unique supplementary cementing material.* Advances in concrete technology, 1992.
107. Rodríguez de Sensale, G., *Strength development of concrete with rice-husk ash.* Cement and Concrete Composites, 2006. 28(2): p. 158-160.
108. Papadakis, V.G., S. Antiohos, and S. Tsimas, *Supplementary cementing materials in concrete: Part II: A fundamental estimation of the efficiency factor.* Cement and Concrete Research, 2002. 32(10): p. 1533-1538.
109. Li, G., *Properties of high-volume fly ash concrete incorporating nano-SiO_2.* Cement and Concrete Research, 2004. 34(6): p. 1043-1049.

110. Bilodeau, A., et al., *Durability of concrete incorporating high volumes of fly ash from sources in the USA.* Materials Journal, 1994. 91(1): p. 3-12.
111. McCraven, S. *The Future of Fly Ash Use in Concrete*. 2013.
112. Papadakis, V.G. and S. Tsimas, *Supplementary cementing materials in concrete: Part I: efficiency and design.* Cement and Concrete Research, 2002. 32(10): p. 1525-1532.
113. Hussain, S., D. Bhunia, and S.B. Singh, *Comparative study of accelerated carbonation of plain cement and fly-ash concrete.* Journal of Building Engineering, 2017. 10: p. 26-31.
114. Pal, S.C., A. Mukherjee, and S.R. Pathak, *Investigation of hydraulic activity of ground granulated blast furnace slag in concrete.* Cement and Concrete Research, 2003. 33(9): p. 1481-1486.
115. Leng, F., N. Feng, and X. Lu, *An experimental study on the properties of resistance to diffusion of chloride ions of fly ash and blast furnace slag concrete.* Cement and Concrete Research, 2000. 30(6): p. 989-992.
116. Cheng, S., et al., *Effects of fly ash, blast furnace slag and metakaolin on mechanical properties and durability of coral sand concrete.* Applied Clay Science, 2017. 141: p. 111-117.
117. Osborne, G.J., *Durability of Portland blast-furnace slag cement concrete.* Cement and Concrete Composites, 1999. 21(1): p. 11-21.
118. Vejmelková, E., et al., *Properties of high performance concrete containing fine-ground ceramics as supplementary cementitious material.* Cement and Concrete Composites, 2012. 34(1): p. 55-61.
119. Scheinherrová, L., et al., *Thermal properties of high-performance concrete containing fine-ground ceramics as a partial cement replacement.* Materials Science, 2015. 21(3): p. 444-448.
120. Malhotra, V.M., *Fly ash, slag, silica fume, and rice husk ash in concrete: a review.* Concrete International, 1993. 15(4): p. 23-28.
121. Behnood, A. and H. Ziari, *Effects of silica fume addition and water to cement ratio on the properties of high-strength concrete after exposure to high temperatures.* Cement and Concrete Composites, 2008. 30(2): p. 106-112.
122. Bhanja, S. and B. Sengupta, *Influence of silica fume on the tensile strength of concrete.* Cement and Concrete Research, 2005. 35(4): p. 743-747.
123. Qing, Y., et al., *Influence of nano-SiO_2 addition on properties of hardened cement paste as compared with silica fume.* Construction and Building Materials, 2007. 21(3): p. 539-545.
124. Unknown. *Pellet granular micro silica fume powder price*. 2018. Available from: http://www.microsilica-fume.com/pellet-granular-micro-silica-fume-powder-price.html
125. Jo, B.-W., et al., *Characteristics of cement mortar with nano-SiO_2 particles.* Construction and Building Materials, 2007. 21(6): p. 1351-1355.
126. Poon, C.S., S.C. Kou, and L. Lam, *Compressive strength, chloride diffusivity and pore structure of high performance metakaolin and silica fume concrete.* Construction and Building Materials, 2006. 20(10): p. 858-865.
127. Mazloom, M., A.A. Ramezanianpour, and J.J. Brooks, *Effect of silica fume on mechanical properties of high-strength concrete.* Cement and Concrete Composites, 2004. 26(4): p. 347-357.
128. Zhang, M.-H. and O.E. Gjørv, *Effect of silica fume on cement hydration in low porosity cement pastes.* Cement and Concrete Research, 1991. 21(5): p. 800-808.
129. Roy, D.M., P. Arjunan, and M.R. Silsbee, *Effect of silica fume, metakaolin, and low-calcium fly ash on chemical resistance of concrete.* Cement and Concrete Research, 2001. 31(12): p. 1809-1813.
130. Bentz, D.P., et al., *Influence of silica fume on diffusivity in cement-based materials: I. Experimental and computer modeling studies on cement pastes.* Cement and Concrete Research, 2000. 30(6): p. 953-962.

131. Scrivener, K., R. Snellings, and B. Lothenbach, *A practical guide to microstructural analysis of cementitious materials*. 2016: CRC Press.
132. Zhang, J. and G.W. Scherer, *Comparison of methods for arresting hydration of cement.* Cement and Concrete Research, 2011. 41(10): p. 1024-1036.
133. Zhang, L. and F. Glasser, *Critical examination of drying damage to cement pastes.* Advances in cement research, 2000. 12(2): p. 79-88.
134. Ligizaki, K.K., *Pore Structure of Cement-based Materials-testing, Interpretation and Requirement*. 2006, New York, Taylor &Francis.
135. Korpa, A. and R. Trettin, *The influence of different drying methods on cement paste microstructures as reflected by gas adsorption: Comparison between freeze-drying (F-drying), D-drying, P-drying and oven-drying methods.* Cement and Concrete Research, 2006. 36(4): p. 634-649.
136. Thomas, J.J., H.M. Jennings, and A.J. Allen, *The surface area of hardened cement paste as measured by various techniques.* Concrete Science and Engineering, 1999. 1(1): p. 45-64.
137. Gallé, C., *Effect of drying on cement-based materials pore structure as identified by mercury intrusion porosimetry: A comparative study between oven-, vacuum-, and freeze-drying.* Cement and Concrete Research, 2001. 31(10): p. 1467-1477.
138. Collier, N.C., et al., *The influence of water removal techniques on the composition and microstructure of hardened cement pastes.* Cement and Concrete Research, 2008. 38(6): p. 737-744.
139. Copeland, L.E. and J.C. Hayes, *The determination of non-evaporable water in hardened portland cement paste*. 1953.
140. Diamond, S., *A discussion of the paper "Effect of drying on cement-based materials pore structure as identified by mercury porosimetry—a comparative study between oven-, vacuum-, and freeze-drying" by C. Gallé.* Cement and concrete research, 2003. 33(1): p. 169-170.
141. Scherer, G.W. and J. Valenza, *Mechanisms of frost damage.* Materials science of concrete, 2005. 7(60): p. 209-46.
142. Marchand, J., R. Pleau, and R. Gagné, *Deterioration of concrete due to freezing and thawing.* Material science of concrete, 1995. 4: p. 283-354.
143. Konecny, L. and S. Naqvi, *The effect of different drying techniques on the pore size distribution of blended cement mortars.* Cement and concrete research, 1993. 23(5): p. 1223-1228.
144. Gillott, J., *Importance of specimen preparation in microscopy*, in *Soil specimen preparation for laboratory testing*. 1976, ASTM International.
145. Taylor, H.F.W. and A.B. Turner, *Reactions of tricalcium silicate paste with organic liquids.* Cement and Concrete Research, 1987. 17(4): p. 613-623.
146. Hughes, D., *The use of solvent exchange to monitor diffusion characteristics of cement pastes containing silica fume.* Cement and Concrete Research, 1988. 18(2): p. 321-324.
147. Feldman, R.F. and J.J. Beaudoin, *Pretreatment of hardened hydrated cement pastes for mercury intrusion measurements.* Cement and Concrete Research, 1991. 21(2-3): p. 297-308.
148. Beaudoin, J.J., et al., *Solvent exchange in partially saturated and saturated microporous systems: length change anomalies.* Cement and concrete research, 2000. 30(3): p. 359-370.
149. Beaudoin, J.J. and B.T. Tamtsia, *Effect of drying methods on microstructural changes in hardened cement paste: an AC impedance spectroscopy evaluation.* Journal of Advanced Concrete Technology, 2004. 2(1): p. 113-120.
150. Gran, H.C. and E.W. Hansen, *Exchange rates of ethanol with water in water-saturated cement pastes probed by NMR.* Advanced Cement Based Materials, 1998. 8(3): p. 108-117.
151. Lide, D.R., *CRC handbook of chemistry and physics. 79th Edition,* 2012.

152. Parrott, L., *Effect of drying history upon the exchange of pore water with methanol and upon subsequent methanol sorption behaviour in hydrated alite paste.* Cement and Concrete Research, 1981. 11(5-6): p. 651-658.
153. Day, R.L. and B.K. Marsh, *Measurement of porosity in blended cement pastes.* Cement and Concrete Research, 1988. 18(1): p. 63-73.
154. Mitchell, L.D. and J.C. Margeson, *The effects of solvents on C–S–H as determined by thermal analysis.* Journal of thermal analysis and calorimetry, 2006. 86(3): p. 591-594.
155. Parrott, L., *Thermogravimetric and sorption studies of methanol exchange in an alite paste.* Cement and Concrete Research, 1983. 13(1): p. 18-22.
156. Dubina, E., L. Wadsö, and J. Plank, *A sorption balance study of water vapour sorption on anhydrous cement minerals and cement constituents.* Cement and Concrete Research, 2011. 41(11): p. 1196-1204.
157. Mmusi, M., M. Alexander, and H. Beushausen, *Determination of critical moisture content for carbonation of concrete.* 2009.
158. Yang, T., et al., *Direct observation of the carbonation process on the surface of calcium hydroxide crystals in hardened cement paste using an atomic force microscope.* Journal of materials Science, 2003. 38(9): p. 1909-1916.
159. Sprung, S., K. Kuhlmann, and H.-G. Ellerbrock, *Particle size distribution and properties of cement: II, Water demand of portland cement.* ZKG, Zement-Kalk-Gips, Edition A, 1985. 38(9): p. 528-34.
160. Celik, I.B., *The effects of particle size distribution and surface area upon cement strength development.* Powder Technology, 2009. 188(3): p. 272-276.
161. ISO, *13320: Particle size analysis by laser diffraction*. 2009: Switzerland.
162. ČSN EN 196-6, *Methods of testing cement - Part 6: Determination of fineness.* Czech Office for Standards, 2010.
163. Tydlitát, V., J. Zákoutský, and R. Černý, *An isothermal heat flow calorimeter for large-volume applications.* Journal of thermal analysis and calorimetry, 2011. 110(2): p. 1021-1027.
164. Yu, R., Z. Shui, and J. Dong, *Using Dehydrated Cement Paste as New Type of Cement Additive.* ACI Materials Journal, 2013. 110(4): p. 395.
165. Doebelin, N. and R. Kleeberg, *Profex: a graphical user interface for the Rietveld refinement program BGMN.* J. Appl. Crystallogr., 2015. 48(5): p. 1573-1580.
166. Payá, J., et al., *Determination of the pozzolanic activity of fluid catalytic cracking residue. Thermogravimetric analysis studies on FC3R–lime pastes.* Cement and Concrete Research, 2003. 33(7): p. 1085-1091.
167. Vejmelková, E., et al., *High-strength concrete based on ternary binder with high pozzolan content.* Struct. Concrete, 2018.
168. ČSN EN 1015, *Methods for Testing Mortar for Masonry - Part 11*, in *Determination of Flexural and Compressive strength of Hardened Mortar*. 2000, Czech Office for Standards: Prague.
169. Gallagher, P.K., M.E. Brown, and R. Kemp, *Handbook of thermal analysis and calorimetry*. 1998: Elsevier.
170. Gaisford, S., V. Kett, and P. Haines, *Principles of thermal analysis and calorimetry*. 2016: Royal society of chemistry.
171. Wunderlich, B., *Thermal Analysis*, in *Encyclopedia of Materials: Science and Technology*, K.H.J. Buschow, et al., Editors. 2001, Elsevier: Oxford. p. 9134-9141.
172. Reed, K.J., M.J. Levchak, and J.W. Schaefer, *Thermogravimetric apparatus*. 1994, Google Patents.
173. Coats, A. and J. Redfern, *Thermogravimetric analysis. A review.* Analyst, 1963. 88(1053): p. 906-924.
174. Ozawa, T., *Thermal analysis—review and prospect.* Thermochimica Acta, 2000. 355(1): p. 35-42.
175. Freeman, E.S. and B. Carroll, *The application of thermoanalytical techniques to reaction kinetics: the thermogravimetric evaluation of the kinetics of the*

decomposition of calcium oxalate monohydrate. The Journal of Physical Chemistry, 1958. 62(4): p. 394-397.
176. Coats, A. and J. Redfern, *Kinetic parameters from thermogravimetric data.* 1964.
177. Flynn, J.H. and L.A. Wall, *A quick, direct method for the determination of activation energy from thermogravimetric data.* Journal of Polymer Science Part B: Polymer Letters, 1966. 4(5): p. 323-328.
178. Carrasco, F., *The evaluation of kinetic parameters from thermogravimetric data: comparison between established methods and the general analytical equation.* Thermochimica Acta, 1993. 213: p. 115-134.
179. Friedman, H.L. *Kinetics of thermal degradation of char-forming plastics from thermogravimetry. Application to a phenolic plastic*. in *Journal of Polymer Science Part C: Polymer Symposia*. 1964. Wiley Online Library.
180. Menczel, J.D. and R.B. Prime, *Thermal analysis of polymers: fundamentals and applications*. 2014: John Wiley & Sons.
181. Groenewoud, W.M., *Characterisation of polymers by thermal analysis*. 2001: Elsevier.
182. Pels, J., et al., *Evolution of nitrogen functionalities in carbonaceous materials during pyrolysis.* Carbon, 1995. 33(11): p. 1641-1653.
183. Teng, H. and Y.-C. Wei, *Thermogravimetric studies on the kinetics of rice hull pyrolysis and the influence of water treatment.* Industrial & Engineering Chemistry Research, 1998. 37(10): p. 3806-3811.
184. Grønli, M.G., G. Varhegyi, and C. Di Blasi, *Thermogravimetric analysis and devolatilization kinetics of wood.* Industrial & Engineering Chemistry Research, 2002. 41(17): p. 4201-4208.
185. Hatakeyama, T., and Quinn, F.X., *Thermal Analysis Fundamentals and Applicatons to Polymer Science: Thermogravimetry*. 2nd ed. 1999: Jhon Wiley and Sons Publications.
186. Rath, J., et al., *Heat of wood pyrolysis.* Fuel, 2003. 82(1): p. 81-91.
187. Samih, S. and J. Chaouki, *Development of a fluidized bed thermogravimetric analyzer.* AIChE Journal, 2015. 61(1): p. 84-89.
188. Ebrahimpour, O., J. Chaouki, and C. Dubois, *Diffusional effects for the oxidation of SiC powders in thermogravimetric analysis experiments.* Journal of Materials Science, 2013. 48(12): p. 4396-4407.
189. Unknown. *Thermal Analysis. A class of techniques to measure chemical or physical properties of a substance as function of temperature or time*. 2005; Available from: http://www.chem.mun.ca/courseinfo/c3110/TGA%20lecture%202011.pdf.
190. Palmer, L.D., *Sources of error in thermogravimetry: balance inclination and specimen temperature.* Journal of Physics E: Scientific Instruments, 1980. 13(9): p. 919.
191. Gurdeep R. Chatwal, S.K.A., *Instrumental Methods of Chemical Analysis: Thermal Methods*. 5th ed. 2002: Himalaya Publishing House.
192. Karlsoom, M., *Thermogravimetry Analysis (TGA)*. 2014, Riphah International University.
193. Di Blasi, C., *Comparison of semi-global mechanisms for primary pyrolysis of lignocellulosic fuels.* Journal of Analytical and Applied Pyrolysis, 1998. 47(1): p. 43-64.
194. Carrier, M., et al., *Thermogravimetric analysis as a new method to determine the lignocellulosic composition of biomass.* Biomass and Bioenergy, 2011. 35(1): p. 298-307.
195. Dweck, J., et al., *Importance of quantitative thermogravimetry on initial cement mass basis to evaluate the hydration of cement pastes and mortars.* Journal of Thermal Analysis and Calorimetry, 2013. 113(3): p. 1481-1490.

196. Payá, J., et al., *Evaluation of the pozzolanic activity of fluid catalytic cracking catalyst residue (FC3R). Thermogravimetric analysis studies on FC3R-Portland cement pastes.* Cement and Concrete Research, 2003. 33(4): p. 603-609.
197. Neves Junior, A., et al., *Early stages hydration of high initial strength Portland cement: Part I. thermogravimetric analysis on calcined mass basis.* Journal of thermal analysis and calorimetry, 2012. 108(2): p. 725-731.
198. Vedalakshmi, R., et al., *Quantification of hydrated cement products of blended cements in low and medium strength concrete using TG and DTA technique.* Thermochimica Acta, 2003. 407(1–2): p. 49-60.
199. Mellado, A., et al., *Immobilization of Zn(II) in Portland cement pastes.* Journal of Thermal Analysis and Calorimetry, 2013. 112(3): p. 1377-1389.
200. Qiao, X.C., C.S. Poon, and C.R. Cheeseman, *Investigation into the stabilization/solidification performance of Portland cement through cement clinker phases.* Journal of Hazardous Materials, 2007. 139(2): p. 238-243.
201. Soin, A.V., L.J.J. Catalan, and S.D. Kinrade, *A combined QXRD/TG method to quantify the phase composition of hydrated Portland cements.* Cement and Concrete Research, 2013. 48: p. 17-24.
202. Dweck, J., et al., *Study by thermogravimetry of the evolution of ettringite phase during type II Portland cement hydration.* Journal of Thermal Analysis and Calorimetry, 2002. 69(1): p. 179-186.
203. De Weerdt, K., et al., *Hydration mechanisms of ternary Portland cements containing limestone powder and fly ash.* Cement and Concrete Research, 2011. 41(3): p. 279-291.
204. Liu, S., Y. Kong, and L. Wang, *A comparison of hydration properties of cement–low quality fly ash binder and cement–limestone powder binder.* Journal of Thermal Analysis and Calorimetry, 2014. 116(2): p. 937-943.
205. Thongsanitgarn, P., W. Wongkeo, and A. Chaipanich, *Hydration and Compressive Strength of Blended Cement Containing Fly Ash and Limestone as Cement Replacement.* Journal of Materials in Civil Engineering, 2014. 26(12): p. 04014088.
206. Dyer, T.D. and R.K. Dhir, *Hydration reactions of cement combinations containing vitrified incinerator fly ash.* Cement and Concrete Research, 2004. 34(5): p. 849-856.
207. Antoni, M., et al., *Cement substitution by a combination of metakaolin and limestone.* Cement and Concrete Research, 2012. 42(12): p. 1579-1589.
208. Wei, J. and C. Meyer, *Sisal fiber-reinforced cement composite with Portland cement substitution by a combination of metakaolin and nanoclay.* Journal of Materials Science, 2014. 49(21): p. 7604-7619.
209. Gruyaert, E., N. Robeyst, and N. De Belie, *Study of the hydration of Portland cement blended with blast-furnace slag by calorimetry and thermogravimetry.* Journal of Thermal Analysis and Calorimetry, 2010. 102(3): p. 941-951.
210. Dweck, J., P.M. Buchler, and F.K. Cartledge, *The Effect of Different Bentonites on Cement Hydration During Solidification/Stabilization of Tannery Wastes.* Journal of Thermal Analysis and Calorimetry, 2001. 64(3): p. 1011-1016.
211. Horpibulsuk, S., R. Rachan, and A. Suddeepong, *Assessment of strength development in blended cement admixed Bangkok clay.* Construction and Building Materials, 2011. 25(4): p. 1521-1531.
212. Horpibulsuk, S., et al., *Strength development in blended cement admixed saline clay.* Applied Clay Science, 2012. 55: p. 44-52.
213. Escalante, J.I., et al., *Pozzolanic properties of a geothermal silica waste material.* Cement and Concrete Research, 1999. 29(4): p. 623-625.
214. Kae-Long, L., et al., *Waste brick's potential for use as a pozzolan in blended Portland cement.* Waste Management & Research, 2010.
215. Pelisser, F., L.R. Steiner, and A.M. Bernardin, *Recycling of Porcelain Tile Polishing Residue in Portland Cement: Hydration Efficiency.* Environmental Science & Technology, 2012. 46(4): p. 2368-2374.

216. Anjos, M.A.S., et al., *Hydration of oil well cement containing sugarcane biomass waste as a function of curing temperature and pressure.* Journal of Petroleum Science and Engineering, 2013. 109: p. 291-297.
217. Govin, A., A. Peschard, and R. Guyonnet, *Modification of cement hydration at early ages by natural and heated wood.* Cement and Concrete Composites, 2006. 28(1): p. 12-20.
218. Peschard, A., et al., *Effect of polysaccharides on the hydration of cement paste at early ages.* Cement and Concrete Research, 2004. 34(11): p. 2153-2158.
219. Payá, J., J. Monzó, and M.V. Borrachero, *Fluid catalytic cracking catalyst residue (FC3R): An excellent mineral by-product for improving early-strength development of cement mixtures.* Cement and Concrete Research, 1999. 29(11): p. 1773-1779.
220. Höhne, G.W.H., W. Hemminger, and H.J. Flammersheim, *Differential Scanning Calorimetry: An Introduction for Practitioners*. 2013: Springer Berlin Heidelberg.
221. Netzsch. *What Is the Difference Between DSC and DTA?* 2016; Available from: https://www.netzsch-thermal-analysis.com/en/landing-pages/what-is-the-difference-between-dsc-and-dta/.
222. Sha, W. and G.B. Pereira, *Differential scanning calorimetry study of ordinary Portland cement paste containing metakaolin and theoretical approach of metakaolin activity.* Cement and Concrete Composites, 2001. 23(6): p. 455-461.
223. Trník, A., et al., *Simultaneous DSC and TG analysis of high-performance concrete containing natural zeolite as a supplementary cementitious material.* Journal of Thermal Analysis and Calorimetry, 2015. 121(1): p. 67-73.
224. Ibrahim, S.S., et al., *Metakaolin as an Active Pozzolan for Cement That Improves Its Properties and Reduces Its Pollution Hazard.* Journal of Minerals and Materials Characterization and Engineering, 2017. 6(01): p. 86.
225. Kocaba, V., E. Gallucci, and K.L. Scrivener, *Methods for determination of degree of reaction of slag in blended cement pastes.* Cement and Concrete Research, 2012. 42(3): p. 511-525.
226. Li, B., et al., *Mesoscopic damage model of concrete subjected to freeze-thaw cycles using mercury intrusion porosimetry and differential scanning calorimetry (MIP-DSC).* Construction and Building Materials, 2017. 147: p. 79-90.
227. Badens, E., et al., *Study of gypsum dehydration by controlled transformation rate thermal analysis (CRTA).* Journal of solid state Chemistry, 1998. 139(1): p. 37-44.
228. Strydom, C., et al., *The thermal dehydration of synthetic gypsum.* Thermochimica Acta, 1995. 269: p. 631-638.
229. Stenseng, M., A. Jensen, and K. Dam-Johansen, *Investigation of biomass pyrolysis by thermogravimetric analysis and differential scanning calorimetry.* Journal of Analytical and Applied Pyrolysis, 2001. 58–59: p. 765-780.
230. Zhang, T., L.J. Vandeperre, and C.R. Cheeseman, *Formation of magnesium silicate hydrate (MSH) cement pastes using sodium hexametaphosphate.* Cement and Concrete Research, 2014. 65: p. 8-14.
231. Lura, P., F. Winnefeld, and X. Fang, *A simple method for determining the total amount of physically and chemically bound water of different cements.* Journal of Thermal Analysis and Calorimetry, 2017. 130(2): p. 653-660.
232. Gómez-Zamorano, L.Y. and J.I. Escalante-García, *Effect of curing temperature on the nonevaporable water in portland cement blended with geothermal silica waste.* Cement and Concrete Composites, 2010. 32(8): p. 603-610.
233. Lam, L., Y.L. Wong, and C.S. Poon, *Degree of hydration and gel/space ratio of high-volume fly ash/cement systems.* Cement and Concrete Research, 2000. 30(5): p. 747-756.
234. Monteagudo, S.M., et al., *The degree of hydration assessment of blended cement pastes by differential thermal and thermogravimetric analysis. Morphological evolution of the solid phases.* Thermochimica Acta, 2014. 592: p. 37-51.

235. Bhatty, J.I., *Hydration versus strength in a portland cement developed from domestic mineral wastes—a comparative study.* Thermochimica acta, 1986. 106: p. 93-103.
236. Pane, I. and W. Hansen, *Investigation of blended cement hydration by isothermal calorimetry and thermal analysis.* Cement and concrete research, 2005. 35(6): p. 1155-1164.
237. Lozano, J.R., *Hidratación de pastas de cemento de con adiciones activas subproductos industriales y materiales de desecho*. 2004, Universidad Autónoma de Madrid.
238. Gruskovnjak, A., et al., *Quantification of hydration phases in supersulfated cements: review and new approaches.* Advances in cement research, 2011. 23(6): p. 265-275.
239. Trník, A., et al. *Differential scanning calorimetry of high-performance concrete with burnt clay shale addition*. 2014. International Conference on Heat Transfer, Fluid Mechanics and Thermodynamics.
240. Pavlík, Z., et al., *DSC and TG Analysis of a Blended Binder Based on Waste Ceramic Powder and Portland Cement.* International Journal of Thermophysics, 2016. 37(3): p. 32.
241. *CEM I 42.5 R - Product sheet* 2014, Českomoravský cement as.: Mokrá, Czech Republic.
242. *ZeoBau 50 - Product sheet*. 2014, ZEOCEM, as.: Bystré, Slovak Republic.
243. *Stachesil S - Product sheet*. 2014, STACHEMA, CZ.: Kolín, Czech Republic.
244. Bottrill, R.S. *Silica fume analysis - A preliminary report*. 1991, Division of Mines and Mineral Resources. p. 1-16.
245. Unknown, *Chemical Information Review Document for Silica Flour [CAS No. 14808-60-7].* National Institute of Environmental Health Sciences, National Institutes of Health, US Department of Health and Human Services, Research Triangle Park, NC, 2009.
246. Chen, J., et al., *Morphological Evolution of Low-Grade Silica Fume at Elevated Temperature*. Vol. 36. 2016.
247. Perraki, T. and A. Orfanoudaki, *Mineralogical study of zeolites from Pentalofos area, Thrace, Greece.* Applied Clay Science, 2004. 25(1-2): p. 9-16.
248. Korkuna, O., et al., *Structural and physicochemical properties of natural zeolites: clinoptilolite and mordenite.* Microporous and Mesoporous Materials, 2006. 87(3): p. 243-254.
249. Breck, D., *Zeolite Molecular Sieves Wiley, New York*, 1974.
250. Mansouri, N., et al., *Porosity, characterization and structural properties of natural zeolite - Clinoptilolite - As a sorbent*. Vol. 39. 2013. 139.
251. Ge, Z., et al., *Characterization and performance prediction of cement-based materials using a simple isothermal calorimeter.* Journal of Advanced Concrete Technology, 2009. 7(3): p. 355-366.
252. Bentz, D.P., M.A. Peltz, and J. Winpigler, *Early-age properties of cement-based materials. II: Influence of water-to-cement ratio.* Journal of Materials in Civil Engineering, 2009. 21(9): p. 512-517.
253. Danielson, U. *Heat of hydration of cement as affected by water-cement ratio*. in *Proc. 4th Int. Symp. on the Chem. of Cem., Washington, 1962*. 1962.
254. Nocuń-Wczelik, W., et al., *Effect of some concrete admixtures on the Portland cement hydration.* Cement Wapno Beton, 2004.
255. Maia, L., et al., *Influence of the cementitious paste composition on the E-modulus and heat of hydration evolutions.* Cement and Concrete Research, 2011. 41(8): p. 799-807.
256. Slamečka, T. and F. Škvára, *The effect of water ratio on microstructre and composition of the hydration products of Portland cement pastes.* Ceramics–Silikáty, 2002. 46(4): p. 152-158.

257. El-Alfi, E., A. Radwan, and S. Abed El-Aleem, *Effect of limestone fillers and silica fume pozzolana on the characteristics of sulfate resistant cement pastes.* Ceramics– Silikáty, 2004. 48(1): p. 29-33.
258. Escalante-Garcia, J.I., *Nonevaporable water from neat OPC and replacement materials in composite cements hydrated at different temperatures.* Cement and Concrete Research, 2003. 33(11): p. 1883-1888.
259. Berry, E.E., et al., *Hydration in high-volume fly ash concrete binders.* Materials Journal, 1994. 91(4): p. 382-389.
260. Lothenbach, B., et al., *Influence of limestone on the hydration of Portland cements.* Cement and Concrete Research, 2008. 38(6): p. 848-860.
261. Borges, P.H.R., et al., *Carbonation of CH and C–S–H in composite cement pastes containing high amounts of BFS.* Cement and Concrete Research, 2010. 40(2): p. 284-292.
262. Parrott, L., *A review of carbonation in reinforced concrete*. 1987.
263. Possan, E., et al., *CO_2 uptake potential due to concrete carbonation: A case study.* Case Studies in Construction Materials, 2017. 6: p. 147-161.
264. Segnit, E., H. Holland, and C. Biscardi, *The solubility of calcite in aqueous solutions—I The solubility of calcite in water between 75° and 200° at CO_2 pressures up to 60 atm.* Geochimica et Cosmochimica Acta, 1962. 26(12): p. 1301-1331.
265. Plummer, L.N. and E. Busenberg, *The solubilities of calcite, aragonite and vaterite in CO_2-H_2O solutions between 0 and 90°C, and an evaluation of the aqueous model for the system $CaCO_3$-CO_2-H_2O.* Geochimica et Cosmochimica Acta, 1982. 46(6): p. 1011-1040.
266. Satman, A., Z. Ugur, and M. Onur, *The effect of calcite deposition on geothermal well inflow performance.* Geothermics, 1999. 28(3): p. 425-444.
267. Lipus, L. and D. Dobersek, *Influence of magnetic field on the aragonite precipitation.* Chemical Engineering Science, 2007. 62(7): p. 2089-2095.
268. Coto, B., et al., *Effects in the solubility of $CaCO_3$: Experimental study and model description.* Fluid Phase Equilibria, 2012. 324: p. 1-7.
269. Smith, G.K., *Calcite straw stalactites growing from concrete structures.* Cave and Karst Science, 2016. 43(1): p. 4-10.
270. Lo, Y. and H.M. Lee, *Curing effects on carbonation of concrete using a phenolphthalein indicator and Fourier-transform infrared spectroscopy.* Building and Environment, 2002. 37(5): p. 507-514.
271. Mostafa, N.Y. and P.W. Brown, *Heat of hydration of high reactive pozzolans in blended cements: Isothermal conduction calorimetry.* Thermochimica Acta, 2005. 435(2): p. 162-167.
272. Lawrence, P., M. Cyr, and E. Ringot, *Mineral admixtures in mortars: effect of inert materials on short-term hydration.* Cement and concrete research, 2003. 33(12): p. 1939-1947.
273. Dittrich, S., J. Neubauer, and F. Goetz-Neunhoeffer, *The influence of fly ash on the hydration of OPC within the first 44 h—A quantitative in situ XRD and heat flow calorimetry study.* Cement and Concrete Research, 2014. 56: p. 129-138.
274. Franus, W., R. Panek, and M. Wdowin, *SEM Investigation of Microstructures in Hydration Products of Portland Cement*, in *2nd International Multidisciplinary Microscopy and Microanalysis Congress*, E.K. Polychroniadis, A.Y. Oral, and M. Ozer, Editors. 2015, Springer International Publishing. p. 105-112.
275. Justnes, H., et al., *A ^{29}Si MAS NMR study of the pozzolanic activity of condensed silica fume and the hydration of di-and tricalcium silicates.* Advances in Cement Research, 1990. 3(11): p. 111-116.
276. Muller, A.C.A., et al., *Influence of silica fume on the microstructure of cement pastes: New insights from ^{1}H NMR relaxometry*. Vol. 74. 2015. 116-125.

277. Zelić, J., et al., *The role of silica fume in the kinetics and mechanisms during the early stage of cement hydration.* Cement and Concrete Research, 2000. 30(10): p. 1655-1662.
278. Yajuun, J. and J. Cahyadi, *Investigation on microstructure of silica fume cement pastes.* WIT Transactions on The Built Environment, 2002. 59.
279. Yajuun, J. and J.H. Cahyadi, *Effects of densified silica fume on microstructure and compressive strength of blended cement pastes.* Cement and Concrete Research, 2003. 33(10): p. 1543-1548.
280. Esteves, L.P., *On the hydration of water-entrained cement–silica systems: Combined SEM, XRD and thermal analysis in cement pastes.* Thermochimica Acta, 2011. 518(1): p. 27-35.
281. Atlassi, E.H., *Nonevaporable water and degree of cement hydration in silica fume-cement systems.* Special Publication, 1995. 153: p. 703-718.
282. Skalny, J.P., *Materials science of concrete 1*. 1989.
283. Sellevold, E. and H. Justnes, *High strength concrete binders part B: Nonevaporable water, self-desiccation and porosity of cement pastes with and without condensed silica fume.* Fly Ash, Silica Fume, Slag, and Natural Pozzolans in Concrete. Fourth International ConferenceAmerican Concrete Institute, 1992. 2(SP-132).
284. Skibsted, J., O.M. Jensen, and H.J. Jakobsen. *Hydration kinetics for the alite, belite, and calcium aluminate phase in Portland cements from ^{27}Al and ^{29}Si MAS NMR spectroscopy*. in *10th International congress on the chemistry of cement*. 1997. Inform Trycket AB.
285. Šavija, B. and M. Luković, *Carbonation of cement paste: Understanding, challenges, and opportunities.* Construction and Building Materials, 2016. 117: p. 285-301.
286. Richardson, I., et al., *The carbonation of OPC and OPC/silica fume hardened cement pastes in air under conditions of fixed humidity.* Advances in Cement Research, 1993. 5(18): p. 81-86.
287. Lim, S. and P. Mondal, *Effects of incorporating nanosilica on carbonation of cement paste.* Journal of Materials Science, 2015. 50(10): p. 3531-3540.
288. Gjorv, O.E., *Silica concrete-protection against corrosion of embedded steel.* Special Publication, 1983. 79: p. 719-730.
289. Abo-El-Enein, S., et al., *Characteristics of lime-silica fume mixtures.* Journal of thermal analysis, 1996. 46(1): p. 275-284.
290. Dambrauskas, T., et al., *Hydration peculiarities of high basicity calcium silicate hydrate samples.* Journal of Thermal Analysis and Calorimetry, 2018. 131(1): p. 491-499.
291. Krolo, P., et al., *Hydration and leaching of the cement-zeolite composite.* Ceramics- Silikáty, 2005. 49(3): p. 213-219.
292. Snellings, R., et al., *Early age hydration and pozzolanic reaction in natural zeolite blended cements: Reaction kinetics and products by in situ synchrotron X-ray powder diffraction.* Cement and Concrete Research, 2010. 40(12): p. 1704-1713.
293. Tydlitát, V., J. Zákoutský, and R. Černý, *Early-stage hydration heat development in blended cements containing natural zeolite studied by isothermal calorimetry.* Thermochimica Acta, 2014. 582: p. 53-58.
294. Barnat-Hunek, D., et al., *The use of zeolite, lightweight aggregate and boiler slag in restoration renders.* Construction and Building Materials, 2017. 142: p. 162-174.
295. Kocak, Y., E. Tascı, and U. Kaya, *The effect of using natural zeolite on the properties and hydration characteristics of blended cements.* Construction and Building Materials, 2013. 47: p. 720-727.
296. Uzal, B. and L. Turanlı, *Blended cements containing high volume of natural zeolites: Properties, hydration and paste microstructure.* Cement and Concrete Composites, 2012. 34(1): p. 101-109.

297. Vejmelková, E., et al., *Engineering properties of concrete containing natural zeolite as supplementary cementitious material: Strength, toughness, durability, and hygrothermal performance.* Cement and Concrete Composites, 2015. 55: p. 259-267.
298. Ghourchian, S., et al., *An investigation on the use of zeolite aggregates for internal curing of concrete.* Construction and Building Materials, 2013. 40: p. 135-144.
299. Yılmaz, B., et al., *Properties of zeolitic tuff (clinoptilolite) blended portland cement.* Building and Environment, 2007. 42(11): p. 3808-3815.
300. Markiv, T., et al., *Mechanical and durability properties of concretes incorporating natural zeolite.* Archives of Civil and Mechanical Engineering, 2016. 16(4): p. 554-562.
301. Kontori, E., et al., *Zeolite blended cements: evaluation of their hydration rate by means of thermal analysis.* Journal of Thermal Analysis and Calorimetry, 2009. 96(3): p. 993-998.
302. Perraki, T., et al., *The effect of zeolite on the properties and hydration of blended cements.* Cement and Concrete Composites, 2010. 32(2): p. 128-133.
303. Uzal, B., et al., *Pozzolanic activity of clinoptilolite: A comparative study with silica fume, fly ash and a non-zeolitic natural pozzolan.* Cement and Concrete Research, 2010. 40(3): p. 398-404.
304. Bilim, C., *Properties of cement mortars containing clinoptilolite as a supplementary cementitious material.* Construction and Building Materials, 2011. 25(8): p. 3175-3180.
305. Valipour, M., et al., *Comparing a natural pozzolan, zeolite, to metakaolin and silica fume in terms of their effect on the durability characteristics of concrete: A laboratory study.* Construction and Building Materials, 2013. 41: p. 879-888.
306. Sabet, F.A., N.A. Libre, and M. Shekarchi, *Mechanical and durability properties of self consolidating high performance concrete incorporating natural zeolite, silica fume and fly ash.* Construction and Building Materials, 2013. 44: p. 175-184.
307. Albayrak, M., et al., *Influence of zeolite additive on properties of autoclaved aerated concrete.* Building and Environment, 2007. 42(9): p. 3161-3165.
308. Fueglein, E., *About the use of IDENTIFY—a thermoanalytical database—for characterization and classification of recycled polyamides.* Journal of Thermal Analysis and Calorimetry, 2015. 121(3): p. 1353-1357.
309. Liptay, G.r., et al., *Atlas of thermoanalytical curves:(TG-, DTG-, DTA-curves measured simultaneously).* 1971: Heyden and Son.
310. Ramachandran, V.S., et al., *Handbook of thermal analysis of construction materials*. 2002: William Andrew.
311. Fueglein, E. and E. Kaisersberger, *About the development of databases in thermal analysis.* Journal of Thermal Analysis and Calorimetry, 2015. 120(1): p. 23-31.
312. Moukhina, E. and A. Schindler. *Automatic evaluation and identification of DSC curves*. in *Presentation during international GEFTA symposium "thermal analysis and calorimetry in industry and research*. 2014.
313. Schindler, A., et al., *Database-supported thermal analysis involving automatic evaluation, identification and classification of measurement curves.* Journal of Thermal Analysis and Calorimetry, 2016. 123(3): p. 2405-2414.

List of figures

List of tables